MSc Thesis

Simulation of the Overall Performance of Glazed Unitised Curtain Walls Under Seismic Action Through Finite Element Modelling and Validation via Full-scale Experimental Testing

Evdokia Stavridou

March 2023

TU Delft

Simulation of the Overall Performance of Glazed Unitised Curtain Walls Under Seismic Action Through Finite Element Modelling and Validation via Full-scale Experimental Testing

Thesis as part of the Master of Science Degree at the Delft University of Technology, to be defended publicly on 31st of March 2023

by Evdokia Stavridou

Student Number: 5378761

Faculty of Civil Engineering and Geo-sciences

Master Track: Building Engineering

Specialisation: Building Physics and Technology

Committee Members

Prof. M. (Mauro) Overend	(Chair)	TU Delft, BK, Structural Design and Mechanics
Dr. S. (Simona) Bianchi		TU Delft, BK, Structural Design and Mechanics
Dr.ir. H.R. (Roel) Schipper		TU Delft, CEG, Applied Mechanics
Ir. P.A. (Paul) Korswagen		TU Delft, CEG, Applied Mechanics
Dr. G. (Guido) Lori		Permasteelisa, Italy, S.p.A

Keywords

building envelope, glazed unitised curtain wall, non-structural elements seismic verification, seismic response, earthquake engineering, seismic verification, performance-based design, finite element modelling, DIANA FEA numerical modelling, result extrapolation, governing failure mechanisms

Cover image retrieved from the internet, Source: Permasteelisa Group

Preface

The current report marks the finalisation of the insightful and beautiful journey of the acquisition of a Master's degree in Building Engineering from Delft University of Technology. Over the past two and a half years, I had the opportunity to acquire valuable knowledge over various topics related to buildings covering a wide range of structural, performance, comfort, as well as sustainability aspects. By attending and fulfilling this program, not only have I gained valuable knowledge and experiences, but my professional as well as personal horizons have broadened. The present research topic arose from my desire to combine two fields of great interest to me, this of the building envelope and its seismic verification.

As for the realisation of my final research project, I would like to express my sincere gratitude to the people who supported and provided me with their knowledge and support. First of all, to the chair of my committee Prof. M. Overend for providing me with suggestions and insightful information regarding the direction of my research. To my supervision Dr. S. Bianchi for her constant guidance and support throughout the long graduation process. To Dr.ir. H.R. Schipper for always clarifying any uncertainty, for providing feedback and for facilitating the effective planning and organising of this challenging topic. To Ir. P.A. Korswagen for his valuable support in the development of the finite element model. To Dr. G. Lori for sharing his expertise in the field of exterior numerical modelling as well as his patience and continuous assistance during our numerous consultation meetings that determined the direction of my research.

Additionally, I would like to acknowledge the Permasteelisa Group for its contribution to the realisation of my research project not only by offering all the useful information regarding the case study examined during this thesis, but also by providing me with the opportunity to participate in the experimental procedure that took place in their testing facilities of the Permasteelisa Headquarters in Vittorio Veneto, Italy in July 2022.

A special thank you to the OMRT team and especially to Vincent Höfte for providing me with flexibility and support during this long graduation process and for allowing me to seamlessly focus on the finalisation of my research.

Finally, my deepest gratitude to my family, Lia, Dialechti, Sakis, Aglaia, Nikos and Tasos, for always encouraging me to pursue my ambitions and for their continuous love and support. Last but not least, I am deeply thankful to my friends, old and new ones, for being by my side and for making this journey even more meaningful. Special thanks to Dimitris and Alexandra for their endless support even during the most challenging moments.

Evdokia Stavridou

Delft, March 2023

Abstract

Although relevant information regarding the structural damage state of curtain walls is available, hardly any information referring to the effect of seismic loading on the overall façade performance and especially the weather-tightness of curtain walls is found in the literature. For that reason, the present research attempts to mainly assess the seismic performance of unitised curtain walls and its subsequent impact on their weather-tightness through the identification of the occurring damage mechanisms based on full-scale façade test measurements and finite element modelling. The numerical model aiming to simulate the seismic behaviour of the façade units tested during the experimental procedure is developed in the DIANA FEA environment.

The current study consists of four distinct parts. The first part refers to the Literature Study and Reference Experiments. There, a state-of-the-art is included, discussing in detail the relevant research areas, namely an introduction to the exterior envelope, the multi-performance of façade systems, the various types of glazed curtain wall systems and their association with seismic events, the principle aspects of current seismic regulations, the typical curtain wall response to seismic events and the most frequent damage mechanisms. Additionally, an introduction to the field of the curtain wall numerical modelling is provided. The previous literature review originates both from the observation of relevant full-scale experimental testing performed in the Permasteelisa SPA facilities and from findings derived from the formation of finite element models, as developed along the current academic progress. Later, the description of the experimental procedure of this specific case study is provided accompanied by the analysis of the curtain wall response to inter-storey drift implementation.

Furthermore, the development of the modelling approach is in detail presented in the second part of the report, the Finite Element Analysis. The curtain wall behaviours considered as well as the mechanisms aimed to be recreated with the simplifications applied are introduced. Additionally, the process of identifying and calculating the main properties of the curtain wall elements are displayed accompanied by the setting of the boundary conditions and the loading implementation. A brief walkthrough of the three main modelling phases, starting from the initial development of the finite element model, continuing to its improvement through its calibration as identified by the experimental results and resulting in its final calibration is also included.

Among the objectives of this research topic is the accomplishment of one of the first global numerical models of a curtain wall system using the DIANA FEA software since no prior modelling of curtain wall elements has been found in the literature. The novelty of this attempt consists of the exploration of the possibilities and limitations of the DIANA FEA software that although is widely utilised for a variety of civil, earthquake and geotechnical applications, it has not yet been used for the numerical modelling of curtain wall systems. In general, the accurate representation of façade systems through numerical models like the one developed in this study aims to provide a better insight of the curtain wall behaviour that will be accurate up to the extent that the performing of typically expensive experimental tests will not be needed for their validation.

A vitally important area of interest of the current investigation is the correlation of the behaviour of the numerical model to the actual experimental results measured and observed on the curtain wall mock-ups while undergoing seismic loading. The calibration of the finite element model that later on takes place forms an interesting challenge of the study, intending for a more realistic representation of the actual performance as recorded during the full-scale testing of the unitised façade elements. Additionally, an assessment of the contribution of structural silicone sealants in the post-earthquake behaviour of unitised curtain walls through the comparative performance of façade samples with dry gasket and systems with structural silicone is performed. The outcomes of this evaluation aim to reinforce the existing knowledge regarding the strengths

and weaknesses of the wet and dry configurations and, consequently, to indicate their appropriate application.

Moreover, the study aspires to contribute to the seismic risk assessment of unitised curtain walls through the identification of the governing ultimate failure mechanisms as observed for the case study examined in the present investigation. The previous evaluation is performed with regards to the structural silicone sealant increase, simulating the transition from dry to wet sealant configurations. For this reason a sensitivity analysis varying over the structural silicone bite is developed with respect to the ultimate failure of the façade element under investigation. In practice, the overall response of the curtain wall system is addressed by evaluating several parameters namely the displacement of representative points of both the glazing and the frame, the distortion and rotation of the curtain wall frame and the maximum stress as defined for each of the components. Moreover, the detection of the largest stress values occurring in every element of the glazed curtain wall configuration is later utilised for the determination of the respective utilisation factors. The latter practically occurs for each of the façade elements through the comparison of their maximum stress with the respective design value. The various outcomes of this research are expected to provide the constructive context for further research in the field of façade response under seismic action.

The third section of this graduation project refers to the impact and conclusions of this specific research. Considerations regarding the procedure followed are also discussed accompanied by suggestions for further research topics. The challenges encountered during this investigation, have been collected and are also included at the end of this study in the form of a list, aspiring to provide helpful indications for a future modeller of a similar numerical simulation. Thereafter, the list of the sources used as a valuable reference is presented.

The fourth and final part of the study comprises the Annexes. There are five different Annexes. The first two supplement the theoretical part of the study, providing further information regarding the curtain wall systems and additional seismic codes. The rest of the Annexes provide a complete set of tables of figures, accompanied by detailed explanation of the main modelling phases, the respective findings and the reasoning for various modelling decisions.

Table of Contents

Symbols

α:	design ground acceleration ratio on ground type A, α_g, for gravity acceleration g, Eurocode 8
a_p:	amplification factor
γ_a:	importance factor
γ_x:	shear strain
δ_{xA}:	deflection of structure A at level x, FEMA 450
Δ_a / h_{sx}:	allowable drift index, FEMA 450
Δ_{aA} :	storey drift that is allowable for structure A, FEMA 450
Δ_{clear}:	total lateral deformation of the glazed curtain wall unit due to the rigid glazing motion
$\Delta_{fallout}$:	relative glazing displacement requirement for the glazing fallout from the curtain wall frame
μ_P:	design ductility
ν:	Poisson's ratio
ρ:	mass density
ρ:	redundancy /reliability factor, FEMA 450
T_a:	fundamental vibration period of the appendage, Eurocode 8
T_1:	fundamental vibration period of the structure for the relevant direction, Eurocode 8
τ:	shear stress
Ω_O:	overstrength factor, FEMA 450
b_p :	rectangular glass panel width
c_1:	gap (clearance) between the frame and the vertical glass edges
c_2:	gap (clearance) between the frame and the horizontal glass edges
$C_p(T_p)$:	horizontal design response coefficient
C_{ph}:	horizontal response factor of the part, NZS 1170.5
C_{pv}:	vertical response factor of the part, NZS 1170.5
C_{vd}:	design action coefficient as determined for the vertical direction, NZS 1170.5
D_p:	relative displacement / inter-storey drift of a component
E:	Young's modulus
F_a :	seismic force applied horizontally in the critical direction
F_P :	horizontal seismic force, FEMA 450

F_{ph} :	horizontal design seismic action, NZS 1170.5
G :	shear modulus
H :	inter-storey height
h :	average value of the roof height above the base, FEMA 450
h_p :	rectangular glass panel height
h_{sx} :	storey height as introduced in the allowable drift Δ_a definition, FEMA 450
I_p :	importance factor of component, FEMA 450
M:	moment of a force
N:	axial force
NCs:	non-structural components
P_{max}:	maximum pressure
Q:	shear force
q_a :	behaviour factor
R_p :	response modification factor of the non-structural component, FEMA 450
R_p :	risk factor, NZS 1170.5
S :	factor related to soil, Eurocode 8
S_a :	seismic coefficient included in the appendage, Eurocode 8
S_{DS} :	acceleration parameter of the short period spectra
T_1:	fundamental vibration period of the structure for the relevant direction, Eurocode 8
T_a:	fundamental vibration period of the appendage, Eurocode 8
T_p:	component period
W_p	operating weight of the non-structural component
z:	component height as measured from the attachment point base and upwards, FEMA 450

Abbreviations

AAMA:	American Architectural Manufacturers Association
ASTM:	American Society for Testing and Materials
DS:	Damage States
EPDs:	Environmental Product Declarations
EPDM:	Ethylene Propylene Diene
EN:	European Norms
FEM:	Finite Element Modelling
FEMA:	Federal Emergency Management Agency
FT:	Fully-Tempered Glass
HS:	Heat-Strengthened Glass
IBC:	International Building Code
IGU:	Insulating Glazing
JASS 14:	Japanese Architectural Standard Specification
JRC:	Joint Research Centre
LCA:	Life Cycle Analysis
NEHRP:	National Earthquake Hazards Reduction Program
NZS:	New Zealand Standards
PACT:	Performance Assessment Calculation Tool
PCM:	Phase Changing Material
PVB:	Polyvinylbutyral
SLS:	Serviceability Limit State
SSG:	Structural Sealant Glazing
ULS:	Ultimate Limit State

Chapter 1

Introduction

Problem Statement

Earthquake events, even the ones with moderate intensities, are known to be responsible for the damage of both the structural elements as well as of the non-structural components of a building. Although the seismic design of structures mainly focuses on the prevention of structural damage, it has been observed that damages occurring to non-structural elements, such as curtain walls, are responsible for a considerable financial impact, remarkably larger than that of structural impairment.

Over the past years, numerous experimental studies have been realised focusing on the seismic performance of curtain wall systems, especially after the realisation that damages of such components apart from resulting in considerable economic losses, they also pose potential hazard. Glass curtain wall systems in particular have been found to be vulnerable to the seismic actions, undergoing various impairments ranging from slight functionality losses to moderate or even severe damages that subsequently lead to both considerable economic losses and costly repairs and can additionally pose significant threat to life safety of the building occupants and the pedestrians (Caterino et al., 2017). Unfortunately, the seismic behaviour of glass curtain walls has not been adequately developed in the existing standards and regulations, therefore the acceptable seismic performance is yet to be defined.

Apart from the experimental testing, various numerical studies have also been performed in the course of recent years aiming to assess the performance of glazed curtain walls during seismic events. Numerical simulations typically attempt to provide a better understanding of the non-linear interaction of the glazing panes and the aluminium frame that importantly affects both the stiffness and the strength of the curtain wall systems while imposed on stepwise incremental loading activities, such as seismic events. The combination of both the experimental and numerical assessment of glazed curtain walls complement each other and eventually enhance the better understanding of the dynamic behaviour of glazed curtain wall components and systems in general. The importance of the latter is highlighted by the continuously increasing need for seismic qualification of curtain wall systems that is gradually becoming a prerequisite for their verification (Huang et al., 2017).

The present study aims to assess the seismic performance of glazed unitised curtain walls, through the combination of experimental results and the insight obtained from a numerical model developed in the DIANA FEA software. In practice, the case study of a full-scale experimental testing realised in the Permasteelisa mock-up test facilities is investigated. For this glazed curtain wall configuration a finite element model is developed, aiming to recreate as faithfully as possible the system response during and after its subjection to seismic activity. The numerical model created and calibrated through the experimental response, provides a useful means for the overall assessment of the glazed curtain wall behaviour under seismic loading. Additionally, the governing damage mechanisms are identified and associated with the respective inter-storey drift ratios and the variation of the glazing-to-frame connection width transitioning from dry to structurally sealed connections. The extent to which a numerical simulation through DIANA FEA software can faithfully approximate the realistic behaviour of a typical glazed curtain wall system as recorded during a full-scale testing is investigated. Finally, this study aspires to provide the constructive context for further insight in the field of façade behaviour and numerical simulation under seismic loading that eventually to facilitate the assessment of a curtain wall seismic response even during the early design stages.

Research Questions

Three are the main research questions addressed in the current study. These are listed in the section accompanied by the sub-questions that supplement and further clarify them.

The main research questions are formulated and presented as follows:

- What is the correlation of the results of the DIANA FEA numerical model, describing the behaviour of the unitised façade elements tested under seismic loading, with the experimental results observed and measured during the full-scale testing?
- To what extent do alternative unitised curtain wall systems (dry vs wet glazed) behave differently under seismic loading in terms of the different damage mechanisms occurring on the façade element?
- What are the possibilities of the results originating from this case study to be extrapolated providing insight for a wider range of similar curtain wall systems?

These main research questions can be further specified while deconstructed into self-contained questions:

- Regarding numerical model development, what level of accuracy can be achieved?
- What are the means of comparison through which the numerical to experimental correlation is realised?
- What is the curtain wall behaviour observed to be mostly affected between dry and wet sealed glazed systems?
- How can the response of each of the curtain wall components be separately assessed?
- What are the governing damage mechanisms and is there any correlation with the variation of the glazing-to-frame connection?

Overall, the foremost aim of this study regarding the assessment of the façade performance under seismic loading is expected to reinforce the current knowledge and to contribute to the optimisation of the façade design and construction procedures as a whole. More specifically, by providing answers to the above research questions this study is expected to indicate to what extent the application of such a numerical model can facilitate the seismic assessment of curtain wall systems even during the early design stages, while also eliminating the need for the realisation of time and resource-consuming full-scale testing.

Research Objectives

Rather than having solely one objective, the present study intends to answer several research topics. It aims to provide insight on the post-seismic multi-performance of the façade elements tested through the

contribution of finite element modelling and to ultimately facilitate the integral assessment and better understanding of the unitised glazed curtain walls' response in general.

1. Study of the Unitised Curtain Wall Seismic Performance through the Identification of the Occurring Damage Mechanisms based on the Full-scale Façade Test Measurements

One of the main research topics is the evaluation of the behaviour of alternative (dry vs wet glazed) unitised curtain wall elements under seismic loading. The assessment is realised in terms of the damage mechanisms occurring on the overall curtain wall behaviour, on the façade elements themselves and their subsequent impact on the enclosure's seismic performance and, supplementary, on its multi-performance The seismic performance is assessed through the application of several in-plane displacements on the façade specimens. In practice, various inter-storey drift intensities are imposed at a certain number of loading circles through a seismic beam. The evaluation of the overall façade performance under seismic loading is expected to reinforce the current knowledge and to contribute to the optimisation of the façade design and construction procedures as a whole.

2. Creation of a Finite Element Numerical Model Simulating the Experimental Seismic Behaviour

Among the objectives of this study is the accomplishment of the first numerical model of a curtain wall system using the DIANA FEA software since no prior modelling of curtain wall elements has been found in the literature. The novelty of this attempt consists of the exploration of the possibilities and limitations of the DIANA FEA software that although is widely utilised for a variety of civil, earthquake and geotechnical applications, it has not yet been used for the numerical modelling of curtain wall systems.

In order to achieve the first modelling of a façade system in DIANA FEA, research on the simulation of similar elements through other finite element software (such as ABAQUS, Visual Analysis, SAP2000, Straus) has been performed. Thereafter, the simplifications and modelling approaches used in other programs have been adapted in DIANA FEA, while also exploring the possibilities of this specific software. The outcome of the study aspires to provide the constructive context for further future research in the field of façade seismic behaviour.

3. Comparison of the Experimental & FEM Numerical Results

The behaviour of the numerical model built in the DIANA FEA software is correlated to the actual experimental results measured and observed on the curtain wall mock-ups while undergoing seismic loading. A calibration of the finite element model later on is performed intending for a more realistic representation of the actual performance as recorded during the full-scale testing of the unitised façade elements. This option provided, allowing for the comparison of the numerical and actual experimental results, forms a significantly important means of verification, evaluating the accuracy of approximations adopted during this numerical procedure and the validity of the modelling approach as a whole.

4. Assessment of the Structural Silicone Contribution to the Curtain Wall Post-seismic Behaviour

The previous is realised through the comparative performance of façade samples with structural silicone and systems with dry gasket. The purpose of converting the structurally sealed (SSG) configuration tested into a dry glazed system in the numerical modelling is to verify and demonstrate the enhancement that structural silicone provides in the seismic performance of the unitised curtain wall systems as opposed to the one of the conventional systems with dry gaskets. The influence of the different connection typologies between the frame and the glazing is evaluated through a sensitivity analysis which is developed through the variation of the adhesive connection bonding the glazing with the frame. The importance of such a sensitivity analysis is highlighted not only by the limited information found in the literature available, but mainly by the insightful information that it provides into the field of result extrapolation. The possibility of extracting results from solely one numerical model related to a much wider range of complex configurations, such as of glazed curtain walls is aimed to be investigated and provide the ground for similar future attempts. The field of the result extrapolation itself is expected to significantly facilitate the seismic behaviour of curtain wall systems, minimising the need for the development of a numerical model for each of the different curtain wall configurations. Therefore, the results of research relevant to the one analysed here are aspired to provide useful information and to contribute to the development of the result extrapolation which is considered of significant importance.

Research Methodology

This specific investigation is conducted by combining several research approaches with the most important ones being the literature review, the full-scale experimental testing as well as the finite element modelling. The latest two are compared and combined in order for the validation of the DIANA model to occur through the data that originated from the lab measurements.

1. Literature Review

Initially, an overview of the available literature including relevant articles, standards & regulations, testing protocols as well as results of similar large-scale tests is performed. The fields under investigation vary from the multi-performance of the exterior envelopes to the façade types and their connection details, the building and curtain wall seismic design, the properties and applications of adhesive connections, the seismic assessment of curtain walls, the seismic regulations and standards, the guidelines for mock-up tests, the finite element modelling of curtain wall systems and a few more. This literature review aims not only to contextualise the present research, but also to substantiate its impact and contribution to the academic field.

2. Analysis of the Full-scale Experimental Testing Results

Regarding the analysis of the full-scale experimental testing results, this is primarily performed by the evaluation of the post-earthquake façade response. In practice, the latter is achieved by inspecting the curtain wall component displacements and deformations and by determining the loss of serviceability state and of the subsequent damages occurred due to the horizontal displacement application that simulates the realistic loading condition. Moreover, by imposing incremental lateral drift demands on the unitised façade elements the different damage states are observed and recorded. The observations above are realised in this study not

only by means of visual inspection but also through monitoring systems, such as displacement transducers monitoring the local and global behaviour of the façade elements.

In order to determine the drift level that occurs horizontally as a result of the earthquake loading, the specified successive levels of displacement are induced on the mock-up façade elements. These accompanied by the prescribed response of the system are listed below:

- 1st Level = H/300: no damage can occur neither in the internal nor in the external components
- 2nd Level = H/200: the external elements should not transcend the permitted stress. The serviceability of the façade needs to be restored by the repair of the structural sealant
- 3rd Level = H/100: components' fall down nor failure of glazing are permitted

The three levels of the horizontal displacement presented above were obtained from the indications of the Japanese standard (JASS 14). The first level refers to a seismic event characterised by high probability, the second one to the highest earthquake event that has been recorded in the past and finally the third level to a seismic event with a return period of 100 years. Moreover, "H" represents the inter-storey height expressed in millimetres.

The seismic performance of the specimens is also evaluated through the investigation of the effect these damage mechanisms have on the multi-performance, namely the weather-tightness and seismic response, of the exterior enclosures. This objective is assessed through a series of static seismic tests, as indicated by the Japanese standards (JASS 14), typically performed whilst a project undergoes a seismic verification, as well as through a modified testing sequence, in order for façade failure conditions to be achieved.

More specifically, through the full-scale experimental testing both the life-safety risk induced by the earthquake loading, which is expected to be limited, as well as the post-earthquake serviceability performance of the façade, that is estimated to be gravely affected, are evaluated.

In practice, the ultimate resistance of the unitised façade elements is typically examined by:

- Air permeability tests, performed following the indications of EN 12152, EN 12153 and
- Seismic tests, where several displacements of various intensities are applied at a certain number of circles in the façade specimens through a seismic beam, according to JASS 14 and AAMA 501.4

3. FEM Simulation of the Unitised Curtain Wall Undergoing Seismic Loading

As for the recreation of the unitised curtain wall system while undergoing seismic loading through the development of a finite element modelling the following research methodology is defined. Aiming for a simulation as close as possible to the realistic testing conditions, a procedure similar to the one followed during the actual testing, where at certain displacements the respective movements of the mock-up are examined, is repeated in the finite element modelling procedure. For this reason, the numerical model developed in the DIANA FEA environment undergoes the same inter-storey lateral drift as this observed during the experimental procedure. Additionally, the respective curtain wall movements are attempted to be recreated, by providing the appropriate boundary conditions and restraints.

Initially the formation of simple numerical models takes place, considering various simplifications such as the spring behaviour of the glass-to-frame connection and the representation of the boundary conditions with

linear properties. At a later stage, when more familiarity with the DIANA FEA environment is achieved, some of these simplifications are replaced aiming for a simulation representative, to the extent possible, of the actual situation. A balance between the simplification criteria and the subsequent error margin introduced, on one hand, and the preservation of both the model complexity and computational time as limited as possible, on the other hand, is the ultimate intention.

4. Comparison of the Testing Measurements & FEM Results

The experimental results and observations are compared and examined for their correlation with the numerical outcomes. The overall behaviour of the numerical model, such as the displacement, the distortion or the rotation of the glazing panels, is expected to be similar with the one recorded in the façade mock-up. Furthermore, a calibration of the numerical model through the measurements acquired from the façade testing is also performed. This option provided, allowing for the comparison of the numerical and actual experimental results, forms a significantly important means of verification, evaluating the accuracy of approximations adopted by this numerical procedure and the modelling approach validity as a whole.

Above the main pillars of the research approach as defined for this study are presented. The flow chart introduced at the end of this chapter (Figure 1.1) graphically presents the workflow followed during this research project.

Analysis & Presentation of Intended Outcomes

An overview of the results obtained from the current study is presented starting from the ones relevant to the assessment of the seismic performance of unitised curtain walls.

1. Study of the Seismic Performance of Unitised Curtain Walls

The damage states (DS) that are expected to be observed and recorded during the full-scale testing of the façade sample units are listed below:

- DS1: Deterioration of the weather protection (water- and air-tightness) of the curtain wall system element. This will be investigated through simple observations, such as the existence of water in the inner side of the glazing system
- DS2: Deformation of the façade elements, in particular in-plane movement of the glass and the framing is expected as well as the relative displacement of the glass to the frame elements. Failure of the gasket is also anticipated at this damage state. The latter will be performed by visual observation as well as recording of the gaskets' movement outside their original place either towards the framing or completely fallen from the curtain wall frame. These kinds of gasket movements indicate either repair or replacement
- DS3: Failure of the glazing or the frame system. Variant conditions can be observed, from confined to extensive cracking, breakage or even complete fall out of the glazing units

For all of the cases above, the drift demand at which these damage states are initiated is recorded.

In general, the ultimate limit, namely the life-safety risk state, of the unitised façade elements under testing caused by earthquake actions is expected to be limited. On the other hand, the post-earthquake serviceability performance, especially the weather-tightness, might be severely affected.

2. Contribution of Structural Silicone Sealants in Unitised Curtain Walls Post-earthquake Behaviour

In the existing literature it is acknowledged that curtain wall elements with structural silicone can absorb part of the seismic drift through the rotation of the units. Further information concerning the additional post-earthquake impact of the structural silicone on the façade details and on the stress redistribution on the unitised curtain wall elements is aimed to be defined through the current study. This behaviour of the curtain wall systems with adhesive connections is also aimed to be compared with the one of the conventional façade systems containing gaskets, widely referred to as dry systems. In general, less stress is expected to be observed in the curtain wall configuration for the cases of the structurally sealed solutions. More specifically, the previous is translated in the curtain wall configuration into the observation of less distortion and more rotation while transitioning from dry to wet seal curtain wall configurations.

For the accurate and detailed assessment of the structural silicone contribution to the post-earthquake behaviour of the façade elements tested, the actual rotations and movements of the curtain wall systems is expected to be accurately presented using tables and diagrams for each of the façade segments. Additionally, figures and visualisations displaying the displacement trends, the stress distribution over the various elements of the façade (e.g. the glazing pane, the gasket/structural silicone), or the initiation of glass cracking etc. of both the dry and wet systems are expected to provide the opportunity for quantitative comparison and eventually for the better understanding of the two configurations examined.

3. Creation of a Finite Element Numerical Model using DIANA FEA

A representation of the façade elements tested during the experimental procedure is attempted through the creation of a numerical model in the DIANA FEA software. The model is expected to respond to the seismic loading in a way similar to the one observed and recorded at the full-scale testing.

The behaviour of the DIANA FEA models to the seismic loading is assessed through the analysis results originating from the software itself. Various diagrams and figures presenting the displacement, rotations and distortions of each façade element in both x and y axes will provide the behavioural overview of the façade elements tested. These figures are later on compared with the respective ones created based on the experimental data. An attempt to minimise the differences that are already expected between the experimental data and the response of the finite element model will be made through the calibration of the latter. Several parameters, mainly the material models and properties of the façade elements (glazing, aluminium frame, gaskets and structural silicones) are evaluated while aiming for the best representation of the actual façade behaviour as monitored through the experimental procedure.

A satisfactory level of accuracy is expected to be achieved mainly through the modification of modelling properties, mostly referring to the properties of the curtain wall components and the boundary conditions. However, a complete correspondence of the numerical and the experimental results is known to be impossible to achieve, due to the inherent inaccuracies introduced into the simulation process through the various simplifications and the inability of approximating the various random effects occurring during the experimental sequence of a mock-up specimen.

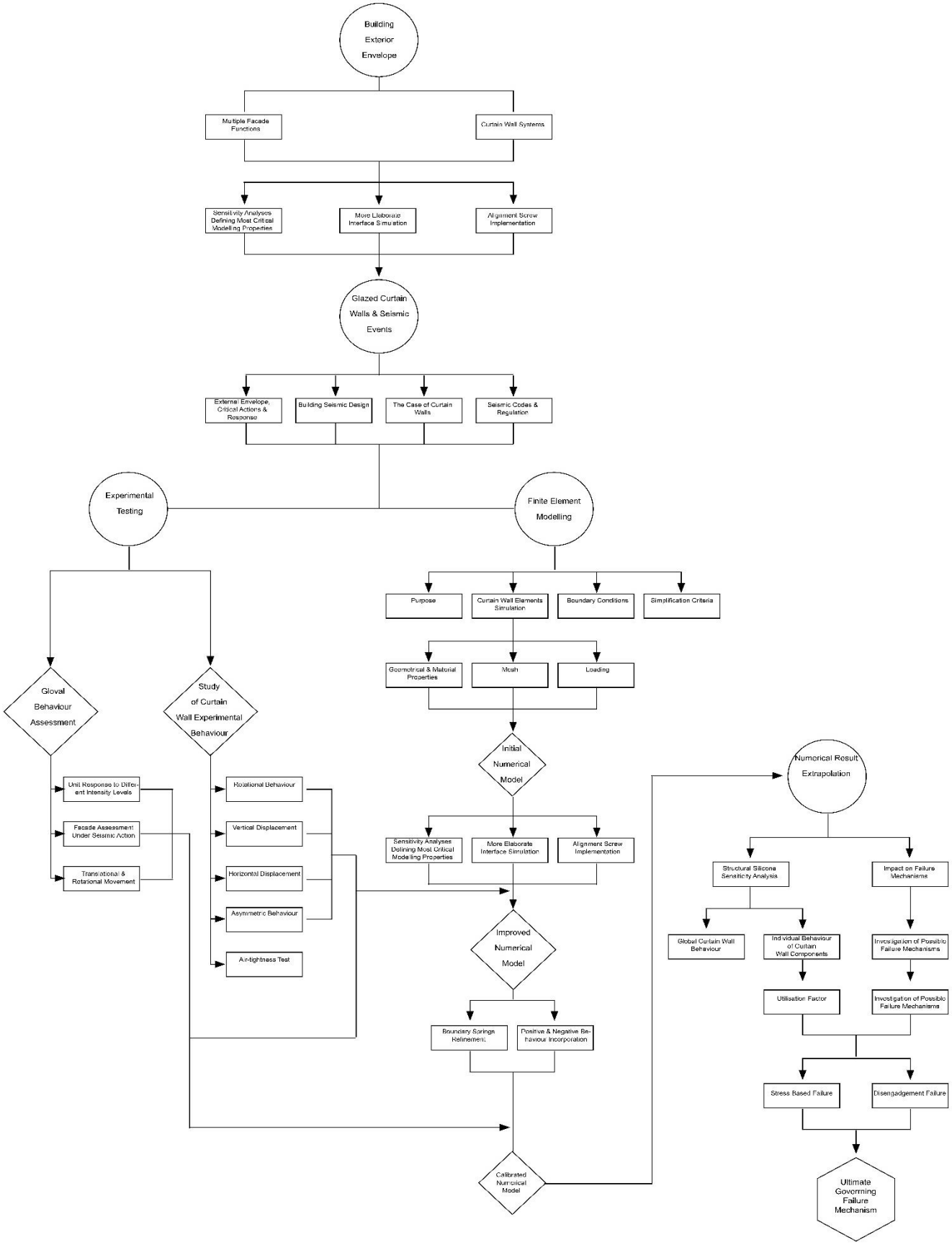

Figure 1.1: Flowchart depicting the research methodology implemented in the present study.

Part I

Literature Study & Reference Experiments

Chapter 2

Building Exterior Envelope

While considering the term façade, the first correlation typically made is with the notion of aesthetics. It is undeniable that the exterior enclosure of a structure defines decidedly, if not entirely, its visual appearance and eventually its identity. However, when aesthetics is applied on architecture broadly and on buildings more specifically, it surpasses the concept of visual impression; instead it is mostly driven by the notions of form and function. In reality aesthetics forms part of the global scope of the optimal building design configuration. In order for the latter to be achieved, various aspects such as the performance design principles, the collaboration of materials, their properties and the associated physics need to be integrated and adequately balanced.

This chapter of the study aims to introduce the above and is considered as a useful introduction to the topics later analysed mainly to the readers not fully familiar with the building sector and the field of façade systems. On the other hand, readers with prior acquaintance with the exterior envelope topics, are encouraged to move forward to the following chapters of the study.

As far as the structure of the present chapter is concerned, an overview of the different functions a façade system typically needs to incorporate is initially presented. Later, the most common typologies related to the different ways of system construction and assembly are introduced. The description of the main façade components follows, accompanied by a short description of the different variations available. The attention is then focused on the different options provided for the connection of the glazing with the frame, more specifically on the mechanical and adhesive connections. Their influence as well as contribution to the curtain wall behaviour is presented, providing the ground for the comparison between the curtain wall dry and wet connections that follows. Finally, an introduction to the fastening systems encountered on façade configurations is presented.

Multiple Façade Functions

For the facilitation of a thorough understanding of the topics later to be discussed, an elementary introduction of terminology relating to buildings and mainly façades is considered essential. The general term “building envelope” is dedicated to the exterior enclosure of a building structure that provides a barrier between the outdoor, environmental and the indoor environment. As a division element it is also responsible for regulating the interactions between the interior occupied areas and the various environmental elements (Frighi, 2022).

The main purpose of the exterior envelope is to achieve the predefined performance levels established for each particular building as well as to provide and maintain internal conditions that are conceived as comfortable by the building’s occupants. Therefore, façades are designed, detailed and constructed aiming to counteract various external phenomena and their influence on the occupied areas depending on the given climatic zone and conditions. The above crucial function of the façade that ensures comfortable conditions for the end users of the buildings and their well-being in general is referred to as weather-tightness.

Another crucial objective of the building envelope that is closely related to the weather-tightness previously mentioned is energy efficiency. By selecting the appropriate type of enclosure and structural detailing, the air and thermal leakages through the façade can be prevented, leading eventually to more efficient heating and cooling of the interior area while saving costs and energy. Moreover, the determination of both the optimal shape and orientation of the building and of the façade’s transparent to opaque ratio not only play a crucial role in controlling the light and natural air intrusion, the temperature and condensation of the interior

but also contributes to the heat gain maximisation during wintertime and to the elimination of heat loss during summertime. The above leads to the energy needs minimisation and, eventually, to the energy consumption reduction (Boswell, 2013).

The structural integrity is an additional important function of the building envelope, consisting in its ability to support both the enclosure itself along with the additional loads and deflections applied to it, such as the in-plane and out-of-plane wind loads. The structural capacity of components, and consequently of the structure as a whole, is an intricate subject depending on numerous parameters such as the properties, thickness, size, geometry, orientation or the selected and applied attachment method.

While examining the building enclosure, a basic division of the exterior envelope in two categories is typically made based on whether the system itself is load- or non-load-bearing. In the first case the exterior enclosure is referred to as load-bearing whereas the rest of the façades are characterised as cladding applications. The load-bearing enclosures accommodate the structural demands of the building since they form part of either the primary or the secondary structural system and transfer themselves both their self-weight and all the exterior forces applied on them to the foundation. The cladding applications on the other hand, which is the category where curtain walls belong to, are only responsible for bearing their self-weight loads along with the additional applied forces and to transfer them to the primary structural system through the anchorage assemblies. More detailed explanations of the anchorage systems and the connection details per façade type in particular are presented.

Last but not least, the accommodation of the movements and deflections is another fundamental function of the building envelope. Thermal movements, inter-storey and seismic drifts as well as deflections caused due to phenomena such as gravity forces and creep need to be sufficiently accommodated by the proper joints and connections of the building envelope. In that way, the exterior enclosure design is relieved from additional stresses that would otherwise be transferred in the enclosure materials themselves, and eventually protected from material buckling or bending (Boswell, 2013). Depending on the type of the building construction and its intended use and function, supplementary functions of the building envelope such as blast, threat or acoustics resistance may also apply.

To conclude, several parameters such as the building’s intended functions, the aesthetic appearance of the structure as a whole, the principles of the performance design and the building physics as well as the forces and elements acting on the enclosure are factors that imperatively affect the selection of the most appropriate exterior enclosure of a building (Boswell, 2013). A façade serving various performance design principles while providing the building with an interesting architectural expression is seen in Figure 2.1.

Figure 2.1: A night view of the Dancing Building façade located in Prague is depicted above. Apart from the aesthetics of a structure, the external enclosure determines several additional parameters, such as functionality and performance design principles (Source: Amazing Czechia).

Curtain Wall Systems

In general, building envelopes and their materials vary from more traditional ones, such as masonry, stone and concrete, to more modern like glass and steel, offering lighter as well as more aesthetically pleasing façades. Over the past years, the ever-increasing desire for transparency and natural light intrusion in the modern buildings as well as the sustainability considerations have broadened the use of glazed façades and extended it to numerous buildings. They can also be retrofitted in the exterior of a building during renovation and upgrade projects.

Apart from offering unobstructed panoramic views, glazed curtain walls allow the entrance of natural light to the building interior (Figure 2.2). Depending on the amount and orientation of the openings, the daylight intrusion as well as the energy retention of the building can be considerably optimised. Curtain wall systems provide numerous design capabilities and flexibilities, not only in terms of the shapes and sizes of the openings, but also on the various materials for the framings and types of the glazing, enhancing in this way freedom to the architectural expression.

Further inherent safety aspects of the curtain walls systems include the prevention of water and air-infiltration, the advanced thermal performance, the lightness and ease of construction (Ilter et al., 2015) as well as the elimination of the fire and smoke spreading between adjacent floors, provided that fire safety aspects have been considered in the design. Curtain walls have been also found to reinforce the structural stability of tall buildings, by contributing to their sway minimisation due to wind. The latter happens due to the energy dissipation through the framing of the curtain wall and its transfer to the building primary structure.

Figure 2.2: One of the main advantages of glazed enclosures is that they provide increased connection with the outside (Source: Karkhana.io).

Critical Aspects

Along with the undeniable advantages of a curtain wall system, a few considerations related to both their design and application exist. More frequently, problems regarding the infiltration or the structural performance of especially the unitised systems arise throughout their life cycle. The main aspects responsible for the gradual deterioration of the infiltration and structural long-term performances are the climatic conditions and the successive wind loads (Ilter et al., 2015). A series of additional considerations as reported by other studies exist, however their importance is dependent on the type and location of the building, therefore they are not considered critical for the general design of the curtain wall systems (Sie, 2007).

On the contrary, the fire safety aspect while using curtain wall systems is a topic that requires additional attention. Due to the gap located between the curtain wall back and the floor slab cladding is normally attached to, smoke, conductive or radiant heat or even the fire itself, easily spread along the building façade between adjacent floors. For this reason, it is important that proper fire safety provisions are included in the façade design. Typical fire safety measures include ensuring the fire resistance of glazing and frames, the fire stops placing along the façade skin, the prevention of the lateral fire spread in case of emergencies, the placing smoke seals at the gaps occurring between the floor slab edge and the curtain wall back. In general, the essence of a fire safety design is the compartmentalisation of adjacent floors and the delay of the fire spread and the combustion gases passage between the building floors (Vigener & A. Brown, 2016).

Over the years it has been concluded that the most impactful aspects of the curtain wall performance that drastically define their performance are the structural integrity, the weather-tightness, the provision for movement and the fire safety design.

Common Curtain Wall Typologies

The glazed curtain wall systems are typically classified to either framed or frameless façade systems based on their structural support. Below an overview of framed and frameless curtain wall systems is presented.

Framed Curtain Walls

Although initially framed curtain wall configurations were made of steel profiles, today the ones with extruded aluminium prevail. Framed curtain walls are designed to accommodate multiple design requirements, such as building movement and sway, thermal conduction and expansion, weather-tightness, sufficient lighting and thermal conditions for the interior while lowering the cooling and heating needs and costs of the buildings. Those types of curtain walls are suitable for multi-storey buildings since they can span between multiple floors. In the following section, the most common aluminium framed curtain wall systems are presented.

Stick-Built

The curtain wall stick-built, or simply stick, system is the traditional curtain wall installation method where each façade unit is installed separately as depicted to the left of Figure 2.3. The mullions (vertical members of the framing) are typically installed first and later the transoms (horizontal rail elements) follow. Usually the frame elements in stick-built systems are rectangular extrusions made of aluminium (Raggousis & Zalok, 2016).

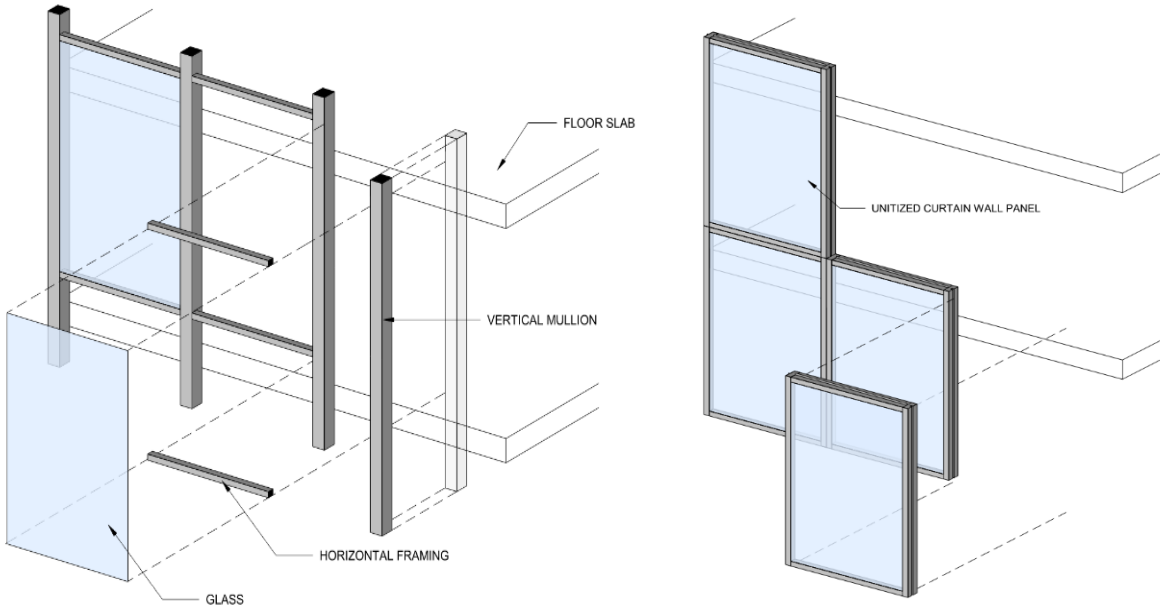

Figure 2.3: In the left schematic drawing, a stick-built system is presented. In this case, the framing (transoms and mullions) as well as the glazing or the opaque panels (spandrels) are erected and connected together on site

piece by piece. To the right, a unitised system is represented where the curtain wall consists of large units that are pre-fabricated in the factory, transferred to the construction site and finally erected on the structure (Source: Building Enclosure).

Even from the early applications of metal curtain walls, the use of the stick system was widespread. The modified application of this technology continues until today mainly due to its advantages which, among others, include the reduced handling and shipment costs as well as the flexibility of the dimensional adjustment based on the site requirements and needs. As for the weaknesses of this installation method, they are mostly related to the time and labour consuming assembly of the curtain wall system that is required to be on site (Sivagnanasundram, 2011).

Unitised

The unitised, also known as modular, curtain walls is a more contemporary compared to the previous design and construction approach, consisting of one storey-height units of either aluminium or steel framing, with the first one applied more frequently. The prefabricated façade units are typically one module wide, however, they can sometimes incorporate more modules (Vigener & A. Brown, 2016). The façade panels are fabricated and assembled in the controllable conditions of a factory, where high quality and product efficiency are assured. The curtain wall units are later transferred on site where, through mechanical handling, are positioned, aligned and fixed to the brackets already placed either on the structural frame or the concrete floor slab. A typical assembly of a unitised curtain wall unit is presented to the right of the Figure 2.3. It is commonly seen that inside the pre-fabricated framework, transparent glazing as well as spandrel panels are mounted.

The installation process of the unitised panels can initiate either from the top or the bottom of the building and typically follows the perimeter of every storey until eventually the entire exposed surface of the building is complete. The aluminium profile is divided into female and male sections, therefore is fabricated in halves each of them containing interlocking components (Raggousis & Zalok, 2016), so that sufficient built-in tolerance can be assured. The latter is essential for the accommodation of movements and adjustments occurring during the installation phase and additionally for the various movements created during the service life of the curtain wall (Sivagnanasundram, 2011).

Due to the required pre-assembly, the application of unitised curtain wall systems is typically more expensive. Additionally, the complexity of the fastening system is higher compared to this of the other framed curtain wall configurations. However, unitised systems are preferred in the high-rise structures since its application does not require any scaffolding on the construction site. They are also more reliable in ensuring water- and air-permeability requirements on the high-rise structures where increased wind pressure occurs (Galli, 2011).

Semi-Unitised Curtain Walling

This curtain wall system is a development of the stick system. In the case of the semi-unitised configuration the mullions are firstly installed independently. Thereafter, the frame pre-assembled units are installed between the mullions. The façade units of this typology can either be continuous, spanning between consecutive storeys, or can be divided into transparent glazing and spandrels, typically non-transparent units

placed in front of the connection of the curtain wall with supporting the floor slab or the beam. Similarly to the stick system, the semi-unitised also requires both increased assembly time and labour force, much greater than those of the unitised curtain wall system.

Figures 2.4, 2.5 and 2.6 depict typical curtain wall applications of stick, unitised and semi-unitised units respectively.

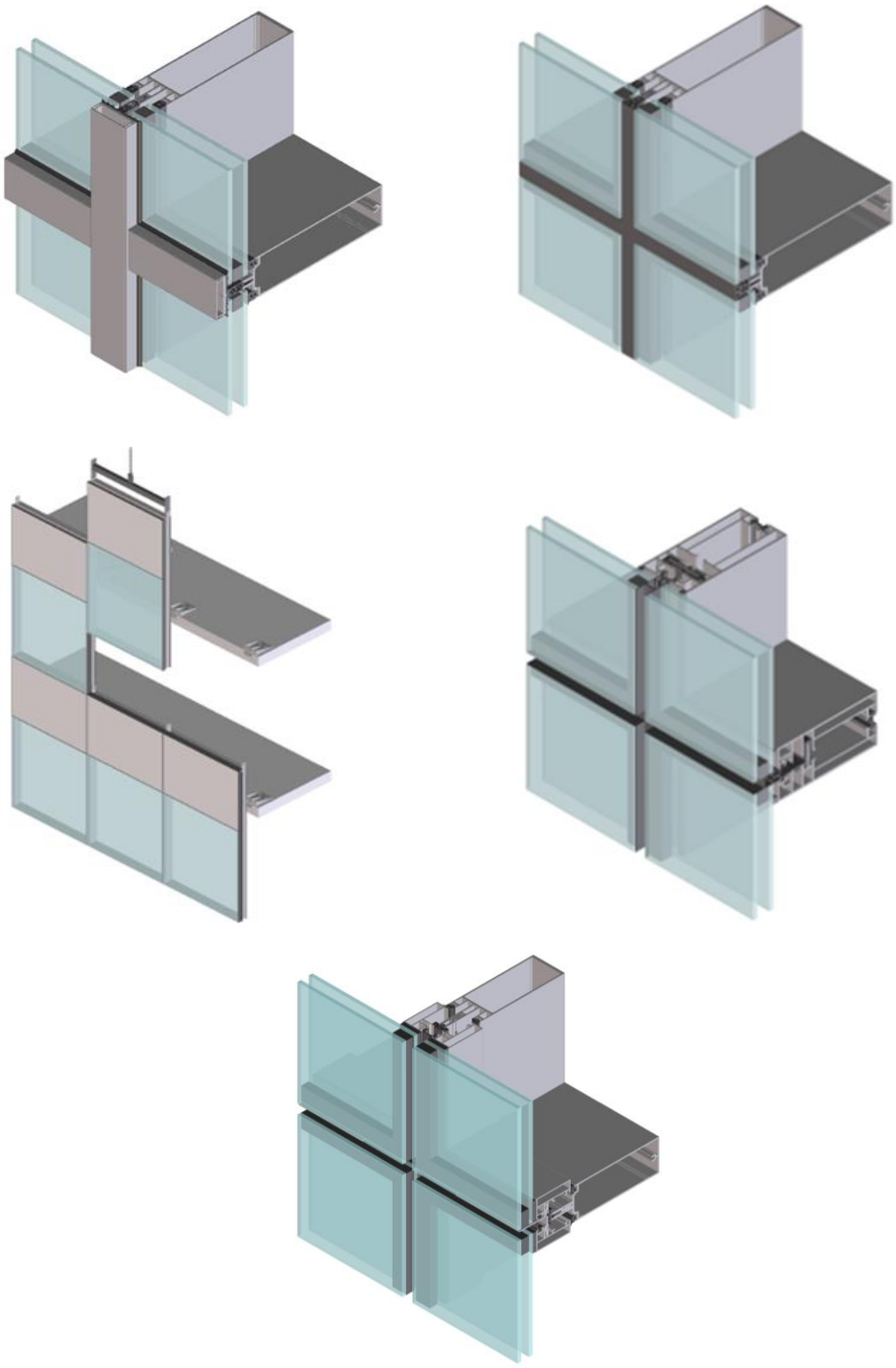

Figure 2.4: In the two figures above typical stick-built systems are illustrated. To the left, a capped configuration is presented. Next, a configuration with a smaller joint aiming to provide a continuous and seamless transparent look is depicted (Source: Glassonweb).

Figure 2.5: In the middle, two unitised systems are presented in the figure above. The individual curtain wall units are constructed in the factory and then transferred on-site where they are attached to the floor slabs of every building level. To the left, the system glazing is structurally bonded on the aluminium profile in the controlled factory conditions. To the right, the glass panes are toggled on prefabricated frame profiles (Source: Glassonweb).

Figure 2.6: Below, a representative semi-unitsed curtain wall system is depicted above. Both the opening and fixed windows have the same external and internal appearances (Source:Source: Glassonweb).

Frameless Curtain Walls

The pursuit of frameless curtain wall systems is ever-growing due to ever increasing desire for transparent designs allowing for more natural light to enter the building. As already mentioned, the higher transparency of buildings has been achieved through the implementation of mainly adhesive connections with the structural silicone being the most common one (Overend et al., 2011). Since the absence of transoms and mullions contributes to the creation of more aesthetically pleasing architectural designs, the field of frameless curtain walls has been vastly developed over the past years allowing also the realisation of units of larger dimensions (Figures 2.7 & 2.8).

Figure 2.7: Though frameless curtain walls the open character of structures can be enhanced. Above the Markthal in Rotterdam, the Netherlands is presented, consisting of a single-glazed cable net façade, the largest of its kind in Europe. The suspended net from which the glass panes hang is constructed of steel prestressed cables. The cable net façade has been designed with sufficient flexibility to safely undergo heavy storms (Source: Patrick van Dijk).

Figure 2.8: The figure above provides an external view of the 12.0 m-height glass cylinder of the Apple Store located in Shanghai, forming the entry to the store placed underground. The cylindrical structure is composed of 62 glass panels, 2.5 m wide and 12.5 m tall. The panels are 6-layers thick and are formed from tempered, ultra-clear, bubble-, strain- and scratch-free glazing (Source: Sivagnanasundram, 2011).

Structural Glazing

A specific type of glazed curtain walls is the structural glazing systems. These systems consist of glazing panes that are either anchored or bonded to the supporting structure with any caps or pressure plate of continuous gasketed aluminium. The glass in these cases can be laminated, monolithic, double-glazing, or insulating triple-glazing (IGUs). The supporting structure might be a glass mullion, or a combination of aluminium mullions and transoms, stainless steel rod, steel blade or cable. Furthermore, for the exterior and the interior sides extruded EPDM or silicone gaskets may be applied or, alternatively, wet sealed silicone (Haber, 2021).

A wide range of structural glazing systems is available on the market. The most frequent ones are listed below (Kekan, 2022):

- Stick system
- Unitised system
- Frameless glazing system
- Two-sided framed glazing
- Four-sided framed glazing
- Fin supported glazing
- Tension system

A structural glazing system widely applied is the “fin supported glazing”. In this type of façade fins, in other words vertical glass sheets, are installed perpendicular to the exposed surface of the building. These glass

sheets are used as reinforcement of the glazed façade. Special silicone sealant as well as fasteners are typically applied in order to secure vins to the rest of the structure (Kekan, 2022).

Moreover, tension systems provide also interesting applications of the structural glazing. In tension systems the façade stresses are imposed on the main load-bearing structure through stainless steel rods or high-tensile cables. In this way, the visible structural elements are considerably reduced. Consequently, the façade transparency is further increased, offering unobstructed outdoor views.

Basic Components

An overview of the curtain wall main components is presented in the following section. Although the readers are expected to have prior knowledge in the field of the exterior envelopes and the curtain walls in particular, a brief description of the principal elements is considered useful. Additional information regarding the curtain wall basic component is provided in Annex I "Insight on the Curtain Wall and its Components". This section of the document is expected to provide complementary information regarded as essential for the readers less familiarised with topics of the exterior envelope.

Frame

A set of both vertical and horizontal profiles and configurations, typically made of aluminium or steel, compose the framing of the façade units as depicted in Figure 2.9. In principle, apart from serving the building aesthetics, the frame material needs to fulfil certain structural demands, namely to support the glazing weight and also withstand wind forces.

The horizontal profiles of a framing unit are widely known as "transoms" whereas the vertical and typically longest ones are referred to as "mullions". Between the two profiles, mullions are the ones receiving the highest stresses since they extend throughout the entire storey height. Transoms are responsible for absorbing some of the wind load received by the glazing and later for unloading to the mullions along with part of the dead loads. The main functionality of mullions, on the other hand, consists of supporting the glazing pane and the unit dead load and of increasing the stiffness of the curtain wall configuration as a whole.

This essential component of the façade configuration, the framing, is responsible for the wind resistance of the exterior envelope, since it absorbs the wind pressure received by the rest of the façade components, for example the glazing pane. For this reason, one of the main characteristics of the façade framing is that it needs to withstand the bending stress. Additionally, it has to adequately collaborate with the fastening system since through that the horizontal forces are transferred from the frame to the structural system. In order for this to be achieved, as it will be later explained in more detail, the fastening system itself needs to be verified for its ability to efficiently maintain and enhance the load path starting from the façade configuration, continuing to the main load-bearing system and eventually the foundations of the structure.

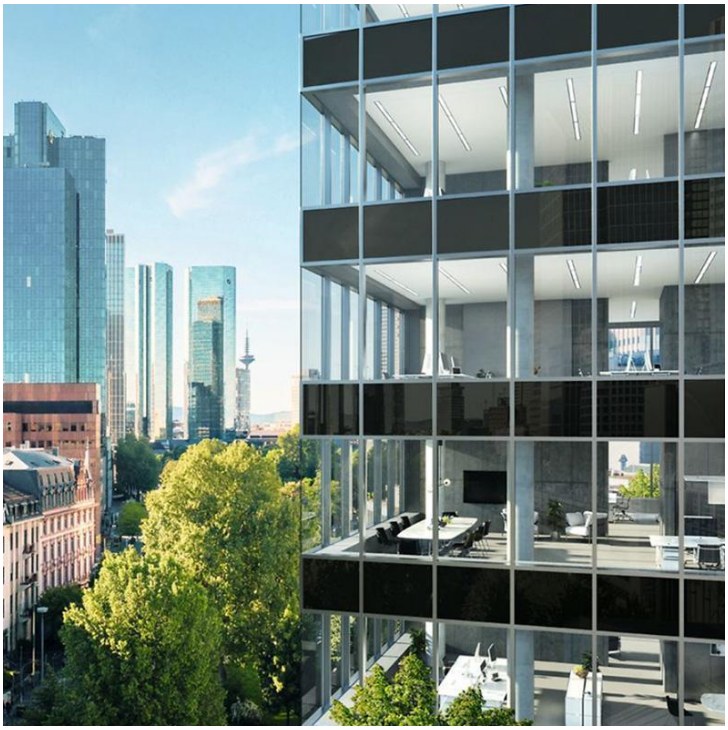

Figure 2.9: A typical curtain wall façade is depicted above. The darker panels are commonly referred to as spandrels. As for the vertical framing elements, they are called mullions and the horizontal ones are transoms (Source: Bespoke Glazing Design).

Glazing

Among the elements of a curtain wall configuration, the glazing is this considered of greater importance not only due to its determinant role in various aspects related to the façade multi-performance, such as the daylight intrusion, glare, thermal insulation, sound proofing etc., but also due to its increased fragility which underlines the need for an integral and safe curtain wall design.

Various glazing typologies are currently available on the market fulfilling the different performance criteria of an exterior envelope. For an elaborate presentation of the properties and applications of various glazing types widely used in the building sector, please refer to Annex I.

Glass-frame Connection

Another important differentiation of the curtain wall systems is related to the connection of the glaze pane to the surrounding frame. The connection traditionally encountered in curtain wall systems is the so-called mechanical consisting of glazing infill panels mounted on a metallic frame. Over the past years though, the ever-increasing desire for more transparency of the buildings resulted in the advance of another type of connection, the adhesive ones.

The majority of the information following in this section is dedicated to adhesive connections, and more specifically to the structural silicone which is commonly used over the past years. Prior to the introduction

of this widespread structurally sealed connection though, a short introduction of the more conservative mechanical connection, which is mainly realised through gaskets, will be presented. This concise presentation of the material, its properties and main functions is also considered useful for the better understanding of the modelling approach followed during this study. It finally provides the ground for the comparison that will later follow between the aforementioned mechanical connection, also characterised as "dry" with the structurally sealed one.

Mechanical Connections

Gasket joints are typical mechanical connections mostly seen in structural assemblies. They consist of various materials, with the most common ones being rubber, steel and different composites. The purpose of the gaskets is to facilitate the force transfer between adjacent components while sealing the intermediate void. These thin materials mostly work under compression, which partially explains their non-linear behaviour.

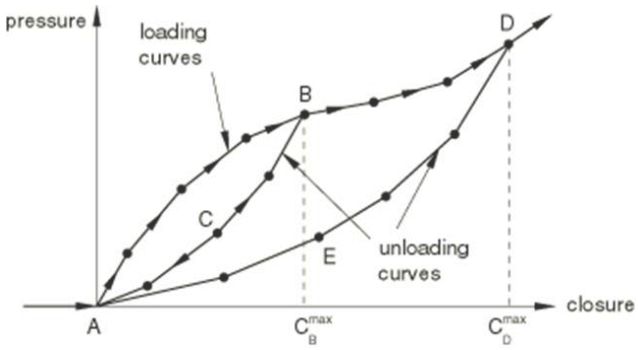

Figure 2.10: The elastic model of a gasket with damage is depicted above. The loading curve illustrates the path that the pressure, alternatively the force, or even the force divided per unit length, follows while the gasket undergoes compression. The upward and downward arrows of the figure represent the loading and unloading paths respectively (Source: Abaqus Analysis User's Guide).

The complex unloading behaviour of a gasket as seen in Figure 2.10 is one of their characteristic properties. Its deformation under the different loading conditions is mostly confined through the thickness. The remaining two directions are typically neglected since both the in-plane stiffness and that of the transverse shear are considerably smaller. The gasket deformation in most of the cases is defined through its closure, a term used to describe the relative displacement of the upper and bottom surfaces of the gasket material (ANSYS, Inc., 2017).

The traditional mechanical connection, realised by dry gaskets, is known as "pressure plate". This pressure plate is typically compressed against the glazing pane and the inner framing profile and then covered by additional mullion covers. In this way the glazing is fixed and tightened against the curtain wall framing. Due to the increased risk of leakages especially in the corner areas or connections of the dry gaskets, the four-sided gaskets solution is applied. In this glazing method, the glazing as well as the infill panels are typically placed from the outside, therefore a scaffolding is usually needed, increasing the installation costs.

An alternative to the previous mechanical connection option is this of the “interior dry glazing”, where both the infill panels and the glazing can be installed to the building from the inside. There dry gaskets are placed from the exterior and although the frame is generally fixed, on the upper interior mullion there is a removable stop element. A quite detailed manipulation is needed in order for the glazing to sill into the glazing pocket. For this type of glazing method, attention should be paid to the ensuring of the water and air-tightness on connection of the removable stop with the rest of the framing. The installation of the spandrels might be only possible from the outside (Vigener & A. Brown, 2016).

Adhesive Connections

As previously mentioned, due to the ever-increasing desire for large glazing areas in buildings, a wide range of adhesive connections has been developed. Although the option of bolted connections in the structural glazing configurations traditionally prevails, the adhesive bonding gradually gains more popularity. The adhesive bonding, contrary to the typical bolted connections that diminish the glazing strength in the locality of the bolt holes, has been proved to ensure efficient cooperation between the supporting element and the glazing by providing a uniform load transfer between the two (Nhamoinesu & Overend, 2012).

A large variety of adhesive products is provided by the current market, covering from glass to steel connections, with the silicone structural sealants being the one mostly applied (Overend et al., 2011). In the structurally sealed joints, high-performing silicone sealant is used instead of gaskets or other mechanical attachments ensuring the flexibility of several structural connections; among others, the bonding of two glass pieces or the attachment of glazing and various panel materials to the metal frame of the curtain wall systems (DOW, 2021, Nhamoinesu & Overend, 2012). These types of connections are extensively documented by various publications, codes and standards (ASTM C1401, 2022, Overend et al., 2011 and AAMA CW-13, 1985). Below the beneficiary attributes and later considerations regarding the implementation of adhesive connections follow.

Beneficial Attributes

When compared to mechanical, structurally bonded connections are proven to contribute to the acoustic, thermal as well as blast performance of the building elevation. Moreover, structural silicone systems, also known as wet systems, by facilitating concentrated support to the glazing, lead to the release of the peak stresses of the latter. Additionally, wet systems provide architectural freedom by allowing the continuity of the glass surfaces around the building envelope (Alcaine et al., 2020).

Based on ASTM (ASTM C1401-14, 2022), when compared to the conventional dry-glazed configurations, structural silicone connections contribute to the elimination of the thermal bridging by the minimisation of the exposed glazing, to the reduction of the cold bridges -namely of the thermal breakage typically occurring on the exposed glazing edges-, to the weather-tightness, the design flexibility and the advanced option for economical glazed applications (Memari et al., 2012).

The main beneficiary attribute of the structurally sealed connections is their flexibility. Additionally, they are characterised by low strength and a thickness typically larger than 6.0 mm, which defines them as thick when compared to the alternative joints (Overend et al., 2011). They are expected to perform better under seismic loading due to the advanced flexibility provided to the attachment of the glazing to the framing by the structural sealant. The previous is substantiated through the attachment of the entire or part of the glazing

to the frame, that minimises the possibility of the glass cracking or breakage due to the interaction of the frame glazing pockets and the glass edges occuring by the racking movements during seismic events (ASTM C1401, 2022). For a typical design of a structural silicone joint, please refer to Figure 2.11.

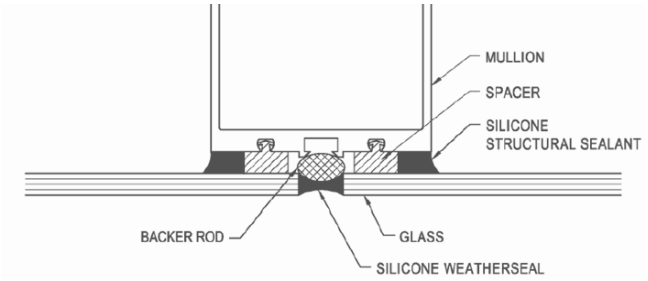

Figure 2.11: Typical structural joint design (Source: DOW, 2021).

In addition, the flexibility of the structurally sealed joints makes them suitable for the differential movement accommodation occurring between the metallic frame and the glazing due to thermal differences. However, the typically low tensile strengths measured for dynamic loading ranging between 0.8 and 1.8 MPa, indicate the structural silicone joints to be inappropriate for the transferring of the higher shear occurring longitudinal that is needed for the composite action in the common steel-glass façade systems (Mocibob, 2008, Nhamoinesu & Overend, 2012). Nevertheless, both the thermal effects as well as the dead loads that the structural silicone has to withstand especially when setting blocks are not incorporated in the structurally sealed configuration are regarded as secondary loads acting on the structural silicone (ASTM C1401, 2022, Iker & Wolf, 1992).

Considerations

Based on the investigation of high strength thermosetting adhesives, stiffer adhesive, typically acrylated and epoxies, can also be used for the glaze-to-metal connection (Overend et al., 2011, Veer et al., 2008). Unfortunately, scarce information is available verifying the use of those adhesives in structural applications mainly due to the absence of reliable models that would accurately indicate both their mechanical behaviour, both in the short- as well as the longer-term (Nhamoinesu & Overend, 2012).

In addition to the considerable advantages of the structural silicone several references as well as the industry itself have raised concerns regarding several aspects of the aforementioned application (Parise & Spindler, 1991, Schmidt et al., 1989, Schwartz et al., 1996, Memari et al., 2012). The unconfirmed material durability on the long-term, the replacement need of the weathered sealant connections, the potential structural sealant incompatibility with various contact materials, such as setting blocks, gaskets, metal finishes, sealants of the insulating glazing units, coatings and paintings, possible defective application of the material and finally the increased reliance of the frame-to-glaze connection on the structurally sealed attachment which can results in decreased redundancy of the structurally sealed systems compared to the mechanical ones are the most important among the recognisable considerations.

Since one of the objectives of the current study is the impact assessment of the mechanically captured connections (dry) on one hand and the wet silicone solutions on the other hand on the curtain wall performance, a detailed presentation of the structurally sealed joints, their properties, typologies, applications and advantages over conventional solutions follows.

Structural Silicone in Curtain Walls

Since the reader is expected to be familiar with main structural joint parameters, such as structural bite and thickness, and their function, their elaboration is omitted from this section. However, a brief presentation of the above is provided as a reference in the Annex I of this study.

Currently, the structural silicone sealants whose application is acceptable by the industry are on- or two-part specially formulated silicone sealants. The sealant joints used for the frame-to-panel connections are widely known as “structural seals” whereas the ones located between neighbouring panels as “weather seals” (Memari et al., 2012).

Over the years both the scientific and the industry field have posed a request for an effective behaviour prediction of various glazing attachment approaches with a specific interest on their response under in-plane racking loading (Broker et al., 2012). Highly insightful test data as well as prediction approaches have already compiled enclosing on one hand two- and four-sided SSG (structural sealant glazing) designs and, on the other hand, stick and unitised façade systems. Although the classification of glazed facade into stick and unitised systems is valid for both dry and wet systems, in this study the attention is focused on the wet configurations.

Four vs Two-sided

One of the most common distinctions between the curtain walls where structural silicone is applied is the number of the glass edges attached through structural sealant to the framing. The two types widely applied are the two- and four-sided structural silicone glazed systems (SSG) which are displayed in Figures 2.12 and 2.13 and are presented in the following section.

For the case of the two-sided SSG type, two edges of the glass panes (either horizontal or vertical, with the vertical ones being the most common case) are attached to the mullions with structural silicone sealants. As for the other glass pane edges, they are captured in the aluminium pockets of the framing system, usually through gaskets, following the dry-glazed system applications (DOW, 2021, Memari et al., 2012). On the contrary, in the four-sided SSG curtain wall systems that are also widely applied on the market, all the edges of the glass pane are attached through a structural sealant to the glazing frame. In this case, the out-of-plane loads, such as wind, are transferred from the glazing to the frame exclusively through the silicone. Consequently, the modulus and the strength properties of the silicone as well as ensuring the sufficient adhesion between the structural sealant and both the aluminium and the glass surfaces are design aspects of vital importance (Memari, Fisher, et al., 2012).

Although the two-sided structural glazing can be fabricated both on-site and, in a factory, for the four-sided case the factory (in-shop) option is generally recommended (DOW, 2021). As far as the waterproofing design of those structurally sealed systems, for the case of the two-sided SSG weather seal is typically included in the joints connecting adjacent glass panels through their vertical edges. For the application of the four-sided SSG on the other hand, weather seals are placed in all the vertical and horizontal joints connecting adjacent panels (Memari et al., 2012).

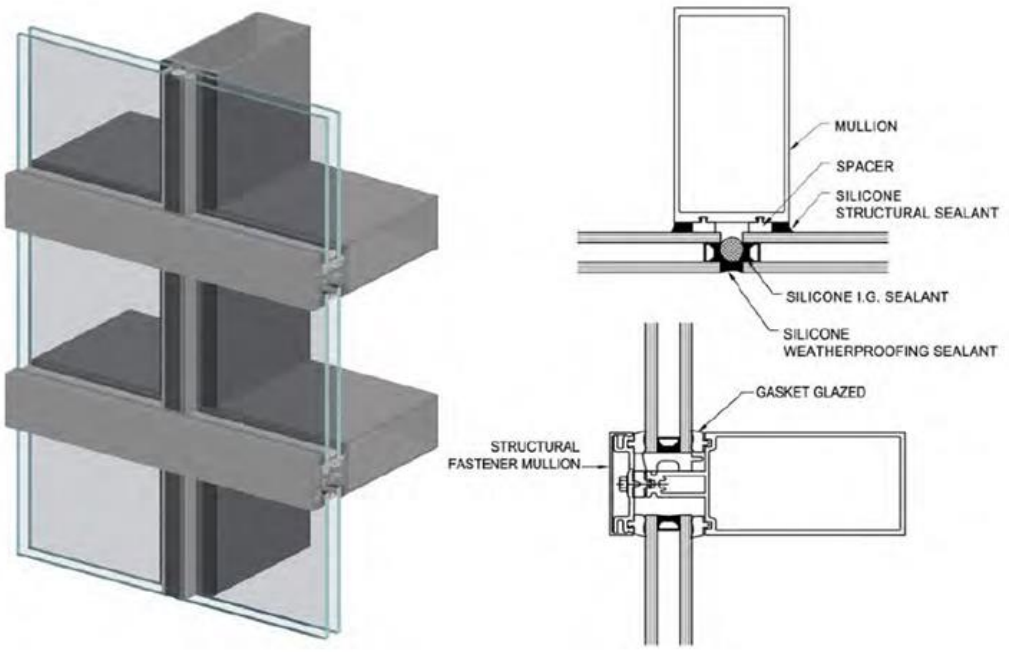

Figure 2.12: Two-sided structural glazing application. In this particular case, the horizontal edges of the glass panes are attached to the mullions mechanically whereas the vertical ones through structural silicone. To the right the structural glazing horizontal (top) and the vertical (bottom) details are seen (Source: DOW, 2021).

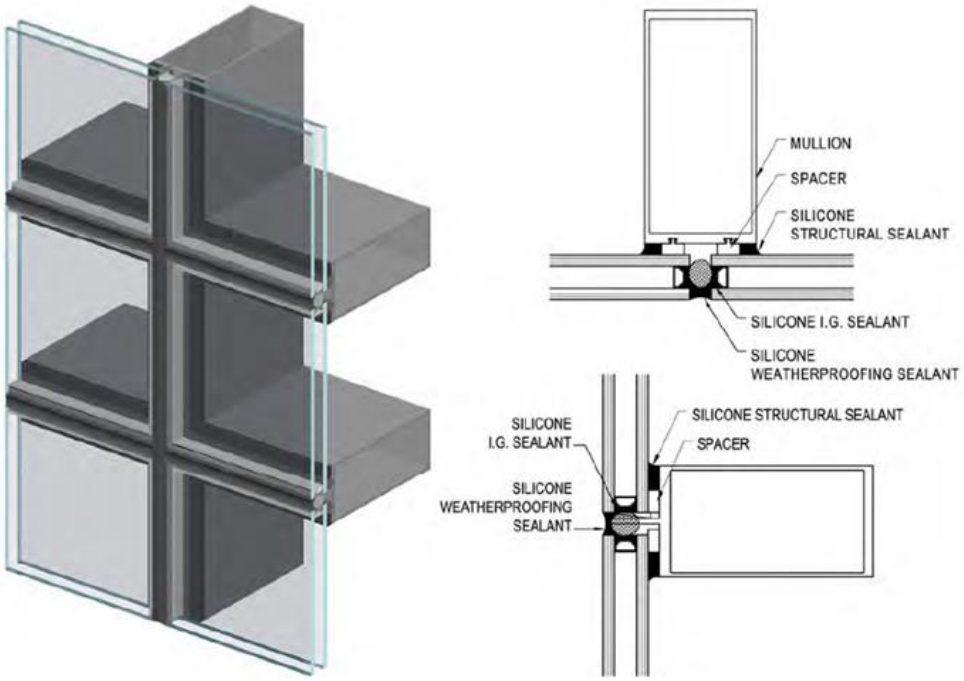

Figure 2.13: Four-sided structural glazing application. To the right the horizontal (top) and the vertical (bottom) details /section are presented (Source: DOW, 2021).

The comparison of four-sided structural silicone systems to two-sided as well as dry-glazed systems forms a topic that has received much scientific attention. One of the first references dates back in 1995 and belongs to EERI (Norton et al., 1994) stating that the glazed configurations to which silicone sealant is incorporated at least in one of their edges, usually perform better compared to the equivalent dry glazing ones (Figure 2.14). Additionally, it has been evidenced (Memari, Chen, et al., 2006) that both the drift as well as serviceability capacities of two-sided SSG configurations, employing structural silicone for the attachment of the two sides of the glazing and mechanical gaskets for the opposite edges, are considerably higher compared to those of equivalent dry-glazed systems.

Other researchers, such as Meimari et al. (Memari, Chen, et al., 2006, Memari et al., 2012) focused on the serviceability performance of structurally sealed systems. They proved through air-leakage tests that air is leaking in both dry-glazed and two-sided SSG systems even for the cases where no sealant damage is visible. It was further noticed that this leakage is further increased due to racking conditions. On the contrary, no air-leakage rates were measured for the four-sided SSG systems tested during those studies as it can be seen in Figure 2.15. The findings of those studies provide the ground for the argumentation that continuous sealant systems, as opposed to discontinuous ones with gasket/sealant transitions or completely dry ones, maintain higher serviceability performance when subjected to seismic racking conditions. Although the statement above is not efficiently proven by a wide range of publications and research findings, there are a few studies (Zarghamee, 1996, Memari et al., 2012) that justify that. Especially Memari et al. (Memari et al., 2012) prove that a four-sided stick-built configuration provides an overall better seismic performance compared to two-sided or dry systems.

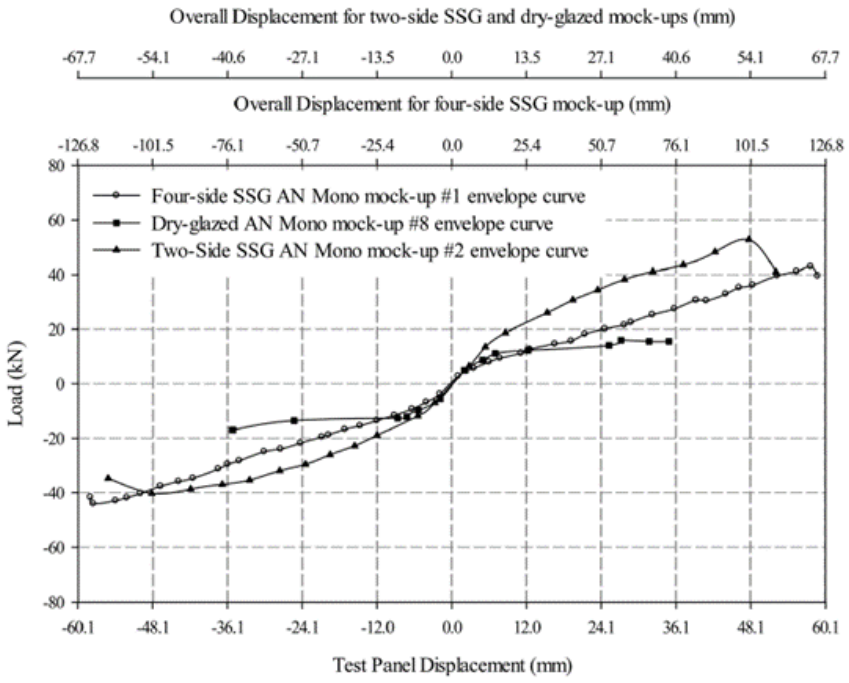

*Figure 2.14: Comparison of the load-displacement correlation of typical four-, two-sided SSG and dry-glazed curtain wall systems. The mock-up configurations tested during this study were stick-built systems and consisted of nine glass panes, with the central panel being the largest one. The dimensions of the central element, which was utilised as a test panel, were 1.83 m high * 1.52 m wide. The drift values measured in the central panel are presented in the displacement scale at the bottom horizontal axis. The actual drift experienced by the complete mock-ups is presented at the top of the graph, in its appropriate scale (Source: Memari et al., 2012).*

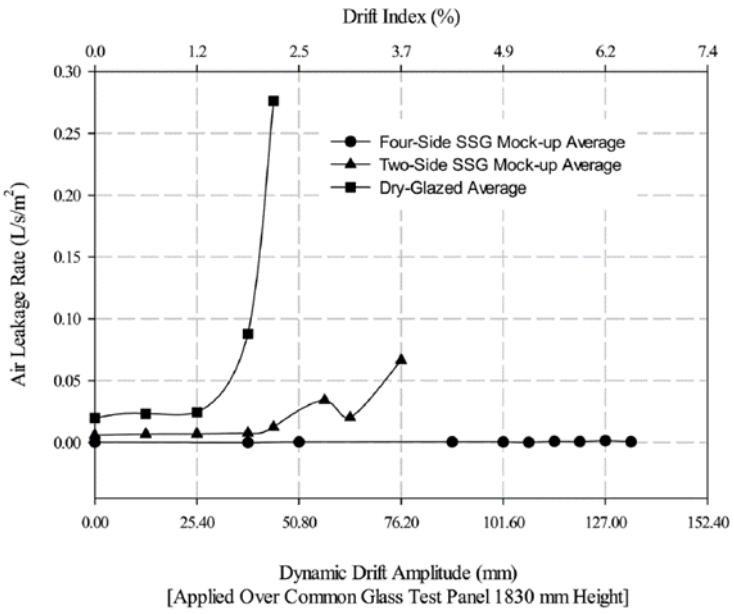

Figure 2.15: The correlation of the dynamic drift ratio and the air-leakage rates measured on the gasket seal and the silicone sealant for the dry and the wet mock-up configurations are presented respectively (Source Memari et al., 2012).

While undergoing inter-storey drift, the glazed structurally sealed systems have been noticed to respond in a particular manner. In fact, the framing typically deforms whereas the glazing pane rotates aiming to adjust to the previous deformation. Both large glazing movements as well as frame deformations can potentially result in multiple failure conditions, namely the glass cracking, breakage or fallout or in the failure, either cohesive or adhesive, of the structural silicone weather seal or bead (Memari et al., 2012).

Although the seismic performance of two-sided SSG façade systems has been examined through a few studies (Memari, Chen, et al., 2006, Behr, 1998), less research has been developed over the four-sided configurations. In fact, this is limited to an older investigation dating back from the 1990s (Zarghamee, 1996) and a few more recent ones (Broker et al., 2012, Memari, Fisher, et al., 2012, Memari et al., 2021). Lately, the industry research over the identification of the four-sided SSG glazed curtain walls' response under seismic racking loading has been increased. The reason for the latter originates from the fact various seismic codes standards, such as the International Building Code (IBC, 2018) or the California Building Standard Code do not explicitly accept the application of four-sided SSG systems in areas of high seismic intensity, mainly for facilities serving healthcare purposes. Consequently. The response of the four-sided systems under seismic action is still a research field in need of more elaboration. In practice, the performance of those systems is expected to be better understood through the realisation of extended laboratory research. The case study examined during this graduation topic forms a representative example of relevant research.

Stick vs Unitised Systems

As already mentioned, over the past years, SSG sealants have been integrated in the curtain wall systems intending to transfer apart from various loads such as wind, thermal or even seismic ones, also deformations from the glazing units to the curtain wall framing (Memari, Fisher, et al., 2012). Structural silicone systems are in principle constructed in controlled environments and hardly ever on site, in an attempt of achieving the proper adhesion of the system by closely monitoring and controlling various external factors such as temperature, relative humidity and dust (Alcaine et al., 2020). It is most frequently seen that the glazed unitised systems are structurally sealed especially when four-sided structural sealing is required. On the contrary, the two-sided configurations are accepted to be installed on the field (Vigener & A. Brown, 2016).

While taking into consideration the seismic design and the overall performance of the façade element, the unitised is frequently chosen over the stick façade system. The reason behind is that the silicone sealant remains adhered to the unitised system, thus can effectively absorb the various stresses caused by dynamic loadings such as wind or the building movements in general. Consequently, in the field of adhesive connections, the unitised compared to the stick system contributes to the minimisation of the racking shear stresses applied to the sealants while maintaining them in the acceptable shear capacity (Memari, Fisher, et al., 2012).

Recent experimental testing (Memari et al., 2012, Memari, Fisher, et al., 2012) comparing the racking evaluation of four- and two-sided SSG curtain wall systems has provided enlightening insight on their seismic performance, mainly on that of the stick systems where normally larger strains are transferred to the structural sealant. The explanation of the latter is justified in the previous paragraph and is enhanced by the fact that in most of the stick system cases, the glazed framing is not constrained per each storey, but it continues over multiple stories. For that reason, the stick-built glazing panel is typically racked under the inter-storey drift, which leads to the transfer of considerable strains to the structural sealants. The unitised systems, on the other hand, are typically discontinuous and structurally interrupted per storey. The above is achieved via the prefabrication of the panels, that are later on placed adjacent to each other with stack joints placed between them. By attaching the glazing panels with stack joints (Figure 2.16), the sliding between the separate units is facilitated, therefore, lower stresses appear in the structural sealant itself (Memari, Fisher, et al., 2012).

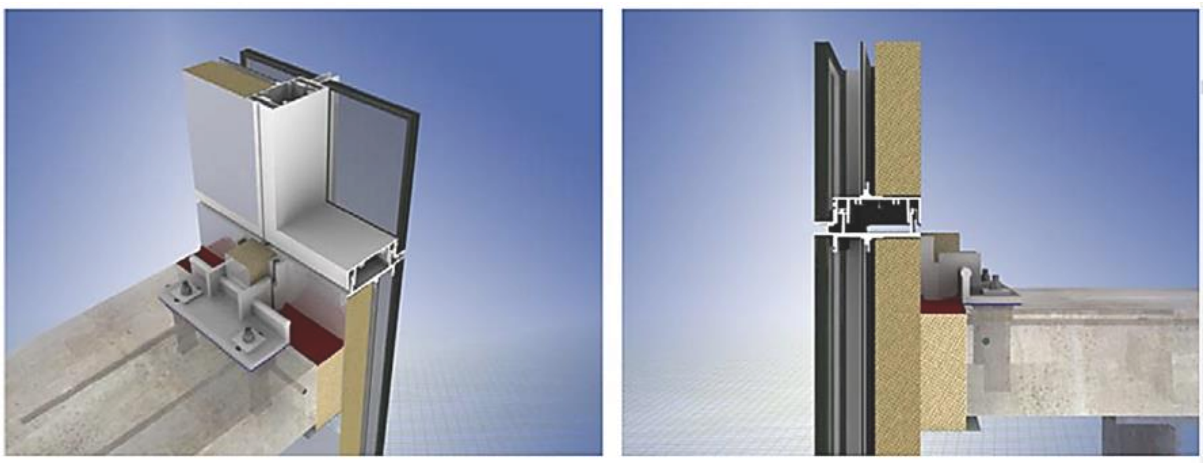

Figure 2.16: Typical stack joints and anchoring system for a unitised four-sided SSG configuration. The stack joints are placed at the top of each floor slab accommodating both vertical deflection and lateral movement. In the renderings above the curtain wall system is presented to be attached to the floor slab above the pair of the

primary mullions through a set of hook plates, a pair at each panel, that are vertically attached to the stack mullions placed below the stack joint of the horizontal direction (Source: Memari, Fisher, et al., 2012).

It is frequently seen that in preliminary considerations and evaluations of a curtain wall design, the most critical case is examined, that is the case where the unitised system does not respond as expected. Instead, its behaviour tends to be similar to the racking stick-built systems undergoing in-plane storey drift. The objective of the examination of this critical condition is to evaluate the reaction of the sealants when exposed to conditions similar to the racking of the frames (Memari, Fisher, et al., 2012).

Fastening System

The attachment of the curtain wall configuration to the load-bearing systems of a building is a topic of high importance determining mainly the safety of the building users, both those inside and outside of the building, as well as the reliability and integrity of the building design in general.

An appropriate fastening system ensures the ability of the exterior envelope to accommodate a large range of actions, not only static but also dynamic ones, by facilitating the attachment of the curtain wall systems to the slab floors. Those attachments are practically realised through the hanging of the curtain wall system from the structural system. The vertical arrangement of the curtain wall systems in most of the cases spans continuously between adjacent floors. An alternative solution which is also seen on the market, with less frequency however, involves the attachment of the curtain wall system in the floor slab of every second floor. Representative anchorage typologies are seen in Figure 2.17.

The majority of the curtain walls are attached to edge beams, most frequently made of concrete, which highlights the need of the edge beams to withstand large deflections that could interrupt the curtain wall function. Alternatively, when the attachment of the curtain wall systems to floor slabs or edge beams should be avoided, steel strong backs are chosen. By applying the strong backs, that are typically hot-rolled sections, the curtain wall elements are able to span along perimeter structural elements, mostly columns.

In order for the safe and efficient fastening of the cladding to be achieved, numerous considerations related to aspects such as those of the load-bearing capacity and tolerance accommodation need to be taken into account. Since the fasteners hold a crucial role in the load path of a building structure, they need to be carefully designed and analysed so that their ability and strength to maintain all the loads likely to be encountered on the building site is verified. Among the wide range of loads those coupling devices forming the fastening system of a structure need to withstand are the following i. the dead load of the cladding itself, mainly formed by its self-weight, ii. the live load additionally introduced by people stepping on the walkaway frequently seen on double-skin façades and iii. forces induced by natural elements, such as thermal differentiation, snow loads concentrated on extended horizontal areas, maintenance loads, seismic loads and positive or negative wind loads created by the wind pressure acting on the façade configuration (Vigener & A. Brown, 2016).

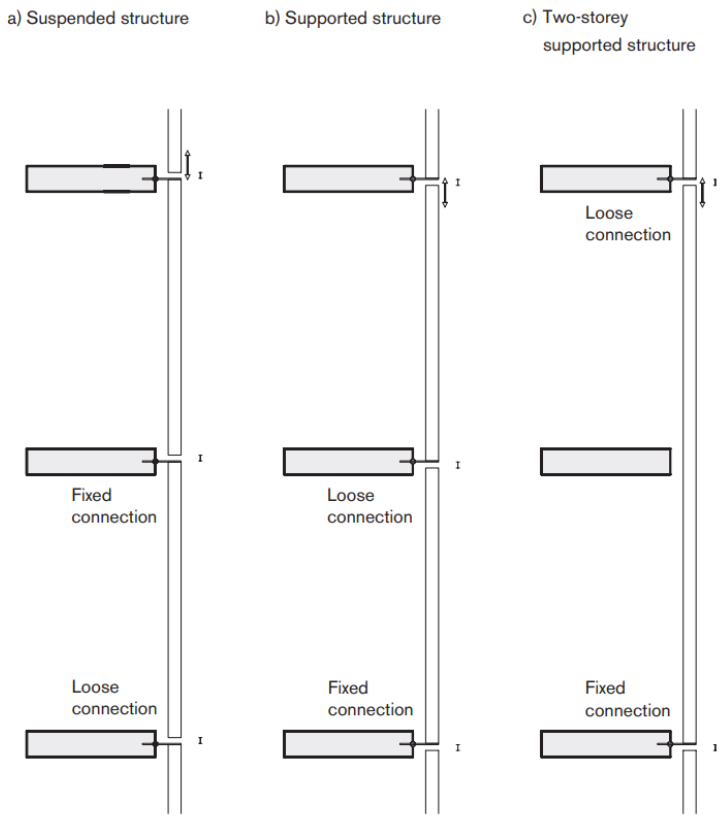

Figure 2.17: The drawing above presents different types of anchorage of a curtain wall system to the load bearing structure of a building. The type of connection defines the load transfer. To the left, the option of a suspended curtain wall is presented, followed by a single-storey configuration in the middle of the figure. Finally, a two-storey curtain wall system is depicted to the right (Source: Knaack et al., 2014).

Additionally, the fastening system in principle must absorb forces created from the interior of the building (indirect effect), such as movements of the primary structural system due to dead and live loads, column shortening or seismic and wind drift (Bârnaure & Voiculescu, 2013). Consequently, it becomes evident that the fastening system needs to provide adequate hardness, tensile and yield strength in order to successfully undertake all the loads acting on the cladding while simultaneously ensuring both its weather-tightness and its integrity.

The second, equally important, function of the fastening system is to provide sufficient tolerance, both in the vertical and the horizontal sense. By ensuring the adequate tolerances, the fastening system ensures that the cladding is able to undertake all the possible movements created either during the installation phase or throughout the building life-cycle. The tolerances are in most of the cases provided by brackets, which usually are composed of steel or aluminium. Brackets themselves are divided into two main categories, the ones used for the coupling of the cladding to the structural system of the building, either concrete or steel slab or other structural elements like beams, and the ones facilitating the fixing of various façade components, such as the glazing vertical supports.

Chapter 3

Glazed Curtain Walls & Seismic Events

Earthquake events, even the ones with moderate intensities, can lead to the damage of both the main structural elements as well as to the non-structural components of buildings such as curtain walls. Although the main concern of the seismic design is the prevention of structural damage, damages occurring to non-structural elements can result in significantly larger financial impact when compared to that of structural impairment. In addition to the increased repair costs, the failure of non-structural elements in many times jeopardises the occupants' safe evacuation normally following an earthquake event and potentially endangers the safety of the pedestrians.

Over the years it has been concluded that the seismic performance of glazed façade units is directly linked to the seismic response of a building. More specifically, the dependency of the latter on the mass distribution and stiffness not only of the building's structural system but also of the non-structural elements has been underlined (Aiello et al., 2018). For this reason, a general introduction to both the critical features acting on the external envelope and to the subsequent response of the latter is essential before diving into the main topic of interest of the present study, the correlation of the curtain wall response under seismic events and the possible failure mechanisms.

Initially, the introduction of the most critical loads typically acting on building structures, namely the wind- and earthquake-actions, is presented. Later, the building response to them is described, followed by the fundamental principles of the building design. Thereafter, the emphasis is transferred to the curtain wall systems specifically, starting from the presentation of the basic loading types acting on them and gradually moving to the exposition of the most common failure mechanisms caused by seismic events. The combination of the two, the over building behaviour followed by this specifically of the curtain walls, is expected to provide sufficient background for the better understanding of the glazed curtain wall failure mechanisms and their seismic design.

Thereafter, a brief review of representative seismic standards and national regulations follows, introducing the main requirements set by contemporary seismic design and substantiating the testing sequences later presented during the current study. The similarities and differences between the analysed national standards will finally be presented aiming for an integrated explanation of the seismic building design as defined from various regions and countries with different building technologies, traditions and expertise.

External Envelope Critical Actions & Response

Among the various failure mechanisms of structures, lateral deflection is a widely known one associated either with ultimate or serviceability limit states. When referring to a larger context, such as the one of a structure, lateral deflection is not limited solely to the examination of the structural elements individually. It goes beyond that and is then called "drift".

In building structures, lateral deflections originate in most of the cases from dynamic forces, mainly seismic and wind ones. For structures located in a seismic zone, both earthquake-induced and wind drift are generally suggested to be calculated. Among the two drifts, the most critical one governs and defines the design of the exterior enclosure. Since the interest of this study mostly focuses on the seismic action and on the seismically induced response of glazed curtain walls, in the rest of the study more attention will be paid to the seismic rather than the wind aspect. However, it is important to mention that the identification of the enclosure storey drift design as presented in the following section is similar for both the wind and seismic drift.

As already mentioned, the response of a structure while undergoing a certain action depends on the nature and intensity of the structure itself. In the case of wind pressure, the reaction of the curtain wall system

typically involves the inward movement of the top transom on the windward building side, and the outward movement for the leeward building side. In general, as the building attempts to “lean” along with the wind, the top transom experiences lateral in-plane displacement (Brenden, 2006).

In the case of the seismic actions, similar movements take place with regards to the ground motion direction. The seismic-induced behaviours of a building and a curtain wall specifically, includes the creation of “seismic drift”. A generic definition of the term would refer to the differential movement of consecutive floors. However, for the better understanding of the notion of the seismic stor(e)y or the inter-stor(e)y drift, the concepts of the storey displacement and drift first needs to be identified.

Inter-storey Displacement & Drift

The storey displacement describes the deflection noticed in a single building storey relatively to the ground level of the structure. Consequently, while moving to higher levels of a structure, the total displacement is expected to increase.

(Inter-) storey drift, or racking, on the other hand, is the deflection of solely one floor relative to that of the previous. Therefore, the storey-drift calculation of level n of a building can be identified through the subtraction of the storey displacement of level n minus the storey displacement of level n-1 (Al-sheikh, 2019). Thus, in order for the storey drift to be calculated, the storey displacements need to be obtained from the building structural analysis. The storey drift can also be expressed as the ratio of the storey drift value to the building storey height. Inter-storey displacement and drift are represented in Figure 3.1.

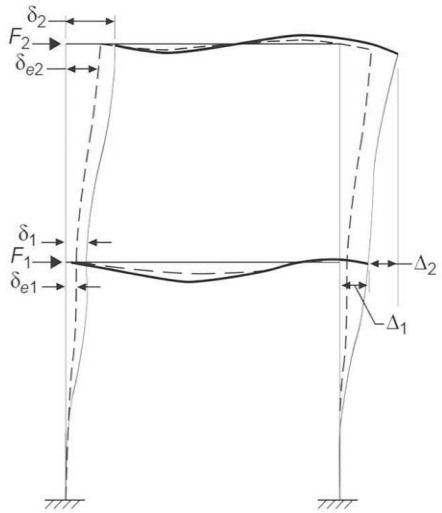

$\underline{Storey\ level\ 1}$

$F_1 = Strength - level\ design\ seismic\ force$

$\delta_{e1} = Elastic\ displacement\ calculated\ for\ strength - level\ design\ seismic\ forces$

$\delta_1 = C_d * \delta_{e1} / I,\ amplified\ displacement$

$\Delta_1 = \delta_1 \leq \Delta_a\ (Table\ 12.12-1, ASCE\ 7-16)$

$\underline{Storey\ level\ 2}$

$F_2 = Strength - level\ design\ seismic\ force$

$\delta_{e2} = Elastic\ displacement\ calculated\ for\ strength - level\ design\ seismic\ forces$

$\delta_2 = C_d * \delta_{e2} / I,\ amplified\ displacement$

$\Delta_2 = \delta_2 - \delta_1 \leq \Delta_a\ (Table\ 12.12-1, ASCE\ 7-16)$

Figure 3.1: Determination of the storey-drift of a typical structure (Source: ASCE 7-16).

Seismic & Wind Allowable Drift Values

Regarding the thresholds of the allowable inter-storey drift, these are specifically defined by various seismic regulations and standards. An elaborate presentation of four typical seismic regulations and their requirements is included in the "Seismic Codes & Regulations" section of the present study. The inter-storey drifts are always related to the building storey height, represented as either "H" or "h", and are typically expressed as percentages or ratios.

Generally, less strict limits are applied on wind-driven drifts not only compared to those corresponding to various damage states, such as glass cracking or fallout and damages in the structural- and weather sealants, but also to the seismic-induced drifts (Memari et al., 2012). The above is substantiated by comparing the value of the wind load drift limit with the equivalent seismic one. Although the allowable drift limit for wind is not specifically stated by most of the norms and regulations, general practices like this stated by ASCE 7, in Appendix CC, define a common wind drift value of H/400 and a wider acceptable drift range between H/200 and H/600 (Al-sheikh, 2019). In order for the comparison of the wind and allowable seismic drift values to be achieved, the requirements indicated by the Japanese regulation are utilised since they are the ones mostly used during the current study. In that sense, the maximum allowable seismic drift of H/100 is four times larger than this of wind (H/400).

Prior to the detailed elaboration of the curtain walls' response to critical external actions, mainly wind and earthquake, and of their most frequent failure mechanisms, an introduction to the basic aspects of the seismic design of buildings is presented. The brief explanation of the principles and of the main requirements of the seismic design applied to typical structures is expected to facilitate the better understanding of the curtain walls' behaviour which, consequently, defines their design.

Building Seismic Design

Since seismic events induce inertia forces to the building structure, and inertia is known to be affected by mass, aspects such as the building mass and stiffness define the building design considerably. It would be ideal if building structures could sustain earthquake events while remaining in the elastic phase. In this way, the building structures would survive even higher seismic intensities without experiencing any damage. Unfortunately, the cost of such structures would be unviable. For this reason, building structures are designed to undergo a certain level of damage, dissipating in this way the energy induced during seismic events. Consequently, the design of building structures against earthquakes is seismic-resistant, rather than seismic-proof (Murty et al., 2012) (Figure 3.2). Only buildings of special importance, like nuclear power plants, deviate from the previous, since these structures are designed to remain elastic while subjected to seismic actions.

The seismic-resistant design, as considered for typical building, requires that the latter should undergo seismic actions of minor, intermediate and severe intensities. The respective requirements are described below and are also depicted in Figure 3.3.

- minor intensity, with typically frequent occurrence, without experiencing any damages to the neither the structural or the non-structural elements
- intermediate shaking, with limited damage to the non-structural and minor to the structural elements
- severe intensity, with low frequency occurrence, without collapsing, allowing only minor damages of the structural element. It is important that during those seismic events any type of human hazard is excluded and also the property of the building itself and of the adjacent ones is preserved.

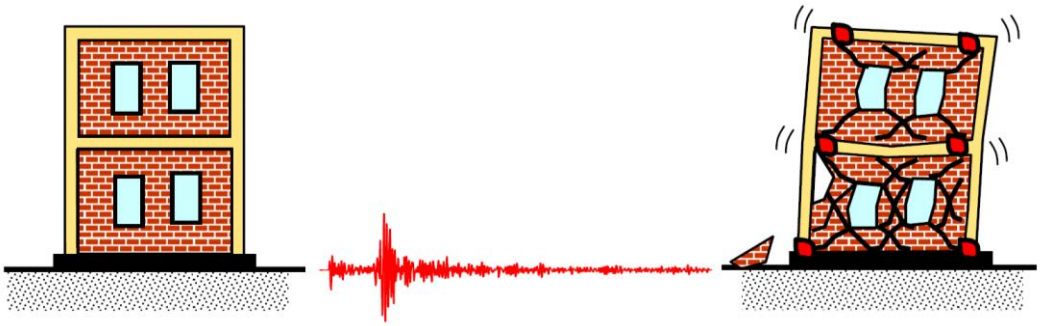

Figure 3.2: The difference between the seismic-proof and seismic-resistant design is depicted above. To the left, a representation of a seismic-proof building, remaining undamaged even after being subjected to earthquake actions, and to the left, the depiction of a damaged structure (Source: Murty et al., 2012).

Therefore, it can be easily understood that typical building structures are designed based on a fraction of the action they would undergo in case they were designed to withstand seismic events of high intensity without any damage, in other words, if they were designed to remain in their elastic phase. According to Murty et al., 2012 this fraction ranges between 8.0 % and 14.0 %. However, buildings are expected to withstand seismic actions of minor shaking without experiencing any structural damage. In order for this to be achieved, the stiffness of the building must be verified to be sufficient.

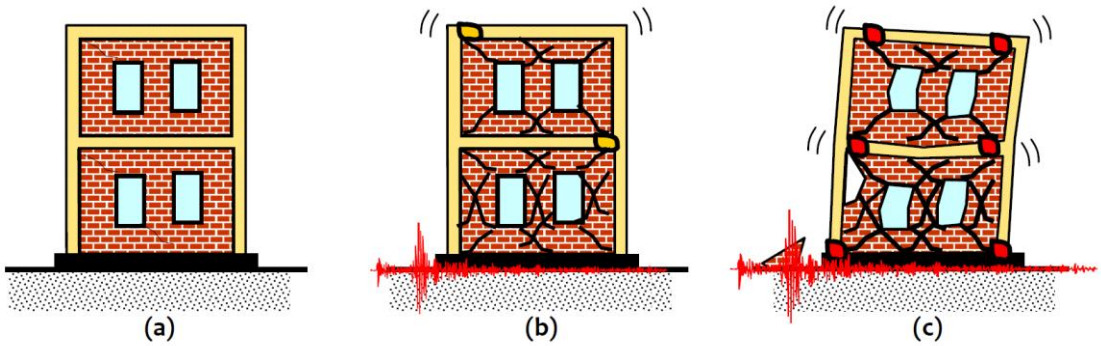

Figure 3.3: The requirements identified by the seismic-resistant building concept applied for typical building structures are depicted above for the three of the seismic intensities individually. (a) Minor seismic intensity: hardly any damage is accepted, (b) Intermediate shaking: minor damage of the structural elements and limited of the non-structural ones (c) Severe seismic intensity: minor damages of structural elements, prevention of the building collapse (Source: Murty et al., 2012).

The Case of Curtain Walls

Curtain wall systems, as typical non-structural elements, are not usually required to withstand seismic-induced accelerations, forces or displacements without collapsing. The reasoning behind that lies on the independence between the integrity of the primary structural system and that of non-structural components. To rephrase the previous, even when non-structural elements, like curtain walls fail or collapse due to the absorption of a fraction of the energy originating from the external acting on the building, the load-bearing capacity of the primary structural system is unaffected.

However, the damaging or, worse, the failure of non-load-bearing systems, like curtain walls, can endanger human safety, both for the building occupants and pedestrians (Rizzo et al., 2021, Lee et al., 2007). Additionally, a possible failure of those non-structural systems can result in another non-structural system, such as a fire-safety mechanism, to interrupt its function causing once again dangerous situations for the people affected or costly damage repairs. The reasons explained above, underline the necessity for understanding, initially, the reaction of the non-load-bearing systems in general and most specifically of curtain walls in earthquakes and for preventing, eventually, the respective damages.

In the following section, common seismically-induced damages of curtain wall systems, their division into limit states and an overview of their general impact is presented.

Load Types Acting on Curtain Walls

The critical loading type acting on a non-load-bearing system can be either a force, displacement, an acceleration or even a combination of the previous. Depending on various parameters, such as the element typology, its position in the structure, or the fastening mechanism, the governing loading condition can be identified. While considering the case of a glazed curtain wall system, some preliminary comments based on the predominant loading condition acting on it can be derived from the available literature.

For claddings of high-rise buildings, air pressure acting both perpendicular and parallel to the façade plane has been found to be the critical load condition defining the system design. In fact, the glass thickness, the infill materials, the framing structural properties as well as the anchorages and connections are mostly driven by the magnitude and nature of the wind actions (Brenden, 2006, Boswell, 2013). In conventional buildings, the wind load is found to be larger, sometimes by even an order of magnitude, than the rest of the loads acting on a façade. More specifically, curtain walls appear to deteriorate more in the glazing area of the panels, mainly due to what has been previously called as the “indirect effect” of an earthquake incident, namely the seismic-induced movements occuring on the areas where the curtain wall is attached to (Bârnaure & Voiculescu, 2013). Consequently, the verification of a curtain wall system as a whole, or of its frame, glazing and fastening components individually, under wind load automatically implies that of the seismic load.

Seismic events and their impact on building structures is another loading type of major consideration. Earthquakes are widely known to be responsible for ground motion and the creation of increased accelerations acting on the building structures. Contrary to the force-type wind loading, inducing wind pressure on the building exposed surfaces, seismic actions belong to the displacement-type of loading as depicted in Figure 3.4. Seismic events create inertia forces to the structure, which in return create stresses

(Murty et al., 2012). Even during earthquakes of generally low intensities, large accelerations combined with the ground displacements act on the structures initially reaching the foundations and later transferred to the primary building structure.

It is important to mention that the determination of the most critical load type acting on curtain wall system is not a straight-forward process, since the nature and magnitude of dynamic loadings such as wind and earthquakes depend on various parameters, such as the building geometry and height of the typology of the surrounding structures, the region, the topography of the environment and many more (Boswell, 2013).

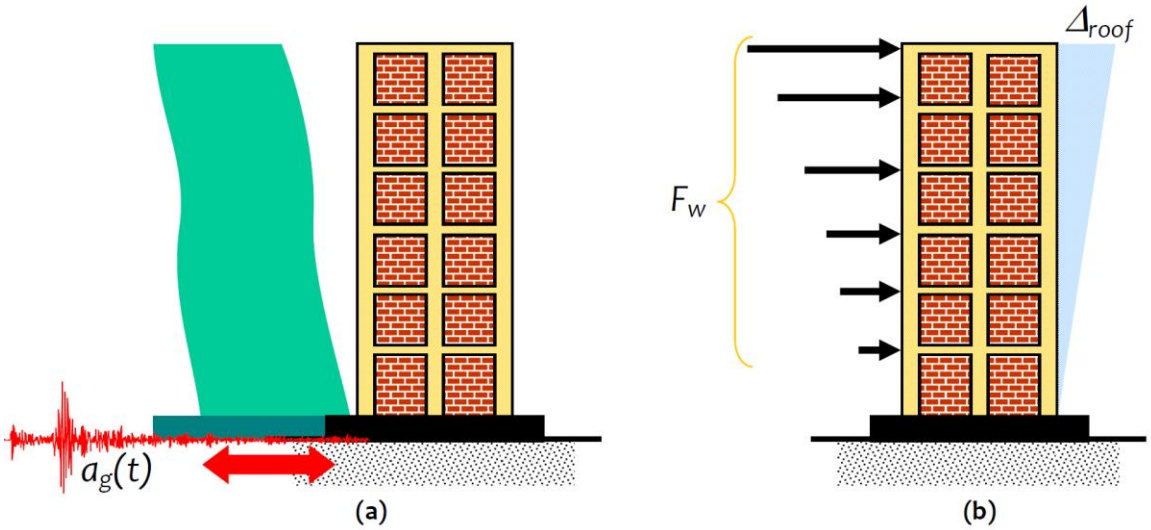

Figure 3.4: In the figure above, the design effect of a building for the seismic is presented to the left. The seismically-imposed displacement is applied at the base of the structure. To the right, the wind pressure acting on the building's exposed area is depicted (Source: Murty et al., 2012).

In general, it has been reported that the in-plane structural behaviour of curtain walls is completely different from the out-of-plane one. While the seismic events are the main reason for the in-plane response of the curtain wall behaviour, the wind load is the one defining the out-of-plane one (Rizzo et al., 2021). The out-of-plane curtain wall response to the wind action is defined by the glazing panel stiffness. A significant out-of-plane torsion is typically noticed on the façade element while undergoing wind actions. The reason for that is the non-uniform distribution of the wind action to the façade surface that subsequently results in the not simultaneous presence of the minima and maxima wind loads on the curtain wall (Simiu & Yeo, 2019, Stathopoulos & Baniotopoulos, 2007, Baniotopoulos et al., 2016).

The in-plane response of the curtain wall elements on the other hand is found to be closely related to the main structure behaviour. The study of various post-earthquake curtain wall responses (Lim & King, 1991, Thurston & King, 1992, Carré & Daudeville, 1999, Filiatrault et al., 2001, Baird et al., 2011, Hosseini, 2005, Caterino et al., 2017) has depicted that the damages were principally caused by the in-plane displacement rate induced by the supporting structure displacements and that the acceleration acting on the curtain wall unit itself had secondary impact (Rizzo et al., 2021). Since the objectives of the present study are closely related to the curtain wall seismic response, the rest of the chapter focuses more on the in-plane rather than the our-of-plane curtain wall behaviour, the respective failure mechanisms and damages.

Earthquake-induced Curtain Wall Damages

Several parameters, such as the glass type and ratio, the framing type, the sealant type, the fixing location, the loading type, the irregularity and the overall stiffness of the building, have been reported to influence the type and extent of the damage of a glazed façade during an earthquake (Bouwkamp & Meehan, 1960). Among the damage mechanisms typically recorded, the gasket dislodging, glass cracking and corner crushing as well as the glazing fallout are the dominant ones (Caterino et al., 2017). More specifically, based on both experimental data and the observation of actual curtain wall response to seismic events, it has been found that the glazing plane, which is fixed by the metallic frame, is typically the element most prone to failure due to its fragile behaviour (Memari et al., 2003, Bârnaure & Voiculescu, 2013). The glazing, in fact, presents a behaviour similar to this of rigid elements since it can only move but not deform. The curtain wall framing on the contrary, is able to easily facilitate the inter-storey relative displacements due to its ductile properties. The latter can be achieved either through the movement of the framing itself or by its shape deformation. The different behaviour of the frame and the glazing during seismic action potentially leads to the contact of the two, resulting in the glass cracking, breakage or even in a complete fallout from the frame (Rizzo et al., 2021).

The previous observations regarding the seismic behaviour of curtain wall systems have been addressed already from the 1960s by Bouwkamp (Bouwkamp, 1961). Additionally, the movement potential of the glazing panels was characterised as large, even reaching relative inter-storey drifts of up to 8.0 %. The previous observation referring to the typical mechanically connected curtain wall systems is substantiated through the large space, mentioned as “c” in Figure 3.5 occurring between the glazing panel and the metallic frame. This space is typically referred to as “clearance”.

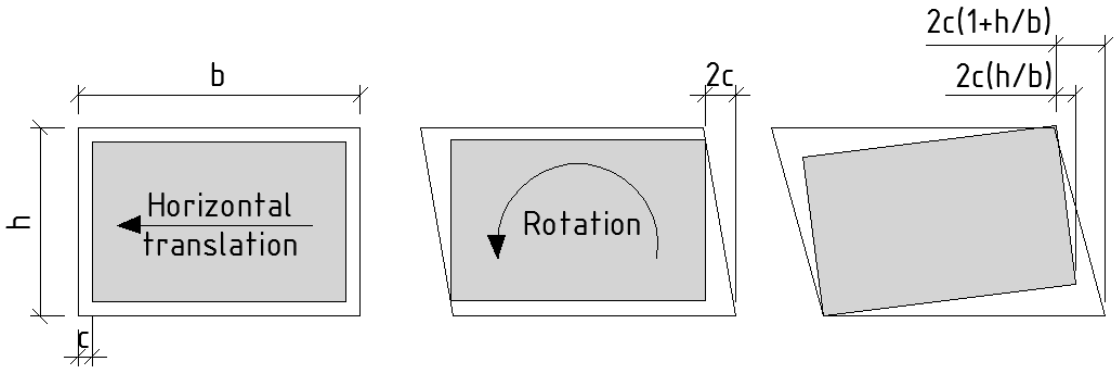

Figure 3.5: In the figure above the in-plane deformation observed in glazed panels when undergoing horizontal shear is presented. To the left the undeflected panel, where the initial frame deformation and the glazing translation within the framing is presented for a displacement applied from the right towards the left. In the middle the in-plane deflection due to the glazing movement is depicted and finally, to the right, the combined in-plane deflection due to both the rotational and the horizontal movement of the glazing (Source: Bârnaure & Voiculescu, 2013).

The in-plane deformation occurring in glazed panels when subjected to lateral loading, was found to occur in two phases as seen in Figure 3.5 (Bouwkamp, 1961). In more detail, the glazing panel is initially observed to translate within the frame following the deformation of the latter. The glazing translation towards the frame interior continues until glazing and frame are in conduct at the two opposite glazing corners as depicted in the middle of schematic representation of Figure 3.5. Thereafter, the glazing panel further rotates up until

the glazing and framing corners align (Bârnaure & Voiculescu, 2013). The total lateral deformation of the glazed curtain wall unit (Δ_{clear}) due to the rigid glazing motion can be found as a function of the width (b_p) and height (h_p) of the panel itself and of the space between the frame and the glazing panel, the clearance (c).

$$\Delta_{clear} = 2c\ (1 + \frac{h_p}{b_p})$$

In case the horizontal (c_1) and the vertical (c_2) spaces between the frame and the glazing differ, the previous equation alters as follows:

$$\Delta_{clear} = 2\ c_1 * \left(1 + \frac{hc_2}{bc_1}\right)$$

By observing the above relations it becomes evident that the ability of the glazing panel to accommodate the in-plane drift is determined by both the distance (c) between the glazing and the frame and the dimensions of the glazing panel.

In general, a seismic ground motion of a lower magnitude is typically associated with damages of the serviceability limit state (SLS), whereas higher magnitudes of ground motions with the ultimate limit state (ULS). Thereafter, during moderate seismic events the serviceability limit state prevails when performing the overall assessment of the glazed façade (Behr et al., 1995). Accordingly, the earthquake-induced damages of the serviceability limit state are extended to a wider part of the structure opposing to the ones of the ultimate limit state given a moderate earthquake.

Replacing of the cracked or fallen-out glass, repositioning or substitution of the glass panels that have shifted or rotated within the glazed façade are only some of the possible repairs that would be needed while restoring the serviceability of a building. As a consequence, the accumulated serviceability repairs of an extended damaged building area not only are considerably costly and time consuming, they can additionally cause inconvenience to the occupants of the building and also reduce the structure's overall weather protection and tightness. In that sense, the importance of understanding and mitigating the damages of the glazed façades under seismic loading is highlighted (Memari et al., 2003).

Serviceability Limit State

Some of the failures that are commonly referred to as “serviceability limit state damages” are concentrated by Memari et al (Memari et al., 2003) described below:

i) Damages at the glass edges that appear either in the form of fragmentation or as perimeter cracking. Fragmentation occurs when glass spalling is noticed in the glass edges whereas in the perimeter cracking, the cracks initiated by local concentrations of stresses due to the connection of glass and frame are noticed along the perimeter of the glass. These types of damage can potentially develop in larger, visible to the human eye, cracks.

ii) Translation and rotation of the glass panels that eventually can lead to water and air infiltration in the envelope of the building.

iii) Degradation of the gasket seal placed perimetrically of the glazing. Such degradation of a gasket can be noticed in the form of distortion, of push-in, of pull-out or of shifting as explained in (Memari et al., 2003). This type of degradation similarly leads to water and air infiltration that causes various problems like corrosion, strains, degradation and general damage in the interior of a structure.

Ultimate Limit State

Damages such as severe glass breakage and/or fallout are ultimate limit states and are considered as threatening to the life safety of both the occupants and the people at the pedestrian level. More precisely, the dominant hazard endangering human life originates from the glass shards detaching from the exterior envelope, which is mainly affected by the production and manufacture procedure followed for each of the glazing types. Following the sequence of the glazing types provided in Annex I of the present study, a brief description of the typical glazing failures as noticed by (Le Bourhis, 2014, A. Behr, 2009) per glazing case is summarised below and presented in Figure 3.6.

The failure of the annealed glazing is considered as the most severe one since it typically results in wide and large shards that are not obtained from the frame after the glazing breakage. Generally, the post-failure glazing situation is defined by the absence of residual strength related to breakage.The previous obviously results in an increasingly hazardous situation with possible piercing or cutting injuries for the pedestrians walking along the glazed external envelope. As for the failure of the heat-strengthened glazing, this is similar to the annealed one with the increased load resistant values of the former being the main difference. This is mostly defined by factors such as the degree of tempering, the glazing surface condition, the environmental as well as the duration of the loading.

The fully-tempered or toughened glazing on the other hand presents a different rapture behaviour due to the high compressive stress which is applied uniformly. For this reason, the glass breakage results in relatively blunt shards of small sizes that are considerably less dangerous compared to the larger ones presented in the annealed glazing. Additionally, an interesting feature of this glazing type is the ability of the glazing plate to remain in the curtain wall framing while undergoing a breakage in the vertical position, unless it undergoes increased horizontal loading.

Figure 3.6: The different breaking patterns for typical glazing types. To the left a representation of the large, pointed and sharp splinters created after the annealed or heat-strengthened glazing rapture are depicted. In the middle, the image of a tempered glazing panel being completely shattered is observed, with most of the shivers falling out of the framing. To the right, a view of a laminated glazing is presented. As seen in the picture, the panel integrity is preserved, with most of the splinters remaining on the frame, adhered to the interlayer (Source: Pioneer Glass).

Last but not least, the laminated glazing after its rapture is also able not to fallout from the framing due to the PVB element that maintains the shards in their original position. The latter is considered as an important advantage of this glazing type since it ensures rain and wind protection of the building interior until the replacement of the damaged glazing is possible. This characteristic renders laminated glazing ideal for sloped glazing applications or for even vertical glazing of curtain walls when increased horizontal loads, such as wind and seismic actions, are expected to act on the external envelope. Generally, aspects such as the breakage pattern, the overall strength as well as the post-failure response of the laminated glazing is determined by various aspects including the type and thickness of both the glazing and the interlayer element.

To conclude, damages frequently seen in curtain wall systems such as glass cracking or sealant damage are not regarded as ultimate limit failures since they do not pose hazard to the human safety. Instead they indicate the need for either glazing or sealant replacement. On the contrary, other types of damages such as the glazing fallout from the curtain wall framing are mostly related to life-threatening failures, therefore they are regarded as ultimate failures of the building enclosure.

The current seismic codes and standards prescribe the provisions for the glazed curtain wall performance with regards to both the serviceability and the ultimate limit states. A more elaborate description of the existing seismic standards and provisions is presented in the following section of the present study.

Seismic Codes & Regulations

It is considered that a brief introduction to the main objectives of the seismic design standards of some of the most seismically active regions of the world contributes to the better understanding of the seismic reaction of structures under the application of seismic motions. This presentation of various national seismic standards and codes also forms the introduction to the experimental procedures of full-scale elements, including among others curtain wall systems, setting in this way the ground for the main aspects, requirements and results expected during the experimental procedure which forms integral part of the present study and is explained in more detail later.

In this introductory section the basic context of national seismic design standards are presented. More specifically, the European Eurocode 8 (Eurocode 8, 2004) and the Japanese JASS 14 standards (JASS 14, 2012) are described below. Additional two more national regulations, the American FEMA 450 (FEMA 450, 2003) and the New Zealand NZS 1170.5 (NZS 1170.5, 2004), are presented in Annex II “Additional Seismic Regulations”. The verification method proposed in each case is mentioned accompanied by the basic relations and tables used for the derivation of the design values, mostly seismic actions and displacements, typically used as a reference for the resistance evaluation of the non-structural elements under examination

against seismic motions. Moreover, the minimum criteria regarded as sufficient for the seismic and life-safety verification of structure are defined per case.

A comparative evaluation focusing on the design indications and specification for non-structural elements of each of the Standards introduced, more specifically for curtain walls, is then addressed. The main similarities as well as the different approaches adopted by the standards examined are underlined in the section devoted to their comparison.

Additionally, a reference to a standard prescribing a typical experimental campaign that evaluates the post-seismic curtain wall performance is presented. Therefore, the description of the AAMA Standards, AAMA 501.4 (AAMA 501.4, 2018) and AAMA 501.6 (AAMA 501.6, 2018) that describes the guidelines of a mock-up test of a glazed storefront system undergoing inter-storey drift is included in Annex II. The aforementioned guidelines provide the basis of the experimental campaign setting aiming for the post-seismic evaluation of glazed curtain wall systems, a topic that forms one of the main objectives of the present study. The importance of experimental results similar to those of the present study is underlined by the ever-increasing need of curtain wall systems for seismic qualification that eventually transforms to a prerequisite for their seismic verification (Huang et al., 2017).

Eurocode 8, European Regulation

The requirements for the non-structural elements of the buildings are described in detail in the 4.3.5 Section of the European standard, (Eurocode 8, 2004), which forms part of the broader section of the code dedicated to the structural analysis. In this specific section the seismic verification of various non-structural elements, also referred to as "appendages", namely curtain walls, railings, partitions, parapets, antennae, gables and mechanical equipment and appendages is analysed. The term appendages has been adopted aiming for a clear distinction between the structural elements and the ones attached to them. It obviously characterises the latter.

The generic requirement that the European standard provides for all the elements of a building and their supports is their resistance to the designed seismic action. This specification by clearly including the term "supports" underlines the importance of fastening and the supporting system in general to the failure-mechanism of appendages.

For the assessment of the seismic action over non-structural elements (appendages) that are not indicated as "of great importance" or "of a particular dangerous nature" a simplification is applied. For the cases mentioned above, a seismic analysis is performed on a model representative of the analysed structures. For the analysis to be realised response spectra of the structural elements providing support to the system providing resistance to seismic actions are additionally required. In practice, a verification of the static horizontal force F_a in the non-structural element is proposed. This seismic force that is applied in the appendage elements is derived as seen below:

$$F_a = \frac{(S_a * W_a * \gamma_a)}{q_a}$$

Where,

F_a: the seismic force applied horizontally in the critical direction. The force is typically applied to the mass centre of the non-structural element under examination

W_a: the weight of the element tested

S_a: the seismic coefficient included in the appendage

γ_a: the importance factor

q_a: the behaviour factor

The seismic coefficient S_a can be derived from the following relation:

$$S_a = \alpha * S * [3 * (1 + \frac{z}{H}) / (1 + \left(1 - \frac{Ta}{T1}\right)^2) - 0.5]$$

Where:

α: the design ground acceleration ratio on type ground A, α_g, for gravity acceleration g

S: factor related to soil

T_a: fundamental vibration period of the appendage

T_1: fundamental vibration period of the structure for the relevant direction

z : appendage height measured above the application level of the seismic action

H: building height calculated from the top part of a rigid basement or the top

It is important that S_a value should always exceed the $\alpha * S$.

In accordance with Eurocode 8, the importance factor (γ_a) cannot be taken less than γ_a= 1.5 for the non-structural elements listed below: tanks and vessels that contain either explosive or toxic substances potentially hazardous for the public safety, anchorage elements included in the equipment and machinery that is included in the life-safety systems.

For the rest of the cases, an importance factor γ_a equal to 1.0 is proposed.

Regarding the behaviour factor (q_a), this can be derived from Table 3.1.

Non-structural element type q_a	q_a
Cantilevering parapets or ornamentations Signs and billboards Chimneys, masts and tanks on legs acting as unbraced cantilevers along more than one half of their total height	1.0
Exterior and interior walls Partitions and façades Chimneys, masts and tanks on legs acting as unbraced cantilevers along less than one half of their total height, or braced or guyed to the structure at or above their centre of mass Anchorage elements for permanent cabinets and book stacks supported by the floor Anchorage elements for false (suspended) ceilings and light fixtures	2.0

Table 3.1: The behavioural factor q_a of non-structural elements (Source: Eurocode 8, 2004).

Considerations

Eurocode 8 clearly recognises the influence of the non-structural elements on the building integrity and the safety of its users. However, a reference specifically referring to the curtain walls is absent. More importantly, apart from examining both the design as well as the fastening of the supporting structure, it requires their verification for resisting the design seismic loading. Therefore, the importance of fastening elements such as the brackets on the seismic resistance of non-structural elements is underlined.

As briefly explained above, Eurocode 8 has adopted a simplified method based on which the seismic action applied on the non-structural elements can be recreated through the imposing of a static horizontal force on the centre of their mass. Although the behaviour as well as the importance of the non-structural elements under examination are determined and weighted through various factors, namely the behaviour (q_a) and the importance (γ_a) factors, this is not the case for the buildings as a whole. The previous consideration implies that aspects such as the building typology, importance and behaviour are not included in the seismic assessment as considered by Eurocode 8.

JASS 14, Japanese Architectural Standard Specification

The extremely high seismic activity of Japan has resulted in advanced building design of structures incorporating seismic considerations. In fact, an entire standard (JASS 14, 2012) of the Japanese codes is dedicated to the façade and curtain wall design. Below the main context of the verification approach proposed by the Japanese Standards aiming for the evaluation and subsequent verification of the curtain wall's behaviour during and after seismic events is presented.

Seismic Energy

One of the main considerations of the Japanese code is the division of seismic energy into two distinct categories: P- and S- waves. The waves that fall into the P-wave category are the primary ones. They are characterised by mostly longitudinal acting and their conveyance is faster. The secondary waves of the S-waves category on the other hand present a slower conveyance and act mainly in the transversal direction.

As specified by JASS 14, in order for the curtain wall structure to be verified as safe, it must withstand the impact forces against both the P- and the S-waves. The definition of the impact forces against P- and S-waves is presented below:

$$Impact\ forces\ withstanding\ P-waves = Vertical\ acceleration\ *\ Dead\ load\ of\ curtain\ wall$$

$$Impact\ forces\ withstanding\ S-waves = Horizontal\ acceleration\ *\ Dead\ load\ of\ curtain\ wall$$

The forces above incorporate a safety verification which involves a common structural analysis. In fact, the cross-section strength is identified through the multiplication of each member by the acceleration speed. The calculated cross-section strength of each component is then compared to the respective allowable short-term stresses. The aforementioned verification mainly considers the location around the brackets. It is important to mention that JASS 14 mainly considers the assessment of the secondary deformation of the curtain wall which originates from the building storey drift.

As has already been explained in previous chapters, the inter-storey drift occurring during earthquake incidents results in relative displacement between successive floors. These relative displacements when induced on curtain wall systems are responsible for the displacement generation of the frames and the glazing. Subsequently, the seismic performance of the curtain wall members needs to be evaluated based on the following verification method.

Grades & Design Requirements

The curtain wall performance under seismic events is evaluated based on three standard design requirements. These three "grades" are related to respective categories of hazard and probabilities of the occurrence of a seismic incident. The three design levels depend on solely one parameter, H, which resembles the inter-storey height and are presented below.

- Level 1 = H/300, This intensity resembles the most frequent seismic actions occurring in Japan. During this design requirement neither the internal nor the external façade elements is allowed to undergo damages
- Level 2 = H/200. This specific grade corresponds to the earthquakes with the largest magnitude recorded in the past. At this level every external component is allowed to stress until certain limits. The possibility of prolonged use depends on the repairability of the sealings
- Level 3 = H/100: The final intensity corresponds to the most intense seismic events that are expected to occur in the upcoming 100 years. During this design requirement, none of the façade components is allowed to drop. Moreover, the glazing of the exterior envelope must remain undamaged and unbreakable

In order for a curtain wall system to be verified according to the Japanese Codes, the unit is required to present the performances associated with each of the three categories respectively.

Overview

Based on the overview presented in this chapter, the Japanese Code JASS 14 takes into consideration different aspects of the façade behaviour while aiming for its seismic verification. A common force-based approach including both vertical and horizontal accelerations imposed on the façade elements during seismic actions is proposed. On the other hand, three distinct design requirements (grades) according to which the façade needs to be verified through its adequate performance are introduced. The combination of those two results in the façade evaluation in terms of various performances, reassuring that the exterior envelope is verified under the complete series of potential seismic events and their corresponding hazard levels. Consequently, the Japanese Regulation can also be described as "performance-based".

An additional reflection upon the Japanese Standard originates from the fact that the performance-based assessment of the façade configuration tested depends solely on a unique façade feature, H, the inter-storey height. This parameter defines the magnitude of the displacement that is statically applied on the façade unit. In that sense, the façade design is displacement-based as opposed to force-based which is more commonly seen among the seismic regulations.

Comparison of the Seismic Regulations

The present section aims to provide a summary of the main aspects of the Seismic Regulations and Standards that were described earlier in this chapter. A comparison between their main considerations also takes place, aiming for a better understanding of how the current Seismic Codes and Provisions identify the required seismic resistance of structures and especially of the non-structural elements, such as the exterior enclosures.

The majority of the codes mentioned above recognise the inter-storey drift of the building structures as the basic means of evaluating either the resistance or vulnerability of curtain wall systems under seismic ground motions. Eurocode 8 is the only exception since it does not include this parameter into its seismic proof verification procedure.

While the inter-storey drift is completely excluded by the Eurocode 8, it is generically included in the New Zealand Standard. In practice, NZS 1170.5 indicates that for the cases where the inter-storey drift is larger than the allowable displacement value of the non-structural elements, this relative displacement should be isolated from the building structure. However, further information regarding the isolation of the specific non-structural element is absent, making the specification rather vague and difficult to interpret. However, the equations specified by the two aforementioned Standards, the European and the New Zealand ones, present noticeable similarities in terms of their components and the incorporation of various coefficients.

On the other hand, both the Japanese and the American regulations clearly include the inter-storey parameter for seismic verification of the non-structural elements. JASS 14 specifies that a horizontal displacement which derives from H, the inter-storey height, is applied on the curtain wall system. In this way, the relative displacement between two adjacent floors that occurs during the seismic actions resulting subsequently in the relative displacement of the glazing and the frames is recreated. Finally FEMA clearly indicates that in order for a non-structural element with a potential to cause life-safety hazards to be verified as seismic proof, apart from the specified seismic forces it also has to adequately accommodate seismic relative displacements.

The following consideration relates once again to the type of the seismic actions applied to the building element whose performance needs verification in terms of its proofness against the seismic actions and more specifically to the vertical acceleration. Only the New Zealand Standard provides the relation based on which the design vertical acceleration applied to the “part” can derive. The Japanese National Standard on the other hand, although mentions the vertical acceleration, which also forms an integral component for the calculation of the impact forces against P-waves, it does not specify any type of equations that could be used for the calculation of the vertical acceleration.

Apart from the Japanese codes, all of the remaining Standards include in their seismic verification approach a specified calculation method based on which the seismic performance of non-structural parts along with this of their supporting elements is evaluated. The common approach includes the determination of the horizontal seismic action that is typically applied to the centre of mass of the component under verification. Most of the equations previously mentioned, especially the ones of the NZS 1170.5 and FEMA, include numerous coefficients aiming to represent the variations over a wide range of parameters, such as ground conditions, importance factors, type of building structures, bracket systems etc. The incorporation of all those

parameters aims to recreate as adequately as possible the particular non-structural element that each time needs to be verified since these verification approaches refer to a broad range of non-structural elements. The exception to the previous one is the Japanese Standard since it includes a specific section exclusively referring to the seismic verification of the curtain wall systems.

Additionally, it is only the American Provisions that include specific requirements for the glazing of various architectural elements, such as of the glazed storefronts, partitions and curtain walls. In more detail, the realisation of mock-up test is indicated aiming for the determination of the relative displacement requirement $\Delta_{fallout}$ of the glazing which is responsible for the glazing fallout from the curtain wall frame. Moreover, special types of curtain walls based on their glazing clearance are specified to be excluded from the typical provisions including the application of seismic forces and, for the cases of architectural elements that could potentially cause life-safety hazards, also of seismic relative displacements in order for the seismic verification to be provided.

Finally, among the regulations analysed above, only the New Zealand set of standards specifies a minimum ductility value for the fastening system of a "part", in other words of a non-structural element. The design ductility μ_P of a non-ductile connection should be considered as $\mu_P = 1.25$ whereas the one of the "parts" itself as $\mu_P = 1.00$ unless specified otherwise.

Seismic Regulations Conclusions

Over the past years, an ever-increasing interest in the investigation of the curtain wall systems seismic performance has been noticed. The latter has been further reinforced especially after the realisation that damages of such components apart from resulting in considerable economic losses, they also pose potential threat for the occupants and pedestrian safety.

Based on a wide range of studies, it has been concluded that the seismic performance of glazed façade units is directly linked to the seismic response of a building. The latter depends on the mass distribution and stiffness not only of the building's structural system but also of the non-structural elements. Additionally, through numerous experimental racking testings on full-size glazed façade systems, it was evidenced that the displacement rate imposed on the tested units is the determining factor largely influencing the seismic behaviour of the façade elements.

Moreover, the provisions of the current seismic codes prescribe the performance levels of curtain wall systems in terms of both their ultimate and serviceability limit states. In order for the ultimate limit state to be preserved during intense seismic loads, the glass fall-out should be prevented. Similarly, the weather-tightness of the external glazing systems is prescribed to be ensured throughout their reference life. Moreover, intending to preserve the integrity of non-structural components, such as claddings and partition walls, the majority of the existing regulations define the maximum inter-storey drift that is allowed to occur to the structural frame. However, specific prescriptions for the verification under seismic loading of glazed curtain wall systems are generally scarce.

The observations and results obtained during experimental procedures such as this of the current study are expected to provide valuable insight on the dynamic behaviour of glazed curtain wall components and systems in general. The importance of the previous is highlighted by the ever-increasing need of façade systems to be in accordance with seismic qualifications and eventually to be seismically verified.

Chapter 4

Experimental Procedure

The following chapter aims to present the experimental test campaign used as a case study for the evaluation of the global behaviour of the unitised façade elements examined and later for the calibration of the finite element model. First, a brief introduction to the background of the experimental studies aiming to assess the seismic performance of non-structural elements in general and of curtain wall systems in particular is presented. Secondly, a description of the present case study examined during the current research is addressed. There a reference to the testing facility as well as the equipment used for the experimental campaign is made.

Later, the characteristics of the façade specimens used upon which the various performance tests were performed are demonstrated. Thereafter, an informative description of the unit response as expected to be observed due to the inter-storey drift application follows. Moreover, a presentation of the monitoring system applied during the experimental procedure is provided. The following section is devoted to the description of the Japanese Regulation (JASS 14) upon which the seismic testing procedure was developed with emphasis on its main reference points. The specific testing protocol followed during the experimental campaign is described, providing an insight of the seismic as well as the air-tightness testing sequence and realisation.

Towards the end of this chapter the curtain wall experimental behaviour is presented with regards to its rotational and displacement behaviour. The asymmetric behaviour of the system, a topic on which this study focused as it will be later seen, is introduced. Additionally, the air-tightness testing implemented in this testing sequence is described accompanied by the presentation of the specimen response. Finally, observations related to the global façade response as originated from the entire experimental campaign are demonstrated. The evaluation of the global behaviour of the unit under seismic action is followed by a brief assessment of its serviceability and ultimate functions.

Experimental Studies on Curtain Walls Seismic Performance

Over the past years numerous studies, both numerical and experimental, have been conducted aiming to assess the reaction and performance of non-structural elements (partitions, openings and walls) as well as of the glazing systems of buildings when undergoing seismic actions (Mosqueda et al., 2008, Lee et al., 2007, Gil, 2019, Sivagnanasundram, 2011). The interest in the seismic performance of curtain wall systems was further enhanced after the realisation that damages of such components apart from resulting in considerable economic losses, also pose potential threat for the occupants and pedestrian safety (Caterino et al., 2017, Aiello et al., 2018).

The earlier studies were focused on the impact of numerous parameters, namely the glazing and the sealant type, the fixing location, the edge strength as well as the loading type. The influence of those parameters was mainly investigated by examining the response as well as the failure mode of glazed window systems undergoing dynamic in-plane horizontal racking tests -either cyclic or unidirectional ones (Aiello et al., 2018, Bouwkamp & Meehan, 1960) whereas fewer studies aimed for the same assessments through out-of-plane racking tests of similar mock-up units (McCue et al., 1978). Following those tests, several researchers investigated the curtain wall response under inter-storey drifts imposed by cyclical displacing floor beams (Pantelides & Behr, 1994, Thurston & King, 1992).

Based on the aforementioned studies it was concluded that the post-seismic performance of the glazed façade unit is closely linked to the overall seismic response of a building that depends on the mass distribution and

stiffness not only of its structural system but also of the non-structural elements (Aiello et al., 2018, Sakamoto et al., 1984). Moreover, through numerous experimental racking testings on full-size glazed façade systems, it was gradually evidenced that the rate of the displacements applied on the tested units is the most crucial factor largely affecting the seismic performance of the façade elements (Lim & King, 1991, Thurston & King, 1992, Carré & Daudeville, 1999).

Over the past years various researchers focused their interest on assessing through experiments a wide range of façade configurations consisting of various framing and glazing elements. Other studies examined the impact evaluation of the glazing unit and the specific glazing type on the overall façade performance (Pantelides & Behr, 1994, Behr, 2001, Memari et al., 2003).

As already mentioned, the investigation of the seismic structural behaviour of various curtain wall systems has been enhanced by the increasing interest in the seismic behaviour assessment of non-structural components. As a result, a wide range of experimental tests has been conducted evaluating various loading protocols (Pantelides et al., 1996). The crescendo test which was also introduced by the AAMA 501.6 recommendations (AAMA 501.6, 2018) is one of the testing protocols that is more widely used. During this test the amplitude of the horizontal racking displacement of the façade systems that could potentially cause the glass panels to fall out is identified.

An additional testing type that is commonly used for the evaluation of a glazing system through a multi-directional base excitement is the shaking table test (Lu et al., 2017, Feng et al., 2010). AC156 (AC 156, 2020) and FEMA 461 (FEMA 461, 2007) have introduced shaking table protocols for the qualification of non-structural components (NCs) since various of the current standards and building codes have posed the seismic qualification of curtain walls under a major seismic incident as a requisite for their seismic qualification and approval (Huang et al., 2017).

Researchers based on the knowledge acquired through numerous experimental practices as well as the study of the curtain wall performance during its life cycle eventually concluded that, despite the seismic qualification of a curtain wall system, additional aspects such as the structural and the infiltration performances of the system have to be verified prior to its approval and construction. The realisation of a sequence of performance tests evaluating mainly the structural strength, air- and water-leakage and thermal performance has gradually become standard practice for custom curtain wall systems applied either on high-rise structures or on buildings with specific requirements for high comfort and confidence levels. Depending on the unique characteristics and prerequisites of a project application, additional performance indicators such as the acoustical, seismic, snow or even dust performance can also be assessed (Ilter et al., 2015).

Regarding the experimental results expected to be observed on the curtain wall under examination during the evaluation of its performance indicators, they are typically categorised in specific damage states (DS) which are presented below:

● DS1: Deterioration of the weather protection (water- and air-tightness) of the curtain wall system element. This is typically investigated through simple observations, such as the existence of water in the inner side of the glazing system.

● DS2: Deformation of the façade elements, in particular in-plane movement of the glass and the framing is expected as well as the relative displacement of the glass-to-the-frame elements. Failure of the gasket is also anticipated at this damage state. The latter is normally verified by visual observation as well as by the recording of the gaskets' movement outside their original place either towards the framing or of the complete falling from the curtain wall frame. These kinds of gasket movements typically indicate either repair or replacement.

● DS3: Failure of the glazing or the frame system. Variant conditions can be observed during this damage state, from confined to extensive cracking, breakage or even complete fallout of the glazing units. The level of these failures is assessed not only through visual inspection, but in more detail through additional monitoring systems such as appropriate pressure sensors, displacement transducers, strain gauges and cameras included in the experimental procedure.

As later explained thoroughly, the performance tests examined during the present study based on which the finite element model is built on, consisted of both weather performance, in practice air-leakage, and dynamic racking tests that were employed on curtain wall assemblies of realistic sizes, commonly known as “mock-ups”. The complete series of performance tests that was performed on the façade models during the experimental procedure is presented in the following section.

Description of This Particular Testing

Following the indications of the current regulations and standards, the curtain wall specimen used as reference case for this study prior to its production and application needed to be approved through a series of laboratory tests. This testing sequence followed the Japanese standards. However, in the absence of a translated version of the experimental setup as described by JASS 14, the brief explanation of mock-up test guidelines as presented earlier in this study, is used as a reference indicating how these tests are typically realised.

These performance tests were conducted on 1:1 scale units of the actual façade specimen, composed of materials, fixing and attachments identical to those of the final product. Since the faithful replication of the actual curtain wall configuration is of vital importance, both the construction as well as the fixing of the sample models to the supporting structure had to recreate the realistic conditions that apply during the instalment of the final exterior wall system. For the reliable assessment of the multi-performance of the façade units it was crucial that the proper environmental conditions, namely the temperature extremes, wind conditions as well as the seismic exposure were adequately simulated.

The sample units used for the performance test were attached to a supporting steel structure consisting of both steel columns and beams, resembling the bearing system of an actual building. Moreover, the adjustability of the beam elements of the steel supporting structure facilitated the reproduction of the building storey height.

Through the full-scale experimental testings both the life-safety risk induced by the earthquake loading, which was expected to be limited, as well as the post-earthquake serviceability performance of the façade, that was estimated to be gravely affected, were evaluated.

In practice, the ultimate resistance of the unitised façade elements was examined by:

- seismic tests, where several displacements of various intensities were applied at a certain number of circles in the façade specimens through a seismic beam as indicated by JASS 14

The serviceability performance of the curtain wall systems under examination on the other hand was evaluated through:

- air permeability tests, performed following the indications of EN 12153

Regarding the expected experimental results, the damage states (DS) that are awaited to be observed and recorded through the aforementioned monitoring system during the full-scale testing of the façade sample units are listed below:

- DS1: Deterioration of the weather protection (water- and air-tightness) of the curtain wall system element. This is investigated through simple observations, such as the existence of water in the inner side of the glazing system.
- DS2: Deformation of the façade elements, in particular in-plane movement of the glass and the framing is expected as well as the relative displacement of the glass-to-the-frame elements. Failure of the gasket is also anticipated at this damage state. The latter is verified by visual observation as well as by the recording of the gaskets' movement outside their original place either towards the framing or of the complete falling from the curtain wall frame. These kinds of gasket movements typically indicate either repair or replacement.
- DS3: Failure of the glazing or the frame system. Various conditions can be observed, from confined to extensive cracking, breakage or even complete fallout of the glazing units. The level of these failures is assessed not only through visual inspection, but in more detail through additional monitoring systems such as appropriate pressure sensors, displacement transducers, strain gauges and cameras included in the experimental procedure. In the case study examined the previous is measured through displacement transducers.

For all the cases above, the drift demand at which these damage states were initiated is typically recorded.

Equipment Setup

It is evident that facilitating an appropriate experimental set up is of great importance while aiming for the evaluation of both the life safety as well as the serviceability limit states of glazed façade systems. The technical equipment required for the realisation of the performance tests included in this specific study the mock-up test facility of Permasteelisa Spa was used.

As for the main point of interest of this research topic, namely the assessment of the seismic and post-seismic performance of the glazed curtain wall elements, the testing chamber of the company facility that involves an intermediate seismic beam was utilised. In practice, the seismic beam through a computer controlled hydraulic system actuator can induce static displacements to the façade specimens tested, resembling the relative inter-storey drift that typically occurs during a seismic event. In this specific setup, where only one series of façade elements was tested representing the exterior enclosure of one floor storey, only the upper beam has the ability to move, whereas the lower beam is fixed. In that way, the seismic drift is introduced in the form of displacement applied on the top of the transom of the façade units through the brackets that reassure the fastening of the exterior enclosure to its supporting structure.

Figure 4.1: Chamber 1. The seismic and weather performance testing facility of Permasteelisa is presented. The seismic beam of the test set up can be noticed in blue (Source: Permasteelisa).

In Figure 4.1 an interesting feature of the testing facility can be seen, the wooden panels located in the perimeter of the façade units under examination. The application of these panels ensures the tightness of the mock-up system which is essential for the evaluation of both water- and air-tightness of the curtain wall configuration. By preventing the air and water drops that are sprayed upon the testing façade models during the performance tests it is ensured that any potential leakage noticed in the interior of the tested element penetrated through discontinuities and leakages of the mock-up itself are prevented.

Figure 4.2: The seismic beam used for the seismic performance tests as seen from the interior of the Chamber. To the right of the picture the interesting feature of the seismic beam is visible, allowing the seismic beam to make a turn of 90.0 degrees. This feature which makes the testing of the corner of two storefronts of a building possible, was not utilised in the case study examined during this study (Source: Permasteelisa).

It is also commonly seen that through seismic beams, accelerations in both directions are simultaneously applied on the façade units examined. However, this is not the approach followed in this specific case study and there are two main reasons for that. To begin with, in order for acceleration to be applied on the mounted façade units a specific software system controlling the acceleration application is required that was not available. Secondly, a complete and thorough structural analysis of the building for which the curtain wall system is designed for, taking also into consideration the exact location of the latter, would have been needed for the determination of the appropriate acceleration. The lack of information regarding the building's structural system, though, is a crucial parameter that makes the acceleration application to the façade units hard to realise. Consequently, only the displacement load induced by the seismic beam, which is also more determining for the seismic behaviour of the exterior enclosure as explained in the previous chapters, is taken into consideration for the evaluation of the seismic performance of the curtain wall system examined. The seismic beam of the specific testing facility is seen in Figure 4.2

In the lower part of the Figure 4.3, the hydraulic system, through which the displacements are induced initially to the beam and thereafter to the façade units tested, is depicted. In the upper part of the image the fastening system of the curtain wall to the seismic beam is presented. Via the two halfen channels located at the top part of the seismic beam the fixing of the bracket is realised.

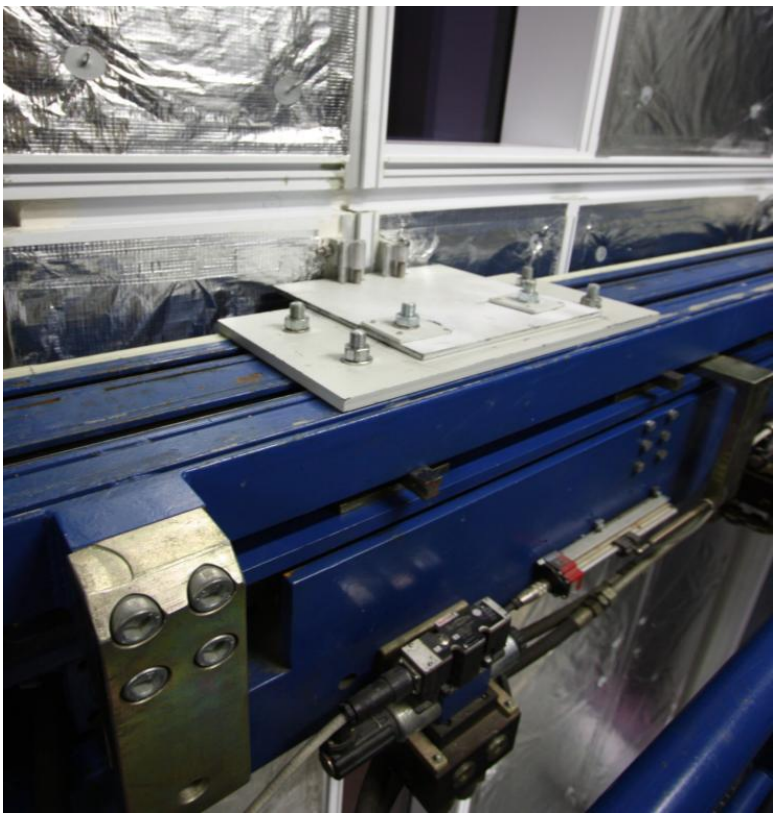

Figure 4.3: The fastening system through two halfen channels at the top of the seismic beam is depicted. In the lower part of the image, the hydraulic system responsible for the displacement or acceleration induction is presented (Source: Permasteelisa).

For the cases where both the upper and the lower beams of the testing setup are moving, a maximum displacement of ± a/2 mm is introduced to each sliding beam in opposed phases, recreating in that way the inter-storey drift of ± a mm. For the experimental procedure examined during this study, the inter-storey drift is introduced to the façade units tested only via the upper beam. Therefore, during the seismic performance testing the seismic beam to which the upper transom of the façade units is attached, "pushes" towards the desired inter-storey drift demand mimicking the relative displacement of the rigid beams of the structural system to which the façade element is supported in the actual situation.

Specimen Presentation

Before presenting in detail the monitoring system as well as the actual procedure that was followed in the experimental performance mock-up setup at the Permasteelisa headquarter located in Vittorio Veneto, Italy, a brief description of the unitised curtain wall specimens tested under seismic action is presented.

Four façade units of the same dimensions have been concluded for the full-scale experimental testing. Since one of the objectives of the experimental testing concerns the impact evaluation of connection between the glazing and the framing, two types of structural silicone joints have been tested. As a result, two of the four units were provided with the SIKA SG-500 and the rest with SIKA SG-550 structural silicone joints as depicted in Figure 4.4. Apart from the type of the silicone applied, also the dimensions of each joint were differentiated. More specifically, the façade units containing the SG-500 type of joints had a dimension of 10.0 * 6.0 mm whereas the ones with the SG-550 type 6.0 *6.0 mm.

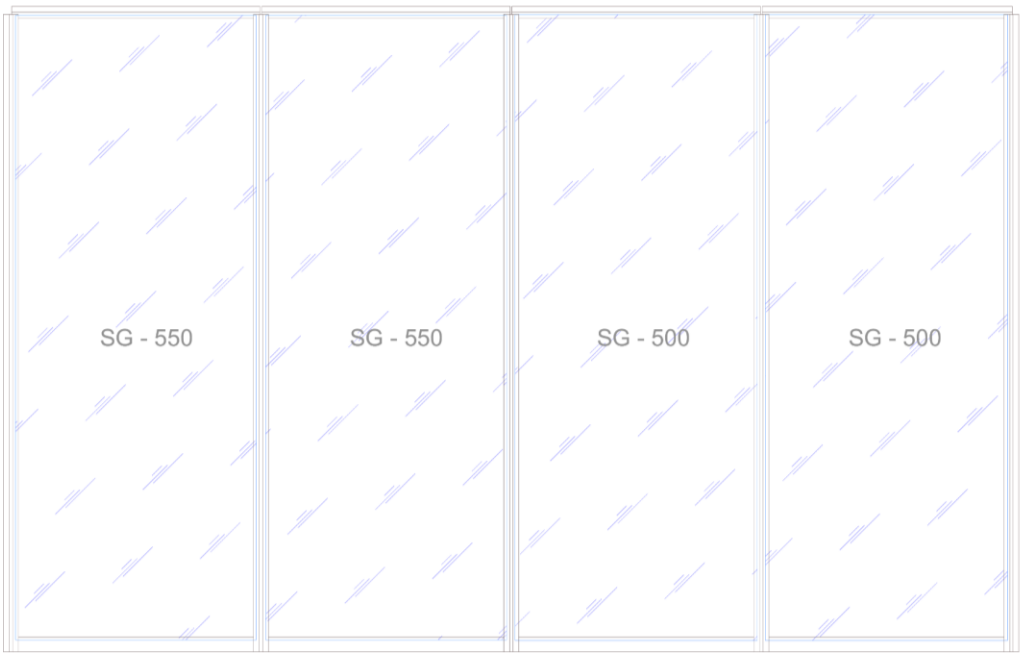

Figure 4.4: The façade units used for the testing campaign are presented. The type of silicone joint applied on each of the units is described (Source: Permasteelisa).

In all cases, the silicone gaskets are placed along the glazing edges providing support to the glaze pane while also preventing the direct conduct between the aluminium frames and the glazing.

As for the glass panel, this is of single glazing with a a thickness of 12.0 mm and dimensions of 1.44 * 3.75 mm. Regarding the mechanical properties of the aluminium and the glass, they are obtained from the literature while considering the classification provided by the respective manufacturer. In more detail, the glass and aluminium weights are 25.0 kN/m^3 and 27.0 kN/m^3 respectively and the Young's modulus is 70.0 GPa for both the materials. In Table 4.1 the technical information of the façade units tested is presented.

Attributes	Description	
Geometry	Height	3710.0 mm
	Width	6040.0 mm
	Inter-storey	3100.0 mm
Element Number	Mullions	8
	Transoms	8
	Starter Sills	4
	Glazed Panels	4
Glass Panels	Thickness	12.0 mm

Table 4.1: The technical and geometrical data of the façade type tested during the experimental campaign are summarised.

The aforementioned specimens were tested simultaneously in the laboratory facility. Each of the façade specimens was mounted between the one fixed and the upper sliding seismic beam of the testing facility as they would have been attached to the actual structure. In particular the exact same brackets aimed to be used during the actual construction of the façade were used for the attachment of the upper transom of the façade units to the two halfen channels located on the seismic beam. The bracket system used for the fastening of the curtain wall is presented through the following details (Figures 4.5 & 4.6) and the respective image taken from the experimental setting itself (Figure 4.7).

As already mentioned, the aim of the present experiment was to determine the serviceability as well as the ultimate limit states of the glazed curtain wall under examination and, therefore, define performance standards of this configuration. It is reminded that typical damages related to the serviceability limit state are glazing movement inside the aluminium frame, gasket dislodging or local glazing crushing. The ultimate limit state is reached when complete glass fallout occurs.

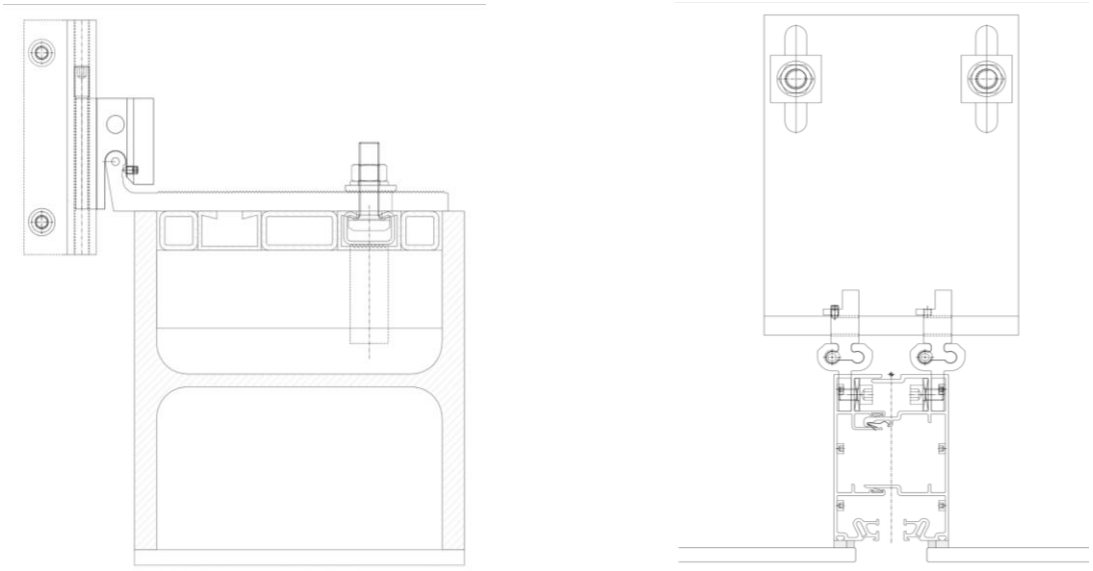

Figure 4.5: Detail drawings of the fastening system of the curtain wall system which is fixed to the seismic beam. The left drawing describes the vertical whereas the right one the horizontal detail of the upper constraint points of the curtain wall system (Source: Permasteelisa).

In order to recreate the conditions met in reality during the performance testing, the upper transoms of the adjacent units were also provided. In practice, the bottom transom of each façade unit tested was connected to the upper transom of the subsequent unit that in reality would have been placed beneath.

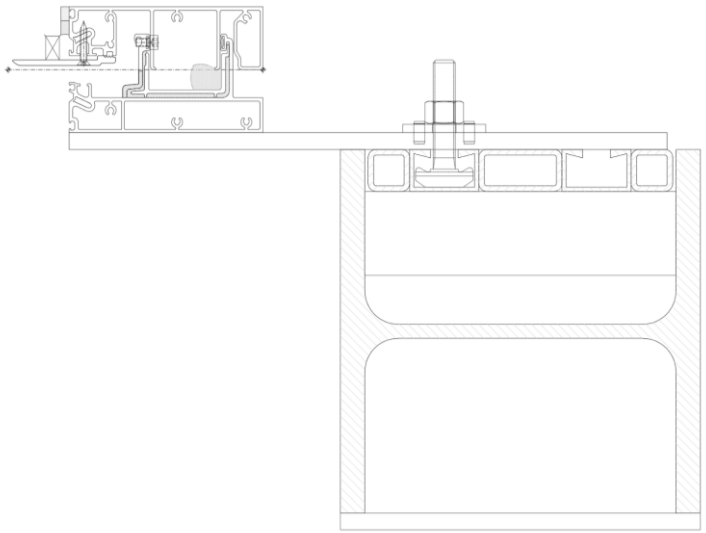

Figure 4.6: Vertical detail presenting the bottom constrain point of the curtain wall system. In particular the connection of the bottom transom to the starter sill is presented (Source: Permasteelisa).

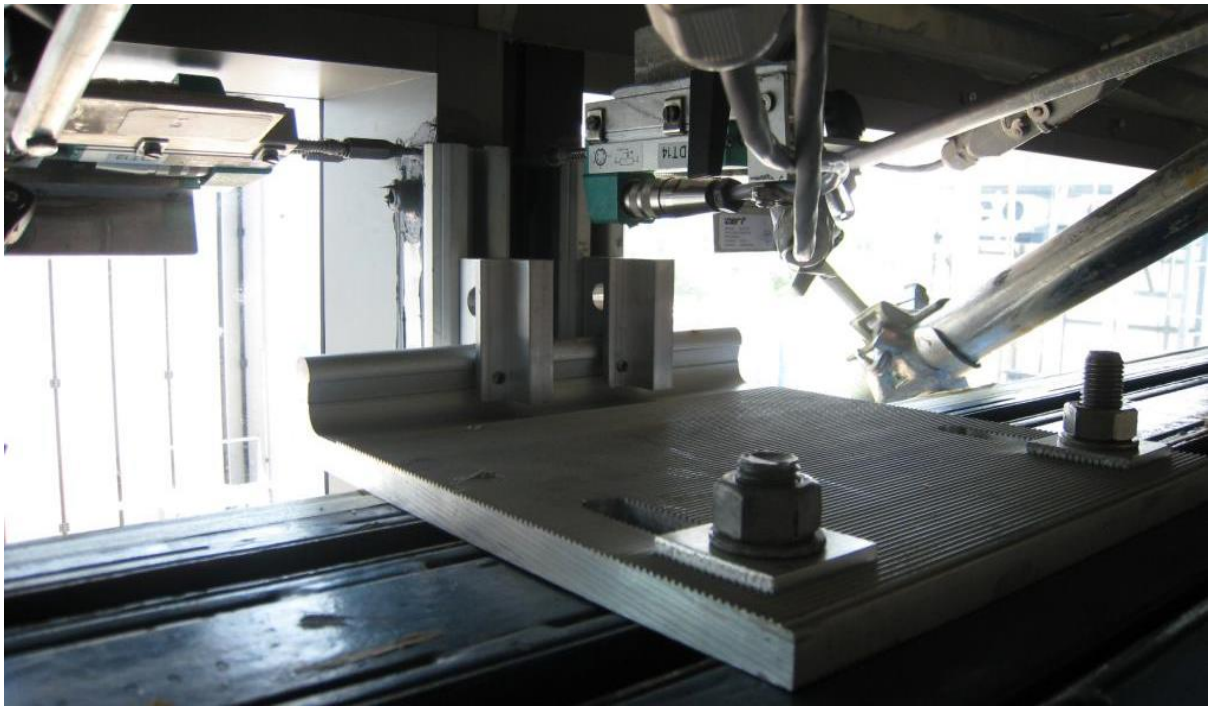

Figure 4.7: View of the fastening system of the curtain wall units as seen from the inside (Source: Permasteelisa).

Curtain Wall Monitoring System & Expected Behaviour

An integral aspect of the experimental testing facilitating one of the main aspects of this study, the post-earthquake response of the façade systems examined, is the monitoring system. Through it, the inspection of the displacements and deformations of the façade components can be measured and, subsequently, the local as well as the global behaviour of the façade system can be assessed.

In order for the adequate monitoring of the façade behaviour while subjected to performance tests and/or seismic events, the monitoring devices need to be placed strategically. Their appropriate installation to strategic façade locations originates from the façade expected behaviour during the displacement application.

As already explained, the glazed curtain wall elements undergo relative inter-storey drift while subjected to seismic action. The façade system is initially expected to rotate rigidly before the shape reformation of the aluminium frame is noticed. This behaviour is presented through the schematic drawings Figure 4.8. During the first distinguishable phase of the seismic application, the façade system including the glazing is observed to rigidly rotate. The rigid rotation of the whole curtain wall is eventually locked through the garter sleeve that is located between the adjacent façade units.

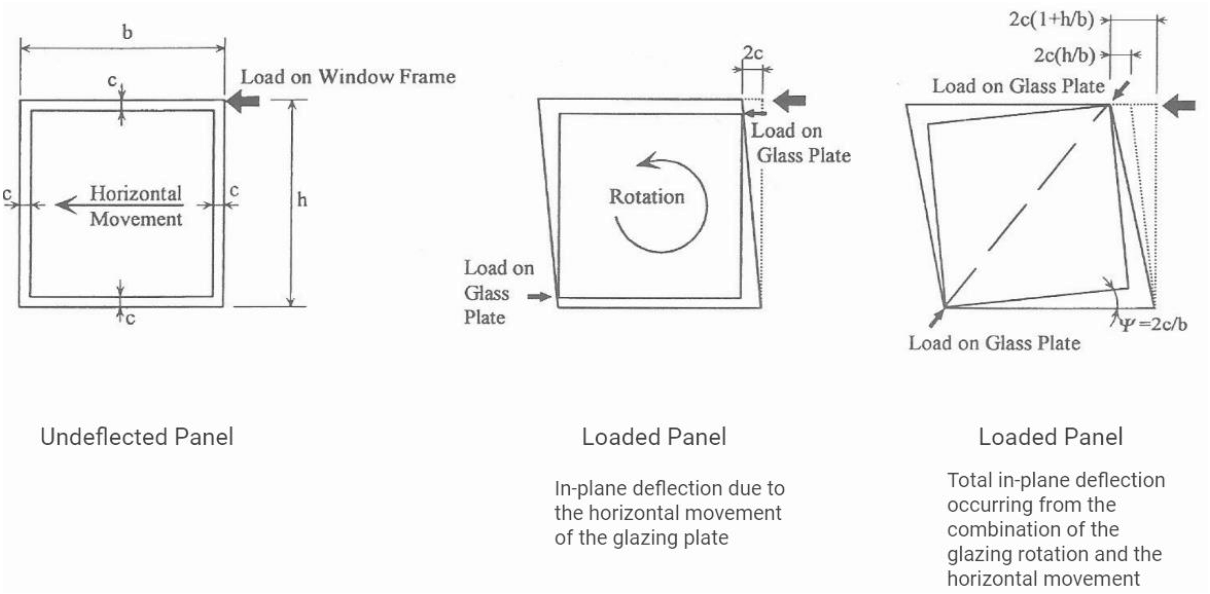

Figure 4.8: In the figure above the different stages at which the glazed curtain wall unit undergoes deformation and, consequently, the glazing gets in conduct with the framing, are depicted. The above representation refers to the cases where relatively weak adhesion is provided between the glazing pane and the frame. The previous allows for the relative movement of the glazing with respect to the curtain wall framing (Source: Sucuoğlu & Vallabhan, 1997).

Following the glazing the rigid rotation, the façade is observed to deform its shape. The initially rectangular shape alters to a rhomboidal one. This particular phase of the shape deformation can be proven critical for the integrity of the glazing pane. The reason lies upon the potential contact of the aluminium frame and the glazing pane which can result in the crack initiation of the latter.

Based on the expected behaviour of the façade specimen, the monitoring system, more specifically the displacement transducers, has been placed accordingly aiming to monitor the diagonal glazing elongation as well as the relative movements of both the glazing pane corners and the mullion-to-transom connections. For an overview of the monitoring mapping, please refer to Figure 4.9.

Moreover, additional displacement transducers have been placed upon the fastening system, aiming for the complete recording of the façade reaction to seismic loading. As depicted in Figure 4.10, the measuring instruments of the fastening system were located internally not only on the bracket but also on the hooks and channels aiming to adequately capture the vertical as well as the horizontal displacements.

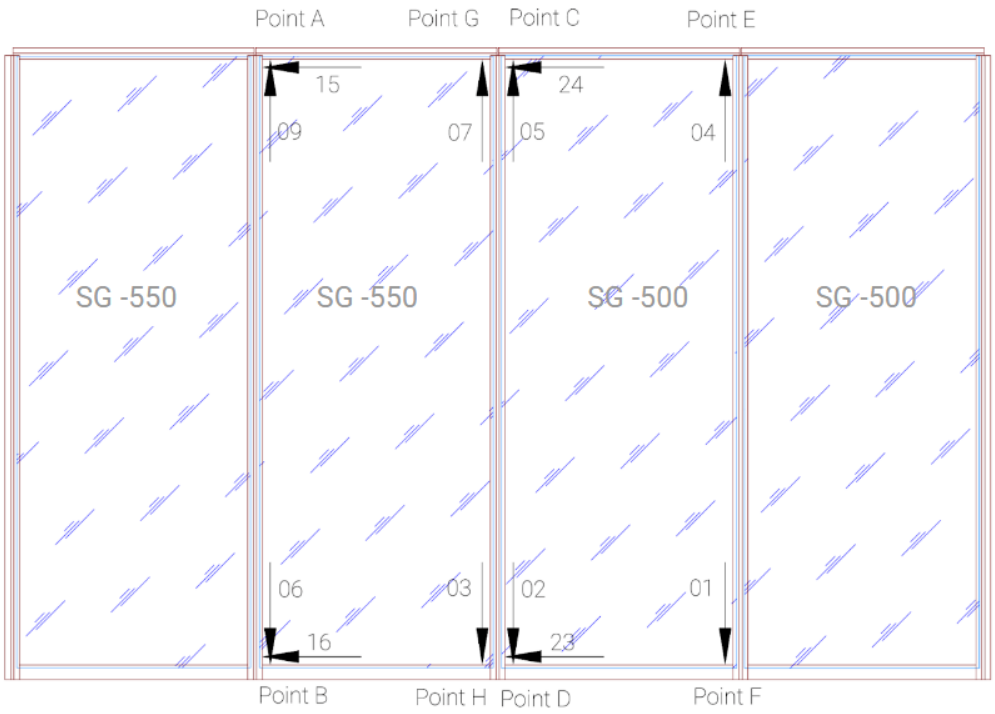

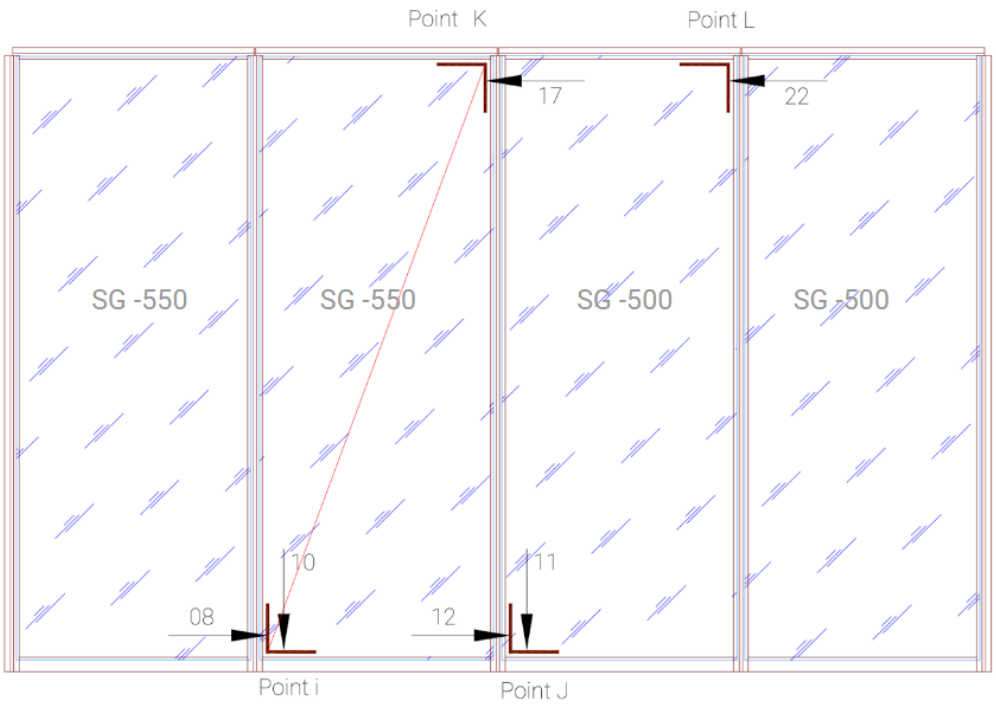

Figure 4.9 Above the location of the displacement transducers is mapped. On top the transducers placed on the framing and below the ones located for the glazing monitoring are presented.

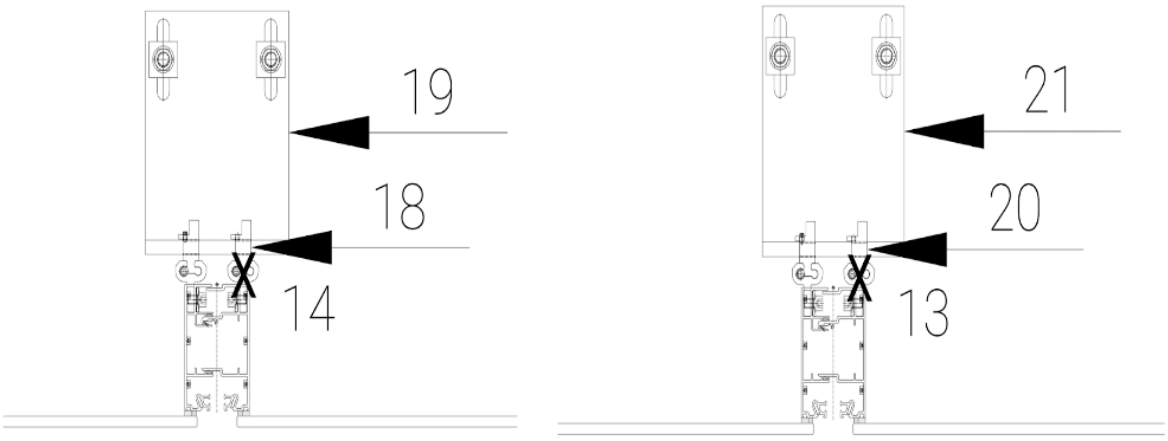

Figure 4.10: The displacement transducers located upon the fastening system to which the façade unit containing SG-500 (to the left) and SG-550 (to the right) is attached to (Source: Permasteelisa).

Testing Protocol

As previously mentioned, the seismic performance of the specimens is evaluated through the investigation of the impact of the displacement application on the multi-performance, namely the weather-tightness and seismic response, of the exterior enclosure. This objective is assessed through a series of dynamic seismic tests, as indicated by the Japanese standards (JASS 14) and typically performed whilst a project undergoes a seismic verification, as well as through a modified testing sequence, aiming to achieve the façade failure conditions.

In order to determine the drift level that occurs horizontally as a result of the earthquake loading, the following successive levels of displacement were induced during the experimental sequence on the mock-up façade elements. The distinct levels of a hazardous seismic incident are defined as presented below:

- 1st Level = H/300 = 12.50 mm: no damage can occur neither in the internal nor in the external components of the façade system
- 2nd Level = H/200 = 18.75 mm: the external elements should not transcend the permitted stress. The serviceability of the façade needs to be restored by the repair of the structural sealant
- 3rd Level = H/100 = 37.50 mm: neither components' fall down nor failure of glazing are permitted

These first three levels of horizontal displacement presented above were adopted from the indications of the Japanese standard (JASS 14, 2012). The first displacement level refers to a seismic event characterised by high probability, the second one to the highest earthquake event that has been recorded in the past and finally the third level to a seismic event with a return period of 100 years. Moreover, "H" represents the inter-storey height expressed in millimetres.

Starting from the lowest intestine (H/300) the displacement sequence increases, initially to the intermediate one H/200 and finally to the largest H/100. For each of the three intensities of the displacement application,

at least five loading cycles need to be implemented on the curtain wall unit. The cyclic manner of the displacement application is presented in Figure 4.11.

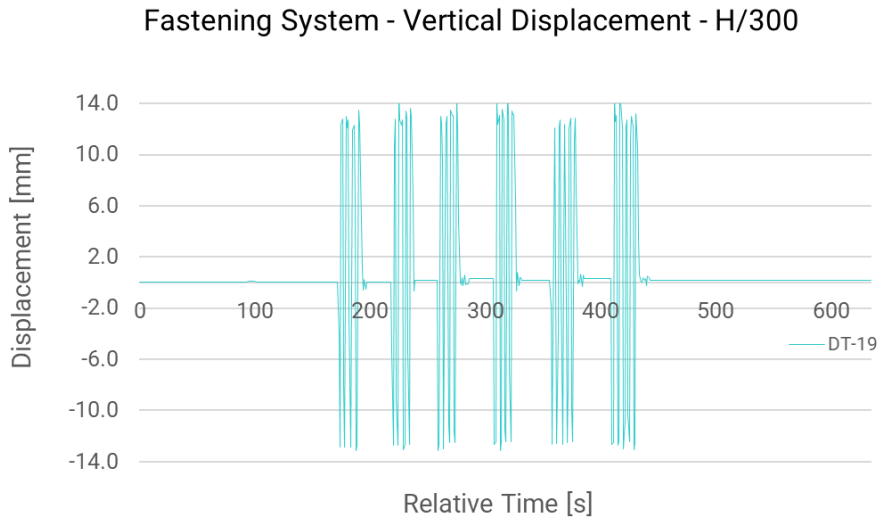

Figure 4.11: In this graph the cyclic displacement applied on the curtain wall units during the testing procedure is presented. The displacement values originate from the measurements as recorded by the transducer DT-19 applied on the fastening system of the unit under examination (see also Figure 4.10). In the present graph, the loading introduced during the first intensity H/300 is depicted. However, the remaining two drift ratios were applied in the same cyclical manner.

Complementary to the displacement application of the curtain wall unit elements that aim to evaluate its seismic behaviour, additional performance tests assessing the air-tightness of the system are performed. In this way, by proceeding with the air-permeability tests the serviceability performance of the curtain wall system is examined. It is reminded that JASS 14 prescribes that for the first displacement intensity, no failure occurrence is considered acceptable. Consequently, for this testing sequence the first air-leakage test is performed both prior to the lowest displacement application (H/300) and immediately after that. In this way, the potential decrease of the system's air-tightness, indicates the deterioration of the façade serviceability performance. The loss of the latter is practically assessed through the air flux increase recorded after the lowest displacement application. In the following paragraph a brief description of this particular testing follows.

During the test procedure the airflow Q_o [m^3/h] passing through the facade specimen is measured. For this to be achieved, a differential pressure, both negative and positive, is typically applied on the chamber. The airflow is monitored via an air flow metre, typically Pitot Tube or a diaphragm, for each of the incremental steps. Thereafter, the total air leakage is divided by the specimen area and the respective figure is plotted and presented on a chart. Typical Standards used as a reference for these performance tests are EN 12153 (EN 12153, 2000) and ASTM E 283 (ASTM E 283, 2004).

Consequently, the testing sequence of the present experimental case consists of the following:

- air-permeability test
- seismic displacement application of the lowest intensity H/300 =12.50 mm, 20 loading cycles

- air-permeability test
- seismic displacement application of the intermediate intensity H/200 =18.75 mm, 10 loading cycles
- seismic displacement application of the largest intensity H/100 =37.50 mm, 5 loading cycles

Experimental Behaviour

The global behaviour of the elements tested under seismic loading can be evaluated through the study of the displacement values as recorded by the monitoring system during the experimental procedure. In the graphs presented on Annex A a detailed overview of the displacement of the most characteristic points of the façade unit is provided.

Based on the experimental data plotted on the diagrams above demonstrating both vertical and horizontal displacements of the façade unit representative points, the global behaviour of the glazed curtain wall system undergoing seismic action can be assessed.

Rotational Behaviour of the Façade

The very first conclusion is that when the examined specimens undergo horizontal displacement, a rotation of the façade unit is recorded. In practice, this rotational behaviour is noticed through the evaluation of the experimental data, deriving from both the vertical and horizontal displacements, of the unit's diametric points. These points are the upper left connection of the top transom and left mullion and the lower connection of bottom transom and right mullion, presented as C and F respectively in Figure 4.9. The naming convention that has been attributed to each of the representative facade and unit points used for the evaluation of the seismic response of the façade unit is also presented.

Vertical Displacement

A second conclusion regarding the global behaviour of the façade unit is related to the amplitude of the vertical point displacements in relation to the horizontal displacement forced on the façade unit. The larger horizontal displacement applied to the curtain wall unit through the seismic beam, the more increased values of vertical displacements recorded on the characteristic points of the tested elements. For substantiating the conclusion above a point among the ones recorded has been used as a reference, namely the upper left point of the frame for the positive displacement application. The respective increment of its vertical displacement as a result of the increase of the horizontal forced displacement that is applied on the façade unit is described below:

- 2.80 mm vertical displacement for an inter-storey drift rate of H/300
- 3.55 mm vertical displacement for an inter-storey drift rate of H/200
- 7.10 mm vertical displacement for an inter-storey drift rate of H/100

Asymmetric Vertical Behaviour

An additional point of interest originated from the analysis of the experimental data is the asymmetrical specimen behaviour with regards to the direction of the displacement applied. As previously mentioned in the "Description of the Particular Testing" section, the displacement forced to the examined specimens is applied through the seismic beam in a cyclic manner. The loading is basically achieved through the displacement application in one direction, followed by the same displacement in the reverse direction. The response of the vertical displacement of the analysis point under the different directions of the external horizontal displacement is characterised as "asymmetric" due to the different and considerably small values recorded under the reverse displacement application.

Figure 4.12 depicts in grey, the initial curtain wall shape and in colour of those occurring after the implementation of the both the positive and negative horizontal displacement recreating the seismic inter-storey drift. In blue the points displaced by the same value are marked (symmetric situation) and in pink the ones experiencing uneven, with respect to each other, vertical displacement (asymmetric behaviour). As seen from this figure, symmetric and asymmetric behaviour exchange between the positive and negative displacement application.

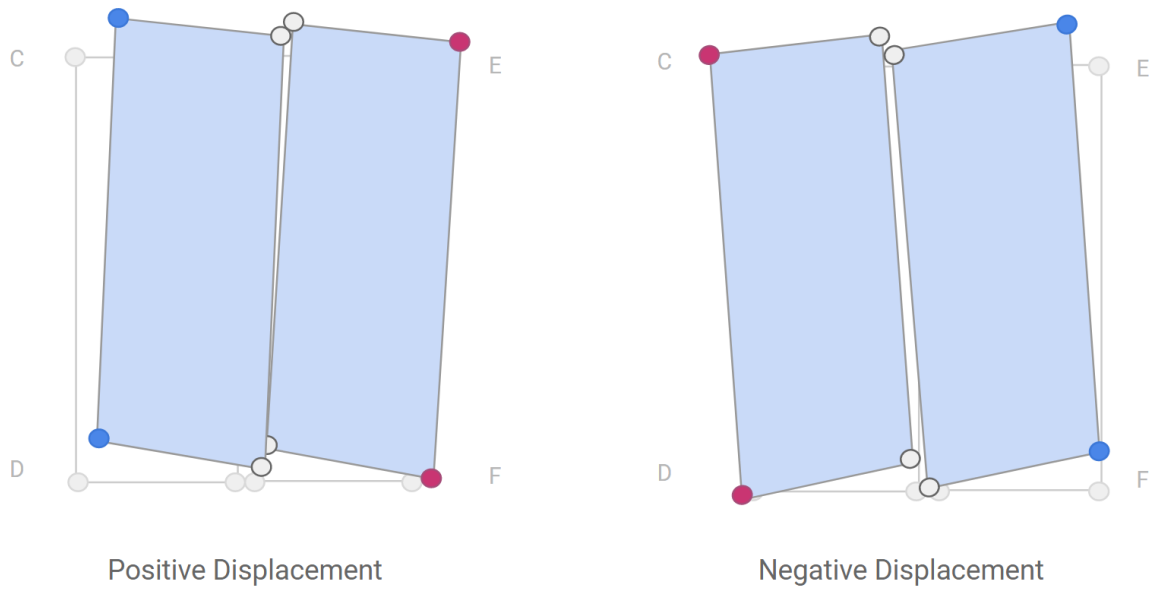

Figure 4.12: The figure above represents the deformed space of two adjacent out of the four adjacent curtain wall units examined during the experimental sequence. The deformed shapes originate from the plotting of the measurements taken during the experimental procedure, therefore recreate the actual curtain wall behaviour as observed during the mock-up test. To the left the façade reaction to the positive and to the right to the negative displacement application are presented.

More details are provided by examining the specific case of the inter-storey drift rate of H/300 both for the positive and negative displacement direction. Following the application of a positive displacement of +12.50 mm, larger and equal vertical to each other displacements of the representative points C and D are recorded (+1.80 mm in both cases) compared to the ones fluctuating around zero (+0.30 and +0.10 mm) measured under the application of the reverse, negative, horizontal displacement, -12.50 mm.

For the case of the other two characteristic points E and F for which the vertical displacement has also been studied, larger displacements are recorded for the negative direction -12.50 mm (+2.50 mm in both points) compared to the ones caused due to the reverse horizontal displacement applied on the façade units tested (+0.17 and -0.56 mm).

It is important to mention that the above is observed while evaluating the complete series of experimental results concentrated during the performance test. Therefore, similar differences between the positive and negative displacement application are also seen in the remaining two intensities, namely H/200 and H/100. For the substantiation of the aforementioned argument, experimental data of representative time-steps both for negative and positive displacements are presented in Table 4.2.

H/300 - Positive Displacement

Unit 2	Glass		Unit 3	Glass	
	I x:	2.25		J x:	2.80
	y:	3.15		y:	2.10
	K x:	11.00		L x:	11.00
	y:	-		y:	-
	Frame			Frame	
	A x:	11.80		C x:	12.00
	y:	2.80		y:	1.80
	B x:	1.85		D x:	2.30
	y:	2.85		y:	1.80
	G x:	-		E x:	-
	y:	0.90		y:	0.17
	H x:	-		F x:	-
	y:	0.10		y:	-0.56

H/300 - Negative Displacement

Unit 2	Glass		Unit 3	Glass	
	I x:	-1.75		J x:	-1.82
	y:	-0.55		y:	0.04
	K x:	-9.65		L x:	-10.25
	y:	-		y:	-
	Frame			Frame	
	A x:	-10.50		C x:	-11.00
	y:	0.40		y:	0.30
	B x:	-1.38		D x:	-1.40
	y:	-0.37		y:	0.10
	G x:	-		E x:	-
	y:	2.00		y:	2.50
	H x:	-		F x:	-
	y:	1.80		y:	2.50

Table 4.2: Above the displacements of the representative frame and glazing points are listed for the positive and negative displacement application. These tables describe the displacements referring to the inter-storey drift with intensity H/300. The response of both façade units, one consisting of a SIKA SG-500 (Unit 2) and the other (Unit 3) of SIKA SG-550 structural silicone joints is presented. Despite their slight quantitative differentiation, the façade units depict an equivalent qualitative behaviour with respect to the order of magnitude of vertical as well as horizontal displacement.

Horizontal Displacement

Regarding the horizontal movement of the unit, that is also differentiated based on the direction of the displacement applied. In fact, for the case of the negative displacement, the horizontal unit translation is restrained by the alignment screw that is placed for connecting the façade unit with the one right below. This connection results more in the deformation of the façade unit rather than in its rotation, instead of the rotational behaviour that is noticed when equivalent horizontal displacement (e.g. +12.50 mm) is applied in the positive direction. The detail of the alignment screw and the 3D drawing are presented to the left and right of Figure 4.13 respectively. In general, the relative restraint between the bottom transom and starter sill at the alignment screw position results in a vertical translation, since the screw is accommodated in a hole on the starter sill and due to the slot is allowed to slide along the bottom transom.

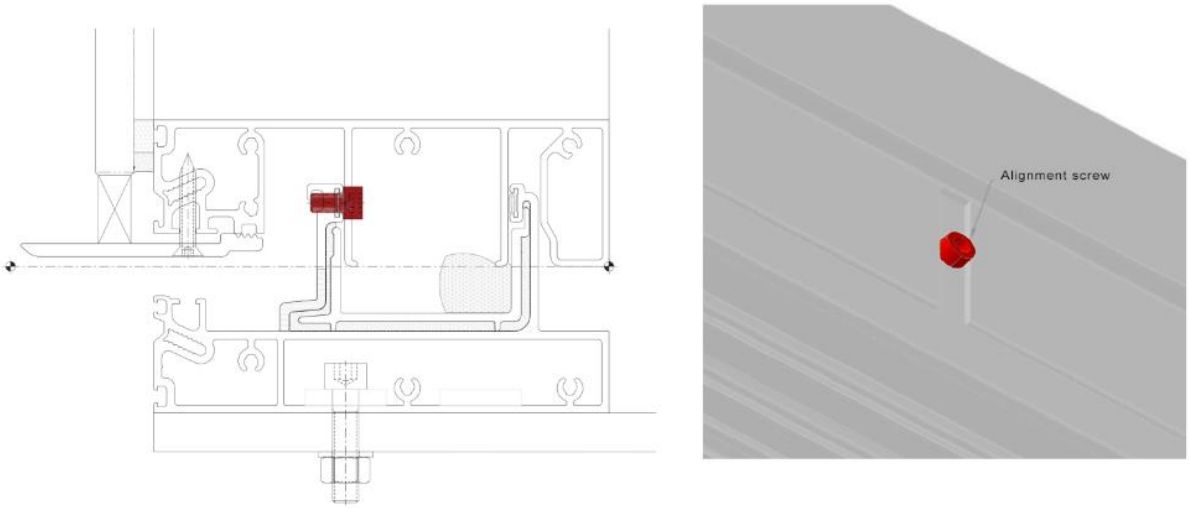

Figure 4.13: The detail to the left presents the connection of the bottom transom and the starter sill. In red the alignment screw is marked, the component that is responsible for the different curtain wall unit behaviour with regards to the horizontal displacement direction. To the right, the 3D drawing provides a better view of the alignment screw location in the curtain wall configuration (Source: Permasteelisa).

For the positive displacement a façade movement which resembles more a rotational behaviour is recorded, whereas for the negative equivalent a deformation similar to a rhomboidal shape is observed.

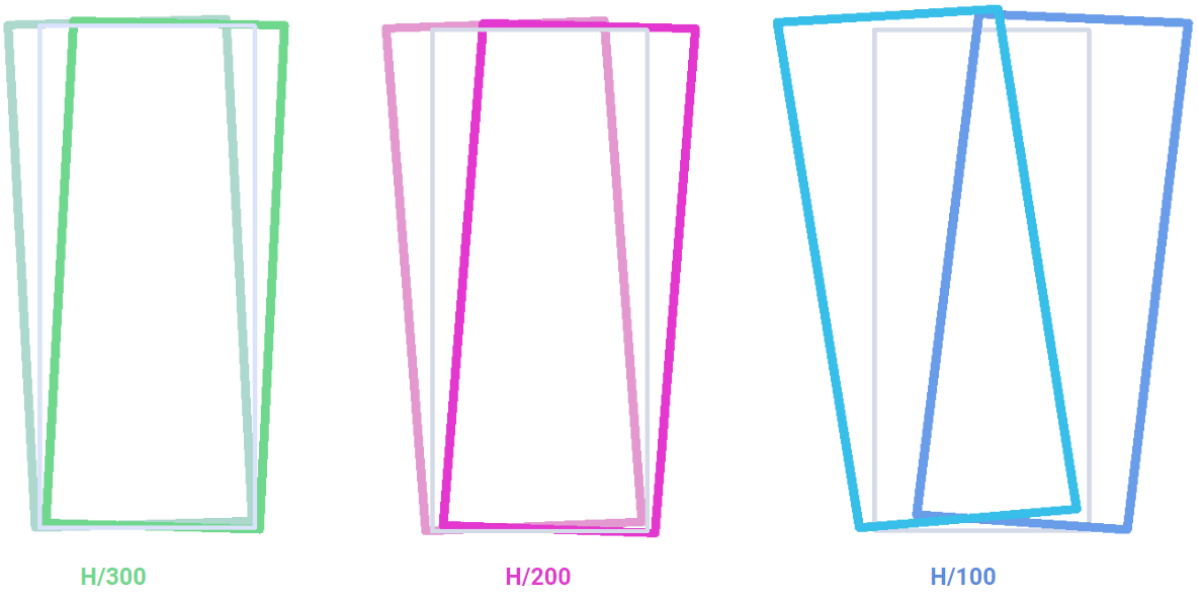

Figure 4.14: In the schematic views presented above the curtain wall response while undergoing the three levels of inter-storey drift is presented. The darker and lighter colours represent the positive and negative behaviour respectively.

The observation made above is depicted in Figure 4.14 and can be proven crucial, especially when considering that the unit rotation, as opposed to deformation, is less likely to result in glass breakage; in the first case due to the uniform unit behaviour, less stress is transferred to the glazing itself, preserving the glass integrity and serviceability. On the other hand, the unit deformational behaviour noticed while responding to negative displacement underlines the urgency of preventing possible risks that result in the glass integrity deterioration especially when considering that several glass damages and failures initiate due to the unit deformation.

Air-tightness Test

As already mentioned previously, during the testing sequence an air-tightness test has been conducted right before and after the implementation of the first and lowest intensity of the inter-storey drift over the curtain wall unit tested. The reason for incorporating it in the experimental sequence originates from the prescription of the reference regulation (JASS 14, 2012) that specifies that after the implementation of the H/300 displacement, the façade needs to maintain its serviceability, without any deterioration of its performance. Therefore, the performance test indicating the potential air-leakage of the façade system was conducted as prescribed by the European regulation EN 12153 (EN 12153, 2000) which is dedicated to the evaluation of the façade system performance while undergoing seismic actions of low intensity.

It is important to mention that this type of testing has not been repeated after the implementation of the intermediate (H/200) and the largest displacement intensities (H/100). The reason for that is the unavoidable maintenance that the curtain wall system is expected to be required after experiencing seismic events of such intensities.

Table 4.3 provides indication on the classification of the curtain wall systems based on the amount of airflow penetrating through the system. It can be easily seen that 1.5 m^3/m^2h is the limit the system should comply with at any pressure level in order for a specific classification to be achieved.

Pmax Air Pressure [Pa]	*Air Permeability [m^3/m^2h]*	*Classification*
150	*1.5*	*A1*
300	*1.5*	*A2*
450	*1.5*	*A3*
600	*1.5*	*A4*
>600	*1.5*	*AE*

Table 4.3: The performance classification of the curtain wall system as originating from the air-leakage test is presented above (Source: EN 12153, 2000).

The realisation of the air-leakage testing is presented in Figure 4.15 and is described as follows. Initially, three consecutive air-pressure increments are applied, with a value 10.0 % larger compared to the maximum pressure P_{max} of the test. Each of the increments is suggested to be implemented for at least three seconds and the air pressure value should be achieved within at least a second. The subsequent increments of 50.0

Pa until reaching 300.0 Pa are indicated to have a duration of at least ten seconds. Thereafter, 150.0 Pa increments follow until the maximum pressure P_{max} is achieved.

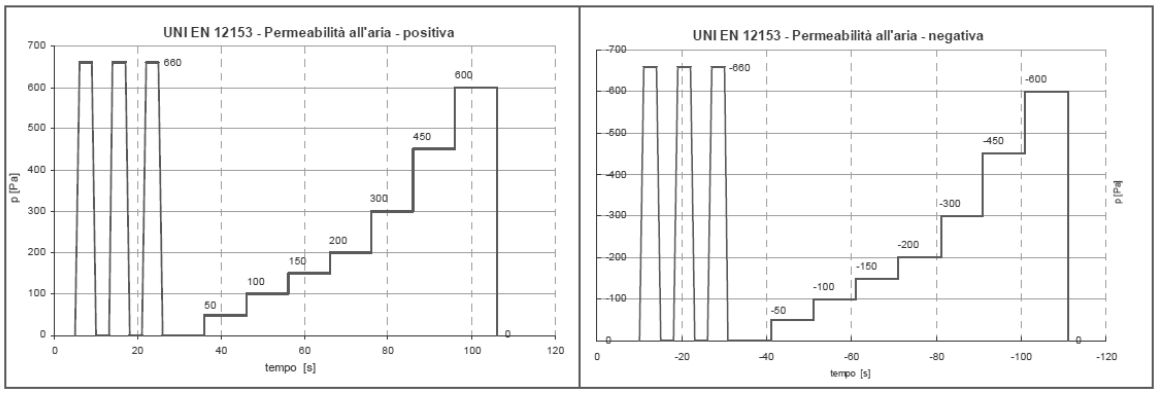

Figure 4.15: The procedure followed for both the positive and negative pressure application during the air-leakage testing is presented above (Source: EN 12153, 2000).

Specimen Response

The curtain wall response to the air-leakage testing prior and after the displacement application of first intensity has been recorded and is presented in Table 4.4.

	Before H/300		After H/300	
Pmax Air Pressure [Pa]	suction *[$m^3/m^2/h$]*	pression *[$m^3/m^2/h$]*	suction *[$m^3/m^2/h$]*	pression [$m^3/m^2/h$]
50	0.64	0.58	0.53	0.55
100	0.81	0.79	0.74	0.77
150	0.86	0.85	0.86	0.81
200	0.99	0.93	0.97	0.98
250	1.13	1.10	1.14	1.13
300	1.32	1.31	1.24	1.26
450	1.72	1.65	1.58	1.56
600	2.00	1.89	1.85	1.90

Table 4.4: The air-leakage testing results as monitored during the suction and pression stages (Source: Galli, 2011).

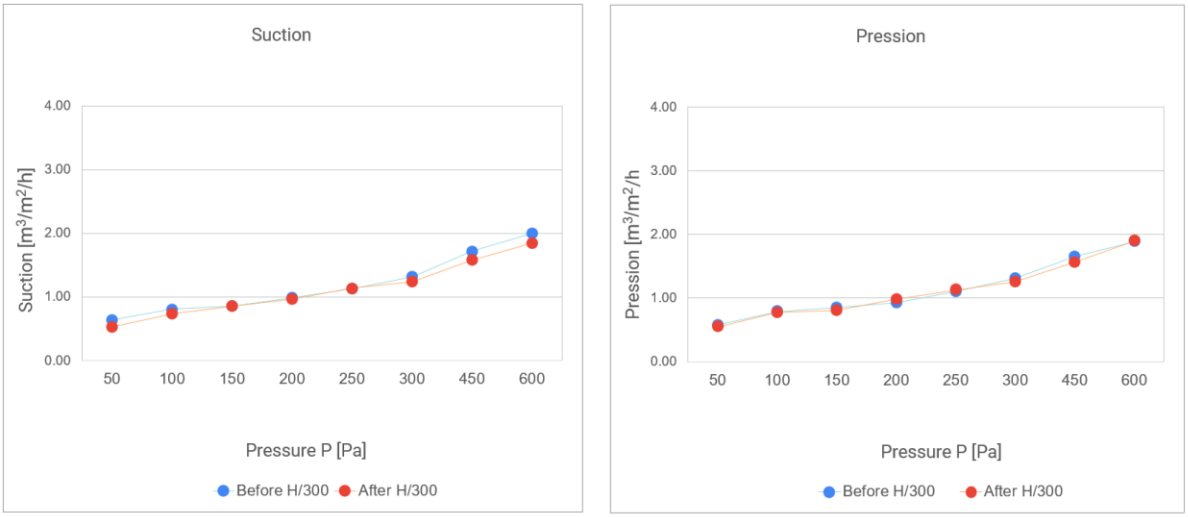

Figure 4.16: The air-leakage as measured before the implementation of the H/300 displacement application both for the cases of Suction and Pression.

Based on the Table 4.4 and Figures 4.16 presented above it can be clearly observed that during the implementation of the first and lowest intensity of the displacement application H/300 the curtain wall mock-up not only maintains, but also improves its performance in terms of air-tightness. Therefore, the JASS 14 requirements are satisfied. This specific curtain wall element is initially classified as A2 and the same classification remains after the displacement application, in accordance with EN 12153.

Global Behavioural Assessment

Unit Response to Different Seismic Intensity Levels

The different response of the glazed curtain wall system based on the levels of the seismic intensity, especially the behaviour during the final loading series corresponding to a displacement of H/100 = 37.50 mm, is probably the most interesting observation regarding the global behaviour of the façade unit tested. When the first cycle of loading is applied corresponding to a horizontal displacement equal to H/300 = 12.50 mm, the unit initiates to rotate. A similar rotational behaviour is recorded during the following series of loading circles of H/200 = 18.75 mm; this time, the unit presents an increased rotation.

As for the third loading series, already from the first loading cycle the vertical displacement of the examined points reaches the highest values recorded in the whole testing sequence. During the second loading circle though, the same vertical values are decreased until they reach almost zero, even from the third loading cycle. Regarding the horizontal displacement of the various test points, this fluctuates at a range below the original displacement value of H/100 = 37.50 mm. So, for the final displacement series, a rotational behaviour of the façade unit similar to the one observed during the previous series of loading cycles, is only recorded during the first loading cycle. Immediately after that, the unit rotational movement is moderated and eventually eliminated already from the third loading cycle. In fact, starting from this third loading cycle, the façade stops rotating and undergoes only a parallel-to-the-unit-plane horizontal sliding.

H/200 - Positive Displacement

Unit 2	Glass		Unit 3	Glass	
	I x:	3.56		J x:	4.53
	y:	4.12		y:	2.90
	K x:	16.00		L x:	16.50
	y:	-		y:	-
	Frame			Frame	
	A x:	17.20		C x:	18.00
	y:	3.55		y:	2.50
	B x:	3.08		D x:	3.90
	y:	3.55		y:	2.20
	G x:	-		E x:	-
	y:	1.04		y:	0.46
	H x:	-		F x:	-
	y:	-0.05		y:	-0.66

H/200 - Negative Displacement

Unit 2	Glass		Unit 3	Glass	
	I x:	-3.64		J x:	-2.90
	y:	-0.52		y:	0.01
	K x:	-14.00		L x:	-14.80
	y:	-		y:	-
	Frame			Frame	
	A x:	-15.85		C x:	-16.15
	y:	0.84		y:	0.56
	B x:	-3.15		D x:	-2.25
	y:	-0.36		y:	0.12
	G x:	-		E x:	-
	y:	2.78		y:	3.37
	H x:	-		F x:	-
	y:	2.80		y:	3.47

H/100 - Positive Displacement

Unit 2	Glass	0	1	2	3	4	5	6	Unit 3	Glass	0	1	2	3	4	5	6
	I x:	15.84	15.84	15.84	15.84	2.23	2.30	2.10		J x:	15.74	18.81	18.81	18.81	1.34	1.41	1.25
	y:	7.76	2.08	-0.90	-0.96	0.39	0.39	0.39		y:	6.42	-2.40	-0.68	-0.37	0.22	0.21	0.20
	K x:	35.00	35.00	-37.00	-36.00	1.70	1.70	1.90		L x:	35.10	36.30	37.50	35.80	1.53	1.43	1.75
	y:	-	-	-	-	-	-	-		y:	-	-	-	-	-	-	-
	Frame									Frame							
	A x:	35.73	35.59	-37.00	-35.80	1.20	1.28	1.29		C x:	36.80	36.80	37.50	34.18	0.97	0.69	0.94
	y:	7.10	1.68	0.44	0.23	0.26	0.25	0.21		y:	6.03	2.33	0.60	0.41	0.28	0.26	0.22
	B x:	19.70	31.40	-35.40	35.40	1.93	1.93	1.93		D x:	14.90	28.80	34.30	33.56	1.29	1.28	1.28
	y:	7.21	-0.59	-3.40	-4.56	-2.32	-2.32	-2.32		y:	5.76	0.39	-4.00	-5.69	-3.73	-3.74	-3.76
	G x:	-	-	-	-	-	-	-		E x:	-	-	-	-	-	-	-
	y:	3.93	1.14	0.17	0.12	0.21	0.19	0.14		y:	2.55	1.46	0.13	0.22	0.31	0.31	0.26
	H x:	-	-	-	-	-	-	-		F x:	-	-	-	-	-	-	-
	y:	2.12	0.33	-0.12	-0.15	-0.02	-0.02	-0.05		y:	0.20	0.59	1.36	1.43	1.59	1.58	1.55

H/100 - Negative Displacement

Unit 2	Glass	0	1	2	3	4	5	6	Unit 3	Glass	0	1	2	3	4	5	6
	I x:	-7.33	-16.29	-31.17	-31.95	2.23	2.30	2.10		J x:	-6.63	-21.30	-31.21	-31.21	1.34	1.41	1.25
	y:	-1.33	0.07	-0.33	-0.20	0.39	0.39	0.39		y:	0.62	1.00	0.47	0.24	0.22	0.21	0.20
	K x:	-30.00	-32.00	-34.00	-34.00	1.70	1.70	1.90		L x:	-30.70	-32.80	-34.40	-34.60	1.53	1.43	1.75
	y:	-	-	-	-	-	-	-		y:	-	-	-	-	-	-	-
	Frame									Frame							
	A x:	-32.45	-33.67	-35.20	-35.39	1.20	1.28	1.29		C x:	-34.16	-34.16	-34.18	-34.18	0.97	0.69	0.94
	y:	2.03	2.86	0.96	0.66	0.26	0.25	0.21		y:	2.82	2.32	0.52	0.34	0.28	0.26	0.22
	B x:	-6.14	-15.00	-30.10	-31.10	1.93	1.93	1.93		D x:	-5.26	-20.70	-32.99	-35.56	1.29	1.28	1.28
	y:	-0.95	0.24	-0.25	-1.71	-2.32	-2.32	-2.32		y:	0.92	1.17	0.33	-2.13	-3.73	-3.74	-3.76
	G x:	-	-	-	-	-	-	-		E x:	-	-	-	-	-	-	-
	y:	5.43	4.91	0.97	0.58	0.21	0.19	0.14		y:	7.78	4.29	1.00	0.67	0.31	0.31	0.26
	H x:	-	-	-	-	-	-	-		F x:	-	-	-	-	-	-	-
	y:	5.50	4.97	0.85	0.39	-0.02	-0.02	-0.05		y:	7.85	4.56	1.59	1.26	1.59	1.58	1.55

Tables 4.5: The first row of tables describes the displacement values corresponding to drift rates of H/200 whereas the second and the third those from the H/100 drift.

While studying the information provided in Tables 4.5, it is observed that for the cases of the lowest intensities only one set of values is used as a reference whereas the detailed displacements of more loading circles are presented for the third and largest displacement intensity (H/100). As already mentioned, the reason for that is that although the behaviour of the façade is uniform in the first two displacement applications, therefore the displacement values measured during the consecutive loading circles are very similar, this is not the case for the third intensity. There the curtain wall units behave differently in every loading cycle, therefore the displacement variation of the representative points is in detail described per

loading step. As for the reference values presented for the lowest and intermediate intensity, although they generally present reduced variation throughout the loading steps, they have derived through the averaging of three or four successive measurements aiming for a more adequate representation.

According to the researcher examining the same experimental results, (Galli, 2011) who also attended the experimental campaign, the façade unit was clearly rotating during the two first displacement series. However, when the third and final loading series was applied, the curtain wall unit was observed to initially rotate. This rotational behaviour was suddenly terminated when the extraction of the alignment screw from its initial place in the transom occurred, accompanied by a sound originating from the façade specimen. After that point, the façade unit kept sliding without rotating as long as it underwent the horizontal displacement corresponding to H/100. Figure 4.17 depicts to the left the slot of the transom inside which the alignment screw is located and to the right the alignment screw itself being fully extracted from the transom.

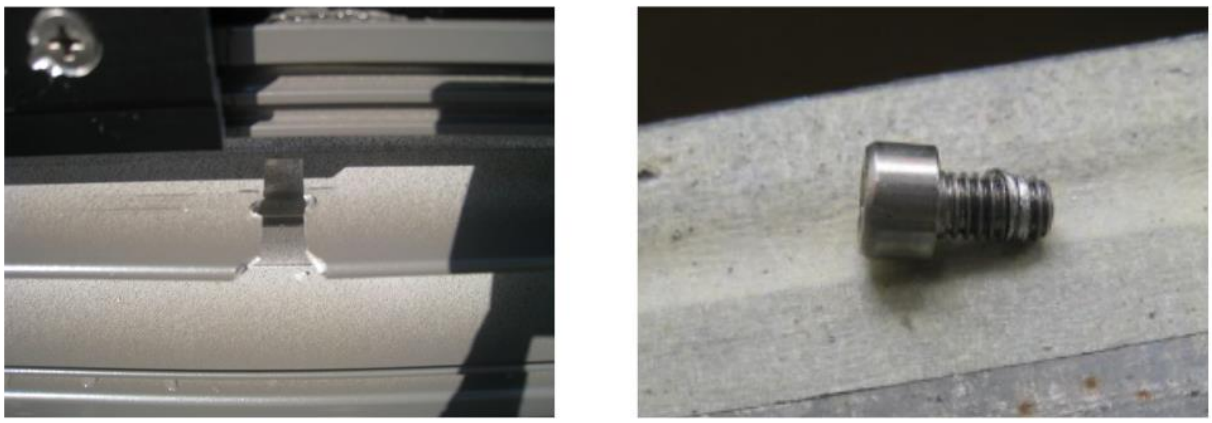

Figure 4.17: To the left, the slot on the transom of the curtain wall unit where the alignment screw is placed is depicted. To the right, the alignment screw after bearing the hole in the transom, is completely extracted from the transom (Source Permasteelisa).

Based on this study, the above situation can be substantiated through the existence of the alignment screw in the façade unit. More precisely, it is attributed to its bearing phenomena to the hole located on the unit transom as depicted in Figure 4.18. The same bearing phenomena can be used for explaining the initial decrease and eventually termination of the rotational behaviour that is observed only at the first two series of H/100 loading. In fact, the reduction of the vertical displacement of the points tested which results in the subsequent unit rotation decrease is adequately explained as follows: As the whole of the transom widens, it can no longer restrain the alignment screw which eventually results in the extraction of the screw from the hole. In the absence of the alignment screw and the limitations applied to the unit movement, the rotational behaviour of the element is no longer facilitated. Consequently, the curtain wall element response while undergoing horizontal displacement is restrained to the horizontal sliding.

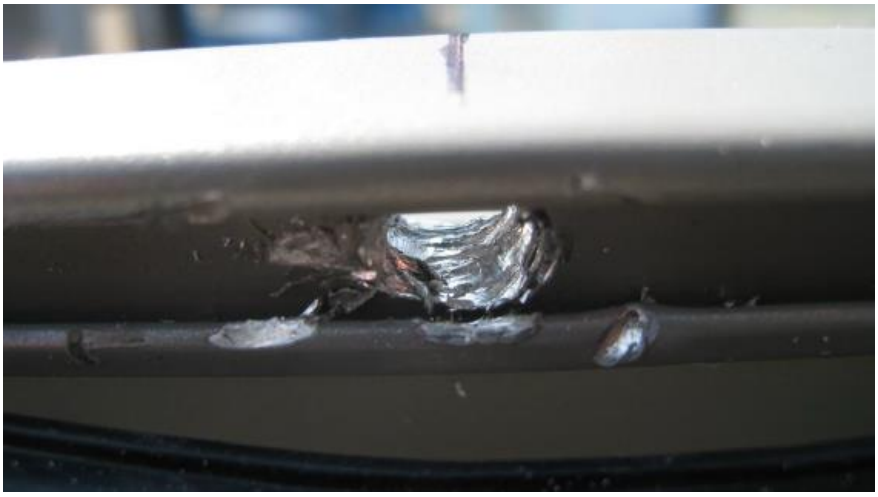

Figure 4.18: The extraction of the alignment screw from its original location in the transom of the façade element. The bearing phenomena after the performance tests recreating the seismic intensities are depicted above (Source: Permasteelisa).

Façade Assessment Under Seismic Action

Apart from the damage noticed on the alignment screw originally applied on the transom ensuring the connection of the façade element with the neighbouring one, no further major damages of either the aluminium frame, the glazing or the fastening system have been recorded during the performance test.

Based on this observation it can be concluded that the unitised curtain wall tested under seismic events behaves in the desired way. In fact, during the application of the first seismic intensity the unit tested appears to fully maintain its serviceability function. For the second level of the seismic intensity where a horizontal displacement of H/200 is applied, not a single damage of the façade elements is noticed. Finally, for the most severe series of loading, the deactivation of the initial deformational as well as deformational behaviour of the façade unit is noticed not later than the first loading cycles. During this phase, no remarkable damages are noticed; instead, the response of the façade unit is restricted to the horizontal sliding. Therefore, the ultimate limit state of the curtain wall unit is also preserved.

Translational and Rotational Movement

The evaluation of the façade unit behaviour is expected to be further reinforced through the assessment of the translational and rotational movements induced to the curtain wall units tested while undergoing different intensities of seismic action.

The above is practically quantified through the study of the diagonal of the façade units tested by means of its i) rotation and ii) elongation/contraction. It is important to mention that the diagonal of the unit is a fictional element introduced in the analysis simply for the ease of assessing the curtain wall unit behaviour. In practice, as already qualitatively defined previously while evaluating the rotational behaviour of the façade, the unit rotation is determined by the combination of the vertical and horizontal movement of the curtain wall unit. In order for the quantification of this rotation, a fictional line connecting an upper transom corner with the diametric one of the lower transoms is created as observed in Figure 4.19.

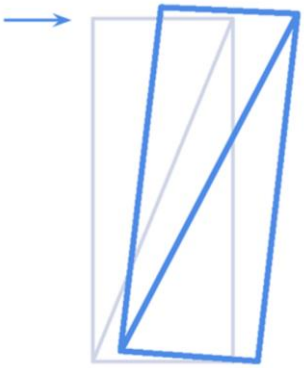

Figure 4.19: In this schematic view the curtain wall unit diagonal is presented to connect the diagonal corners of the curtain wall unit. The coloured deformed shape represents the unit response to the horizontal displacement application. As seen in the visualisation, the diagonal is also affected. Therefore, the rotation, elongation or contraction of the diagonal can be defined based on the initial state of the diagonal.

In order for the more elaborate evaluation of the curtain wall response, separate diagonals are defined for the framing and the glaze pane. This diagonal fictional line, of both the glazing and the framing, is then evaluated based on its rotational and/or translation movement it undergoes while following the curtain wall unit response to the different displacement application rates.

Below, the respective values representing the translational/rotational movement of the curtain wall diagonal, therefore of the units tested in general, are concentrated and presented for each of the three seismic level intensities. Initially the information regarding the frame of the façade unit is provided in Table 4.6. Thereafter, the respective information for the glazing is presented in Table 4.7.

Rotational / Translation Movement & Deformation of Frame						
Displacement	H/300		H/200		H/100	
Silicone Type	SG-500	SG-550	SG-500	SG-550	SG-500	SG-550
Rotation [deg]	0.14	0.13	0.17	0.19	0.43	0.39
Diagonal Elongation [mm]	0.89	0.80	1.13	1.05	2.44	2.38
Diagonal Elongation [%]	0.022	0.020	0.028	0.026	0.061	0.060

Table 4.6: The translational and rotational unit response as expressed by the frame diagonal is depicted above. The values provided refer to the two types of structural silicone joints, SG-500 and SG-550 and to the three displacement applications rates H/300, H/200 and H/100.

As expected, the rotation of the unit as well as its diagonal elongation increases as the external deformation applied on the façade unit becomes larger. However, it can be argued that the deformation of the aluminium frame as expressed through its diagonal remains in a limited state, not even reaching an amount of 1.0 % even during the third and more severe drift rate application.

Rotational / Translation Movement & Deformation of Glazing						
Displacement	H/300		H/200		H/100	
Silicone Type	SG-500	SG-550	SG-500	SG-550	SG-500	SG-550
Glass Rotation [deg]	0.14	0.13	0.18	0.19	0.29	0.32

Table 4.7: The rotational behaviour of the glazing pane is depicted in the table above for the different displacement intensities and for the two structural silicone types implemented in the curtain wall configuration tested during this experimental campaign.

The different behaviour of the glazing compared to the one of the aluminium frame is depicted in the values of the Table 4.7. Although the glazing pane follows the aluminium frame movement by rotating due to the structural silicone that ensures the glazing-frame connection, the glazing behaves rigidly. Therefore, under the seismic action applied to the façade units tested, the glass plate appears to rotate but not to deform its shape. Consequently, zero deformation of the glazing diagonal is observed.

Structural Silicone Joint Impact

An additional interesting topic examined through this experiment relates to the evaluation of the impact that a structural silicone joint has over the global seismic behaviour of the façade elements examined. As previously explained in this chapter, two different silicone joints have been assessed during the experimental sequence. In more detail, as previously described in this chapter and previewed in Figure 4.9, the first as well as the second units were provided with a SIKA SG-500 joint whereas the remaining two with a SIKA SG-550 silicone joint. The dimensions of the structural silicone joints also differentiated, with the first having 10.0 * 6.0 mm and the second one 6.0 * 6.0 mm.

Below, the influence of the two structural silicone joints on the façade overall behaviour is previewed in terms of the different rotational behaviour of the frame first and of the glazing afterwards.

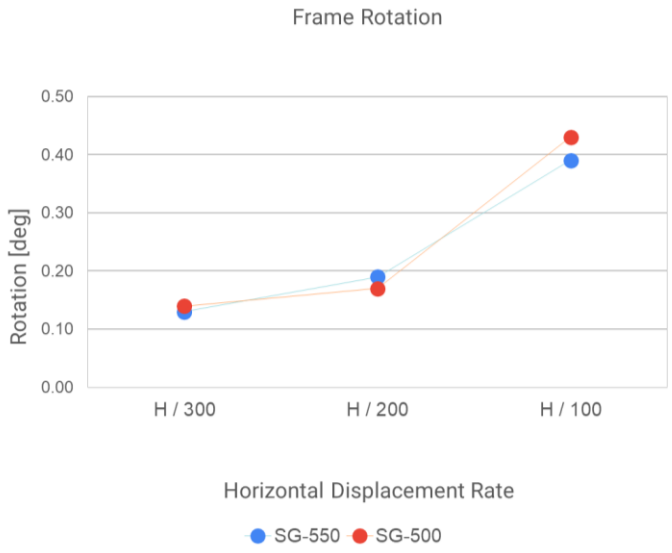

Figure 4.20: In the figure above the variation of the frame rotation is presented as recorded during the experimental campaign for each of the three displacement rates.

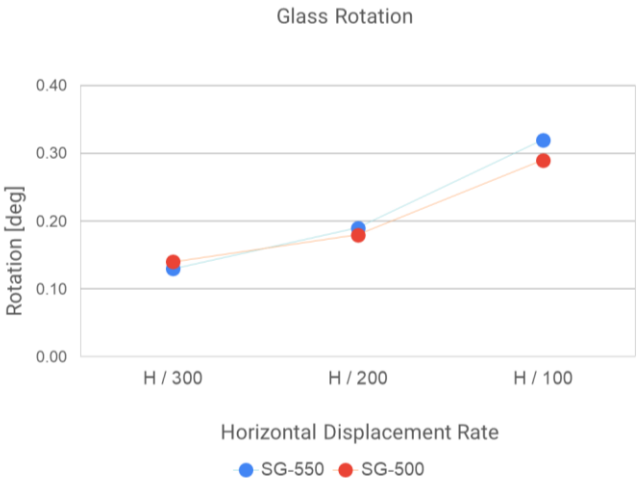

Figure 4.21: Similar to the previous figure, the response of the glazing rotation with regards to the different displacement values, in practice drift rations, is presented.

Based on the graphs presented in Figures 4.20 and 4.21 above, it can be concluded that the different structural silicone joints indeed affect the global behaviour of the façade unit while subjected to seismic loadings. However, the response of the different units is not completely unrelated; in fact, the curves expressing the behaviour of the façade units follow the same trend only presenting little qualitative differences, which in any case does not overpass the range of a rotation of 0.5 degrees.

Taking into consideration that the implementation of the structural silicone in a curtain wall configuration primarily aims to enhance the glazing pane collaboration with the aluminium frame, it can be argued that the structural silicone SG-500 provides weaker connection between the aforementioned elements as opposed to SG-550. In the first case, the rotational movement of the frame and the one of the glass plate are less relevant to each other compared to the respective ones recorded for the units with SG-550 joints. For the third and hardest seismic intensity for example, the rotation of the frame is measured as 0.29 mm and for the glass as 0.43 mm in the case of SG-500. For the units with SG-550 on the other hand, the same values range at 0.39 mm and 0.32 mm respectively proving that the rotational movement of the glazing follows closer the one of the frames, therefore that SG-550 is less deformable and stiffer than SG-500.

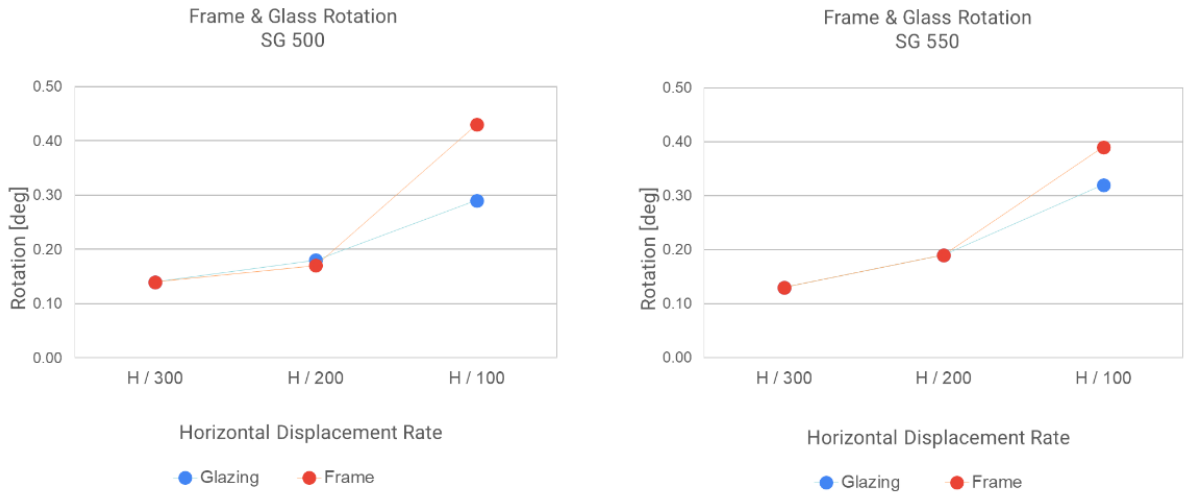

Figure 4.22: In the figure above the rotational behaviour of both the glazing and the framing combined are presented for the case of the structural silicone joint SG-500 to the left and of SG-550 to the right respectively.

The aforementioned point can be further substantiated by the fact that the frame rotation in the case of SG-500 is increased compared to that of SG-550 as a result of the stronger restrain that the stiffer glazing provides in the case of SG-550. Although in both cases the glass plane behaves rigidly, in Figure 4.22 it appears that the frame rotational behaviour is more affected in the case of SG-500, therefore higher collaboration between the façade elements is achieved.

According to the previous, the cooperation of the two façade elements, namely the aluminium frame and the glazing, can be defined and, if needed, enhanced through the application of the proper structural silicone joint. As it can already be seen by comparing SG-500 and SG-550, the stiffer and less deformable the connection is, the greater the frame-to-glazing collaboration.

Part II

Finite Element Analysis

Chapter 5

Finite Element Modelling

The purpose of this chapter is to present the modelling approach that has been adopted during this specific research topic. Initially a short literature review of finite element modelling, its emergence, evolution and overall importance is outlined followed by the aim of the current finite element modelling. Additionally, a reference to the simplification criteria considered for this study is included.

Later, the geometrical and material properties determination of the principal curtain wall components simulated during this finite element modelling is presented. In this section of the study the elements used for the simulation of each of the curtain wall elements are demonstrated separately accompanied by relevant substantiation. Additionally, the calculation process followed for the identification of the main material properties is also depicted. Moreover, an overview of the meshing options, the loading as well as the boundary conditions applied on the model provide the outline of the first set of parameters that composed the initial version of the numerical simulation.

Thereafter, a set of notions frequently repeated in the study is presented in the sense of clarifications. The second phase of the modelling approach during which a better insight of the properties and the overall behaviour of the finite element model is then presented. This is the modelling stage that eventually results in what is referred to as the improved version of the initial numerical model.

The further elaboration of the numerical approach developed during the previous modelling stages is introduced later. This modelling stage essentially forms the calibration process of the DIANA simulation. In practice, a better correspondence of the numerical model to the equivalent experimental behaviour is attempted through the more accurate implementation of the allowable movements of the façade and the update of the displacement restraints as determined by the boundary conditions. Eventually, a more accurate recreation of the actual curtain wall behaviour is achieved.

A concise overview of all the attempts made for the further improvement of the initial DIANA model is then presented. Later various considerations related to the possibilities and points of improvement of the current modelling approach are listed. Finally, the conclusions and main findings of this modelling approach are outlined at the end of the present chapter in the Numerical Response Assessment section.

Importance of Finite Element Modelling

A brief introduction to the fundamental aspects of the finite element modelling is considered essential for contextualising the topics later to be discussed in the present section. A finite element model (FEM) is a numerical model that aims to represent as closely as possible the behaviour of an actual system. In order for this to be achieved, the following parameters need to be defined (Galli, 2011):

- The geometry of the physical system itself
- The materials of the system along with their properties, identified through constitutive equations
- The constraints as well as the external loadings applied into the system, typically defined by the boundary conditions selected
- The analysis approach that is applied, mainly identified through the selection of the appropriate solver

In general the incorporation of the finite element method in the numerical simulations has been proven to contribute to the thorough understanding of the curtain wall behavioural analysis when subjected to seismic action. In addition, numerical simulations are ideal for the determination of the parameters affecting the limit state deformation capacity of curtain wall systems, while constituting a useful validation means of various laboratory results. Ultimately, numerical simulation can provide a viable alternative to the generally costly, time and resource consuming mock-up testings (Bârnaure & Voiculescu, 2013).

Literature Review of Numerical Studies

Various numerical studies have also been performed over the past years aiming to assess the performance of glazed curtain walls during seismic events. The importance of the analytical formulations in the prediction of the glazed systems drift capacity has been identified already almost half a century ago. A mentioned previously on the current study, already from the 1960s, Bouwkamp and Meehan (Bouwkamp & Meehan, 1960) proposed the presentation of the glazing panel displacement when undergoing in-plane loading as the composition of a rigid rotation until the glazing-to-frame conduct is achieved and of a compressive deformation on the glazing diagonal occurring after the aforementioned contact. This assumption formed the basis for Sucuoğlu and Vallabhan (Sucuoğlu & Vallabhan, 1997) for the development of an analytical procedure related to the drift capacity of the glazed frames. This specific analytic formulation was later applied by Sivanerupan, Wilson et al. (Sivanerupan et al., 2009) during their drift capacity and seismic demand evaluation.

The first attempt of substituting the full-scale mock-up tests with prediction models has been proposed by Memari, Behr et al. (Memari et al., 2000). In practice, the ultimate drift prediction of glazed curtain walls was suggested. Later, a rating system evaluating the seismic cracking drift of existing curtain wall systems was suggested by Memari and Shirazi (Memari & Shirazi, 2002). This rating system was based on a system assigning points to the curtain walls with regards to the seismic drift demand and the mechanical as well as geometric properties of each of the systems. Later, a finite element model accompanied by an experimental calibration was proposed by the same researchers aiming to contribute to the predictions of the behaviour of both existing and new glazed curtain wall systems. More specifically, this finite element aimed to provide insight on the identification of the seismic drift at which glass cracking or fallout occurs (Memari et al., 2007, Memari et al., 2011).

More recent approaches include the simulation of stick curtain wall systems and the comparison of the numerical results with the experimental equivalent ones (Caterino et al., 2017). Objectives such as the impact of the non-linear interaction of the aluminium with the glazing on the overall stiffness and strength of the composite configuration while subjected to incremental loading were intended to be answered.

In general, over the past years the interest of both the researchers and the industry as well has been shifted to the development of numerical models able to accurately predict the lateral response of various façade systems. Numerical simulations typically attempt to provide a better understanding of the non-linear interaction of the glazing panes and the aluminium frame that importantly affects the stiffness as well as the strength of the curtain wall systems while imposed on stepwise incremental loading activities, such as seismic events. Other relations and phenomena that underpin the mechanical global behaviour of glazed curtain wall systems that are typically aimed to be reproduced through numerical models are the deformability of the aluminium frame, the clearance between the aluminium frame and he glass panels, the

mechanical distortion of the gaskets, the glass-to-gasket friction as well as the rotational stiffness of the mullion-to-transom connection (Casagrande et al., 2017, Caterino et al., 2017).

The ultimate purpose of the utilisation of finite element models in the multi-performance and mainly seismic assessment of glazed curtain wall units is the eventual elimination of the necessity for developing the generally expensive full-scale experimental testing.

Case Study Simulation

Purpose

The finite element model developed during the existing study can be evaluated initially by reviewing the overall results and the proximity of the model behaviour to the one observed during the experimental procedure when undergoing similar loading conditions. It is additionally expected to contribute to the better understanding of the seismic drift correlation with the actual damages and failure mechanisms of glazed curtain wall systems. Eventually, while combined with relevant studies attempting to relate numerical with actual experimental results, interesting suggestions regarding the improvement and development of the current seismic design and verification methods are expected to arise.

Finally, this modelling attempt aspires to lay the basis for the initiation of the curtain wall finite element modelling through the sophisticated software DIANA FEA, that despite its wide application in numerous sectors, such as geotechnical, dams and dikes, reinforced concrete applications and many more, it hasn't been utilised yet for the examination of curtain wall systems through numerical modelling.

Simplification Criteria

In order to approach the actual behaviour of the unitised curtain wall system that has been experimentally tested under seismic loading, a number of simplifications had to be adopted. The reason for that lies both on the principle of finite element modelling that is the deconstruction of the actual physical model in simpler elements as well as on the available possibilities of the boundary conditions set by the DIANA FEA software. The ultimate purpose is to eliminate the approximations introduced in the model since they inevitably affect its sensitivity in presenting accurate results.

Therefore, the simulation of the actual curtain wall unit through a finite element model commenced with the consideration of various simplifications. Later on, based on the familiarity gained with the numerical approach followed by the DIANA FEA software and on the numerical behaviour observation with respect to the one recorded during the experimental sequence, some of the initial modelling simplifications converted into more educated approaches.

In- & Out-of-plane Curtain Wall Behaviour

One important aspect of the present modelling procedure is the clarification of the curtain wall behaviours aimed to be captured in the existing model. Generally, in order for the overall curtain wall behaviour under seismic action to be assessed, the development of a bi-directional model capturing both the in- and out-of-

plane behaviours is required. Although, plenty of existing studies (Bouwkamp & Meehan, 1960, Sucuoğlu & Vallabhan, 1997, King & Lim, 1988, Pantelides & Behr, 1994, Behr et al., 1995) have focused solely on the in- or out-of-plane curtain wall response managing to assess key interactions and behaviours important for the curtain wall analysis considerably well, the incorporation of both the behaviours in a single model is generally considered better practice, especially when a multi-hazard analysis is intended.

As already mentioned in Chapter 3 the out-of-plane response of the curtain wall system is mostly related to the wind pressure acting on the previous, whereas the in-plane behaviour is mostly driven by seismic actions. Moreover, it has been also reported that the wind pressure determines the design as well as the verification process of the curtain wall configurations and their components (Behr, 2009, Willford, 2006) since it is typically larger, up to an order of magnitude, compared to the seismic actions applied on the building structures. However, seismic norms and regulations typically prescribe the façade verification while subjected to force since the latter is perceived as more significant for the building interior and is additionally more comparable to wind-induced action over the non-structural elements of a building at lower heights. Therefore, representative seismic regulations, such as NZS and FEMA, when considering the design and modelling phase of typical unitised curtain wall systems, clearly specify their seismic, instead of wind, verification. In any case, both the façade unit as a whole and every component individually, needs to be designed and verified for a stronger action, such as that induced by wind, irrespectively of the seismic verification requirements (Galli, 2011).

Based on the elaboration provided above, the study of only the in-plane behaviour of the curtain wall unit is considered acceptable. Undeniably, the incorporation of the out-of-plane movement in addition to the in-plane capture would lead to a more realistic simulation of the curtain wall system examined. Nevertheless, when considering the additional complexity and error margins inevitably introduced to the modelling procedure on one hand and the significantly larger impact the seismic actions have on the in-plane compared to the out-of-plane curtain wall behaviour, it becomes evident that the simplification of the modelling procedure to include solely the in-plane behaviour is both acceptable and efficient. The efficiency mentioned in this context relates to the considerable reduction of the model complexity and computational time, relieving it from the introduction of extra simplifications and further inaccuracies. For this reason, several experimental testings, including the one carried out in this specific case study involve only the in-plane direction.

In the following section, the modelling procedure realised in the present study is described. In particular, the selection of the modelling elements used for the simulation of each of the curtain wall components is presented accompanied by the respective substantiation. Moreover, additional modelling aspects such as the boundary as well as the loading conditions are also listed below.

Curtain Wall Elements Simulation

After the main simplifications and approximations introduced during this simulation are outlined, the actual modelling process followed by this study is described. Initially the elements chosen for the simulation of each façade component are presented. The overview of the material properties later attributed to them complements the simulation approach incorporated for this numerical modelling.

Geometrical & Material Properties

Frame

Moving to the curtain wall framing, the aluminium sections of mullions and transoms were introduced to the numerical model as beam elements. It is important to mention that the exact extruded profiles were not inserted in the simulation. Instead, the external dimensions as well as the respective moment of inertia were calculated and later introduced to the DIANA environment. The reason for not importing the accurate but extremely complex extruded mullion and transom profiles is that additional model complexity as well as computational time would have been introduced in the numerical simulation. Additionally, the limitation of the educational version of the software regarding the maximum threshold number of the elements analysed made the need of the framing profiles simplification into equivalent less complex elements almost imperative.

Finally, the selection of beam elements to represent the aluminium frames instead of the actual detailed extruded profiles, was partially made taking into consideration the need for an effective way of simulating the transom to mullion joint. Since the attempt to join different profiles would inevitably introduce additionally larger approximations to the modelling procedure, the much simpler option of the beam elements was decided to be implemented, offering also the option of connecting the elements with either unites or rigid connections, that typically allow the modeller to define the degrees of freedom attributed to the model. For this specific modelling case, all the three degrees of freedom available were restrained, not allowing the relative rotation of the connected elements. This modelling approach does not follow the actual situation completely faithfully since in reality the transom-to-mullion connection presents a rotational stiffness. However, this stiffness is not that large to completely restrain the rotation of the elements. In any case an intermediate modelling approach would recreate more accurately the realistic situation. Nevertheless, the current modelling approach is still considered adequate for the effective representation of the actual situation.

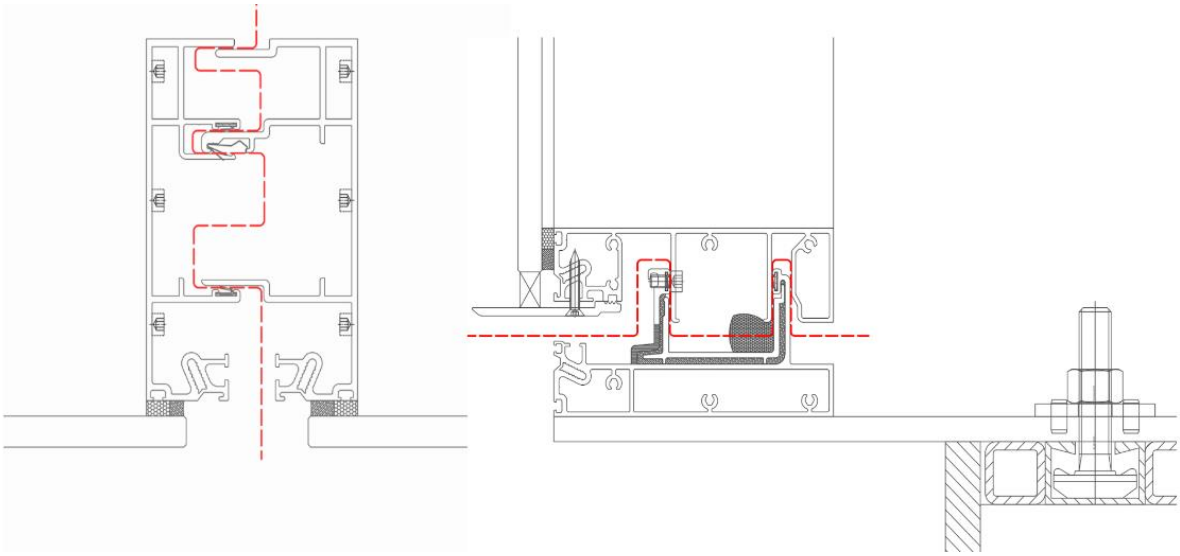

Figure 5.1: In the details above, the division between the adjacent framing profiles, to the left of the left and right mullion and to the right the lower transom on top from the bottom transom/ starter sill, are presented. The red line indicates the boundary between the framing areas used for the calculation of the respective equivalent area

and moment of inertia eventually introduced as properties to the arbitrary shapes of the aluminium framing elements in the DIANA environment.

Although the complicated framing profiles as seen in Figure 5.1 were chosen to be simulated through simplified 2D-beam elements the actual geometrical characteristics and properties of the framing elements were attempted to be captured. In order for this to be possible, the DIANA option of "arbitrary shapes" was selected, so that parameters such as the equivalent cross-section area as well as the respective moment of inertia could be introduced in the software. For this reason, a closer study of the details of the façade elements tested and thereafter simulated through the numerical procedure examined in this chapter, had to be conducted. Also, for the calculation of parameters above, namely the framing cross-section and the moment of inertia, the respective commands of the Autocad software were utilised and were proven highly helpful.

In practice, by implementing into the Autocad environment the detailed drawings of the left and right mullion and of the upper and lower transom, creating the respective regions and subtracting the void areas, the actual aluminium areas remained. For these areas, the useful properties of the area [mm^2] as well as the moment of inertia [mm^4] were extracted. Although Autocad calculated two principal moments of inertia with respect to the centroid of the configuration (I & J), the one obtained from the weakest axis (J) was introduced in the DIANA environment. This decision was based on the fact that only the 2D behaviour of the curtain wall is evaluated, and therefore simulated. In addition, only one property of the material inertia was required by the DIANA environment. For this reason, based on the values of the dimensions, the prevailing axis was decided to be the weakest one.

A procedure identical to the one described for simulation of the mullion and transom elements was also followed for the representation of the starter sills into the numerical modelling. The reason being that, as previously explained, in practice starter sills are the upper transoms of the façade unit that in real cases would exist below the curtain wall unit under examination.

Glass

One of the most important aspects of the modelling procedure refers to the curtain wall element that, based on the information provided above, is the one most commonly seen to break or even fallout from the framing unit causing the curtain wall configuration to fail. In the current modelling procedure, the glazing itself was decided to be simulated through shell elements. The selection of this particular element is ideal for the further division into numerous regular plates of reduced dimensions during the meshing required for each numerical analysis. However, the most interesting aspect of this simulation aspect is the correct recreation of the retaining system that eventually attaches the glazing to the aluminium frame of the curtain wall system.

The vital importance of the adequate simulation of the retaining system is recognised when the following is considered. The efficient modelling of the retaining system defines to a great extent the ability of the numerical model to recreate the large stiffness of the glazing material on one hand as well as its rigid behaviour that eventually defines the stiffness of the entire glazing unit. More importantly, the connection of the glazing unit with the adjacent unit framing is the principal parameter defining the appropriate collaboration between the glazing pane and the framing, and consequently, the ability of the numerical model to realistically capture the actual unit behaviour under a seismic event.

Regarding the material properties attributed to the aluminium as well as the glazing elements, these were linear and are presented in Table 5.1.

Linear Material Properties			
	Aluminium	*Glazing*	*Units*
Young's Modulus (E)	*70000*	*70000*	N/mm^2
Poisson's Ratio (v)	*0.23*	*0.25*	-
Mass Density (ρ)	*2.7e-0.9*	*2.5e-0.9*	T/mm^3

Table 5.1: The linear properties attributed to the aluminium framing and the glazing respectively for the numerical model developed in the DIANA software.

Glazing-to-Fame Connection

Finally, another modelling aspect that was proven to be challenging was this of the material connecting the glazing with the frame. The idea prevailing while deciding over the correct representation of this material was that a single material should be applied in the numerical procedure, simulating not only the material properties of the silicone connection between the glazing and the frame itself, but also the entire range of interactions between this silicone material with both the glaze and frame of the curtain wall unit.

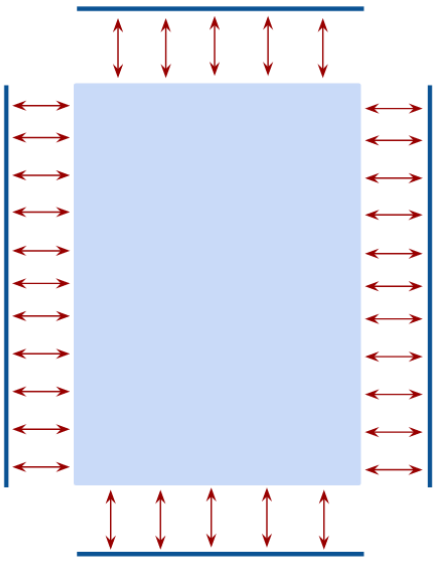

Figure 5.2: Above, the connection between the glazing and the adjacent aluminium framing is presented by the red arrows of the schematic representation. Through the implementation of this element in the numerical procedure, all the non-linearities of the material, its time-dependent behaviour as well as the mechanisms occurring on its interface with the frame and the glazing are attempted to be included.

The previous decision of combining all the properties and interactions of the glazing-to-window connection and attributing them to solely one material is considered to be more efficient than the alternative option, consisting of the simulation of multiple elements. In the latter case, an element identifying the connection element itself, either the gasket or the silicone, and additional interface elements recreating the bonding and interaction of this material with the frame and the glazing separately would be needed. It can be easily understood that additional uncertainties and approximations would have been introduced, especially since relevant information regarding the type of the elements and their respective properties needed for the numerical simulation is missing from the available literature.

For this reason, structural line interfaces are selected to be modelled for the representation of the structural silicone connecting the glazing with the aluminium curtain well frame as well as the interrelations of this material with both the glazing and the framing. In practice the edges of the glazing pane were continuously connected with the frame located perimetrically of the framing. Due to this interface implementation approach, not a specific working direction, either x or y, had to be assigned. Instead, by inserting the interface connection in each of the four sides of each of the glazing pane with the adjacent framing element, the respective connection working in both x- and y- directions was established as seen in the schematic representation of Figure 5.2.

Below the selection of the specific material property is discussed. For the connection of the glazing with the frame, as already mentioned 2D structural line interfaces were selected. Therefore, an infinite number of springs connecting the glazing with the adjacent frame was defined.

Regarding the material properties introduced to the DIANA software, these were initially linear ones. However, after a long series of interactions performed during the calibration of the model based on the experimental results, it was concluded that more accuracy of the adhesive connection was needed. The previous was achieved by the implementation of the nonlinearity of the material. In order for this to happen, the mechanical performance under shear and tensile loading had to be identified. Fortunately, useful information was found from relevant published studies of the literature (Silvestru et al., 2018) and is presented in Figure 5.3 below. For the numerical model utilised in this study, the properties referring to the SIKA material were utilised, since this was included in the curtain wall configuration tested during the experimental sequence.

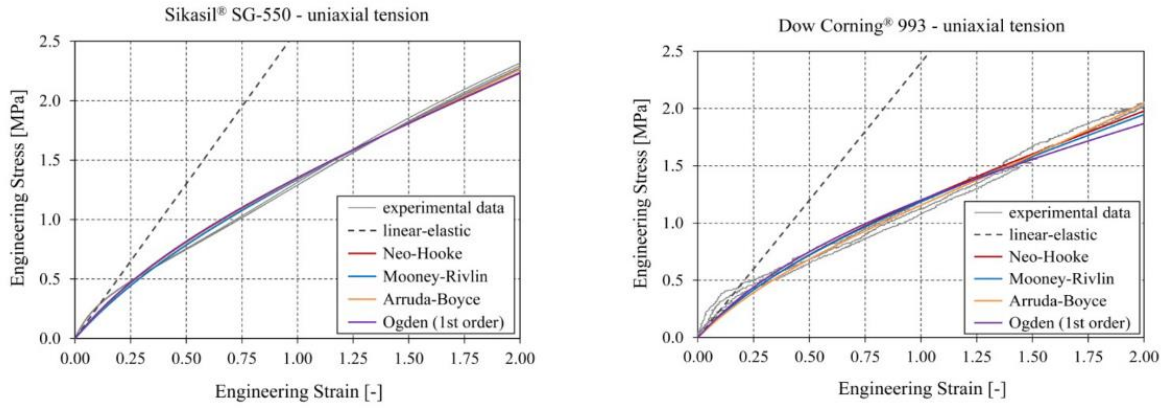

Figure 5.3: The stress-strain curves for the adhesive connections for the uniaxial tensile tests found in the literature are depicted. These curves were used as a reference for the plotting of force-elongation diagrams of the interface connecting the glazing with the frame (Source: Silvestru et al., 2018)

In more detail, the stress-strain curves obtained for two representative adhesive connections, (DOW 993 and Sikasil SG-550) were later transferred into force elongation and later traction-displacement diagrams. These conversions of the curves were necessary, since the non-linearity of this material model representing the structural silicone in DIANA is introduced by the plotting of the respective traction-displacement diagram as seen on Figure 5.4. More specifically, for the translation of the aforementioned diagram to the force-elongation curves, initially and to traction-displacement later, various engineering values such as the dimensions of the reference cross section area A, the initial measurement length Lo, the extension of the measurement length ΔL etc. had to be utilised.

It is important to mention that although the structural silicone values were only obtained for tensile behaviour, they were used for the compressive behaviour as well. The reason for that is that it was observed that the respective values were needed in order for the DIANA model to run, otherwise fatal errors occurred preventing the running of the analysis from happening. Although information regarding the correlation of tensile and compressive behaviour of the adhesive connection was searched for, not a clear conclusion was made based on the information available in the current literature. Therefore, due to the lack of research evidence, the tensile behaviour of the adhesive structural silicone joint was recreated, in practice mirrored, for the compressive behaviour of the material.

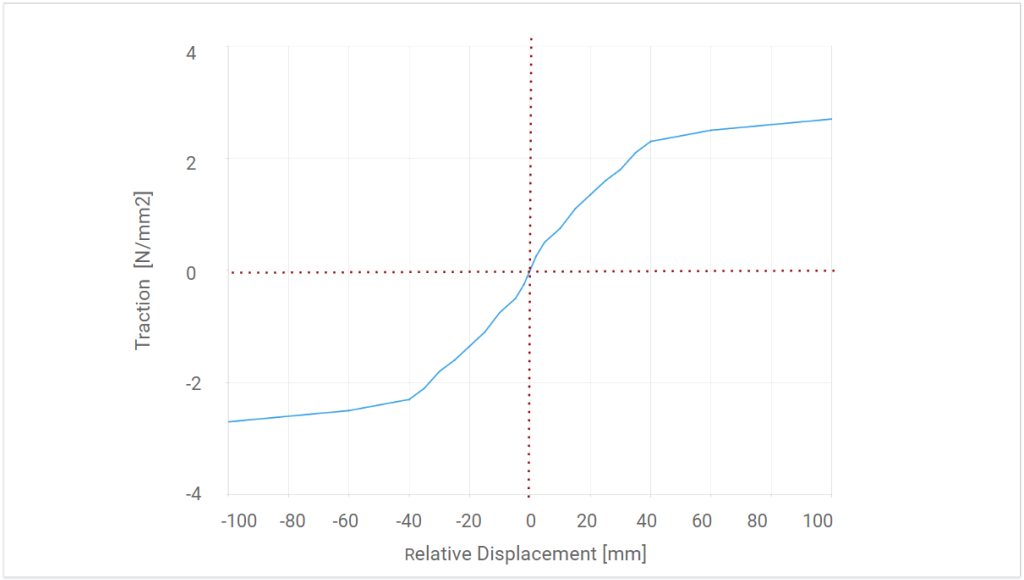

Figure 5.4: The non-linear elasticity of the structural silicone connecting the glazing with the frame is introduced in the DIANA environment through the traction-relative displacement curve as seen above. In order for the analysis to run for the two displacement directions, apart from the tensile, the compressive behaviour also had to be provided. For this reason, the information found for the tensile behaviour was mirrored with respect to axes x and y that are also marked in red dotted lines in the figure above.

Frame-to-Frame Connection

As already mentioned all the four façade units used in the actual experimental procedure were decided to be included in the numerical simulation. The alternative option would include the simulation of solely one façade unit, an approach that was actually followed by the investigation of Galli, (Galli, 2011) while performing a similar attempt of recreating the same experimental case by developing a representative numerical model, this time in a different software.

For the current modelling approach, however, all the four units were decided to be modelled, in an attempt to identify whether the sequence of more than one unit would somehow affect the behaviour of the façade unit. The previous was intended to be checked mainly through the comparison of intermediate and the edge units, in practice by comparing the displacements of representative frame corner points of the units examined. For this reason, a certain connection was needed to be implemented in the numerical model, bonding the adjacent curtain wall units.

The element decided to be introduced for the recreation of the aforementioned connection was an interface. This option of introducing practically numerous springs connecting the adjacent frames was considered as the optimum solution for the continuous bonding of adjacent elements as opposed to the implementation of a finite number of springs, localising the connection of the adjacent elements. Additionally, for the similar connection bonding the bottom transom of the unit analysed with the adjacent starter sill the same interface element was used. The realisation of both the mullion-to-mullion and bottom transom-to-starter-sill connections through interface elements is depicted in the schematic view of Figure 5.5.

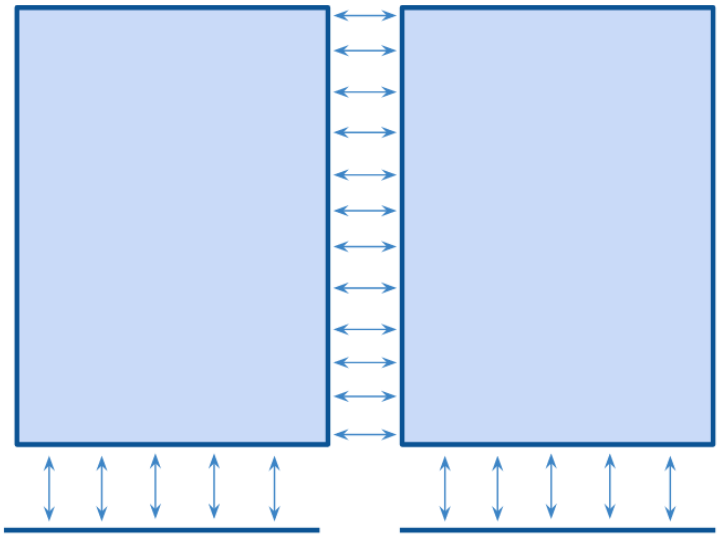

Figure 5.5: In the schematic presentation above the implementation of the interfaces to the glazing-to-frame and frame-to-frame connections is depicted. The blue arrows identify the connection realised between adjacent frames, bonding right and left mullion profiles on one hand and the bottom transom with the starter sill below on the other hand.

One important aspect of the modelling approach that relates to the simulation of the adjacent curtain wall units is the initial distance introduced between them while setting up the model. In practice a distance of 10.0 mm was introduced between the neighbouring units which originated from the actual distance occurring between left and right mullion in the connection as observed in Figure 5.6. Based on this figure, it is obvious that in both the cases of mullion-to-mullion connections and the bottom-to-transom connections the relative movements that results in the elements moving away from each other is unrestrained, up until a certain point of course, whereas the opposite resulting to the elements getting closer is restrained. Therefore, the recreation of this inherent distance that mullions need to overcome before they get in touch was thought to be beneficial for the more realistic simulation of the actual curtain wall behaviour.

As already mentioned, the frame-to-frame connection modelling intended to provide the numerical DIANA model with the ability to capture the actual interrelation of the adjacent curtain wall units. For this reason the elements as well as their properties that are actually compressed in case of the adjacent framing elements contact, after overcoming the initial distance between them, had to be identified through the proper material model. For simplification purposes, it was concluded that these elements are the accessories, such as gaskets, implemented in the curtain wall configuration for this specific reason, namely to relieve potential actions occurring during the conduct of the adjacent aluminium elements. Therefore, the linear properties of this specific connection bonding the adjacent framings were obtained from a typical material used for gaskets, Ethylene Propylene Diene (EPDM).

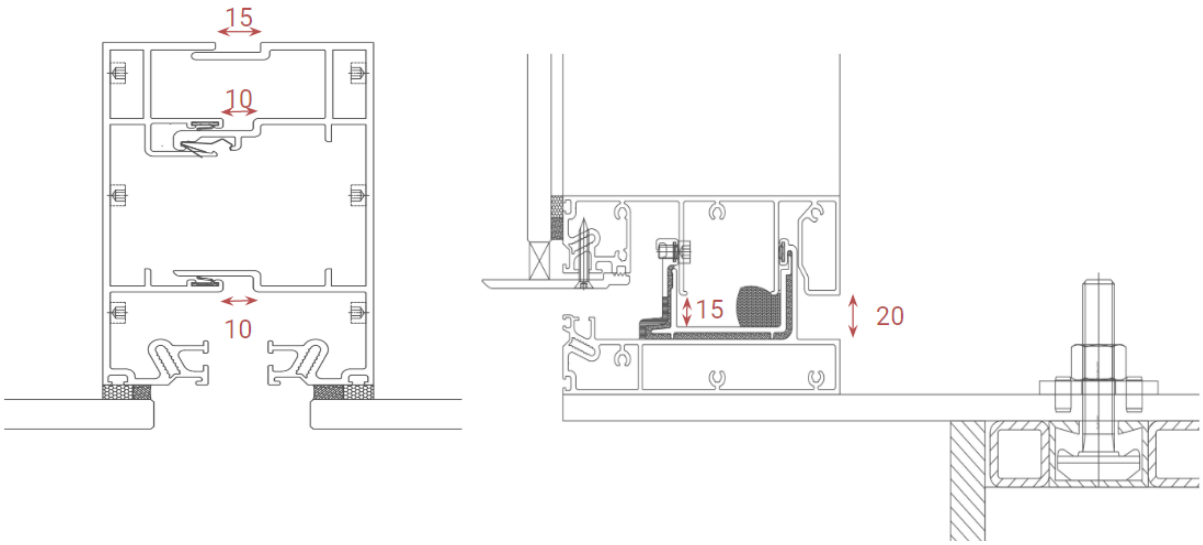

Figure 5.6: In the figure above, the connection detail of the adjacent framing elements is presented. To the left, it can be seen that although the units can move almost freely away from each other, while an external action forces them to move towards each other, a certain distance of almost 10.0 mm has to be overcome before the actual connection of the left and right mullion. To the right, a similar case is observed for the bottom transom and starter sill connection. Here the distance that needs to be surpassed before the elements are in conduct is slightly larger, around 15.0 mm.

Finally, for simplification purposes, the same material properties as the ones used for the glazing-to-frame connection were also attributed to the bottom transom-to-starter sill connection. The reason for this lies again on the simplified approximation that the material first to be activated when the conduct between adjacent framing profiles occurs is the gasket material, therefore its properties were utilised for the identification of the respective properties, namely the shear and normal shear modulus, as explained for the glazing-to-frame connection. Figure 5.7 depicts the four units of the finite element model as seen in the DIANA environment. The various connections occurring between the various components is also depicted.

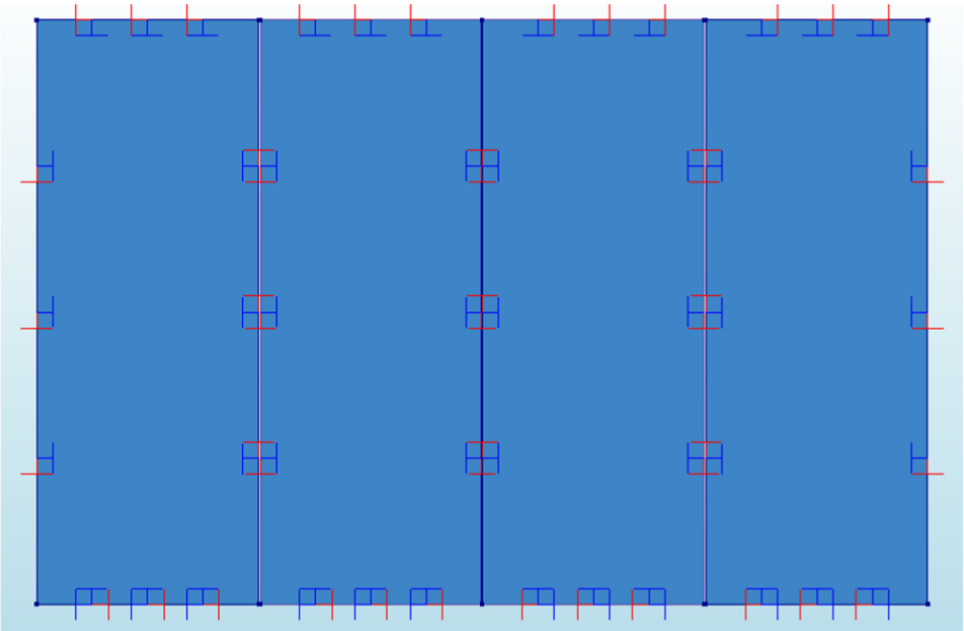

Figure 5.7: The figure above is obtained from the DIANA environment and visualises the modelling of the different curtain wall elements comprising the mock-up unit of the four subsequent units. The larger blue area represents the glazing, whereas the perimetrical thin lines that are coloured in darker blue depict the framing. Although not visible in the picture, the starter sills are placed right where the bottom transoms of each curtain wall unit are located. The blue and red lines forming represent the various interfaces, connecting either the glazing with the frame, the adjacent mullions or the bottom transom with the starter sill.

Mesh Definition

In practice, while defining the meshing of a numerical model, the latter is divided into small elements and points. The amount of those sub-elements, and subsequently their dimension, defines the level of accuracy of the analysis performed on one hand and the computational time on the other hand. It is therefore essential to define what is the largest possible element size that is still able to capture the material behaviour desired. A typical approach consists of the setting of a certain mesh size, followed by additional tests with larger and smaller sizes. By comparing the previous cases and defining their differences, the largest mesh size that still captures the desired level of accuracy is selected.

A common practice in the simulation of large elements through finite element modelling is to differentiate over the level of detail throughout the same element. The idea is that a denser grid is provided only in the areas where more detail is needed, whereas for the rest of the area less detailed analysis is performed. In that way the unnecessary detail of the model is avoided, which results in the reduction of the computational time. In this specific modelling case the previous approach could be translated into defining larger mesh sizes at the centre of the glazing pane compared to the critical areas around the glazing edges connected to the adjacent framing where more accuracy is needed.

However, while evaluating the size of the existing numerical model, the differentiation of the meshing size is expected to provide only limited computational benefit. Additionally, the increased interest of the present study for the identification of the interface behaviour and its interaction with the surrounding elements indicates the imperative need of the proper collaboration of the aforementioned elements. In practice, in

order for the interface to work properly, it is important that both the nodes on the two sides of the interface are more or less equally spaced. In that regard, the element size of the aluminium frame and of the glass pane at least around the glazing edges should be the same. For these reasons, a uniform meshing of 50.0 mm as depicted in Figure 5.8 is utilised by the present numerical approach.

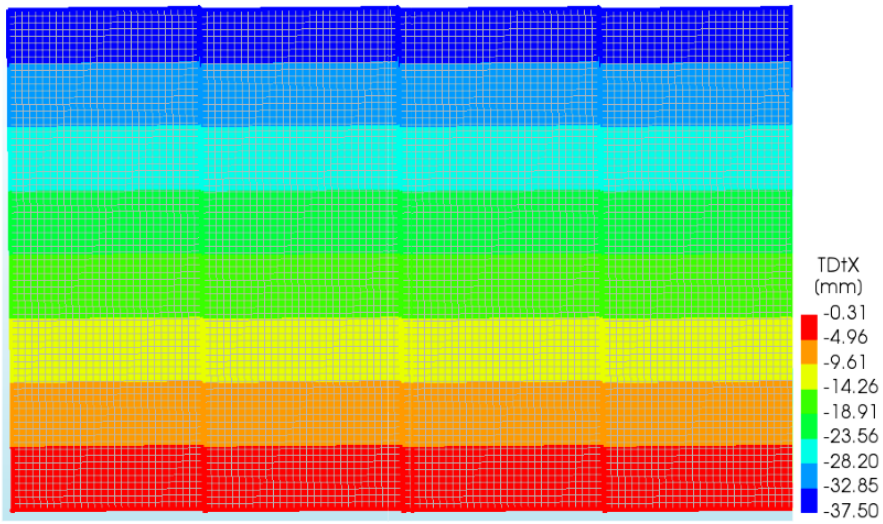

Figure 5.8: A preview of the result section of the four curtain wall units is presented above. In this specific case the units have undergone a negative displacement equal to the largest displacement applied on the unit H/100 = 37.5 mm. It is observed that the meshing is uniform throughout the area analysed.

Loading

Finally, the explanation of the key aspects of the current modelling development is complemented by an introduction to the loading possibilities as well as the one chosen for this modelling approach. As also mentioned previously, during the experimental procedure, the imposed displacement was applied to the upper part of the curtain wall units through the seismic beam in a cyclic manner, at a certain number of circles. Initially the displacement, as defined by the Japanese standards JASS 14 for H/300, H/200 and H/100 respectively, was applied in one direction, e.g. the positive and later the unloading of the system followed. Thereafter the same displacement value was applied in the opposite direction. The previous loading application was repeated several times, resulting in the simulation of a cyclical loading condition.

For the recreation of this specific testing condition in the present study, a monotonic loading was considered as the most appropriate approach balancing the adequate approximation of the loading condition actually applied during the experiment, the complexity of the numerical model in terms of the properties introduced and their compatibility.

Although the incorporation of the cyclic loading was attempted, its implementation was soon abandoned due to the detection of a crucial limitation of the DIANA software. In more detail, it was noticed that the introduction of the cyclic loading to the modelling procedure would overrule the implementation of the nonlinear properties introduced to the numerical model for the more accurate recreation of the actual behaviour. Therefore, facing the challenge of selecting either the implementation of the cyclic loading, therefore the consecutive loading and unloading of the system, or the preservation of the nonlinearities of the elements modelled and their properties, the latter was chosen.

Moreover, while searching for relevant information in the literature available, an interesting observation regarding the similar response of systems undergoing monotonic and load-reversal tests was found (Caterino et al., 2017). An additional reason that underlined the choice of the non-linearities over the cyclic loading originated from the fact that numerous material properties would need to be identified in order for the accurate loading and unloading behaviour to be captured. The latter would inevitably result in further simplifications and, almost certainly, the introduction of additional errors.

Therefore, the preservation of the nonlinearity in the model and the subjection of the latter to monotonic loading was eventually selected.

More precisely, a structural nonlinear analysis was performed with incremental displacement. In this way, the loading condition was gradually increased through the introduction of the proper steps and factors. Since the numerical model behaviour needed to be evaluated and captured for the three different displacement intensities, in accordance with the indications provided by JASS 14, the following loading combinations were tested throughout the modelling process:

- 25 loading steps with a factor of 0.50, for H/300
- 25 loading steps with a factor of 0.75, for H/200
- 25 loading steps with a factor of 1.50, for H/100

Additionally, it is considered essential to refer to the convention used during this study regarding the positive and negative displacement application. The displacement applied in fashion similar to this presented to the left of Figure 5.9 is considered as positive whereas the one depicted to the right as negative.

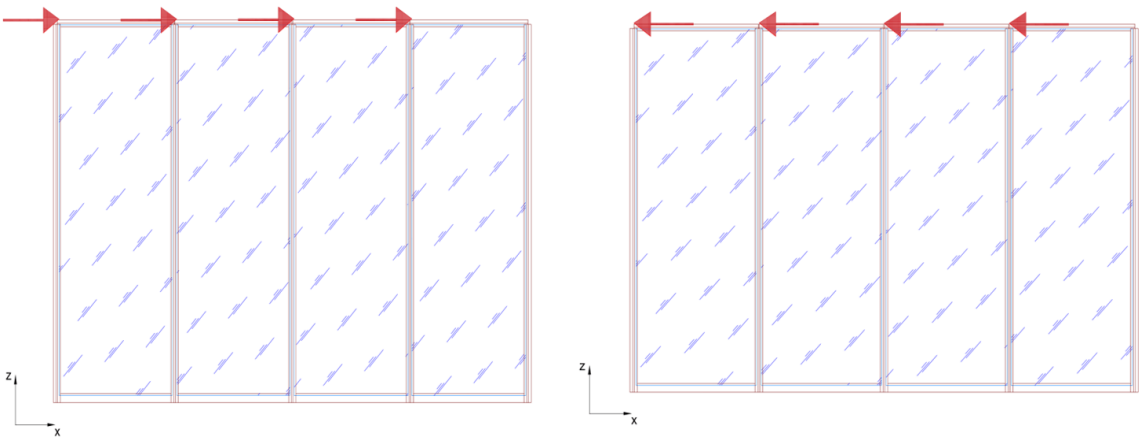

Figure 5.9: The convention of the positive and negative sign used in the current study. To the left the positive and to the right the negative displacement applications are depicted. The displacements are always applied on the upper left framing corner of each of the curtain wall units tested.

Boundary Conditions

One of the crucial elements of a façade system that needs to be verified cautiously for all the possible loading conditions and combinations acting on it is the constraint system. The overall constraint system of the

examined façade elements has been approached through the use of simplified constraint points. The purpose of representing the actual fastening system with simpler constraint points is to prevent the creation of complex stress mechanisms that are extremely hard to control and verify.

In this section the boundary conditions eventually applied to the numerical model are presented. As explained in detail earlier in this chapter, the initial boundary conditions as assumed from the study of the detailed drawings were slightly different and also less in number compared to the ones finally applied to the model. During numerous sensitivity analyses aiming for the calibration of the DIANA model in order to better recreate the experimental results, insightful indications were provided for the slight modification of properties roughly calculated initially for the boundary conditions. Of course, both the main calculation approach as well as the magnitude of values remained the same, therefore are presented below. For a more elaborate insight on the reasoning for the initial boundary conditions, the findings of the initial set of sensitivity analyses that indicated the model sensitivity to various boundary condition parameters and the substantiation for their further modification, please refer to Annex B, "Improvement of Initial Numerical Model".

In order for the accurate representation of the curtain wall behaviour while subjected to horizontal displacement to be achieved, the boundary conditions of both the vertical and also the horizontal displacements of the curtain wall units had to be defined. In general the option of the "boundary springs" offered by the DIANA environment was utilised for the implementation of both the vertical and horizontal restaurants of the unit. Before diving into a more detailed description of properties applied to each of the boundary springs separately, a simplified schematic representation of the over boundary conditions applied to the model is considered insightful.

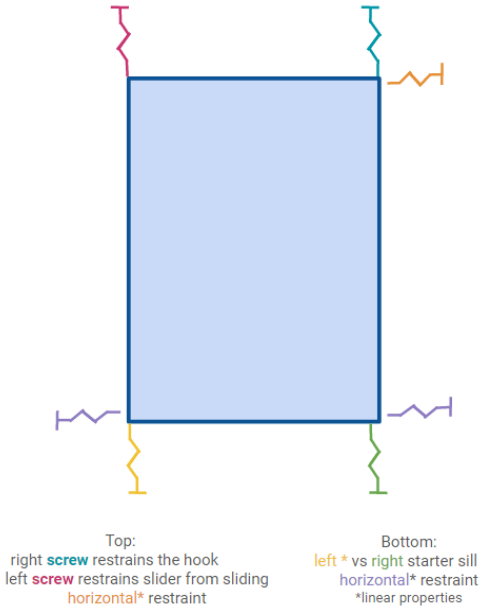

Figure 5.10: In the schematic representation above, the different boundary conditions applied on the numerical model are represented. The different colours indicate different properties, whereas the asterisk (*) the cases were linear properties were attributed. Obviously, the non-linear properties were provided to the boundary springs not characterised by an asterisk.

As seen in the schematic representation of the overall boundary conditions presented in Figure 5.10, boundary springs are defined in the numerical model, aiming to connect the corner areas of the frame to the surrounding environment. Initially the properties attributed to the boundary springs were linear. However, after studying the curtain wall response especially with respect to the vertical displacements, the need for more complex properties became obvious. Below a concise description of the boundary conditions applied on the vertical and later on the horizontal sense are presented.

Vertical Restraints

In more details, the vertical upper boundary condition of the façade unit which is in practice realised through the bracket elements, allows the unit to move upwards, if needed, but not downwards. Similarly, boundary springs were applied to the two edges of the lowest part of the curtain wall unit, connecting the starter sill with the environment, to what the software considers as ground.

What is essential to mention is how the properties attributed to the upper and lowest vertical constraints of the curtain wall unit were computed. Initially, the stiffness K of both the boundary springs was found. After calculating the spring stiffness for both the upper and the lowest boundary springs, the respective force-elongation diagrams originated through the implementation of Hooke's Law. The identification of the force-elongation diagrams was vital for the description of the non-linear behaviour of the constraints of the curtain wall unit.

A more detailed elaboration of the non-linearity of the boundary springs, on the way this has been assessed with regards to the experimental behaviour and eventually incorporated in the numerical modelling is described in the sections "Boundary Springs, Non-linear Stiffness Properties" and "Starter Sill Boundary Springs Differentiation" that follows later. Additionally, a comprehensive explanation related to the differences between the right and left upper boundary conditions and how they have been eventually captured in the present numerical approach is included in section "Upper Boundary Restraints Modification" of the present chapter.

Horizontal Restraints

As already mentioned, in the current modelling procedure the displacement is applied on the top frame corner, whereas in the actual experimental case it is applied on the seismic beam and through that to the curtain wall frame. According to the experimental measurements, under the horizontal displacement application the top corners of the frame displace by the same distance as the magnitude of the displacement applied, namely 12.5 mm for the case of the H/300 = 12.5 mm displacement application, 18.75 mm for the the H/200 = 18.75 and 37.5 mm for the case of the largest displacement of H/100 = 37.5 mm. The same displacement, however, does not occur to the lowest part of the frame. As seen in Figure 5.11, there the displacement is almost half.

There a horizontal displacement of the same duration is noticed, of a smaller value though. The latter indicates that a restraint needs to be applied at the lower part of the curtain wall unit also in the horizontal sense. Since in the absence of the latter the units tested would be noticed to slide/translate under the action of the imposed displacement, it becomes evident that a certain restrain of the horizontal displacement is needed. Therefore, in order for the experimental behaviour to be recreated to the extent possible, boundary springs were also applied to the lowest part of the curtain wall unit and more specifically to the starter sill, connecting each of the edges to the ground.

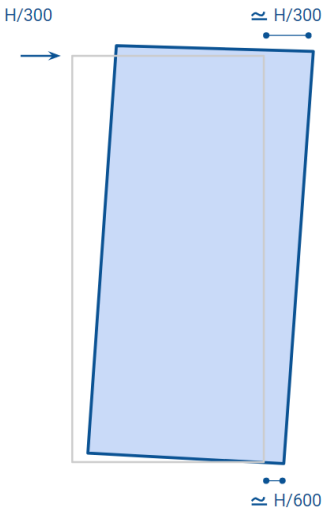

Figure 5.11: In this figure the curtain wall response to the positive inter-storey ratio of H /300 is depicted. Similar behaviour is noticed for the negative direction as well. Regarding the horizontal movement of the curtain wall unit, the upper part of the frame is noticed to displace at a value almost equal to the imposed displacement. On the contrary, the lower part of the façade unit presents a smaller horizontal displacement.

In reality, an element similar to this simulated through the boundary springs is not included in the curtain wall configuration. This limitation of the horizontal movement observed in the lower part of the actual façade unit, though, is assumed to be offered by the adjacent curtain wall units. Therefore, the exact information needed for the indication of the stiffness properties of this boundary condition was missing. Additionally, the absence of measurements for the horizontal displacements of the lowest framing corner of the unit, point F as seen in Figure 5.12, hindered the understanding of the curtain wall behaviour in the horizontal sense both regarding its upper and lower part. For these reasons, the stiffness of these boundary springs was calibrated based on the experimental measurements. In practice, the stiffness initially used for the boundary springs restraining the vertical direction was used and it was later adjusted appropriately so that the horizontal displacements of the numerical model would match those of the experiment. Eventually linear properties of a relatively small value, 20 N/m, were attributed to this boundary spring.

Regarding the horizontal movement of the upper part of the curtain wall unit, this is also partially restrained. Similarly to the case of the lower part of the unit, the importance as well as the stiffness identification of this boundary condition was mostly defined through the calibration process based on the experimental values. Again, the lack of information for the horizontal behaviour of one of the upper corner points, point E of Figure 5.12, introduced further challenges in the understanding and subsequently recreation of the curtain wall behaviour. Therefore, several runs of sensitivity analysis aiming to assess the impact of the horizontal restraint in the numerical model response to the horizontal displacement implementation were evaluated. Eventually, a set of linear properties was identified resulting in the numerical simulation to respond in a way similar to this monitored during the experimental procedure. In reality, among several stiffness values tested, the one value initially calculated for the upper bracket spring was included in the final numerical model.

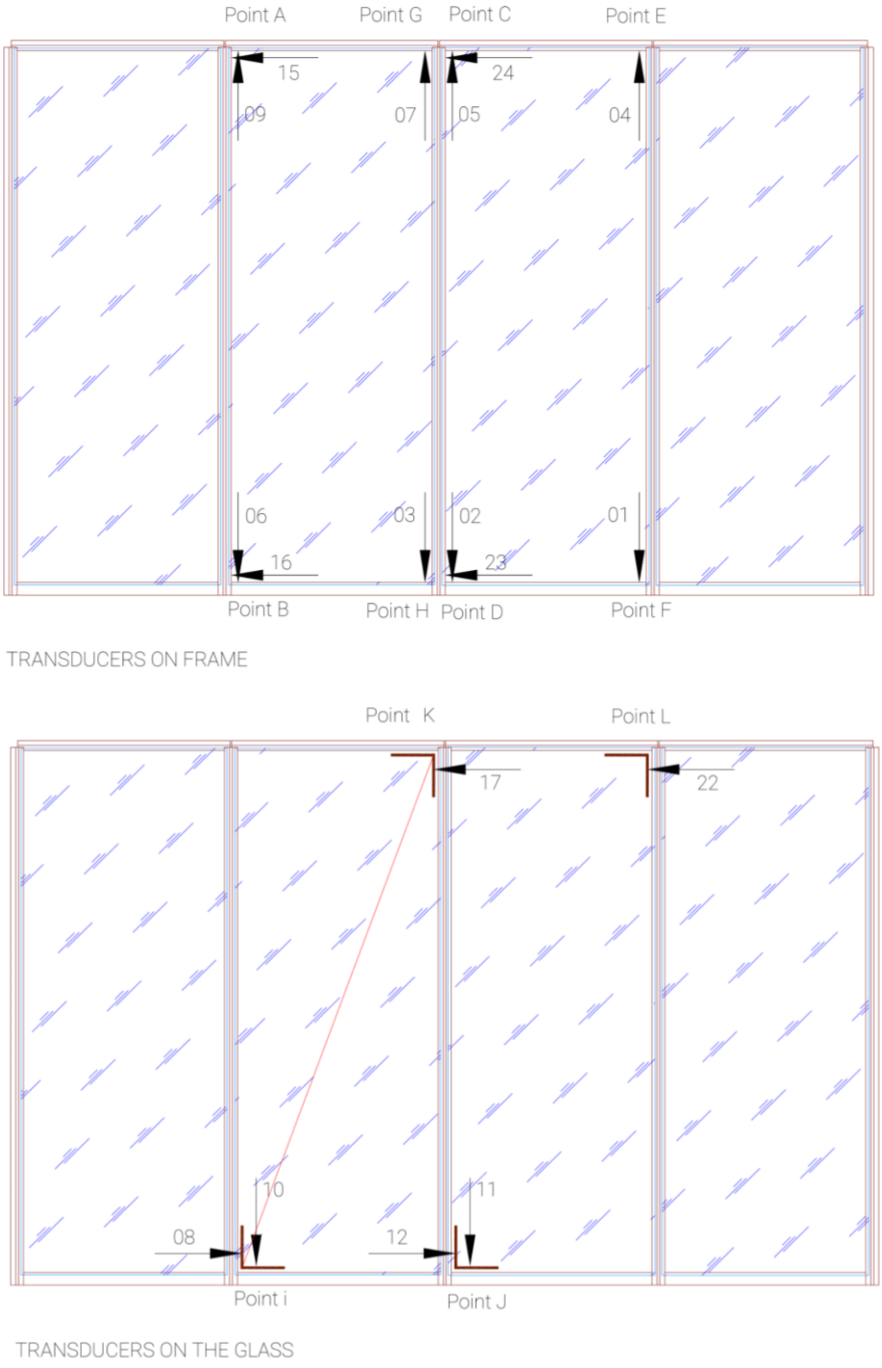

Figure 5.12: The naming convention used for the points under examination is presented. The figure above depicts the points of the framing whereas the scheme below the ones of the glazing. The direction of the arrows was used for the appropriate interpretation of the experimental values monitored during the experiment.

Clarifications

Before diving into the details of the sensitivity analyses conducted and the improvement of the numerical model in terms of the accurate representation of experimental behaviour, a brief presentation of some notions

that are frequently referred to throughout the study follows. To start with, the set of the points and their naming convention used for comparison of the displacements is presented in Figure 5.13.

Additionally, a quick reference to what later on is quite frequently referred to as asymmetrical behaviour of the curtain wall unit with respect to the positive and negative displacement application is considered essential for the better contextualisation of the overall procedure later explained in this chapter.

In practice, during the experimental procedure it was noticed that the façade unit, while subjected to a horizontal displacement, does not present equal behaviour to both the positive and negative directions of the displacement application. Figure 5.13 depicts this situation. In more detail, the points marked in blue represent the test points displacing symmetrically with respect to each other. On the contrary, the points marked in red are those that display asymmetrical behaviour. The term "asymmetrical" aims to express the numerical inequality of the points belonging to the same mullion, points C and D for the positive and E and F for the negative displacement. Simultaneously, it can be argued that this asymmetrical response of the curtain wall system is presented in a symmetrical manner with respect to the displacement application. To rephrase the previous, the exact same asymmetrical behaviour observed in the left mullion of the façade unit when the former is subjected to a positive displacement application is noticed on the right mullion for the negative displacement.

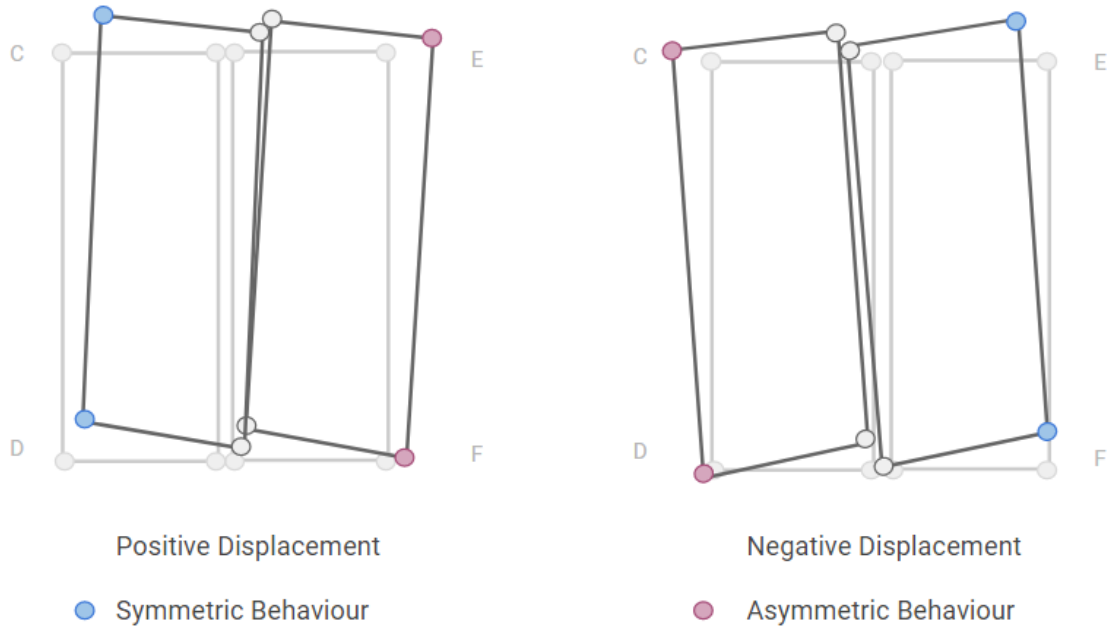

Figure 5.13: The reaction of the façade under positive to the left and negative to the right displacement application is presented.

Numerical Model Improvement

Eventually, the determination of all the properties and interrelations needed for the DIANA model to run, a detailed description of which was previously presented, resulted in the development of the initial version of the numerical model. The second step of the modelling procedure involved the further improvement of the

initial model based on the measurements of the curtain wall behaviour as recorded during the experimental campaign. In practice, the acquisition of a better understanding of the numerical model behaviour was attempted through the run of various sensitivity analyses aiming to demonstrate what properties of the model affect its behaviour the most.

A total of thirty variations (scenarios) of the initial numerical model were tested. The target of this modelling stage was the implementation of various aspects in the finite element model with the most important ones being the accurate correspondence of the experimental and numerical displacements, the integration of the two different façade responses (negative and positive) and finally the introduction of the non-linearity while modelling various elements that eventually results in a simulation closer to the actual situation. Below a short review of the properties tested during this modelling phase is presented.

- the first series of sensitivity analysis focused on the differentiation of the linear properties of the starter sill in the vertical (y) direction, whereas
- the second testing sequence on the linear properties of the same boundary condition related to the horizontal (x) direction
- the third analysis category concentrated on the other boundary element, the upper bracket, and more specifically to both the linear and non-linear properties defining the x and y directions respectively
- the fourth and final sensitivity analysis varied over the properties of the same boundary condition, the upper bracket boundary spring again both in the vertical (y) and horizontal (x) direction. This time non-linear properties were attributed to all the aforementioned parameters

Since the present is regarded as an intermediate step of the numerical modelling, the detailed explanation of this modelling step is omitted from this section. Instead, a thorough description of the property variations and individual conclusions of this sensitivity analysis series is presented in Annex B. Below the final remarks originating from this simulation phase are presented, providing the ground for the better understanding of the next modelling phase, the numerical model calibration that is discussed later.

While examining all the different scenarios tested during this series of sensitivity analysis, the following observations are made. To begin with, the dynamic behaviour of the curtain wall response while subjected to a horizontal displacement is underlined. It becomes obvious that, when varying over the properties of either the upper bracket or the starter sill boundary springs, the improvement of some displacement values of a representative curtain wall point inevitably results in the compromising of the displacement behaviour of other façade points. The latter occurs irrespectively of the linearity or the non-linearity of the Additionally, while studying the complete series of the sensitivity analyses performed, some scenarios are observed to better approximate the reference values measured during the experimental sequence of the mock-up. Those scenarios are concentrated into Table B.6 of Annex B and formed the basis for the additional sensitivity analyses performed during the numerical calibration explained in the next section.

Additionally, it is important to highlight that during this modelling phase the behaviour of the numerical model while subjected to positive and negative horizontal displacements was identical. To rephrase the previous, the representative points of the curtain wall units appear to have almost the same displacement in absolute values, with the only difference being their sign. Obviously, the values with a negative sign for the displacement application of one direction, present a positive one for the remaining direction.

In order for the improvement of the existing numerical model to be achieved, practically through recreating the different negative and positive behaviour of the glazed curtain wall system as noticed during the experimental campaign, the implementation of an additional component, of the alignment screw, is

investigated. The modelling of this curtain wall component that was not implemented during the initial simulation, is aspired to, on one hand, provide better representation of the relative vertical displacement of the upper and lower framing points, and on the other hand to incorporate the positive and negative behaviours of the actual curtain wall system into one DIANA model. It is reminded that both the goals mentioned previously were not achieved during the first series of sensitivity analyses leading to what was previously characterised as the improvement of the initial modelling approach.

Alignment Screw Implementation

A detailed explanation of the façade element behaviour tested under seismic action has been provided in Chapter 4 of the present study. There an extensive reference to a specific part of the configuration, the alignment screw which is depicted in red in Figure 5.14, and to its contribution to the façade behaviour is made. It is substantiated that due to this element the façade unit responds differently to the two opposite horizontal displacements applied through the seismic beam. In practice, a shape deformation is noticed when the façade unit undergoes a negative displacement. Moreover, when the positive equivalent displacement is applied, the façade specimen is noticed to rotate.

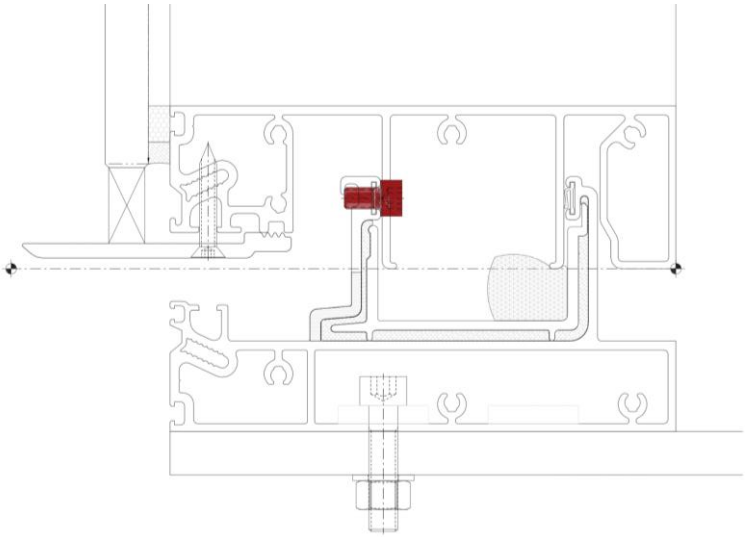

Figure 5.14: In this figure the detail of the connection of the bottom transom with the starter sill is presented. The alignment screw connecting the two elements is highlighted in red.

This asymmetrical behaviour of the façade unit was attempted to be captured in the finite element model built during this study. In order for this to be achieved, the location of the alignment screw had to be identified. After consulting the expert who was in charge for the design of this specific façade configuration, it was found out that the screw was placed in the bottom transom connecting it with the starter sill at a distance of 400.0 mm from the right mullion. Since the location was identified, the actual behaviour of the element had to be considered and, thereafter, transferred to the numerical model. It was concluded that the alignment screw operates as a link connecting the two adjacent elements, bottom transom and starter sill, restraining the movements in both X and Y axes while allowing rotations.

An elaborate explanation of the various options considered and of the steps eventually followed during the modelling of the alignment screw accompanied by the respective behaviour of the model is presented in the Annex C, Alignment Screw Implementation of the present study.

The findings of the investigation of the alignment screw application are briefly presented here. In short, while exploring alternative modelling approaches for the alignment screw integration, it was concluded that this specific DIANA model is not sensitive to the application of the alignment screw. The previous is substantiated by the already stiff connection between the transom and the starter sill. It is concluded that the previous does not allow any changes to be introduced to the façade behaviour while introducing additional restraints at the location of the alignment screw.

Current Modelling State Evaluation

After completing this modelling stage, the first findings regarding the model sensitivity to the boundary spring properties originated. Mainly the impact of the properties introduced by both the x- and y- direction of the upper bracket and the starter sill was investigated. After concluding to an improved set-up of the boundary springs, this time also for the x- direction and not only for the y-direction as was the case for the initial modelling phase, the first insight on the model behaviour was obtained.

However, various aspects of the modelling still need to be refined. Among others, the more accurate recreation of the restraints as defined by the boundary springs, the better correspondence of both the frame and glazing displacement values to those recorded during the experimental process and of course the incorporation of the positive and negative curtain wall behaviour into solely one DIANA model. It is reminded that the latter was attempted with the application of the alignment screw which unfortunately did not manage to enhance the modelling approach with the desired behaviour.

For all the reasons previously mentioned, an additional modelling phase is considered essential during which the numerical approach already developed will be able to ever better recreate the glazed curtain wall behaviour as noticed during the full-scale experimental testing.

Numerical Model Calibration

Below, the adaptations of the numerical model and its properties performed during the calibration of the numerical model through the comparison of the previous with the experimental behaviour are presented. For a more detailed explanation of each of these aspects accompanied by the respective comments, figures and tables please refer to Annex D, Numerical Model Calibration.

As already mentioned previously, during this modelling phase a better approximation of the numerical simulation and the experimental curtain wall response is intended. By modifying the displacement restraints defining the façade boundary conditions, a more precise recreation of the movements actually allowed is intended.

The gradual introduction of non-linear properties determining the stiffness of the boundary springs is attempted to better capture the realistic curtain wall behaviour that is allowed to move upwards but restrained to displace to the opposite direction. Additionally, the overall façade behaviour as well as the displacement of each of the curtain wall representative points is aimed to better approximate the one of the experiment.

Furthermore, the incorporation of the two different curtain wall behaviours, one responding to the positive and the other to the negative displacement application is attempted to be captured in solely one numerical model, which up until this modelling stage has not been achieved. The previous goals are realised through the investigation of the impact several parameters have on the numerical model and the appropriate modification of the existing boundary conditions, as explained in detail later in this chapter.

Boundary Springs, Non-linear Stiffness Properties

After defining the mechanical properties of the bracket connections of the upper frame and the starter sill based on their stiffness K, another challenge arose, this time related to the identification of the asymmetrical behaviour that the actual constraints present with respect to the direction of the movement, either upward or downward as previously mentioned. In short, both boundary conditions allow the upward movement of the curtain wall unit but restrain the one downwards. The essence of the uncertainty was related to the correct way of scripting to the software, the movement to the allowable direction and the prevention of the opposite. In practice, for half of the diagram the force-elongation properties previously calculated had to be preserved, whereas for the rest extremely stiff conditions had to be provided, preventing in this way the downward movement.

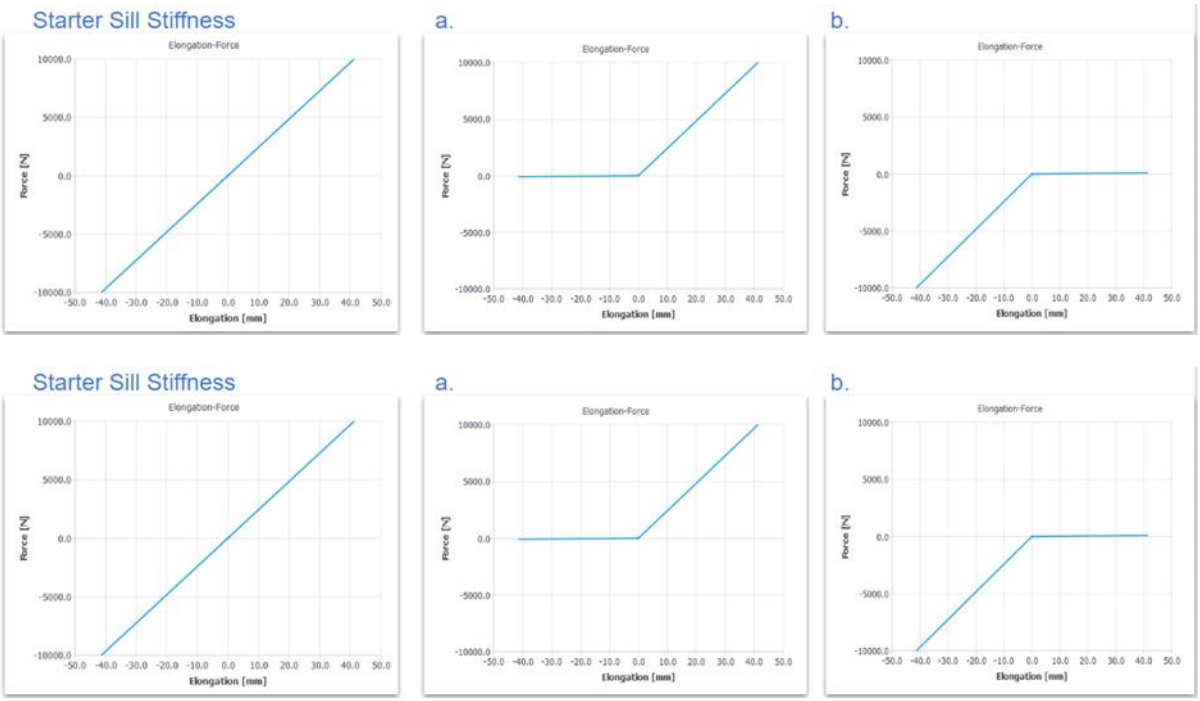

Figure 5.15: In the figure above the scenarios referring to the variation of the upper bracket and starter sill boundary springs are presented. To the left, the completely linear properties of the starter sill and the upper bracket brackets initially calculated from Hooke's Law, based on the spring stiffness initially defined, are presented respectively. Scenarios a, b, refer to the two possible ways of implementing to DIANA the desired behaviour of the starter sill allowing upward but no downward movement of the unit. Scenarios c and d are the

equivalent for the upper bracket. Initially the scenarios referring to the starter sill and later for the upper bracket boundary conditions were tested separately while preserving the properties of the other boundary spring linear. This sensitivity analysis attempted to determine the most appropriate combination of upper bracket and starter sill boundary spring properties that more accurately recreate the experimental, therefore actual, curtain wall behaviour. Later, all the possible combinations of joined non-linearity of the upper and lowest boundary springs were tested (ac, ad, bc, bd).

This uncertainty regarding the software correct interpretation of the downward and upward movement through the implementation of force-elongation properties of the material model was overpassed through a respective sensitivity analysis. In short, all the possible scenarios varying between the non-linear properties of the upper bracket boundary spring initially and of the starter sill stiffness later as seen in Figure 5.15 were tested. The detailed process is described in Annex D, Further Calibration – Boundary Springs Sensitivity Analysis. Below, in Figure 5.16 the approximation of each of the scenarios tested to the reference values is depicted.

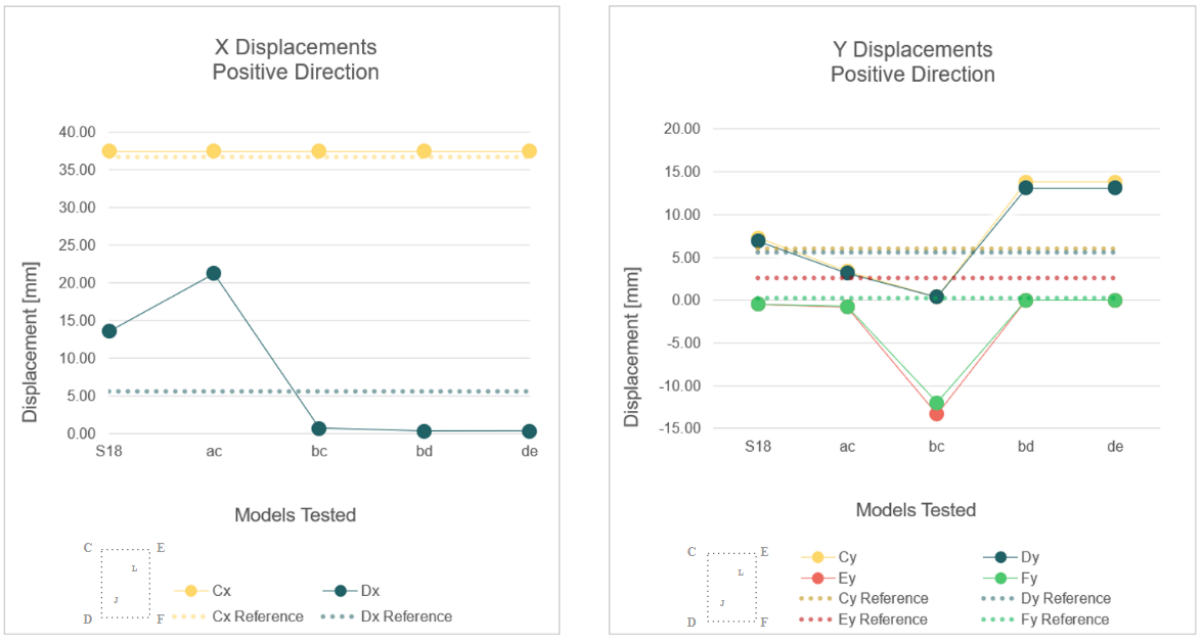

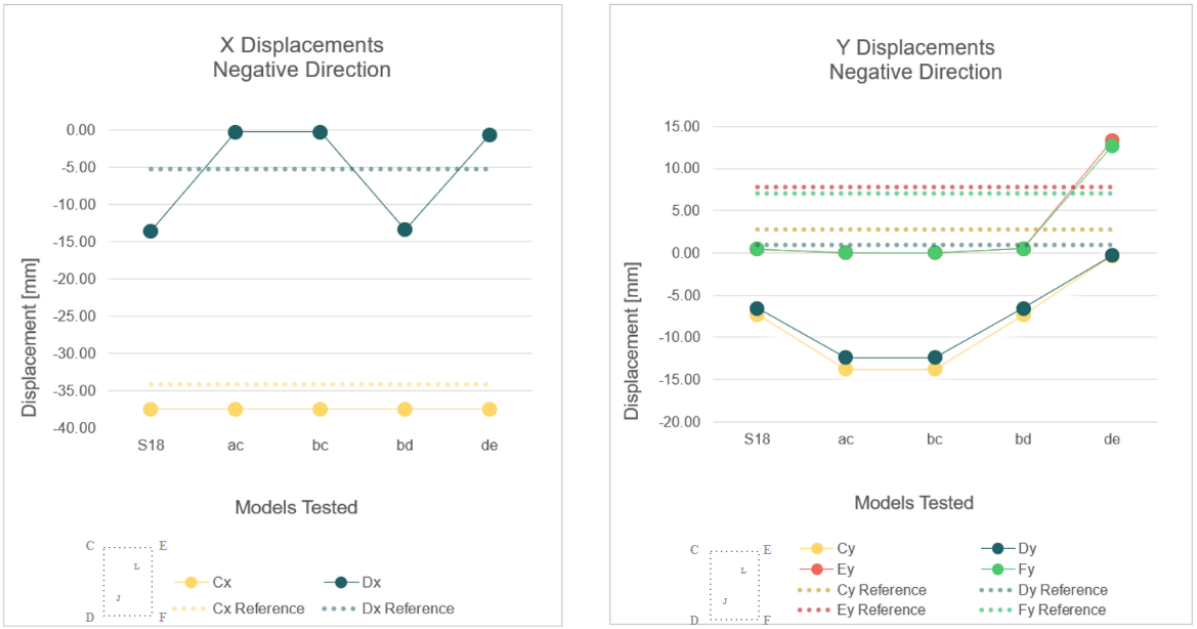

Figure 5.16: The figures above represent the different displacement values of the characteristic points C, D, E & F that are used as a reference for the evaluation of the proximity of the numerical behaviour to that of the actual experimental response to the positive and negative displacement application respectively. In dotted lines, the experimental values that are used as a reference are presented, following the same colour coding as defined for each of the characteristic points. It is seen that less values are presented for the x displacements and this is due to the lack of the experimental reference. It has been decided that only the values for which a reference exist, will be presented since only by means of comparison as such the proximity of each scenario tested can be indicated. Based on the response of the numerical model to the implementation of non-linear properties to the boundary springs, it can be concluded that the combinations including the upper bracket properties defined by scenario d are the ones approximating better the reference behaviour plotted in dotted lines.

Eventually, the more appropriate identification of the actual unit behaviour, being able to move upwards but not downwards, was found to be achieved by the combinations including the non-linear properties of the upper boundary bracket as described by the scenario d. However, regarding the properties defining the starter sill boundary condition, apart from the observation that scenario d results in a better approximation of the numerical behaviour to the experimental one while compared to this of scenario c, not a straightforward conclusion could be made.

The reason for the latter partially lied on the inability of the model to present an adequate approximation of the positive and negative experimental results simultaneously. It is reminded that the curtain wall behaviour presented a slightly different response to the positive and negative displacement application, a behaviour that was in detail described in the beginning of this chapter. Therefore, an additional calibration of the numerical model followed with respect to the non-linear properties of the starter sill boundary conditions.

Starter Sill Boundary Springs Differentiation

Based on the observation of the previous sensitivity analysis an additional hypothesis that would result in the numerical model to better recreate the experimental curtain wall behaviour was examined. The influence of slightly differentiating the properties attributed to the right and left starter sill on the numerical recreation of the positive and negative experimental behaviour simultaneously was investigated. An overview of the different scenarios tested is presented in Figure 5.17.

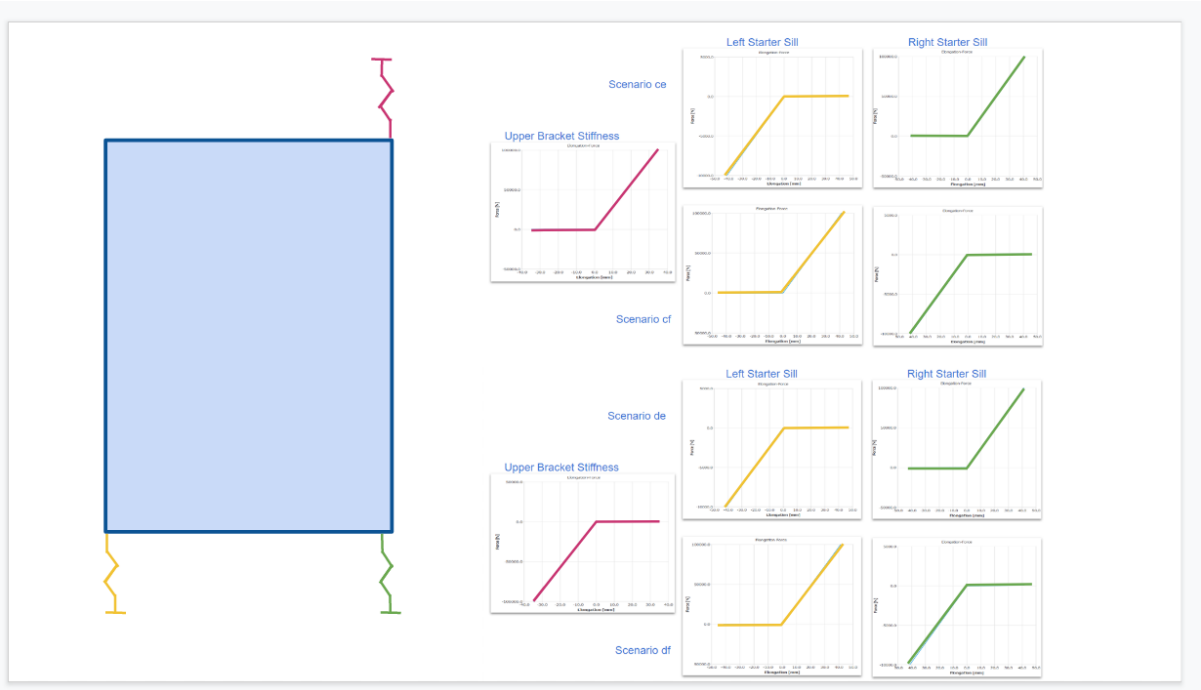

Figure 5.17: The above figure concentrates all the cases tested in order for the impact of the implementation of opposite non-linear properties on each of the starter sills to be assessed. The diagrams viewed correspond to the force-elongation properties attributed to the respective boundary condition. For better visualisation, the same colour coding of the properties defined to each of the boundary springs tested is identical to that of the simplified scheme presented to the left.

The study of the respective findings, as presented in the "Further Calibration – Boundary Springs Sensitivity Analysis" section of the Annex D, resulted in some interesting observations. Initially, the stiffness mechanism that leads to the more accurate behaviour of the numerical model for both the positive and negative displacement applications, as already indicated by the increased proximity between the numerical and experimental results, was verified to be the one presented by scenario d. Additionally, it was noticed that due to the differentiation of the properties describing the starter sill boundary spring stiffnesses, the numerical model appeared to recreate better some experimental displacement values, especially for the case of the negative displacement and more specifically the vertical displacements of points E and F, with a level of approximation that hadn't reached before. The latter proved that the discretisation of the left and right boundary springs can provide a solution for this specific modelling approach, that aims to correspond to the actual situation by providing different curtain wall response depending on the direction of the displacement applied on the curtain wall unit.

While paying extra attention to the experimental behaviour of the numerical model, and more specifically to the vertical displacement of the upper left framing point, it was noticed that this specific area was moving considerably more compared to the respective experimental behaviour. On that ground the concept of the introduction of additional boundary conditions restraining the vertical movement of also the left upper point of the frame was investigated.

Upper Boundary Restraints Modification

It is reminded that during the initial modelling phase and up until the stage described in the previous section, only vertical restraint implemented on the upper area of the façade unit was located only on the right part of the glazed curtain wall unit, whereas the left upper corner was free to move upwards. The concept of this differentiation between the right and left restriction of the vertical movement of the curtain wall unit adopted during the initial modelling approach originated from the different function of the two upper brackets that in reality serves the accommodation of possible thermal expansion.

For this reason, while considering the function of the curtain wall unit having one of the upper brackets fixed while allowing the other to be vertically displaced in case needed, a vertical boundary condition was applied only to the right upper frame corner. By closely studying the curtain wall behaviour and its sensitivity to the property alterations gradually performed previously, second thoughts regarding the validity of the previous assumptions arose that resulted in the following findings.

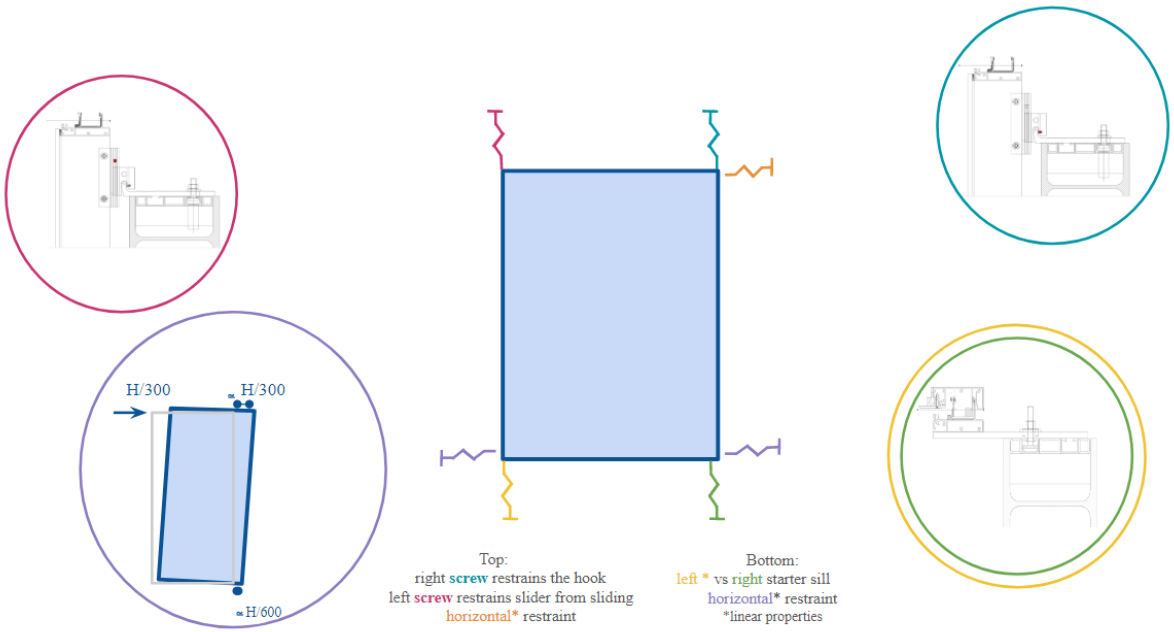

Figure 5.18: The schematic representation of the final boundary conditions applied to the numerical model is depicted above. The implementation of the additional boundary spring located on the top left corner of the curtain wall frame is visible in pink colour.

Eventually, it was concluded that an additional boundary condition also limiting the upward vertical displacement had to be integrated complementary to the existing boundary spring of the right upper framing corner. The newest and final set of the boundary springs is depicted in Figure 5.18. The reason for this extra boundary not previously included in the numerical modelling is that the focus was concentrated solely on the impact of the brackets located on the façade unit upper part instead of the connection as a whole. Therefore, the impact of the rest of the connection components, e.g. of the hook, the slider or the connecting elements between them, was overseen. This direct interpretation of the bracket function to the vertical movement of the façade unit upper areas resulted in a less realistic representation of the actual façade behaviour. In practice, for the upper part of the façade unit the upward movement is possible and unrestrained, whereas the reverse is prevented. The interesting point though is that although the vertical downward movement of the façade unit is generally restrained, the façade element preventing it is not the same for the left and right part of the frame.

As it can be also seen from the detail in Figure 5.19, the right connection there is a screw restraining the hook, therefore preventing the vertical movement of the unit downwards. The upward vertical movement of the façade though is not restrained by the right bracket since the hook is free to slide into the slider. On the other hand, this screw is not present on the connection of the upper left side of the façade unit. However, the downward vertical movement there is also prevented due to the conduct between the hook and the slider. In practice, the movement downwards is restrained by the screw located at the top of the hook that makes it impossible for the slider to slide, at least until a certain position. In this way, regardless of the existence of the screw existence between the hook and the floor bracket, when the façade unit is forced to be displaced downwards this movement will be restrained due to the conduct of the hook and the floor bracket.

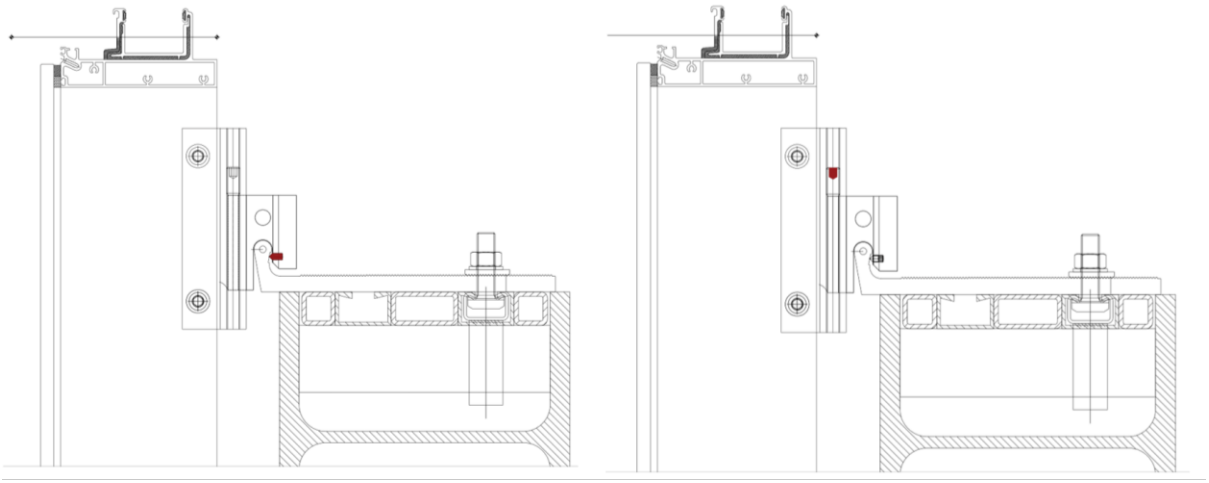

Figure 5.19: Detail of the upper fastening of the façade unit to the supporting structure. The difference between the left and right upper boundary conditions of the façade unit is the reaction of the floor bracket and the hook and lies on the need for the displacement accommodation. In practice in the right connection the screw, which is more accurately referred to as grain, connects the hook with the floor bracket rigidly. Therefore, the hook is fixed to the floor bracket which results in these rigidly connected elements having the same vertical displacement. On the other hand, the upward vertical movement of the unit is possible since the hook is allowed to slide inside the slider. This upward movement, though, is only allowed until a certain point above which the unit disengages from the hook. Although the aforementioned screw is not present in the left connection, the vertical movement downwards is still restrained due to the conduct of the hook and the slider. The upward movement is also allowed since there as well the hook can slide inside the slider.

The reason for the difference between the left and right fastening of the façade to the supporting beam is that one of the two connections, here the right one, needs to be fixed whereas the other one, the left in this façade configuration, has to accommodate the horizontal (lateral) movement making the thermal expansion and/or conduction of the façade units possible. What is important to underline is that in both the cases, left and right, the façade unit is free to move upwards but restrained to move in the reverse direction.

After processing the numerical results of the new series of the sensitivity analysis including the additional boundary spring in the location of the left upper bracket, that are also presented in Figure D.13 of Annex D and Tables D.6 & D.7 of its Supplement, it was concluded that some of the scenarios run were presented to have better approximation with the equivalent experimental results, especially for the case of the negative displacement application. More specifically, considerable improvement was noticed in the vertical displacement of points E and F, approximating the experimental values with a deviation of 6.0 % compared to that of 38.0 % that was achieved by the numerical models without the implementation of the extra boundary spring.

Regarding the influence of the additional boundary to the curtain wall behaviour under the positive displacement application, not an equivalent improvement was noticed there. The previous can be substantiated when considering that the fist sets of calibrations were performed with respect to the reference experimental values originating from the positive curtain wall behaviour. In any case, the implementation of the additional boundary spring did not result in the further deviation of the numerical behaviour from the one used as a reference.

To conclude, the modelling of the left boundary spring resulted in an overall positive impact of the modelling procedure. In fact some of the various scenarios tested during this sensitivity analysis, especially for the negative displacement application, resulted in acquiring a behaviour closer to this measured during the experimental sequence.

Incorporation of Positive & Negative Behaviour

As already mentioned in the latest statement, there were some DIANA modelling variations resulting in numerical results closer to those of the experiment, therefore not solely one working optimally for the negative and positive displacement application simultaneously. In more detail, scenario de presents numerical results closer to the ones monitored for the negative displacement application, especially the ones describing the vertical displacement of points E and F, whereas scenario df recreates better the curtain wall behaviour as recorded for the positive displacement.

The final modelling attempt aiming to combine the optimal negative and positive façade behaviours into one single DIANA model was based on the previous observation. In this way, the parameters of scenarios de and df each of which recreates better the one of the two displacement applications examined were merged into one optimised DIANA model. The detailed response of the numerical model to these changes can be studied in Figure D.14 of Annex D and in Table D.8 of its Supplement.

In practice the modelling parameter the properties of which were modified in order for the efficient combination of the previously two optimal scenarios, de and df, was the stiffness properties of the boundary spring connecting the left starter sill edge with the ground. Therefore, the non-linear properties determining the stiffness of the left boundary sprung as presented during the previous sensitivity analyses were modified into the initial linear ones. Figure 5.20 schematically presents in yellow the linear stiffness properties of the

left and in green the non-linear properties of the right starter still. This stiffness alteration of only one of the two boundary springs resulted in a more accurate curtain wall behaviour, compared to the experimental one, while subjected to positive displacement.

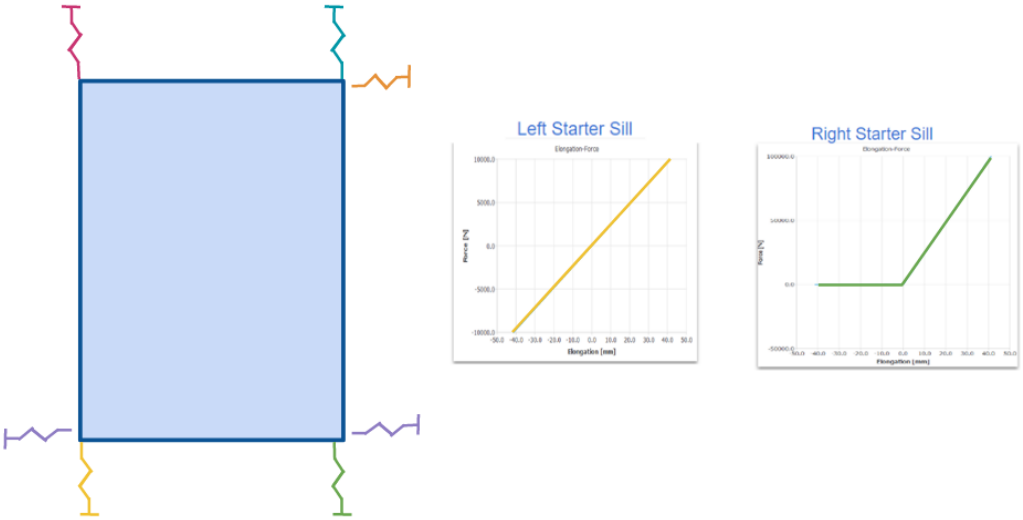

Figure 5.20: In the schematic representation presented above the different boundary springs applied to the curtain wall unit are depicted. Each colour indicates different material properties. The slightly different trend of the properties attributed to the two boundary springs of the starter sills are depicted to the right. It is clearly seen that for the left case, the non-linear properties were reversed to the linear ones.

On the downside, after the modelling of the additional boundary condition restraining the upward movement of the unit to its left corner, the horizontal displacement of point D was noticed to deviate more from the experimental reference values, compared to its experimental approximation before the implementation of the extra boundary condition. As a consequence, the glazing point J located adjacently to the framing point D, was seen to displace more compared to the experimental situation. The previous observations refer to the curtain wall behaviour while undergoing only the negative and not the positive displacement. In fact, for the positive displacement application the curtain wall configurations tested recreate better the experimental results.

Calibration Overview

During the modelling approach previously explained in detail, a series of sensitivity analyses was performed aiming for the improvement of the initial DIANA model. This initial version of the numerical model was developed after the calculation of the properties and interactions of all the principal curtain wall components was realised. Primarily, a set of analyses was performed attempting to identify the properties of the numerical model that influence the most its response to the horizontal displacement application. Consequently, various indications regarding the modelling directions that would result in the numerical model originated and, eventually, resulted in the first improvement of the initial DIANA model. Based on the observations made during this phase and on the better understanding of the modelling behaviour that was gradually acquired, additional hypotheses on how the numerical model could be further calibrated with respect to the reference experimental values were identified.

To begin with, the alignment screw implementation into the numerical model was investigated for its impact on the curtain wall behaviour with respect to both the negative and positive displacement applications. In practice, the asymmetric behaviour that the actual façade element was observed to have during the experimental sequence is in reality attributed to the influence of the alignment screw. Therefore, it was considered that the modelling of this curtain wall component would result in the DIANA model to better approach the actual situation by recreating both the negative and positive curtain wall behaviours simultaneously.

According to the results originating from this analysis stage, it was concluded that the two modelling approaches of this additional façade component, the alignment screw followed during this study, were not able to efficiently recreate the desired curtain wall behaviour. The existing interface connecting the starter sill with the bottom transom is presented to be stiff up to the extent that does not allow the alignment screw implementation to influence the model behaviour. Therefore, it is noticed that by reducing the stiffness of the aforementioned connection, the effect of the alignment screw implementation on the overall curtain wall behaviour increases. Nevertheless, the reduced value of the transom-to-starter sill connection stiffness deviates considerably from the realistic properties of typical products actually applied by the industry.

Furthermore, additional calibrations of the numerical model are attempted, varying over two of its main properties, the stiffness of the boundary springs connecting the upper bracket and the starter sill with the environment. The reason for this calibration originated from the need of the numerical model to recreate closer the actual façade unit behaviour, of being able to displace upwards but restrained for the opposite direction, a limitation introduced by the aforementioned boundary springs. In practice this curtain wall behaviour is intended to be modelled through the transition from the linear stiffness properties of the boundary springs to non-linear ones restricting the downward unit movement while allowing the upward. Initially, the stiffness modifications were applied to the numerical model separately for the upper bracket and the starter sill boundaries conditions. Later, while aiming for the even more realistic recreation of the façade behaviour as monitored during the experimental series, the asymmetrical properties of both the upper bracket and the starter sill boundary springs were investigated simultaneously.

The aim of this sensitivity analysis was the correction of some façade displacements, in a way that the numerical values would more closely recreate the experimental behaviour. All of the scenarios tested during this as well as the following runs of sensitivity analyses were performed for both the positive and the negative displacement aiming to facilitate the complete evaluation of each of the parameters tested in the overall behaviour of the façade units tested.

Based on the first indications originating already from the sensitivity analyses conducted in the previous modelling phase as explained in Annex B, “Improvement of Initial Numerical Model” where the impact of all the possible combinations of the asymmetrical stiffness properties of the upper bracket and the starter sill boundary springs was evaluated, the following indication derived. The discretisation of the stiffness properties of the two starter sill boundary conditions improves the overall curtain wall behaviour, more specifically its asymmetrical response while subjected to the two different displacement directions. For this reason, four additional numerical scenarios were tested during which the stiffness properties attributed to the left starter sill were the mirrored version of the ones defined for the right starter sill boundary spring.

Although the numerical values of those last versions of the DIANA model are improved, it is observed both for the positive and negative behaviour of the numerical model that an additional boundary condition applied to the upper left part of each of the façade units tested would provide further improvement. In practice, an extra boundary condition recreating the upper bracket that in reality connects the left part of the façade unit with the supporting seismic beam, was applied to the numerical model aiming to eliminate the vertical

movements of the numerical model that were increased compared to the respective experimental measurements.

Finally, based on the further improved numerical results originating from the latest DIANA model variations, a final calibration is performed. The scope of this procedure is the refining of specific façade displacements by combining the scenario providing closer-to-the-experimental numerical values for the positive direction with the one performing better for the negative displacement. After a short series of runs, a final version of the numerical model recreating better, compared to all the previous versions, the experimental behaviour of the glazed curtain wall façade unit while undergoing both positive and negative displacement application is developed. This final version of the numerical model is characterised as “calibrated model”.

After this final calibration, a considerably adequate approximation of the behaviour of the numerical model is achieved with respect to the behaviour recorded for the negative and positive displacement application during the experimental procedure as depicted in the graphs of Figure 5.21.

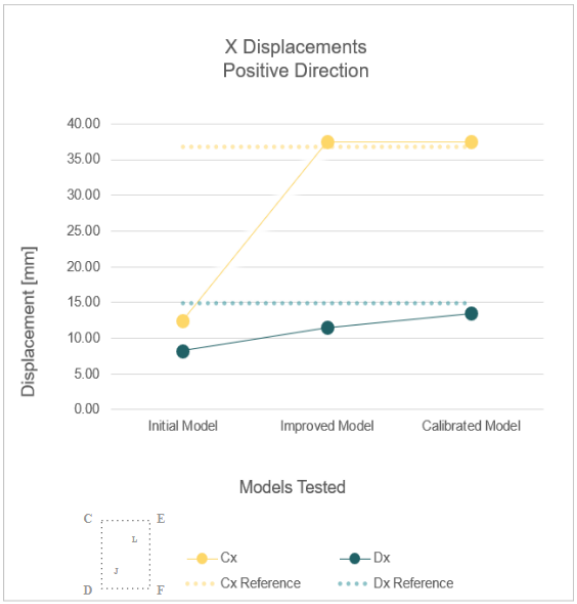

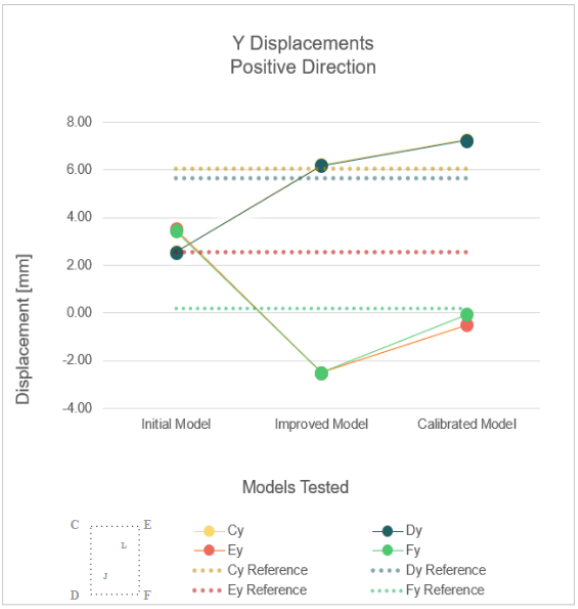

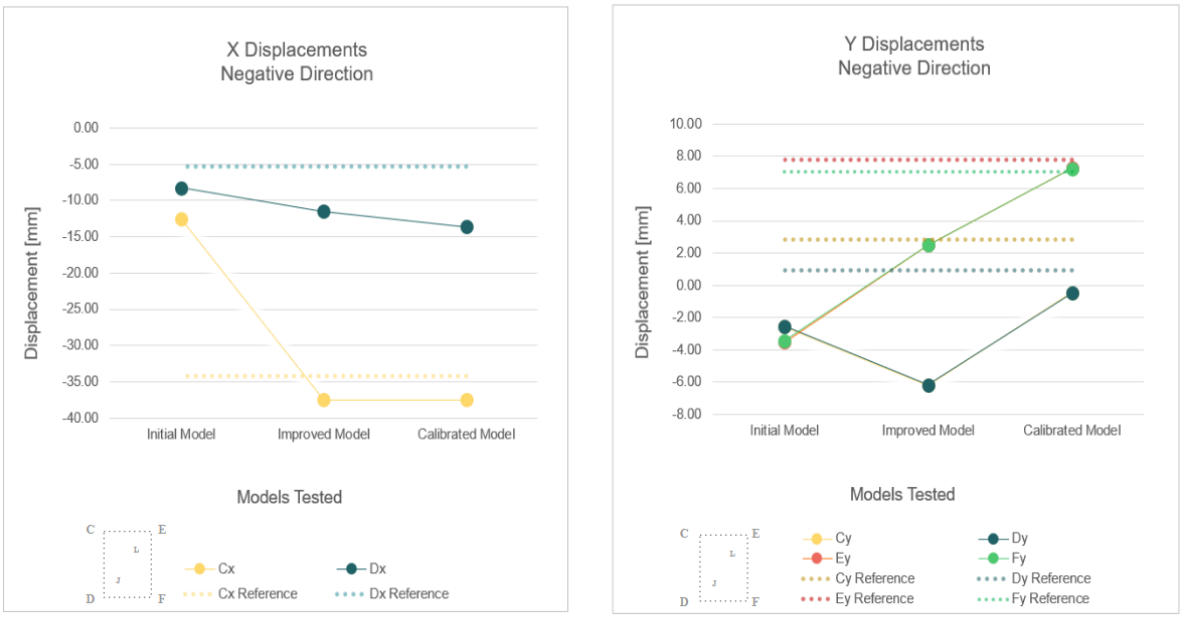

Figure 5.21: In the figure above the variation of the vertical and horizontal displacements for the positive and negative displacement application is presented above for the three distinctive versions of the numerical model, namely the initial, the improved and finally the calibrated version.

Below, some considerations as originated from the modelling development of the current study are provided. Later, a brief overview of the characteristics of the calibrated version of the numerical model follows in the "Numerical Response Assessment" section of this chapter. Additionally an evaluation of the level of accuracy achieved during this modelling approach is provided through the comparison of the numerical response with the reference experimental values.

Considerations

Despite the improvement in the accuracy of the numerical model to faithfully recreate the actual curtain wall response under seismic loading, the stiffness modifications of the boundary springs applied during this modelling phase, especially those of the starter sill boundary springs, are under discussion.

In an attempt to provide a closer to the reality simulation of the façade configuration, the starter sill properties indicating the stiffness of the boundary springs should be symmetric and not asymmetric as presented for the calibrated version of the finite element model. The reason for concluding in attributing non-identical properties to the two starter sill boundary conditions that provide the connection of the system to the ground originates from the need of the incorporation of the two different façade behaviours into solely one numerical model. It is reminded that the different behaviour of the curtain wall unit resulting from the inter-storey drift implementation and the two opposite directions, positive and negative, is in practice ascribed to a specific curtain wall component, the alignment screw. The modelling of the previous element and of its function was attempted, however the desired façade behaviour was not able to be captured. Therefore, the different

response of the curtain wall unit to the opposite displacement applications was eventually captured in the numerical simulation through the modification of stiffness properties of the starter sill boundary springs.

Apart from considering the symmetric approach of the two boundary springs, the bottom transom-to-starter sill connection should be attributed with very small stiffness. The reasoning behind that lies on the 14.0 mm gap which is present between the two coupled elements. In practice the two components only come into conduct when the façade unit is forced to go down and after overcoming this 14.0 mm distance.

The reason for not introducing the aforementioned features in the finite element modelling originates from the difficulty in the determination of the connection properties representing in a simplified way the actual connection. Eventually it is concluded that the linear properties of the gasket material located between the starter sill and the bottom transom would be attributed to this connection. As for the scripting of the unit's function aiming to allow its upward movement but to restrain the respective downward, this is transferred to the starter sill boundary conditions. As mentioned in the previous chapters, a long series of sensitivity analyses has been performed, in order for the stiffness properties that recreate best the actual façade behaviour to be defined.

Below, some conclusions related to the modelling approach developed during this study are presented. The first consideration refers to the decision to model all the adjacent curtain wall units aiming for the more accurate recreation of the actual interrelations occurring between them. The second one is related to the interrelation of the experimental and numerical results and how the latter can reinforce the better understanding of the former.

Influence of Modelling Adjacent Units

One of the goals of the current modelling approach was the identification of the impact of modelling various curtain wall units as instead of merely one. In practice, it is noticed that no different values are observed when comparing an intermediate curtain wall unit with ones located at the edges of the façade unit sequence. While examining the possible explanations that can substantiate the possible inability of the system to capture the interrelation of the adjacent curtain wall units, two possible explanations arise. The first one relates to the friction parameter that is not introduced in the properties definition of the modelling process and is expected to be essential for the correct representation of the actual situation. A second explanation for the inability of this modelling approach to represent the relation between the adjacent units is inherent distance that is initially introduced between the adjacent elements of about 10.0 mm.

The idea behind this approach is based on the actual distance that is observed between the left and right mullions, which in practice needs to be overcome in order for the adjacent mullions to be in conduct, therefore actual stress to be applied on them. An alternative modelling approach that could potentially result in a different response of the system that was not tested in this specific study but is highly suggested for further elaboration, includes the remodelling of the adjacent units with the elimination of their distance and the implementation of this feature, of the adjacent frames being able to move freely away from each other but being restrained while moving towards each other, after the initial distance placed between them is overcome.

No further action related to the improvement of the frame-to-frame connection was decided to be included in the present topic since that would include either the implementation of friction parameters of the aforementioned connection, that are not broadly available as resulted from brief research on the available literature and typical manufacturers. Additionally, the limited measurements of only the intermediate curtain

wall units, therefore, lack of a complete set of experimental values referring to both the intermediate units and the ones on the edges, is a restrictive factor for any possible validation means of the numerical model. However, this topic is considered as an interesting topic for future development and research.

Interrelation of Numerical & Experiential Results

Finally, during the modelling procedure one really interesting observation regarding the correction of the numerical approach based on the comparison of its behaviour with that noticed during the experiment was made as already mentioned previously. In more details, while studying the results of the initial versions of the DIANA model, an irregular behaviour was noticed in the mullion-to-transom connection. In fact, following the displacement application on the curtain wall unit, the frame connection appeared to be discontinuous, highlighting the necessity for its correction by implementing an element reassuring the collaboration of the two by practically meeting on solely one node.

Observations like these underline the interrelation of the finite elements modelling procedure and their contribution to the better understanding of the way a complicated system like this of a curtain wall operates. This particular finding pointing out the need of the transom-to-mullion connection continuity is intuitive, especially when considering mullions and transoms as 2D beam elements connected to each other; in that sense, it becomes evident that the two components eventually need a commonly shared node. However, the previous is representative of similar observations that might occur, leading to the modification of the numerical model and subsequently to the improvement of its accuracy.

All in all, by applying all the mechanisms a modeller considers as essential to adequately recreate an existing configuration to their simulation and visualising the respective results, important misinterpretations or even omissions can arise. In this way, not only the numerical model can be improved to recreate the actual situation more adequately but, more importantly, a better understanding of the real configuration and the way it operates is achieved.

Numerical Response Assessment

As already mentioned, the calibrated version of the finite element model resulted after running numerous sensitivity analyses and testing various options that aimed for the sensitivity assessment of the present model. Gradually, the first series of sensitivity analyses resulted in the improvement of the initial numerical model and the latter was then developed into the calibrated version.

In this final version of the numerical model development both the positive and the negative behaviours of the curtain wall element are captured. Although in reality a specific curtain wall component, the alignment screw, is considered responsible for the different behaviour of the curtain wall unit with respect to the displacement application, this feature of the curtain wall configuration was not successfully included in this specific numerical approach. Although alternative options were tested, its implementation did not provide the model with the desired behaviour. For this reason, the desired curtain wall behaviour was managed to be captured through modification of the properties defining the function of the boundary conditions. More specifically, the latter originated through the calibration of the starter sill boundary springs that were provided with slightly different stiffness. The previous does not fully correspond to the realistic situation, since there similar restraining properties are expected for both the starter sill supports.

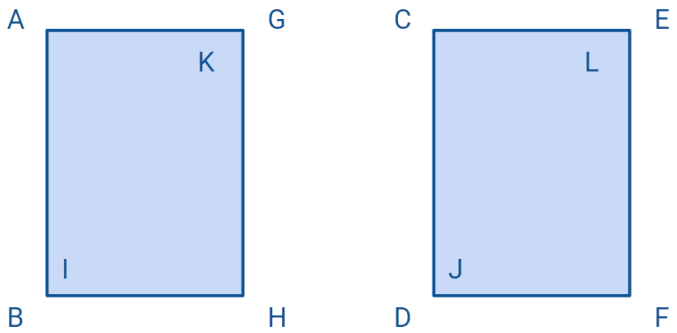

Figure 5.22: A schematic representation used as a reminder for the naming convention followed during this numerical approach.

While comparing the accuracy of the model response in the two different directions of the displacement application as seen in Tables 5.2, better performance is noticed for the case of the positive displacement. There, all the displacement values approximate the experimental behaviour in a range of 30.0 % which is considered as adequate for this global approach of the curtain wall behaviour. For the case of the negative displacement thought, the horizontal movement of point D, of the lowest left corner of the curtain wall unit, is noticed to displace more compared to the value originating from the experimental campaign which is used as reference. Consequently the adjacent glazing point, point J as referred to by the naming convention followed in the study and presented in Figure 5.22, displays a similarly large displacement compared to that measured in the actual mock-up testing. It is reminded that those two horizontal displacements deviating more than 30.0 % from the reference values refer only to the negative displacement application.

Additionally, the global curtain wall behaviour is in general accurately recreated by the calibrated model as noticed by Tables 5.2. However, the current modelling approach did not manage to capture faithfully a specific unit movement, this defined by the one of the upper brackets connecting the curtain wall unit with the primary structural systems. For the case of the positive displacement application, the movement not captured is this of the upper right corner part (point E) whereas for the reverse loading condition the upper left (point C). Although in reality these two points are noticed to displace upwards, this is not achieved by the numerical simulations. On the contrary, a downward movement is noticed which contradicts with the situation occurring in reality. It is worth mentioning that the final numerical model refinement presents a better approximation of these values. However, their accuracy still remains outside the boundary of 30.0 % that has been defined for this study.

As already explained while setting up and modifying the boundary conditions, in reality the presence of the upper bracket of the curtain wall system restrains the unit's downward movement. Therefore, a downward displacement of the upper corners of the unit are not considered accurate. However, the limitation of the movement of these areas to almost zero is considered as acceptable. Since the aforementioned values are known to not adequately recreate the realistic behaviour, their values in the tables are marked in grey, indicating that less attention should be paid to them and more to parts better recreating the actual experimental behaviour.

However, it is important to underline that although some of the aforementioned displacements are considered not to recreate the experimental behaviour quite accurately, in reality they refer to a difference of only a few millimetres. By studying a bit closer the displacement values themselves, it becomes evident that even for the case of the largest displacement application, the differences between the numerical and experimental

values do not exceed 1.5 mm with the largest difference noticed to be 3.0 mm. Therefore, the actual deviations of the numerical model from the experiential behaviour are considered limited.

Comaprison of Initial, Improved & Calibrated Models									
	Positive Displacement				Negative Displacement				
	Experiment Values	Initial Model	Improved Model	Calibrated Model	Calibrated Model	Improved Model	Initial Model	Experiment Values	
Glass									Glass
J x:	15.74	8.38	12.10	14.20	-14.20	-12.10	-8.38	-6.63	J x:
y:	6.42	2.68	6.18	7.36	-0.56	-6.18	-2.68	0.62	y:
L x:	35.10	7.30	36.20	36.20	-36.20	-36.20	-7.3	-30.70	L x:
Frame									Frame
C x:	36.80	12.50	37.50	37.50	-37.50	-37.50	-12.5	-34.16	C x:
y:	6.03	2.57	6.21	7.28	-0.46	-6.21	-2.57	2.82	y:
D x:	14.90	8.25	11.50	13.50	-13.60	-11.50	-8.25	-5.26	D x:
y:	5.76	2.54	6.18	7.24	-0.49	-6.18	-2.54	0.92	y:
E x:	-							-	E x:
y:	2.55	3.51	-2.50	-0.49	7.28	2.50	-3.51	7.78	y:
F x:	-							-	F x:
y:	0.20	3.44	-2.51	-0.05	7.25	2.51	-3.44	7.85	y:

Comaprison of Initial, Improved & Calibrated Models									
	Positive Displacement				Negative Displacement				
	Experiment Values	Initial Model	Improved Model	Calibrated Model	Calibrated Model	Improved Model	Initial Model	Experiment Values	
Glass									Glass
J x:	15.74	-47%	-23%	-10%	114%	82%	26%	-6.63	J x:
y:	6.42	-58%	-4%	15%	-191%	-1097%	-532%	0.62	y:
L x:	35.10	-79%	3%	3%	18%	18%	-76%	-30.70	L x:
Frame									Frame
C x:	36.80	-66%	2%	2%	10%	10%	-63%	-34.16	C x:
y:	6.03	-57%	3%	21%	-116%	-320%	-191%	2.82	y:
D x:	14.90	-45%	-23%	-9%	158%	119%	57%	-5.26	D x:
y:	5.76	-56%	7%	26%	-153%	-770%	-375%	0.92	y:
E x:	-							-	E x:
y:	2.55	38%	-198%	-119%	-6%	-68%	-145%	7.78	y:
F x:	-							-	F x:
y:	0.20	1664%	-1387%	-127%	-8%	-68%	-144%	7.85	y:

Tables 5.2: The tables above provide an overview of the progress noticed during the development of the numerical approach. In coloured columns the experimental values that are used as reference values are depicted. Thereafter, the numerical results of the improved and finally the calibrated versions of the finite element model are depicted. For the better assessment of each approach with respect to its proximity with the reference value the second table is provided. There, the values approximating the experimental equivalent within a range of 30.0 % are marked in green background. However, since the percentage values can be misleading, especially since they refer to displacement of millimetres or even fractions of millimetres, the first table where the actual numerical values are presented is also depicted.

Alternative Evaluation Means

Although the close study of the displacement values and their modification based on the various property alterations is considered as the most direct means of evaluation indicating the level of proximity the numerical approach manages to achieve with respect to capturing the desired behaviour, the exploration of alternative means of assessment is considered necessary. The reason for evaluating the curtain wall behaviour through additional aspects is that a wider scope of the global behaviour is generally suggested for the overall assessment of the unit.

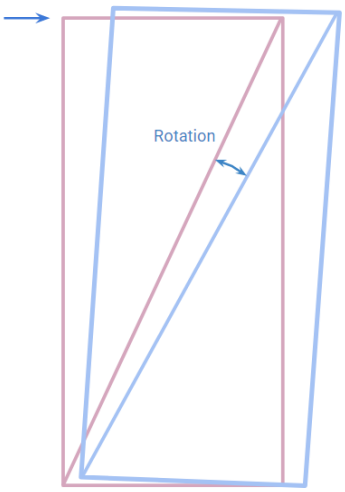

Figure 5.23: In the schematic representation above the undeformed shape of the unit prior to its loading is depicted in pink. The curtain wall response to the horizontal displacement implementation is presented in light blue colour. The angle marked in the scheme indicates the rotation angle based on which the following evaluation is realised.

Typically, the curtain wall unit rotation is considered as such. In accordance with an earlier research (Galli, 2011) analysing the same case study, the unit rotation is evaluated through the fictional diagonal element, a topic already introduced in Chapter 4 “Experimental Procedure”. The rotational angle determining the rotational angle is presented in Figure 5.23. Thereafter, relevant information regarding the procedure followed for the evaluation of the unit rotation is presented.

Contrary to the approach followed by the previous study where a spring element was used and the rotation of this was later evaluated, in this research study the rotation of this fictional diagonal element derives from the calculation of the angle created between the initial diagonal line of the unit, corresponding to the undeformed shape of the latter, and the one created for the deformed version of the curtain wall configuration.

Result Post-Process Standardised Workflow in Grasshopper

Aiming for the accurate calculation of the aforementioned rotation angle as well as the facilitation of the process a numerical workflow has been developed in the grasshopper environment. In practice the post-process of the numerical results originating from the DIANA environment was proven to be time consuming

and elaborate, therefore prone to calculation errors. In an attempt to simplify and standardise the calculation process and quickly extract the results desired, a grasshopper script has been developed. A brief introduction to its contribution to the numerical procedure and its functionality follows below.

The first part of the workflow is dedicated to the reading of the excel tables derived from the result tab of the DIANA environment. Those tables were manually extracted for each of the six frame and glazing points used as reference (points C, D, E, F, J and L) and for their displacements both in x and y direction. Therefore these tables needed primarily to be introduced in the grasshopper script. Then each of the displacement values, x and y, is attributed to the respective point, and are eventually combined with the initial coordinates previously provided for each of the points, the new locations of the point derive.

The formation of all the representative points is followed by the creation of the lines representing the aluminium transoms and mullions. Additionally, the diagonal element of the deformed unit is created as previously explained by identifying its initial and final point being the diagonal corners of the unit.

After the creation of the deformed unit and is respective diagonal, the post process of the data initiates, aiming for the calculation of various aspects such as the unis rotation, both of the frame and the glazing, the calculation of the diagonal elongation as well as the frame distortion. This data post-processing is performed in the panels coloured in green as seen in the script overview of Figure 5.24. The evaluation of these results is later discussed in the section that follows, dedicated to the extrapolation of the results.

After the creation of the deformed unit and is respective diagonal, the post process of the data initiates, aiming for the calculation of various aspects such as the unit rotation, both of the frame and the glazing, the calculation of the diagonal elongation as well as the frame distortion. This data post-processing is performed in the panels coloured in green as seen in the script overview of Figure 5.24. The evaluation of these results is later discussed in Chapter 6 which is dedicated to the result extrapolation.

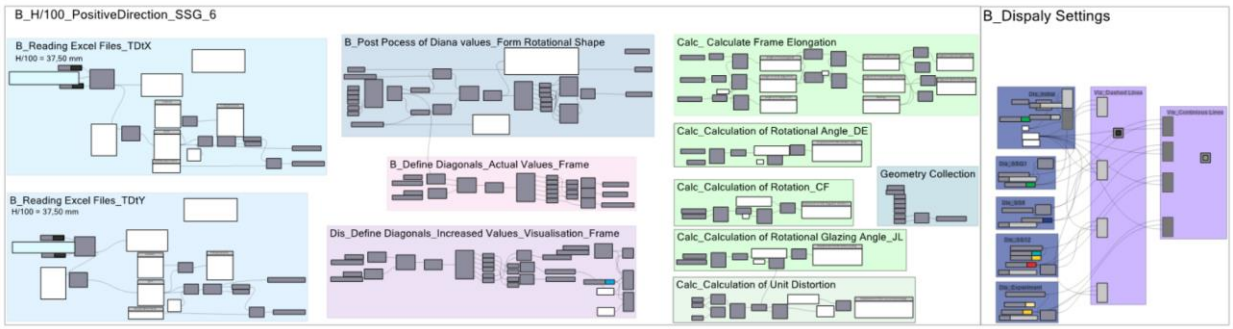

Figure 5.24: An overview of the script developed in grasshopper aiming for facilitation and the standardisation of the result post-process is presented above.

Additionally, a parallel function of the script is the visualisation of both the initial undeformed unit and of the deformed one. Of course, for the better visualisation result a magnifying factor of ten is applied to this section dedicated to the visualisation of the unit. In general, this grasshopper script developed for the present study has been widely used through the entire modelling phase and has been proven to considerably reduce the calculation time. Moreover, its contribution to the easier study of the numerical response altering based on the various modifications of the model parameters is considered valuable.

Returning to the main core of the model evaluation with regards to its proximity to the experimental results, an additional means of assessment utilised in this study is the unit rotation as already discussed. The approach followed during this study for its calculation has just been introduced. The process of the diagonal element creation is depicted in Figure 5.25. An overview of this parameter and its variation with respect to the different modelling approaches is presented in Figure 5.26.

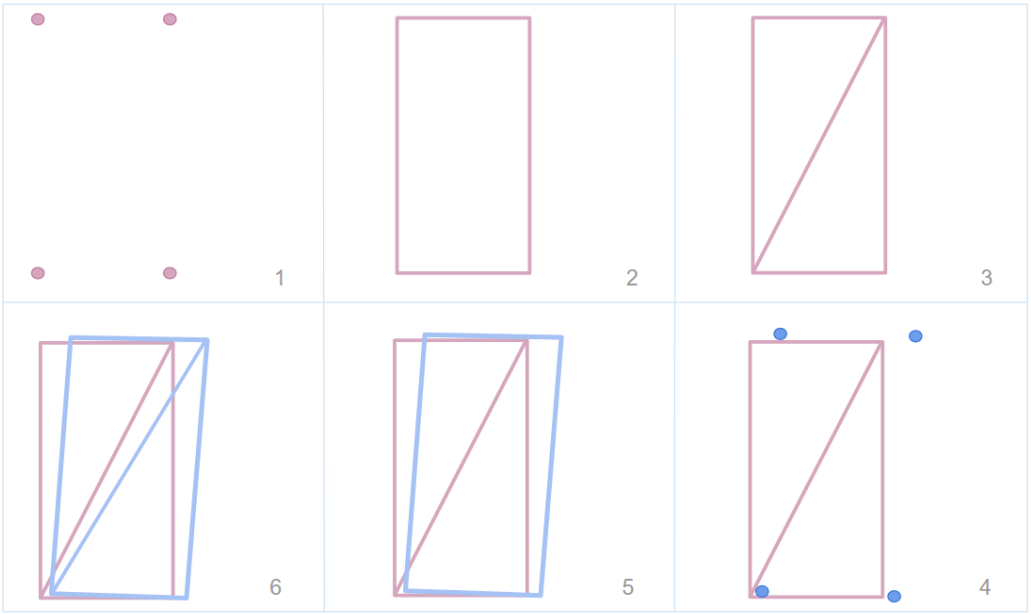

Figure 5.25: Above the concept followed during the grasshopper script starting from the initial undeformed condition and gradually moving to the deformed one and the creation of the diagonal element is presented.

The information obtained from Figure 5.26 provides useful insight regarding the progress of the numerical modelling and the approximation with the reference experimental values eventually achieved. The numerical values originating from a similar study conducted in another simulation software with a slightly different numerical approach are also included in this graph in order to serve as reference (Galli, 2011).

An interesting topic to notice is the gradually better approximation the DIANA models appear to achieve to the experimental reference values, depicted above in the dotted line. The initial version of the numerical model results in a frame rotation that recreates the one of the actual curtain wall units less faithfully compared to the rest of the approaches presented here. In fact it is the only DIANA version among the representative ones depicted above, that provides numerical results that deviate more than the values originating from the similar research approach that is used here as a reference.

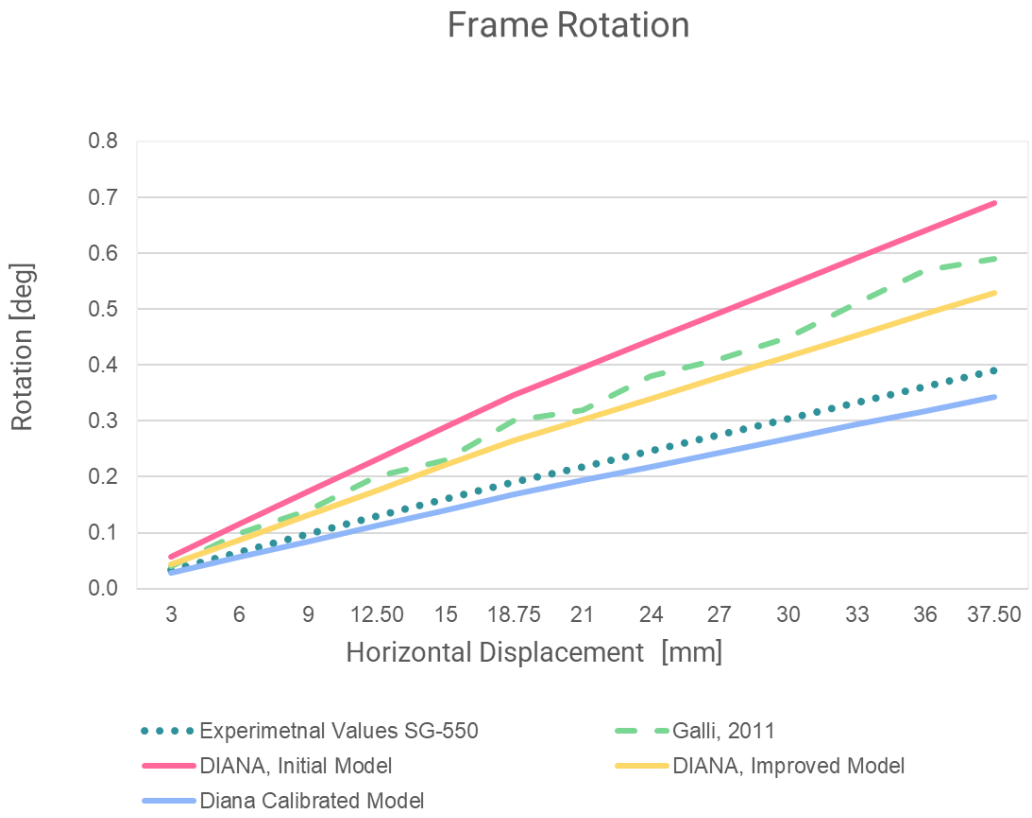

Figure 5.26: In the graph presented above an overview of the frame rotation as captured by the transducers during the experimental procedure or simulated through the different modelling approaches is presented. The experimental values monitored during the full-scale testing campaign are presented in the turquoise dotted line. The light green dashed line depicts the numerical values originating from the similar study performed for the same case study while following a slightly different modelling approach (Galli, 2011). Finally, the continuous pink, yellow and purple lines display the different versions of the DIANA model. This graph provides an insightful indication of the level of proximity achieved by each of the numerical simulations.

As already mentioned, the intermediate (improved) as well as the final (calibrated) versions of the DIANA numerical approach manage to capture more accurately the frame rotation as recorded during the mock-up test. This increase of the accuracy level is recorded not only with regards to the initial DIANA model but also with the similar study previously conducted, simulating the same curtain wall system.

Moreover, apart from the unit rotation, additional means of evaluation, such as the unit distortion and the diagonal elongation that are depicted in Figure 5.27, have been used for the assessment of the numerical model behaviour and its proximity to the experimental behaviour. Their implementation as well as the respective outcomes are in detail described in the following section referring to the result extrapolation. There, apart from the extreme scenarios tested, the intermediate case with structural silicone bite equal to 6.0 mm is also investigated. This last scenario is the final, calibrated version of the model. Thus, the unit evaluation with respect to the actual behaviour is addressed there.

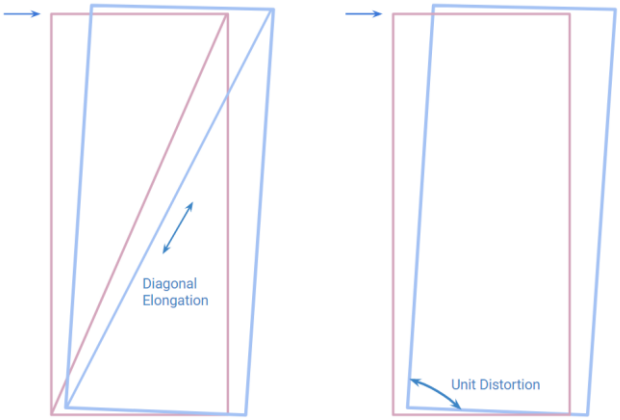

Figure 5.27: The alternative means used for the evaluation of the curtain wall behaviour are seen in this schematic representation. The diagonal elongation is assessed both in terms of mm and as percentage with respect to the initial diagonal length. The unit distortion is calculated as the relative difference of the initial and final angle of the mullion and transom connection.

Chapter 6

Numerical Result Extrapolation

The latest stage of the modelling simulation refers to the extrapolation of the results originating from the previous experimental validation. In more detail, the result extrapolation focuses on the investigation of additional modelling aspects. The latter is expected not only to provide a thorough insight on the mechanisms and overall behaviour of the façade system tested, but also to indicate the expected behaviour of similar curtain wall configurations. In that sense, the findings originating from this specific modelling approach are attempted to cover a wider range of glazed curtain wall systems, providing useful insight without requiring the development of an additional numerical model.

In order for broader conclusions to be extracted covering a wider range of curtain wall systems, the last series of analyses initially concentrates on the structural silicone sensitivity analysis. While performing this sensitivity analysis of the glazing-to-frame connection, a gradual transition from dry to the structurally sealed curtain wall system occurs. In practice, the set of analyses initiates from a very small bite of structural silicone representing the smallest stiffness of the aforementioned connection. Later, and while the silicone bite gradually becomes larger, the stiffness of the frame-to-glazing connection respectively increases. In this way, one of the main research questions this specific study aims to answer, that referring to the different seismic behaviour of the unitised curtain wall system based on either a dry or a wet connection type, is tackled.

During this incremental increase of the structural silicone thickness, the respective behaviour of the curtain wall as a whole and of its main components is evaluated. In more detail, the relation of the maximum stresses and the load path observed on the curtain wall in general are intended to be identified for different displacement rates and in function of dry (gasket) and wet (silicone) systems. The detailed study of the curtain wall elements separately also aims to validate the comments mentioned in Chapter 4, “Experimental Procedure” related to the positive contribution of structural silicone to the façade behaviour mainly due to the elimination of the stress occurring in the system.

Another, equally important goal of this final modelling stage which closely correlates to the structural silicone sensitivity analysis is the extrapolation of the ultimate governing failure mechanism of curtain wall systems similar to this under examination. Therefore, the overall reaction of the façade system will be assessed, through the evaluation of various parameters, such as the frame distortion and rotation, the displacements of representative points of both the frame and the glazing as well as the maximum stresses of all the façade components. Furthermore, the identification of the largest stresses occurring in the various curtain wall elements, will later facilitate the comparison with the respective design values.

Structural Silicone Sensitivity Analysis

Throughout this last phase of numerical simulation, and more specifically via the structural silicone sensitivity analysis during which different thicknesses of the structural bite are evaluated, one of the main research questions posed by the proposal of this study is assessed. In more detail, by gradually transitioning from a very small structural bite to larger ones, the cases of both the dry and the structurally sealed connections are aimed to be recreated. In this way, alternative with respect to their connection typology unitised curtain wall systems are evaluated under their different reaction to seismic actions and in terms of their damage mechanisms.

Additionally, the aforementioned sensitivity analysis realises the extrapolation of the observations already made from the previous stages of the current research. In more detail, the result extrapolation of the existing

study is mainly achieved through the recreation of a wider variety of glazed curtain wall configurations. It is reminded that up until this modelling stage, only the case of structurally sealed systems has been analysed, more specifically with a representative thickness bite of 6.0 mm.

Regarding the methodology of the structural silicone sensitivity analysis, it is performed between a minimum silicone thickness of 1.0 mm and a maximum of 12.0 mm. The rest of the scenarios face an incremental increase of 2.0 mm. The previous resulted in the examination of seven in total scenarios, with structural silicone thickness of 1.0, 2.0, 4.0, 6.0, 8.0, 10.0 and 12.0 mm respectively. Moreover, the running and analysis of all these scenarios is repeated for both the positive and the negative displacement application, aiming to provide an holistic evaluation of the curtain wall behaviour. Although quite a lot of intermediate scenarios have been tested during the sensitivity analysis, only three representative ones are included and presented in the evaluations, explanation and representations that follow. These are the lower and upper limit, namely with structural silicone thickness of 1.0 and 12.0 mm, and additionally the intermediate case of 6.0 mm which is also the base case used in the previous stages of the modelling procedure.

With respect to the observations originating from the frame-to-glazing connection sensitivity analysis that is evaluated during the current section, a few preliminary indications were already made based on both the findings of relevant literature and the observations of a similar sensitivity analysis performed during the earlier stages of this study's finite element modelling. Regarding the level of stresses anticipated from the structural silicone sensitivity analysis, this is expected to be minimised while moving from the dry to the wet solutions. Additionally, due to the better cooperation of the curtain wall elements that is typically noticed in structurally sealed systems compared to the configurations containing gaskets, the first ones are expected to accommodate larger displacements before their failure.

Below a schematic overview of the curtain wall behaviour for three representative scenarios of the sensitivity analysis is presented. The initial undeformed shape of the façade unit under examination is presented in grey colour, whereas the numerical results of the DIANA models comprising of 1.0, 6.0 and 12.0 mm structural silicone thickness are depicted in purple, blue and pink colour respectively. Their visualisation into a single figure aims to provide insight on the impact of the structural silicone thickness on the finite element model built for this specific case study. Additionally the experimental results are included in this figure, coloured in light blue, aiming to compare the numerical behaviour with the equivalent experimental (Figure 6.1).

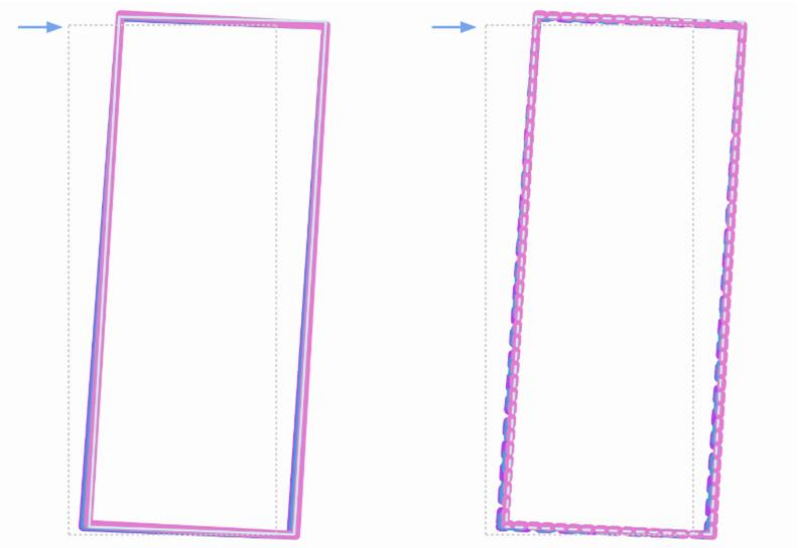

Figure 6.1: The façade behaviour under the largest positive displacement applied during this testing sequence of H/100 = 37.5 mm is seen in the figures above. In grey, the initial undeformed shape of the façade unit is presented. In light blue the façade behaviour as monitored during the experimental procedure is shown, and finally the representative DIANA models with the different silicone joints (1.0, 6.0 and 12.0 mm) are depicted in purple, blue and pink respectively. In order for the façade behaviour to be clearly seen, a magnification factor of 10.0 has been applied to both the x- and y-displacements of the façade unit. The same behaviour is presented to the left in continuous and to the right in dashed lines for the better assessment of the unit behaviour.

In the following section a detailed overview of the observations made during the current sensitivity is presented. Initially the overall curtain wall response is evaluated with respect to the structural silicone increase. Subsequently, the attention is transferred to each of the curtain wall components and their respective behaviour separately.

Global Curtain Wall Behaviour

While observing the global curtain wall behaviour as depicted in Figure 6.2, it becomes evident that in general, a good approximation of the experimental result has been achieved through the numerical modelling developed during this research.

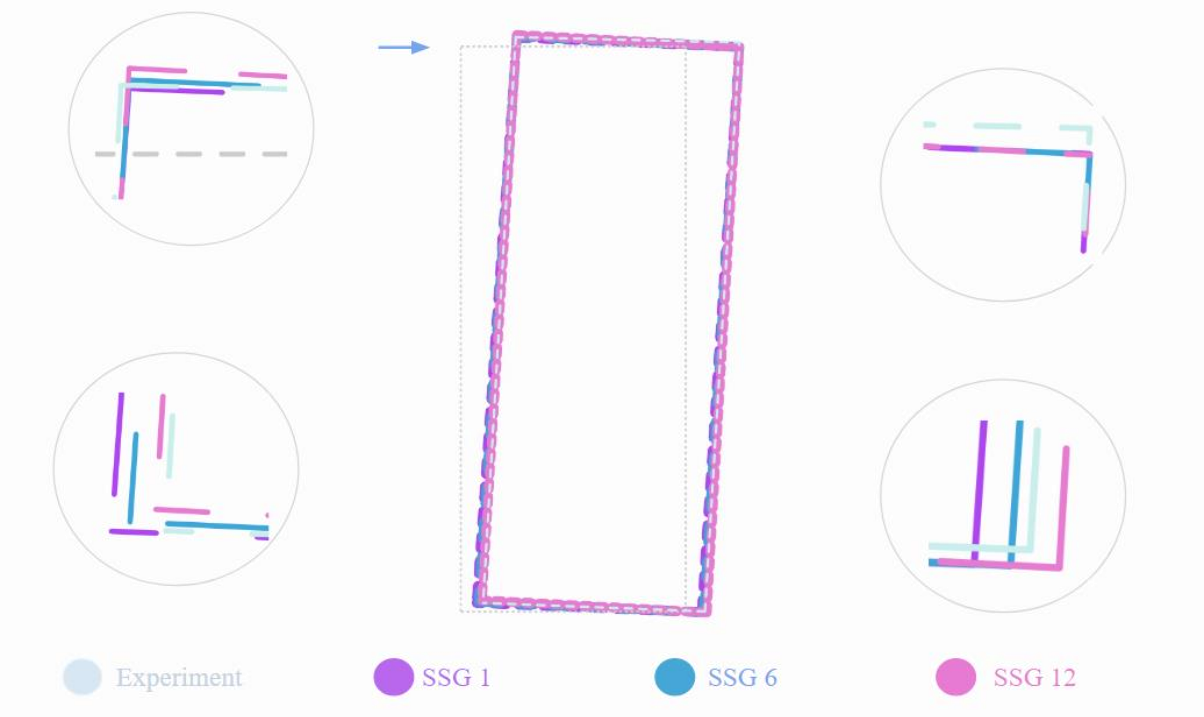

Figure 6.2: In the figure above the response of one of the curtain wall units imposed to a positive in-plane horizontal displacement is depicted. In grey the initial position of the curtain wall unit is presented. In light blue the experimental behaviour as monitored by the displacement sensors is depicted. Finally, in purple, blue and pink the representative scenarios of the structural silicone sensitivity analysis are presented. A magnification

factor of 10.0 has been applied to both the vertical and horizontal displacements for illustrative purposes. Additionally, for the better evaluation of the model response a closer look is provided to the framing corners.

An observation also mentioned during the previous modelling stages is also verified here. This observation refers to the curtain wall behaviour captured with less accuracy compared to the rest is that of the upper right corner as seen in Figure 6.2. Although this curtain wall point in the experimental case is observed to displace upwards, this has not been captured in the numerical simulation. Instead, a minor displacement approximating 0.0 has been considered as acceptable. The latter presents an improvement achieved during the improvement phase of the initial numerical model, since the finite element model is at least not seen to move downwards. It is reminded that a downward movement of corner farming is considered as unacceptable, due to the restraint imposed in reality by the bracket, preventing the curtain wall element from moving downwards.

Alternative Assessment Means

Since the evaluation of the unit behaviour with respect to the structural silicone thickness is a complex topic difficult to be directly evaluated, a combination of various means of evaluation has been selected and presented below. These alternative assessment aspects are expected to provide an elaborate and integrated evaluation of the curtain wall system global response.

The decision of the means of evaluation included in this specific study is made after relevant research in studies with similar interest and scope. Additionally, the results obtained from a graduation research focusing on the same case study (Galli, 2011) are also incorporated in some of the assessments that follow, providing a comparative evaluation of the different finite element modelling approaches developed by the two different studies. It is reminded that the main difference between the two simulations is the selection of a different software, with the initial study using Straus7 whereas the present one DIANA FEA.

Although most of the simplifications included during the modelling approach are similar, a few differences are noticed mainly with regards to the elements and material models used by each of them for the simulation of the curtain wall behaviour. The previous selection was also affected by the different possibilities and limitations of the respective software. In any case, a previous simulation of the same case study undoubtedly provides a good means of comparison and reference, especially while combined with the experimental values that serve as a reference. However, not all the means of assessment used in the present chapter have also been incorporated by the similar study. For this reason, a reference to the previous study is only made when the relevant data is available.

Regarding the additional means of the curtain wall unit evaluation, these are concluded to be the rotation of the unit diagonal expressed in degrees, the diagonal elongation expressed in mm and in the form of percentages as well as the distortion of the façade unit. Before diving into the assessment of those alternative curtain wall expressions, an overview of the way the displacement values of the representative points is affected based on the structural silicone bite alterations is presented.

Displacement Comparison

As already mentioned in Chapter 4, the experimental behaviour of the curtain wall system analysed has been recorded through a set of transducers strategically applied on representative locations of mainly the framing and secondary the glazing of façade configuration tested. Subsequently, the displacement recordings obtained from the experimental campaign, expressing the vertical and horizontal movement of characteristic points is used not only for the visualisation of the curtain wall experimental behaviour but also as reference indicating the approximation of the finite element study and the different variations tested.

Similarly to the previous modelling stages, where the improvement of the finite element model and, thereafter, its calibration was achieved by observing the variation of the displacement approximation with respect to the experimental values, an overview of the curtain wall behaviour and how this is affected by the different thicknesses of the structural silicone bites is offered by Tables 6.1 presented below.

Positive Displacement, H/100, Strucutral Silicone Sensitivity Analysis Point Displacements									
Glass	Experiment	Improved Model	S.S.1	S.S.2	S.S.4	S.S.6	S.S.8	S.S.10	S.S.12
J x:	15.74	14.20	11.80	13.00	13.90	14.20	14.40	14.50	14.60
y:	6.42	7.36	7.05	7.20	7.31	7.36	7.38	7.40	7.41
L x:	35.10	36.20	35.70	35.90	36.10	36.20	36.20	36.00	36.30
Frame									
C x:	36.80	37.50	37.50	37.50	37.50	37.50	37.50	37.50	37.50
y:	6.03	7.28	5.74	6.51	7.05	7.28	7.40	7.47	7.53
D x:	14.90	13.50	10.50	12.00	13.10	13.50	13.80	13.90	14.10
y:	5.76	7.24	5.72	6.48	7.02	7.24	7.36	7.44	7.49
E x:	-		36.00	36.00	36.00	36.00	36.00	36.00	36.00
y:	2.55	-0.49	-0.38	-0.44	-0.47	-0.49	-0.50	-0.51	-0.51
F x:	-		10.50	12.10	13.20	13.60	13.90	14.00	14.10
y:	0.20	-0.05	-0.40	-0.46	-0.50	-0.52	-0.53	-0.54	-0.54

Positive Displacement, H/100, Strucutral Silicone Sensitivity Analysis Point Displacements									
Glass	Experiment	Improved Model	S.S.1	S.S.2	S.S.4	S.S.6	S.S.8	S.S.10	S.S.12
J x:	15.74	-10%	-25%	-17%	-12%	-10%	-9%	-8%	-7%
y:	6.42	15%	10%	12%	14%	15%	15%	15%	15%
L x:	35.10	3%	2%	2%	3%	3%	3%	3%	3%
Frame									
C x:	36.80	2%	2%	2%	2%	2%	2%	2%	2%
y:	6.03	21%	-5%	8%	17%	21%	23%	24%	25%
D x:	14.90	-9%	-30%	-19%	-12%	-9%	-7%	-7%	-5%
y:	5.76	26%	-1%	12%	22%	26%	28%	29%	30%
E x:	-								
y:	2.55	-119%	-115%	-117%	-119%	-119%	-120%	-120%	-120%
F x:	-								
y:	0.20	-127%	-307%	-336%	-357%	-367%	-372%	-375%	-377%

Negative Displacement, H/100, Strucutral Silicone Sensitivity Analysis Point Displacements									
Glass	Experiment	Improved Model	S.S.1	S.S.2	S.S.4	S.S.6	S.S.8	S.S.10	S.S.12
J x:	-6.63	-14.20	-11.80	-13.00	-13.90	-14.20	-14.40	-14.60	-14.70
y:	0.62	-0.56	-1.67	-1.11	-0.72	-0.56	-0.48	-0.43	-0.39
L x:	-30.70	-36.20	-35.70	-35.90	-36.10	-36.20	-36.20	-36.30	-36.30
Frame									
C x:	-34.16	-37.50	-37.50	-37.50	-37.50	-37.50	-37.50	-37.50	-37.50
y:	2.82	-0.46	-0.36	-0.41	-0.45	-0.46	-0.47	-0.47	-0.48
D x:	-5.26	-13.60	-10.60	-12.10	-13.20	-13.60	-13.90	-14.10	-14.20
y:	0.92	-0.49	-0.39	-0.44	-0.47	-0.49	-0.50	-0.50	-0.51
E x:			-36.00	-36.00	-36.00	-36.00	-36.00	-36.00	-36.00
y:	7.78	7.28	5.74	6.51	7.05	7.28	7.40	7.47	7.52
F x:			-10.50	-12.00	-13.10	-13.60	-13.80	-14.00	-14.10
y:	7.85	7.25	5.72	6.48	7.03	7.25	7.37	7.44	7.50

Negative Displacement, H/100, Strucutral Silicone Sensitivity Analysis Point Displacements									
Glass	Experiment	Improved Model	S.S.1	S.S.2	S.S.4	S.S.6	S.S.8	S.S.10	S.S.12
J x:	-6.63	114%	78%	96%	110%	114%	117%	120%	122%
y:	0.62	-191%	-369%	-279%	-216%	-191%	-178%	-169%	-163%
L x:	-30.70	18%	16%	17%	18%	18%	18%	18%	18%
Frame									
C x:	-34.16	10%	10%	10%	10%	10%	10%	10%	10%
y:	2.82	-116%	-113%	-115%	-116%	-116%	-117%	-117%	-117%
D x:	-5.26	158%	101%	130%	151%	158%	164%	168%	170%
y:	0.92	-153%	-142%	-147%	-151%	-153%	-154%	-154%	-155%
E x:									
y:	7.78	-6%	-26%	-16%	-9%	-6%	-5%	-4%	-3%
F x:									
y:	7.85	-8%	-27%	-17%	-10%	-8%	-6%	-5%	-4%

Tables 6.1: In the tables above the numerical values of the displacements of the curtain wall representative points are displayed. Following the presentation approach also followed in the previous modelling phases the results are presented for the positive and negative displacement applications separately. The tables presenting the numerical values are followed by the respective ones expressing the level of proximity of each of the values with respect to the reference experimental values. The values marked in green background are the ones that approximate the equivalent experimental behaviour within a range of 30.0 %.

Similarly to the previous stage of the modelling approach, where the final calibrated numerical model was defined, the numerical model appears to recreate better the curtain wall behaviour when undergoing a positive displacement application. In principle, the same substantiation provided during the calibration of the final numerical model also applies here since no further modifications to the boundary conditions property is made. In more detail, all the reference points appear to approximate the reference values within a range of 30.0 % as seen from Tables 6.1. The exception to that is of course the vertical movements of points E and F that, as already analysed previously, cannot follow the experimental behaviour. As already mentioned previously, this weakness of the modelling is regarded as accepted since at least these points do not move downwards. Therefore, the points marked in grey are not further examined for their response. The

numerical results corresponding to the negative displacement application, though, present slightly less approximation to the experimental results.

Only limited information can be extracted regarding the unit overall behaviour with respect to the structural silicone sensitivity analysis based on the modification of the displacement values of the reference points. More importantly, the examination of the displacement originating from the various scenarios analysed is utilised for the realisation of additional assessment approaches, namely the evaluation of the framing and glazing rotation and the diagonal elongation. These are expected to provide a better overview of the global curtain wall behaviour and its sensitivity to the modification of the structural silicone bine. More details on the implementation of the displacement values to these evaluation methods follow in the upcoming sections.

Frame & Glazing Diagonal Rotation

The evaluation of the curtain wall rotation has been decided to be another means of comparison between the numerical and experimental results. The assessment of the rotational curtain wall response to the variations of connections, either mechanical or adhesive, is considered as an important indicator of the overall curtain wall performance. The previous is substantiated by the fact that multiple researchers have also used it in the past as a means of comparison and, eventually, concluded in a direct relation between the curtain wall connection type and the unit rotational behaviour. In practice, as already mentioned previously in this study in Chapter 2, several researchers have concluded that adhesive curtain wall configurations as opposed to mechanical ones are reported to record larger rotation.

Therefore, the assessment of the unit rotation is considered as an interesting aspect for evaluation providing a useful indicator for the curtain wall behaviour and how this is affected by the different connection typologies. The approach followed for the calculator of the unit rotation through its diagonal is the same as the one analysed earlier in Chapter 5 during the “Numerical Response Assessment” and is schematically presented in Figure 5.23. Additionally, it is reminded that the evaluation of the diagonal rotation is a combined assessment of the rotational behaviour of the glazing pane and the aluminium frame of the unit.

Similarly to the evaluations of the numerical model previously performed, the workflow created in through the grasshopper script has been utilised. While plotting the initial coordinates of the reference points the undeformed shape of the curtain wall unit is created. Later, by importing the displaced values of the same points the final shape of the curtain wall unit along with the diagonal are created per case. The differences in the length and rotation of the diagonal are calculated from the script itself. These values are later concentrated and presented in Figure 6.3 and Tables 6.2 as seen below.

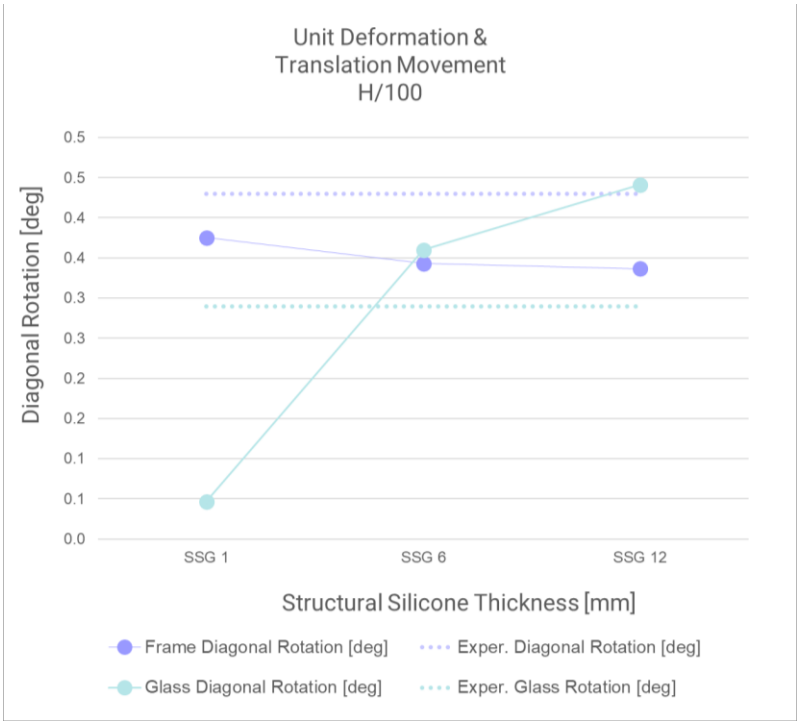

Figure 6.3: The variation of the diagonal and framing rotation with respect to the structural silicone thickness is presented in the figure above for the three representative scenarios of structural silicone bite of 1.0, 6.0 and 12.0 mm. The previous are referred to as SSG 1, SSG 6 and SSG 12 respectively. Although an increase of the glazing rotation is observed with the increase of the structural silicone bite, a decrease is noticed in the aluminium frame.

Rotational / Translation Movement & Deformation of Frame H/100					
Means of Assessment	Experiment		DIANA Models		
	SG-500	SG-550	SSG 1	SSG 6	SSG 12
Frame Diagonal Rotation [deg]	0.430	0.390	0.375	0.343	0.337

Rotational / Translation Movement & Deformation of Glass H/100					
Means of Assessment	Experiment		DIANA Models		
	SG-500	SG-550	SSG 1	SSG 6	SSG 12
Glass Diagonal Rotation [deg]	0.29	0.32	0.0466	0.3601	0.4412

Tables 6.2: In the tables above the rotation of the framing (up) and of the glazing (below) is expressed in degrees. The angle calculated is the one formed between the initial diagonal and the one originating for the curtain wall unit that is being deformed as a result of the horizontal displacement application.

While studying the rotational behaviour of the frame and the glazing pane separately, a situation similar to this presented during the evaluation of the experimental procedure, presented in Chapter 4 is recognised. More precisely, for less stiff structurally sealed connections, previously this of SIKA SG-500 here of SSG 1, the frame appears to rotate more compared to the cases where stiffer connection between the glazing and the frame is ensured.

On the contrary, for the systems with reduced thickness of structural silicone, the rotation of the glazing is less compared to that of the configurations with increased silicone bite. This indicates that the increase of the structural bite enhances the collaboration of the frame with the glazing, which results in the glazing following closer the frame behaviour by rotating. This rotation is larger in value compared to the one of the dry systems, here approached as adhesive connections with a minimum thickness. The aforementioned conclusions coincide with the observation made for the experimental behaviour which is explained in the section "Translational and Rotational Movement" of Chapter 4 and is presented in Figures 4.20 and 4.21.

Diagonal Elongation

Similarly to the calculation of the unit rotation, the derivation of the curtain wall unit diagonal is also utilised for the determination of the diagonal elongation. Again, the initial length of the fictional diagonal derives by the initial position -x and y coordinates- of the diagonal corner points of the unit. While applying in all the representative points the respective vertical and horizontal displacements, the new position of those points derives. Subsequently, the diagonal line connecting the bottom left and upper right corner of the unit is respectively modified. By comparing the final and initial length of the diagonal fictional element corresponding to the deformed with the respective length of the undeformed unit condition, the elongation or contraction of the diagonal line derives.

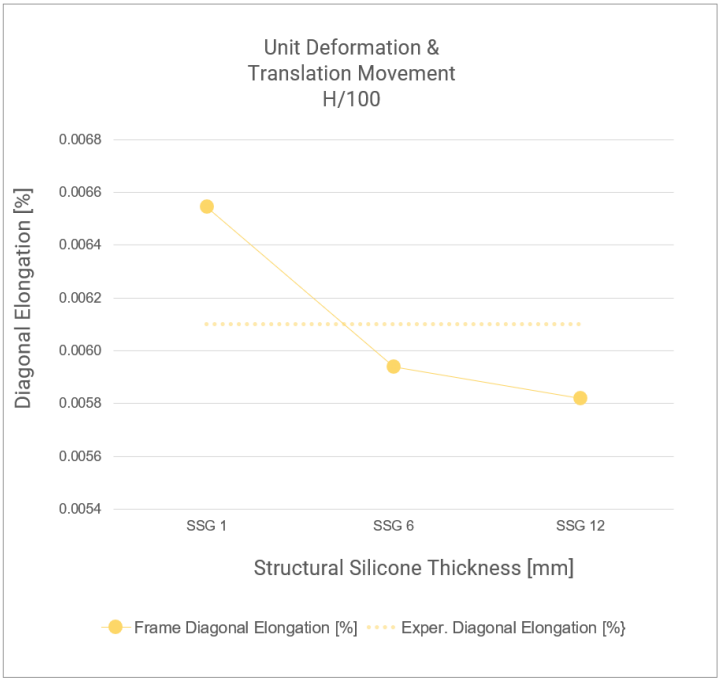

Figure 6.4: In this figure the variation of diagonal elongation expressed in the form of percentage is presented.

Rotational / Translation Movement & Deformation of Frame H/100					
Means of Assessment	Experiment		DIANA Models		
	SG-500	SG-550	SSG 1	SSG 6	SSG 12
Frame Diagonal Elongation [%]	0.0061	0.0060	0.0065	0.0059	0.0058

*Table 6.3: Above the frame elongation for the two experimental cases to the left and for the representative scenarios of structural silicone are introduced as percentages. It is reminded that the SIKA SG-500 joints have dimensions of 10.0 * 6.0 mm, whereas the ones with SIKA SG-550 6.0 * 6.0 mm.*

The diagonal elongation as a means of evaluation has been selected to be expressed both in terms of millimetres and as percentages as seen below in Figures 6.4 and 6.5 and in Tables 6.3 and 6.4. The schematic representation indicating the way of assessment of the unit distortion is depicted in Figure 5.27.

This means of assessment is mainly introduced as an indicator verifying the finite element model to adequately recreate the curtain wall behaviour as noticed during the experimental procedure. As seen from Tables 6.3 and Table 6.4, the values referring to the SSG 1, simulating the dry connection, deviate from the ones obtained from the experimental curtain wall response. The previous is a logical outcome, substantiated by the fact that the reference values originate from the curtain wall system tested during the experiment, which as already mentioned, consists of wet sealed configurations.

On the contrary, for both the intermediate case of structural silicone thickness of 6.0 mm, which is also the base case scenario used in all the previous modelling phases, and for the scenario with the largest bite of structural silicone (12.0 mm) the numerical values approximate better and extremely closely the reference ones. More specifically, the two expressions of the diagonal elongation not only follow closely the reference values, they also present the same trend as the one noticed during the experiment. In other words, the diagonal elongation slightly reduces as the structural silicone thickness increases, with the latter indicating the transition from structurally sealed connections with less to similar ones with more stiffness.

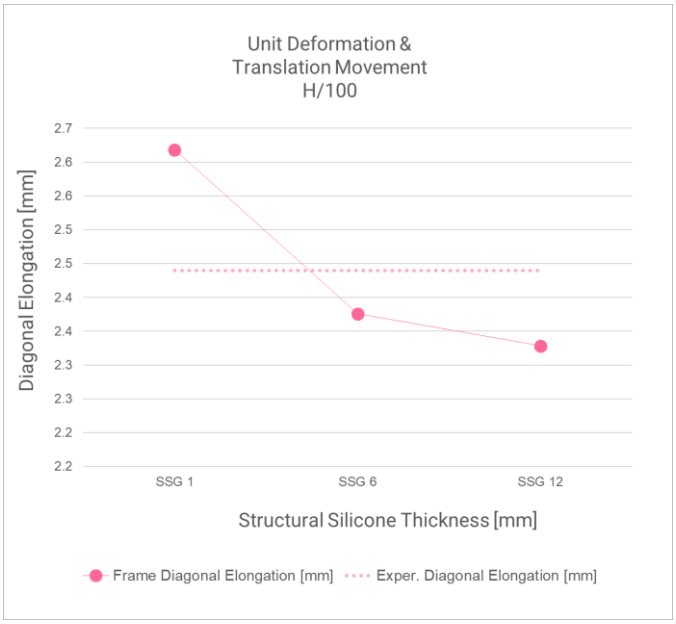

Figure 6.5: The same variation of the frame diagonal is visualised here in the form of millimetres. Again, the variation is depicted with respect to the three representative structural silicone scenarios.

Rotational / Translation Movement & Deformation of Frame H/100					
Means of Assessment	Experiment		DIANA Models		
	SG-500	SG-550	SSG 1	SSG 6	SSG 12
Frame Diagonal Elongation [mm]	2.4400	2.3800	2.6184	2.3758	2.3283

Table 6.4: The table presents the actual numbers as originated from the calculation of the diagonal elongation through the grasshopper script.

Frame Distortion

Finally, the curtain wall unit response to the alteration of the structural silicone bite is evaluated through the frame distortion. In practice, for the derivation of the unit distortion the angle between the transom and the mullion has been evaluated. Figure 5.27 provides a visual indication on the way the frame distortion is considered.

It is important to distinguish the difference between the rotation and distortion of a unit. Whereas in the case of the rotation the aforementioned angle remains 90.0 degrees, in the distortion two of the angles formed between the transom and mullion increase and the remaining decrease their angle. This is practically how the distortion has been evaluated in the current study. The respective results are depicted in Figure 6.6 and Table 6.5.

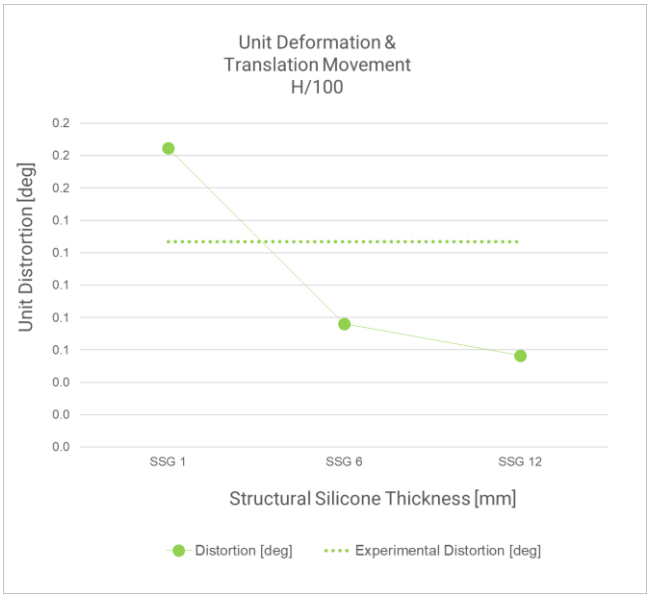

Figure 6.6: In the figure above the response of the curtain wall unit to the alteration of the structural silicone bite is presented through the frame distortion. Similarly to the previous cases, the values presented correspond to three representative scenarios of the structural silicone sensitivity analysis.

Rotational / Translation Movement & Deformation of Frame H/100					
Means of Assessment	Experiment		DIANA Models		
	SG-500	SG-550	SSG 1	SSG 6	SSG 12
Distortion, Transom-to-Mullion Angle [deg]	0.1269	0.5360	0.1846	0.0762	0.0566

Table 6.5: The numerical values describing the frame distortion are presented above. As seen both from both the figure and the table, the distortion is expressed as the difference between the initial right angle of 90.0 degrees and the deformed angle as calculated for the unit which responds to the horizontal displacement application.

What needs to be highlighted is that in this study, when referring to the angle that describes the distortion of the transom-to-mullion connection, not the exact angle of the two elements as measured for the unit deformed shape is presented. Instead, the difference of the latter and the right angle of the undeformed unit is described, characterising only the distortion occurring to the unit as result of the inter-storey drift applied on the upper part of the unit.

Observations

Based on the data originating from the previous tables and mainly from the clear intersection of two specific parameters, the diagonal frame elongation [%] and distortion of the transom-to-mullion corner [deg], with the respective dotted lines representing the experimental values, it can be concluded that the values for the

intermediate scenarios of structural silicone thickness 2.0, 3.0 and 4.0 mm should also be calculated. In practice, it is noticed that while gradually moving from structural thickness of 1.0 to 6.0 mm, these two parameters expressing the corner distortion and the frame elongation meet the reference experimental values. The latter will indicate the exact thickness of the silicone bite that for this specific modelling procedure returns the better approximation to the experimental behaviour.

The detailed behaviour of the numerical model can be seen from Table 6.6, where the correspondence of the numerical to the experimental values is represented in the form of percentage. In this case, the values marked in green background represent deviation from the experimental values within a range of 20.0 %.

Rotational / Translation Movement & Deformation of Frame H/100							
Means of Assessment	Experiment	DIANA Models					
	SG-500	SSG 1	SSG 2	SSG 3	SSG 4	SSG 6	SSG 12
Diagonal Rotation [deg]	0.4300	0.3751	0.3550	0.3494	0.3437	0.3432	0.3365
Diagonal Elongation [mm]	2.4400	3.4500	2.7200	2.2450	1.7700	0.8400	0.3800
Diagonal Elongation [%]	0.0061	0.0065	0.0062	0.0060	0.0060	0.0059	0.0058
Distortion, Transom-to-Mullion Angle [deg]	0.1269	0.1846	0.1305	0.1109	0.0914	0.0762	0.0566

Rotational / Translation Movement & Deformation of Frame H/100							
Means of Assessment	Experiment	DIANA Models					
	SG-500	SSG 1	SSG 2	SSG 3	SSG 4	SSG 6	SSG 12
Diagonal Rotation [deg]	0.4300	-13%	-17%	-19%	-20%	-20%	-22%
Diagonal Elongation [mm]	2.4400	41%	11%	-8%	-27%	-66%	-84%
Diagonal Elongation [%]	0.0061	7%	2%	-2%	-1%	-3%	-5%
Distortion, Transom-to-Mullion Angle [deg]	0.1269	45%	3%	-13%	-28%	-40%	-55%

Table 6.6: Four different assessment methods of the structural silicone sensitivity analysis are presented above. On the table below, the values for which their approximation to the equivalent experimental result fluctuates between -20.0 % and 20.0 % are presented in green background.

According to the table above, the numerical models with structural silicone thickness of 2.0 and 3.0 mm recreate closer the experimental behaviour. However, the fact that the above values refer to an extremely increased level of detail, rotations of less than 0.5 degrees and diagonal elongations of 0.001 %, should be underlined. Of course, some of the inconsistencies of the numerical compared to the experimental model

existing already from the previous stages, for example the one of the top right corners of the frame not being able to move upwards in accordance with the experimental behaviour, also affect the model behaviour in terms of its translation and rotational movement. Therefore, the selection of the most appropriate silicone joint based solely on the sensitivity analysis above where limited variation between the numerical values is observed, is of minor priority.

The more important aspect of the sensitivity analysis is to present the overall façade behaviour and how this is affected by the thickness of the joint connecting the glazing with the aluminium frame. The main points originating from the study of this behaviour are concentrated and presented in the following section.

Comparison with Expected Unit Behaviour

Following the presentation of the various assessment means of the façade behaviour with respect to the structural silicone sensitivity analysis, the comparison of the unit response as originated from the numerical modelling and the one described from the current literature takes place.

With respect to the curtain wall unit rotation, the model response as originates from this sensitivity analysis is verified for its accuracy while compared to the behaviour noticed during the experimental campaign. This quantitative verification is substantiated by the fact that the structural silicone thickness alteration affects the curtain wall behaviour in a way similar to that observed in the experiment, while comparing units composed of weaker structurally sealed connections (SG - 500) with others of stiffer connections (SG -550).

By examining the curtain wall behaviour with regards to its distortion, it can be noticed that while moving towards the wet configurations the distortion values decrease. The latter coincides with the expected unit response since it indicates better coupling between the glazing and the frame. Although the qualitative assessment of the numerical behaviour is in accordance with the unit behaviour as noticed during the experimental sequence, the numerical values themselves present a slight deviation. This deviation does not exceed the 0.5 degrees as seen from Tables 6.7, therefore it is in practice negligible.

Rotational / Translation Movement & Deformation of Frame H/100					
Means of Assessment	Experiment		DIANA Models		
	SG-500	SG-550	SSG 1	SSG 6	SSG 12
Frame Diagonal Rotation [deg]	0.4300	0.3900	0.3751	0.3432	0.3365
Frame Diagonal Elongation [mm]	2.440	2.380	2.618	2.376	2.328
Frame Diagonal Elongation [%]	0.0061	0.0060	0.0065	0.0059	0.0058
Distortion Transom-to-Mullion Angle [deg]	0.1269	0.5360	0.1846	0.0762	0.0566

Rotational / Translation Movement & Deformation of Glazing H/100			
Means of Assessment	Experiment	DIANA Models	

	SG-500	SG-550	SSG 1	SSG 6	SSG 12
Glass Diagonal Rotation [deg]	0.29	0.32	0.0466	0.3601	0.4412

Tables 6.7: The different means of evaluation are collected facilitating the assessment of the frame (up) and the glazing (below). Both the experimental values including a less stiff silicone connection (SG-500) and a stiffer one (SG-550) are presented aiming to provide a direct comparison to the similar stiffness increase introduced by the silicone sensitivity analysis. The numerical values observed here refer to the last and largest intensity of displacement application, with a range of 37.50 mm, which responds to a drift ratio of H/100.

Finally, it can be argued that the previous remarks are in agreement with the expected unit behaviour as mentioned previously. It has already been stated that apart from the increase of the rotation, additionally a decrease of the unit distortion is expected to occur while moving from dry to wet façade systems. The latter is verified in this sensitivity analysis since the distortion values calculated for the angle of the transom-to-mullion connection are observed to decrease as the structural silicone thickness increases.

While starting from the minimum structural silicone bite and gradually increasing it until it reaches its maximum value, an overall understanding of the individual curtain wall components and the unit as a whole can be derived. Additionally, the impact of the transition from dry to wet systems with regards to the failure mechanisms of the individual façade components can be assessed, also in relation to different displacement applications. These topics are addressed in the following sections.

Individual Behaviour of Curtain Wall Components

As already mentioned, one of the main objectives of the present phase of the research is the identification of the governing failure mechanism with respect to the structural silicone width increase. For this reason the critical parameter per façade component, namely the glazing, aluminium frame and the structural silicone, needs to be defined. The elaboration of the results originating from the DIANA environment facilitates the decision of the latter. Below the critical aspects determining the potential failure per component are presented.

- The maximum stress for the glazing
- The maximum stress of the frame cross section
- The shear deformation for the gasket/structural silicone

More information regarding the calculation of those critical strength indicators is provided in the following section. The method applied is presented per façade element separately.

Glass

Initially, the maximum stress appearing in the glass plane had to be identified from the numerical results of the DIANA models. Regarding the location of the largest stresses of the glazing pane, this is typically observed around the glass pane edges and in the connections with the framing. As originates from relevant literature, this is expected to be found close to the lower corner of the curtain wall elements.

For this finite element simulation modelled in the DIANA environment, the stress information was obtained from the "Cauchy Total Stresses" section of the "Results" tab for each of the scenarios tested, both for the negative and positive displacement application. In this specific result representation both the orientation as well as the magnitude of the respective stresses are presented. Although the stress distribution over the glazing pane was varying depending on the variation of the structural silicone bite, only the maximum stress value was considered in each of the cases. The location of the area presenting the maximum stress is not specifically mentioned since the latter does not affect the determination of the utilisation factor.

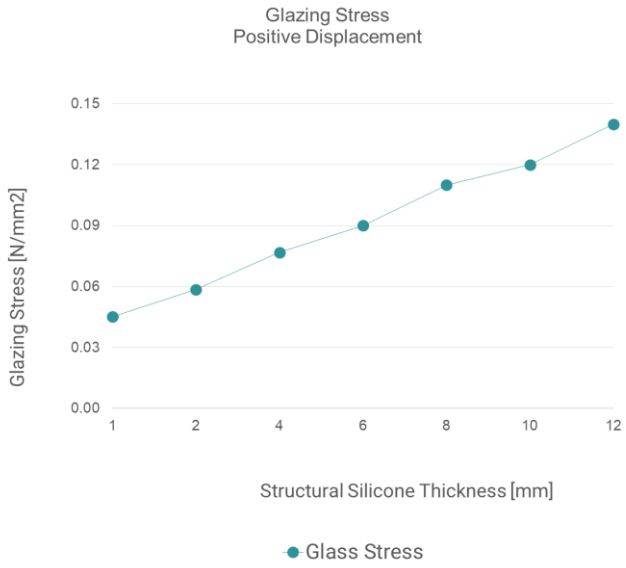

Figure 6.7: In the figure above the relation between the maximum stress observed on the glazing pane for the positive displacement application with the largest intensity H/100 is depicted with respect to the increase of the structural silicone bite.

According to Figure 6.7 presented above, the maximum stress noticed on the glazing appears to increase in relation to the structural silicone thickness. This behaviour contradicts the one we would expect while gradually moving from systems with dry connections to wet ones. Intuitively, due to the better collaboration that is normally achieved between the frame and the glazing when they are structurally sealed, a decrease of the maximum stress should be noticed. A possible explanation for the opposite behaviour observed is found in the modelling approach used.

In practice, the clearance of the dry glazing occurring between the glazing and the frame has not been included in the simulation. In reality, the initial clearance -in other worlds gap-, between the frame and the glazing needs to be covered in order for the connection of the two to happen and thereafter the stress to occur. Since this clearance is not captured in the current simulation, the frame-to-glazing connection is not

realistically represented. The previous mainly refers to the cases of the small thickness of structural silicone, which has already mentioned previously, resembles the mechanically captured connections.

A qualitative assessment of the stress distribution as observed in Figure 6.7 indicates for the cases of 1.0 mm structural silicone thickness a symmetric behaviour is observed both on the positive and negative cases of the displacement application. However, this symmetric behaviour gradually disappears while moving to larger structural silicone thicknesses.

From the seismic point of view, it can be suggested that for the dry glazed systems more attention is required to the clearance so that the connection of the glazing and the frame that eventually results in the initiation of the glass stress is prevented. The latter is concluded by observing that the larger stresses are measured in the glazing area where the adjacency of the glazing pane and the aluminium mullions occurs. Apart from this observation however, the utilisation factor as originated from the glazing measurements cannot be a safe indicator for the glazing breakage.

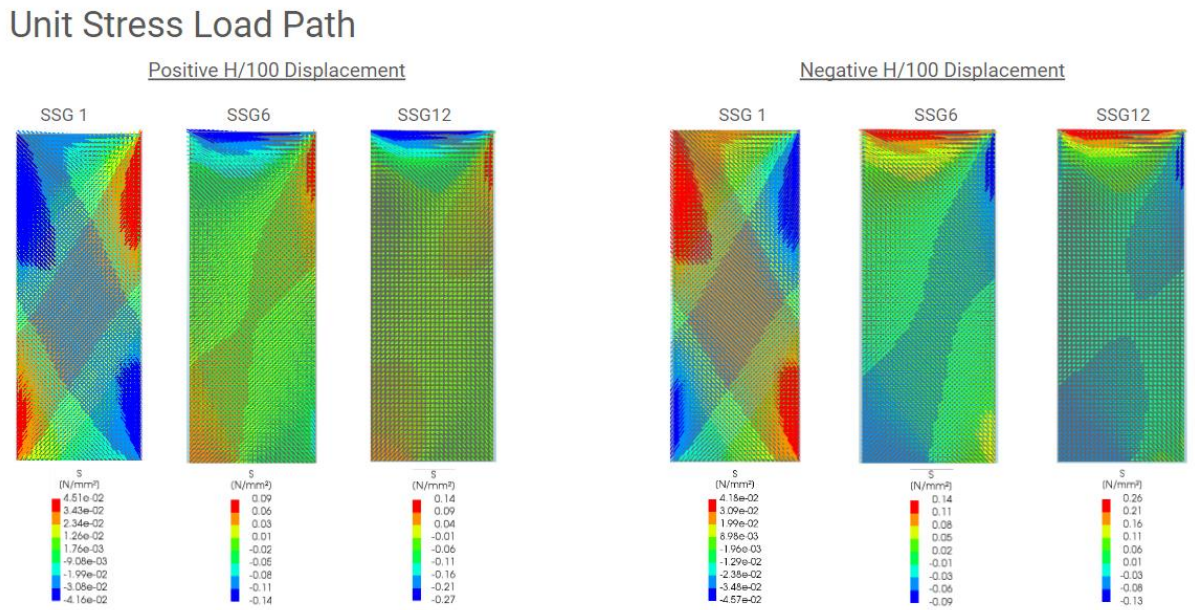

Figure 6.8: Above the loading path of the glazing unit as changing based on the different thickness of the structural silicone connection is presented for the positive (left) and negative (right) displacement application and the largest inter-storey ratio (H/100).

However, for the evaluation of the possibility of the glazing to crack, not only the investigation of the maximum stress values is important, but also the assessment of their distribution. More specifically, the flows of the glass surface presenting a reduction of the local strength are considered as important indicators. If in the flow there is a stress large enough to open the flow, then the glazing crack initiates. Therefore it is frequently seen that a crack can initiate in a glazing location with a peak flow even if the maximum stress is not located there. The previous happens since the probability of glass breakage does not only depend on the respective peak stress values but also on the way the stress is distributed.

In this way, by taking a closer look at Figure 6.8, it might be suggested that even if larger stresses are observed in the scenarios with structural silicone thickness 6.0 and 12.0 mm, the scenario with 1.0 mm resembling the dry connection might crack first. The previous hypothesis is explained by the fact that the larger stress values observed in the first cases occur only in a small glazing area, whereas in the case of the mechanically-captured system the relatively smaller stress has a larger stress distribution. Therefore, the probability of having a crack in the curtain wall configuration with a dry connection is eventually bigger.

Frame

The mechanical properties of the aluminium frame are known to be modified based on parameters such as its tempering process and general treatment. Based on the literature available and on various manufacturers, the mechanical properties of the typical curtain wall materials, glazing, aluminium framing and the connection between the previous, either gasket or structural silicone, were obtained. In more detail, the shear and axial strength of the aluminium frame [N/mm^2 or MPa] was defined as follows.

Initially the maximum shear (Q_y) and axial (N_x) forces of the curtain wall framing cross-section were obtained. Although the shear stress applied on the aluminium frame was expected to be the critical action, in practice the axial is several orders of magnitudes larger. For this reason and since the axial force of one element, e.g. the transom, works as the shear action to the perpendicular element, here the mullion, the axial stress values, instead of the shear ones, resulted to be the most critical factor.

Below the modification of the axial and shear forces as well as of the moment of the frame are presented in Figure 6.9 aiming to provide an overall view of the frame response to the increase of the structural silicone bite.

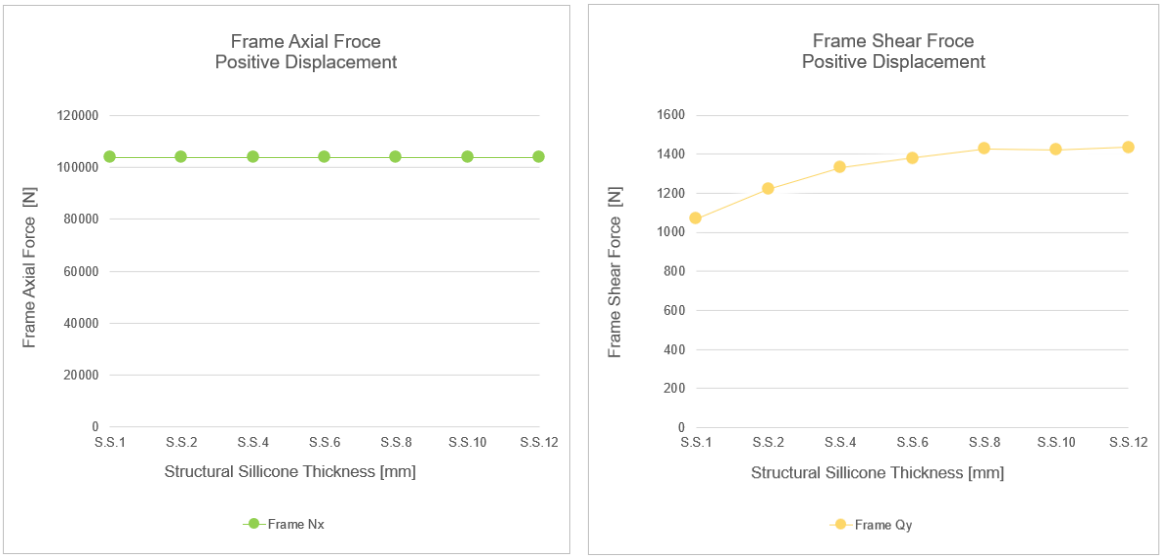

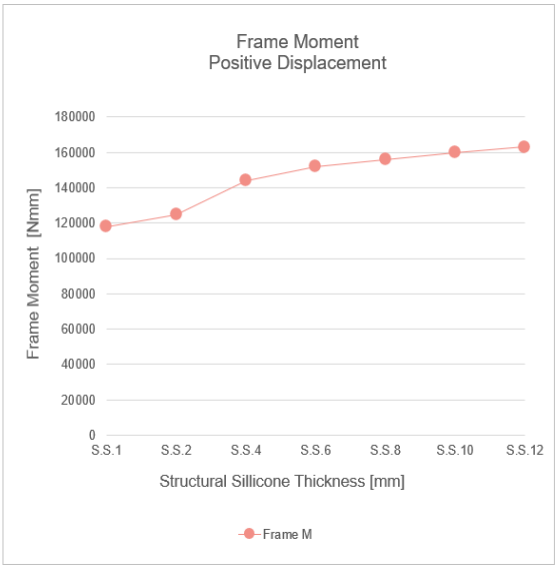

Figure 6.9: The variation of the axial and shear forces (top) and the moment (below) with regards to the structural silicone thickness increase is presented above.

According to the figures provided above, both the shear force and the moment appear to increase as the glazing-to-frame connection gradually transforms from what is simulated as dry connection to a wet solution. The axial force on the other hand does not present a noticeable variation. It is however obviously larger compared to the shear force as measured for the cross section. A detailed presentation of how the axial force is modified with respect to the structural silicone thickness is presented in Table 6.8

Glazing-to-Frame Connection

Finally, the shear deformation of the connection between the glazing and the aluminium frame was decided to be used as the determining factor for the definition of the respective utilisation factor since the shear strength is expected to be equivalent or even surpass the tensile one (Memari et al., 2012). For this reason, the shear deformation was determined through the “Interface relative displacement” field of the DIANA result section. An overview of the results obtained from DIANA which are related to the glazing pane is seen in Figure 6.10.

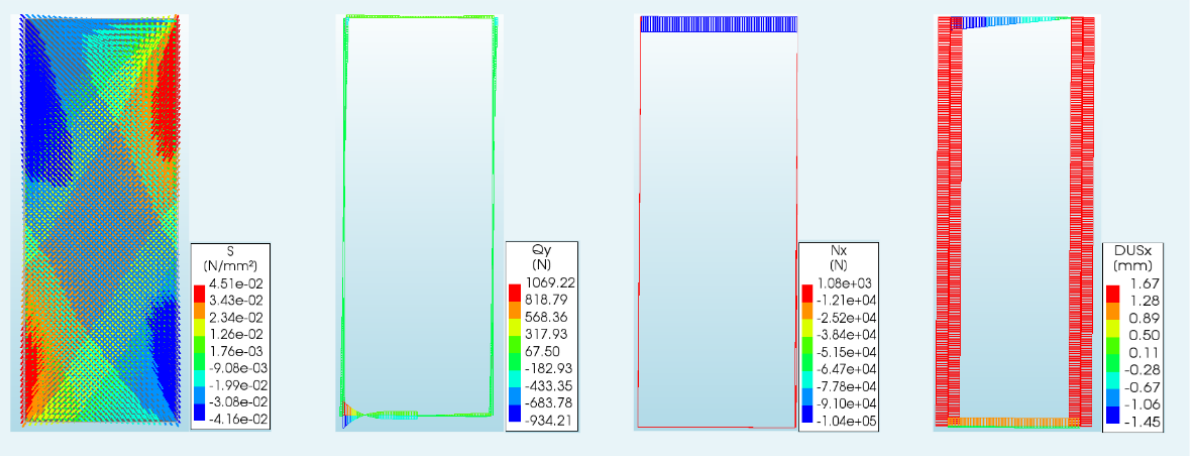

Figure 6.10: The figure above provides a qualitative indication of the results obtained from the Result tab of the DIANA environment. To the left, the contouring expressing the orientation as well as the magnitude of stresses on the curtain wall unit as resulted from the run of the non-linear analysis is seen. In the middle, the shear as well as the axial forces as calculated from the cross section of the frame and to the right the relative displacement of the glazing-to-frame connection as measured for the x-axis are presented.

Utilisation Factor

An efficient means of representation of the behavioural change of each of the curtain wall components and of the approximation to the failure threshold is the utilisation factor "u". In practice, this factor is formed for each of the façade components through the division of the maximum stress by the respective design strength.

In order for the assessment of the governing mechanism to be checked the thresholds above which failure is indicated need to be determined for each of the façade unit components separately. Initially, the critical design value for the glazing has to be identified. Although the glass strength is considered as a complex topic depending on various parameters, among which the load duration, a typical value of 20.0 MPa can be considered as a representative design value. When the numerical values of the DIANA model appear to surpass the design value threshold, the initiation of glazing breakage, or at least cracking, is considered. Of course, this exceedance of the design value does not imply the simultaneous cracking or general failure of the actual glazing element. Although, only one specimen over a larger range is realistically actually broken, the adaptation of the design values' concept as the means of the material properties evaluation is typically considered as good practice.

Regarding the evaluation of another important façade component, the aluminium frame, the maximum stress of its cross section appearing at the frame connection can provide the threshold indicating the respective failure mechanism. As already mentioned previously, based on the observations made on the framing cross-section, the axial forces were found to be larger than the shear ones. Therefore, the axial forces are the determining factor and for this reason they are obtained for the calculation of the aluminium frame utilisation factor. Consequently, the axial stress S_{xx} is divided by the yield stress of the material. The latter value is considered equal to that of an aluminium alloy typically used for curtain wall framing, Alloy 6061, 276.0 MPa (AZO, 2012, Cavallo, n.d.). Important information related to the calculation of the utilisation factor as

originated for the frame component is presented in Table 6.8. The derivation of this factor led eventually to the creation of Figure 6.11.

Calculation of the Frame Utilisation Factor			
SSG Thickness [mm]	Axial Stress on Top Transom Sxx [N/mm²]	Yield Stress of Aluminium Alloy 6061 [N/mm²]	Utilisation Factor [-]
1	77.0665	276	0.2792
2	77.0665	276	0.2792
4	77.0665	276	0.2792
6	77.0474	276	0.2792
8	77.0474	276	0.2792
10	77.0474	276	0.2792
12	76.9676	276	0.2789

Table 6.8: The variation of the axial stress S_{xx} as measured in the top transom is presented in the table above in relation to the gradual increase of the structural silicone thickness. It is quickly observed that the axial stress is slightly decreasing as the structural silicone thickness increases. Additionally, the yield stress of the aluminium alloy 6061 used for the frame of the façade configuration is also presented. Based on the two previous the utilisation factor of the aluminium frame is calculated and presented on the latest column.

Finally, the shear deformation indicates the failure of the third unit component, either the gasket for the dry systems or the silicone for the structurally sealed configurations. As introduced earlier, the shear deformation is determined through the relative displacements of the interfaces used to simulate the glazing-to-frame connection. A summary of the way those displacements are extracted and thereafter utilised for the final determination of the utilisation factor is presented in Figure 6.11.

In general, while the façade unit moves as a response to the displacement application, due to the relative movement of the framing and the glass, the silicone deforms in both the axial and the shear direction. For this reason, in the silicone bite both shear and axial strains are normally observed. Consequently, while heading to the formulation of the utilisation factor of the structural silicone, these two strains need to be considered in order for the axial and shear combined effect to be accounted for. However, since in the current modelling procedure the numerical model is only two-dimensional (2D), the axial parameter is missing due to the lack of the out-of-plane movement.

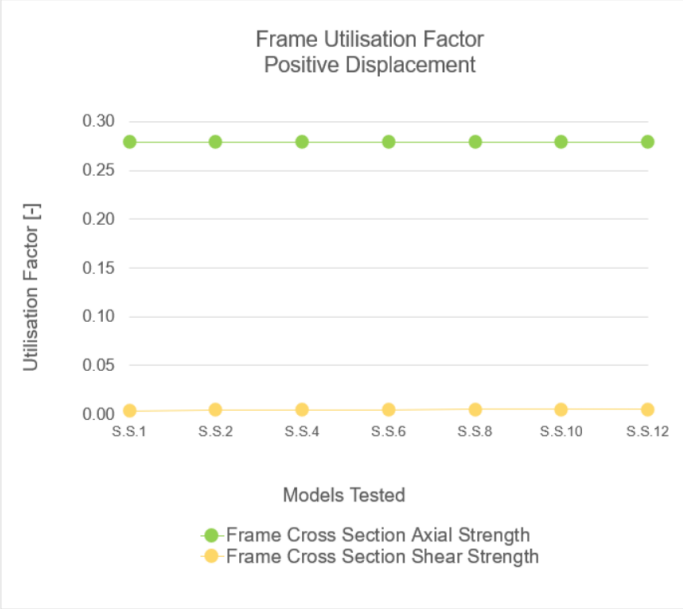

Figure 6.11: The aluminium frame utilisation factor as calculated for the axial and shear strength. As seen above, the factor deriving from the axial strength is much larger compared to that of the shear strength.

In this way, while considering only the in-plane movement of the connection joint, the relative displacement of the structural silicone is determined based on the maximum x- and y- displacement measurements. Later, the shear strain γ_{xy} is defined as follows: The equivalent displacement is divided by the initial length of the area upon which the structural silicone connects the framing with the glaze pane.

Information Needed		
Shear Modulus G		
SIKA SG-500	0.105	MPa
SIKA SG-550	0.130	
DOW 995	0.295	
DOW 983	0.398	
Shear Stress τ		
Design Value	0.140	N/mm²
SIKA SG-500	0.105	
SIKA SG-550	0.130	
DOW 995	0.931	
DOW 983	0.938	

Table 6.9: Geometrical and mechanical properties of the various structural silicone joints examined.

After the calculation of the shear strain γ_{xy}, the shear stress τ_{xy}, can also be derived, by multiplying the first with the shear modulus of the silicone connection G. Initially, only this of SIKA SG-500 is utilised, since this is the material used for the façade unit of the experiment which measurement values were used as a reference for the numerical modelling calibration. Later, more materials are considered, as seen from Table 6.9 in an attempt to capture the impact of the selection of different materials. This impact of the different silicone properties attributed to the DIANA model is visualised in Figure 6.12. Based on this figure, the use of different connections affects the utilisation factor values. Among the materials tested, the ones of DOW present lower shear stress on the structural silicone material itself, subsequently smaller values of the utilisation factor.

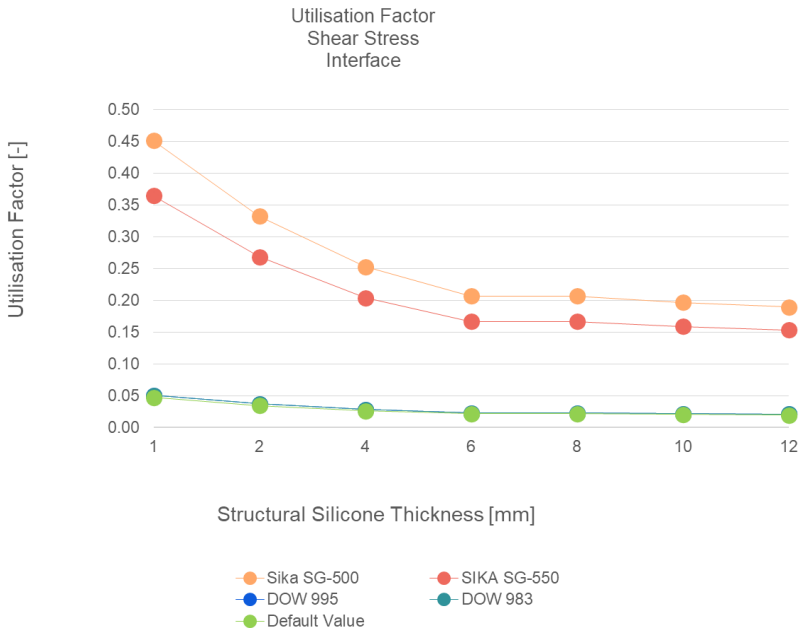

Figure 6.12: The variation of the shear stress measured on the glazing-to-frame connection in relation to the silicone thickness is presented. Several silicone materials were considered as depicted in the coloured legend.

In Figure 6.13 the utilisation factors of the basic elements of the façade configuration, frame, glazing and silicone joint connecting the two previous are presented. As seen below, the glazing is not included in the same diagram presenting the utilisation factor of the frame and structural silicone. The explanation relevant to this has already been mentioned previously. The behaviour of the glazing pane is noticed to not realistically capture the actual situation in the current modelling approach. For this reason the utilisation factor of the glazing is also not captured in the following figures displaying the different utilisation factors of the curtain wall unit.

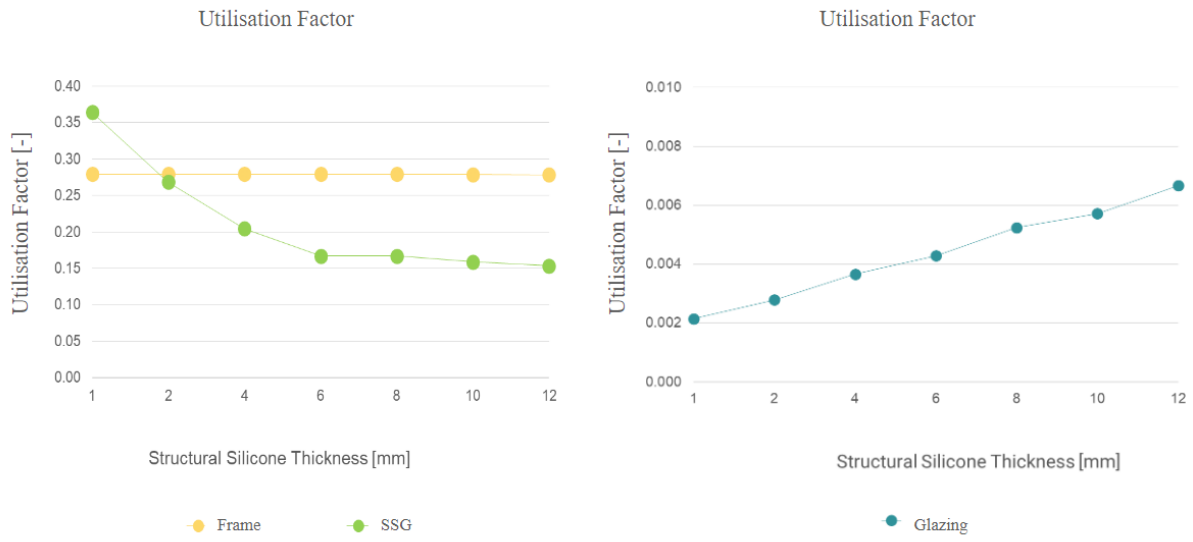

Figure 6.13. The utilisation factor of the main façade components, frame, silicone joint and the glazing are presented in the figure above.

Findings

As it can be clearly seen from the utilisation factors determined for each of the curtain wall components separately, there is a certain modification of the values with respect to the structural silicone thickness, however this is not large to the extent that the different utilisation curves coincide. The latter indicates that the variation of the structural silicone bite does not influence the curtain wall behaviour up to the extent that, depending on the silicone thickness, different components define its failure. Instead, the situation observed above indicates the stress of the cross section of the frame being the more critical failure mechanism among these of the glazing and structural silicone.

By examining Table 6.8, it can be concluded that the axial stress of the frame measured on the top transom is considerably large. Regarding its variation over the increase of the structural silicone thickness, the axial stress of the frame appears to gradually decrease as the thickness of the structural silicone joint increases. This reduction of the frame axial stress subsequently results in the reduction of the respective utilisation factor. It is important to mention though that this axial stress decrease is extremely small. The latter can be substantiated by the fact that aluminium is known to be a material considerable stiffer compared to the structural silicone, therefore the increase of the adhesive joint is expected to affect the behaviour of the façade as whole and, consequently, this of the frame up to an extent. However, not extremely large modifications are expected to be observed in terms of the utilisation factor.

Regarding the silicone joint, it is seen that less stress occurs in the material while moving from smaller to larger structural silicone thicknesses. This observation coincides with the intuitional explanation, since while more material is available to receive certain actions, the stresses occurring to it are decreased. On the contrary, for the façade configurations containing smaller silicone bite, increased stresses are developed, leading to higher values of the respective utilisation factor.

Finally, the utilisation factor resulting from the maximum stress measurements of the glazing appears to increase with respect to the structural silicone bite increase. Therefore, its value for the cases resembled in this modelling approach as wet solutions appear to be slightly larger compared to this originating from the mechanically captured façade configurations. This contradicts to the behaviour that would be normally expected, that would indicate the decrease of the maximum stress occurring on the glazing, subsequently the gradual decline of the respective utilisation factor values. A possible explanation to this could include the omittance of the clearance modelling in the current simulation. Since the initial gap between the glazing and the frame has not been modelled, the conduct of the glazing and the frame instantly occur leading subsequently to the instant stress initiation.

For this reason, it can be concluded that the utilisation factor as defined for the glazing case does not express the probability of glass cracking in general but only the probability of the peak values occurring on the glazing pane. As already explained previously and verified by the respective figure indicating the stress distribution on the curtain wall unit, in many cases the most important factor defining the possibility of a glazing unit to crack is the distribution of the stress rather than the actual peak stress. By examining this factor both for the negative and positive displacement application it can be observed that a larger distribution of the stress occurs on the glazing pane of the scenario representing a mechanically-captured curtain wall element -structural silicone thickness of 1.0 mm. The latter indicates increased cracking probability for this case of the dry-glazed façade system compared to the other representative scenarios of the structural silicone sensitivity analysis, where although larger stress values are noticed, these are distributed in a smaller area of the glazing pane.

Ultimate Governing Failure Mechanism

Stress-based Mechanisms

An additional interesting aspect of this research stage is the identification of the maximum displacement rate that can be accommodated before the actual design strength of the weakest curtain wall component is surpassed. To rephrase the previous, the identification of the displacement at which the actual failure of the various façade elements is expected is intended as part of the result extrapolation.

In case the largest displacement applied during the experimental series, which is H/100 = 37.5 mm, none of the curtain wall components is observed to surpass their design values, the drift ratios, more specifically the displacement actions, applied on the curtain wall system are increased until the point where at least one of the components fails. In practice, though, these design values based on which the utilisation factors derive are generally below the ones that define the actual failure of the components. Nevertheless, the findings of this topic are expected to clarify how the variation of the glazing-to-frame connection width affects the governing ultimate failure mechanism of the curtain wall configuration examined.

Making use of the information already originated from the behavioural analysis of each of the curtain wall components individually, an indication of the ultimate failure mechanism of the specific curtain wall configuration simulated during this study can arise. More specifically the ultimate drift ratio under which failure occurs to the curtain wall unit is identified as follows. In Figure 6.14 the variation of both the utilisation factor (to the left) and of the drift ration (to the right) are presented.

Through the largest utilisation factor noticed in the façade configuration, in this case the one determined for the framing, and while using the drift ratio at which this specific utilisation factor value has been calculated (H/100), the increase of the displacement that will lead the utilisation factor to reach the value of 1.0 can be easily derived. It is important to mention that for the simplification of the process the previous is calculated by assuming linear behaviour.

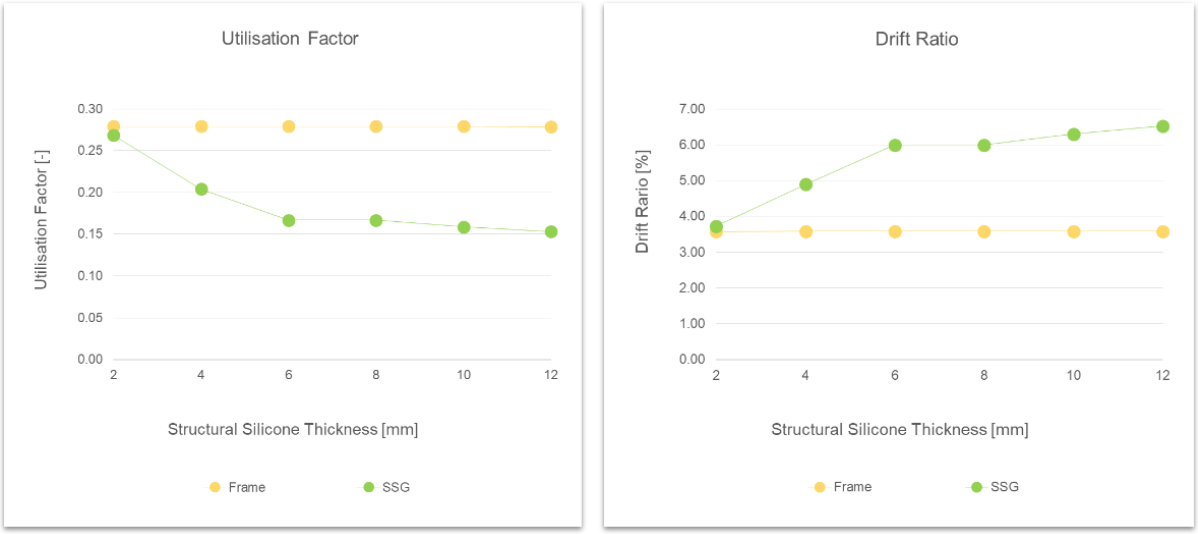

Figure 6.14: The graphs presented above express variation of the utilisation factor (to the left) and of the drift ratio (to the right) with respect to the structural silicone thickness. The influence of the glazing-to-frame connection on the ultimate failure mechanism can be easily assessed.

For a better understanding of the previous process a brief presentation is shown below.

Failure Identification

* Assuming Linear Behaviour

- for H/100 = 37.05 mm → utilisation factor ≃ 0.28
- Failure at an displacement increase of 1/0.28 = 3.60

  → ultimate stress of the element at 37.50 * 3.60 ≃ 135.0 mm

  → failure at a drift of ≃ H/28 or a drift ratio of 3.6 %

Disengagement Failure Mechanism

While studying the behaviour of similar façade configurations to the seismic displacement under experimental sequences identical to the one examined in this study, it was noticed that apart from the stress-

based failure mechanisms, the unit disengagement can be proven the governing factor leading the façade unit to fail.

In fact, during the last phase of the experimental procedure it was observed that for a very large displacement application the curtain wall unit failed but not because of the failure of one of its main components, namely the glazing, the frame or the structural silicone connecting the two previous ones. Instead, a disengagement of the façade unit was recorded due to the increased vertical displacement occurring on the bracket that eventually resulted in the disengagement of the mullion from the bracket.

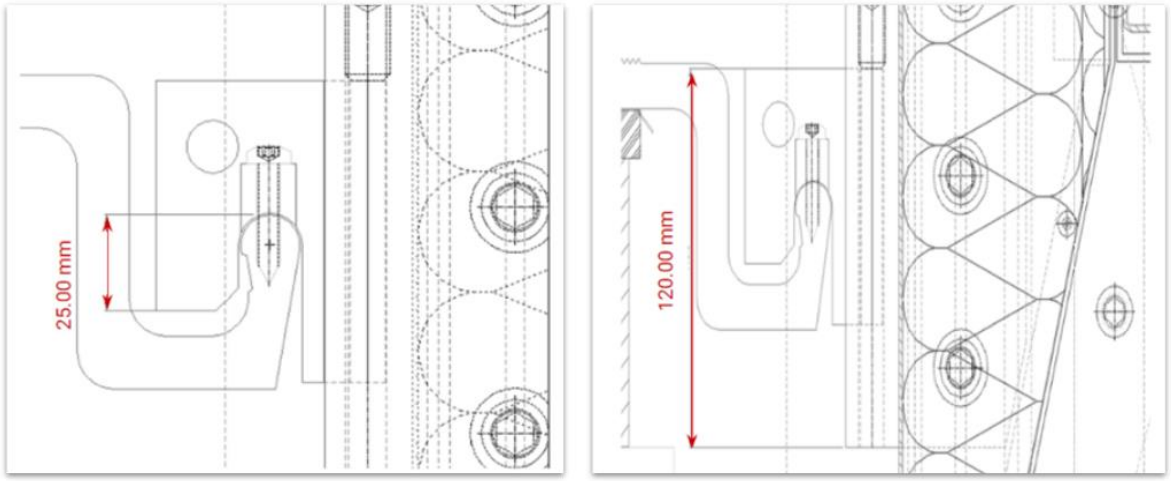

Figure 6.15: In the details above the left and right brackets connecting the curtain wall unit of the recent experiment to the structural system are presented. The vertical distance that the curtain wall unit needs to overcome in order for the disengagement to occur is different for the two brackets. As seen above, this distance is limited in the case of the left bracket, around 25.0 mm whereas for the right case is considerably larger (Source: Permasteelisa).

As seen from the details presented above in Figure 6.15, the maximum disengagement range of the unit depends on the displacement direction. The reason behind that is that not in both the left and right upper attachments of the curtain wall unit the hook is fixed to the floor bracket. For this reason, in one direction the governing mechanism is the hook disengagement of the floor bracket is 25.0 mm and in the other case 120.0 mm.

Since the threshold of the movement above which the disengagement occurs varies per curtain wall design, the above findings were translated into the case study examined in this paper.

In practice, the disengagement of the unit from the hook occurs in the upper bracket connection which is not fixed to the floor bracket, when the displacement of the slider along with the façade surpasses the limit of 25.0 mm as shown in Figure 6.16. For the remaining upper bracket connection though, a much larger margin for vertical displacement of the unit is allowed, around 120.0 mm, due to the fixing of the hook to the floor bracket. It is noticed that the same thresholds for the left and right upper bracket are observed in both the curtain wall configurations, namely the one of the present case study and this of the similar experiment recently performed. Consequently, the disengagement of the façade unit is a more critical failure mechanism for the direction of the displacement applications that results in the larger vertical displacement of the left upper part of the façade unit.

For this reason, an additional failure mechanism, this of the unit disengagement due to the hook disengagement from the floor bracket, is also analysed. Prior to the determination of the respective utilisation factor, the maximum vertical movement occurring in the upper points of the curtain wall needs to be defined as a function of the different scenarios of the structural silicone sensitivity analysis tested.

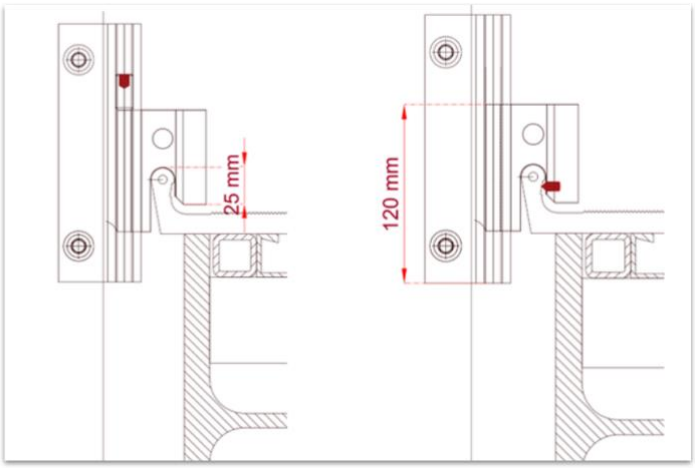

Figure 6.16: To the left, the vertical distance the unit needs to surpass in order for the disengagement to occur. To the right, the much larger vertical displacement that the façade unit needs to undergo is depicted. The difference between the two is substantiated through the screw located on the right connection, here depicted also in red, fixing the hook to the floor bracket. For the left connection, in the absence of this screw, the hook is free to disengage from the floor bracket if exceeding the 25.0 mm vertical displacement, leading to the disengagement of the curtain wall unit (Source: Permasteelisa).

The respective utilisation factor expressing the vertical displacement threshold above which disengagement occurs is also defined and presented in Figure 6.17. This failure mechanism is then combined with the previously derived ones that focus on the max stress received by the main façade components. The above results in a combined figure concentrating the respective utilisation factors simultaneously expressing the ultimate unit behaviour as defined by the two criteria, namely the stress and unit movement. The visualisation of the previous, seen in Figure 6.18 facilitates the identification of the governing failure mechanism and how this is modified by the structural silicone bite increase.

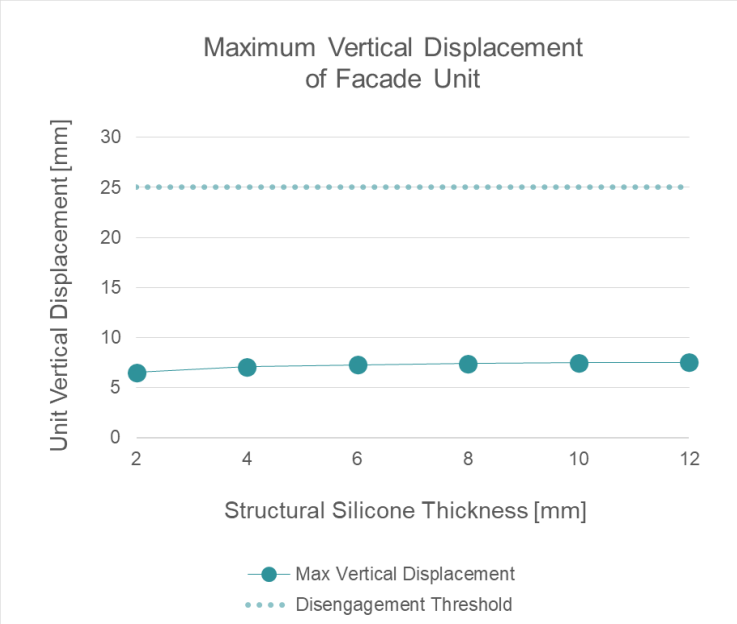

Figure 6.17: The maximum vertical displacement of the façade unit under examination observed on the upper frame corners of the façade unit.

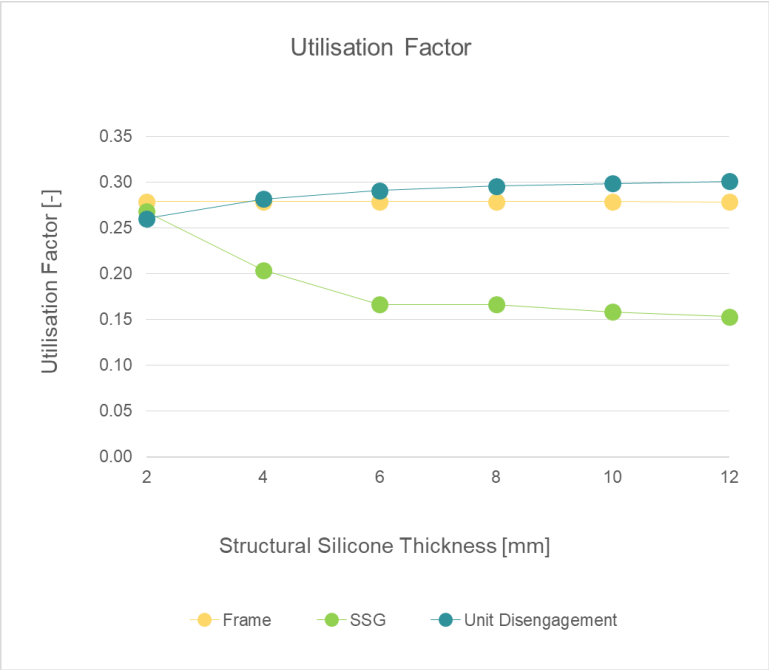

Figure 6.18: In the figure above the two maximum stress-based failure mechanisms of the frame and the structural silicone joint are presented accompanied by the additional failure mechanism indicating the possibility of the unit disengagement.

What is interesting to notice is that based on the structural silicone bite, the failure mechanism of the curtain wall unit is modified. In more details, for a structural silicone thickness less than 4.0 mm, the frame axial strength prevails as the governing damage mechanism. For the cases where the structural silicone bite is larger though the unit disengagement is the factor more prone to lead to the unit to fail.

The comment above proves the importance of the sensitivity analysis performed examining the impact of the structural silicone thickness. In fact, it is evidenced that different properties can be attributed to the curtain wall behaviour simply by varying over the connection bite, or even by the connection type itself since in this sensitivity analysis a wide range starting from the mechanically until the adhesively captured joints is covered. Moreover, possible weaknesses of the specific façade unit can be identified, allowing for the prevention of possible damages or even of the ultimate failure.

Similarly to the procedure followed previously, the ultimate displacement that will result in the curtain wall unit to fail is calculated based on modified utilisation factor. In more detail, for the scenarios closest simulating the case of dry gasket connections, therefore with a reduced structural silicone bite less than 4.0 mm, the governing displacement rate remains as calculated previously, at 135.0 mm (a drift of H/28 or drift ratio of 3.6 %) and it is determined by the frame axial strength.

The latest conclusion, which identifies the unit disengagement as the governing factor leading to the failure of the façade unit, indicates that the ultimate stress is less and therefore needs to be recalculated. Again linear behaviour is assumed for matters of simplicity. For the same drift intensity H/100, the calculation initiates from a larger utilisation factor, this time 0.30 as opposed to the previous 0.28, see Figure 6.18. The governing stress of the unit that results in the ultimate failure of the latter is calculated at 125.0 mm. The previous is translated in a drift of H/30, alternative a drift ratio of 3.3 %, and refers to the cases where the structural silicone bite is larger than 4.0 mm.

As presented previously, the previous process is modified as follows:

Failure Identification
* Assuming Linear Behaviour

- for H/100 = 37.50 mm → frame utilisation factor ≃ 0.28

  → ultimate stress of the element at 37.50 * 3.60 ≃ **135.0 mm**

  → failure at a drift of ≃ **H/28** or a drift ratio of **3.6 %**

- for H/100 = 37.50 mm → disengagement utilisation factor ≃ 0.30

  → ultimate stress of the element at 37.50 *(1/30) ≃ **125.0 mm**

  → failure at a drift of ≃ **H/30** or a drift ratio of **3.3 %**

In Figure 6.19 the correlation between the drift ratio variation and the structural silicone bite is presented.

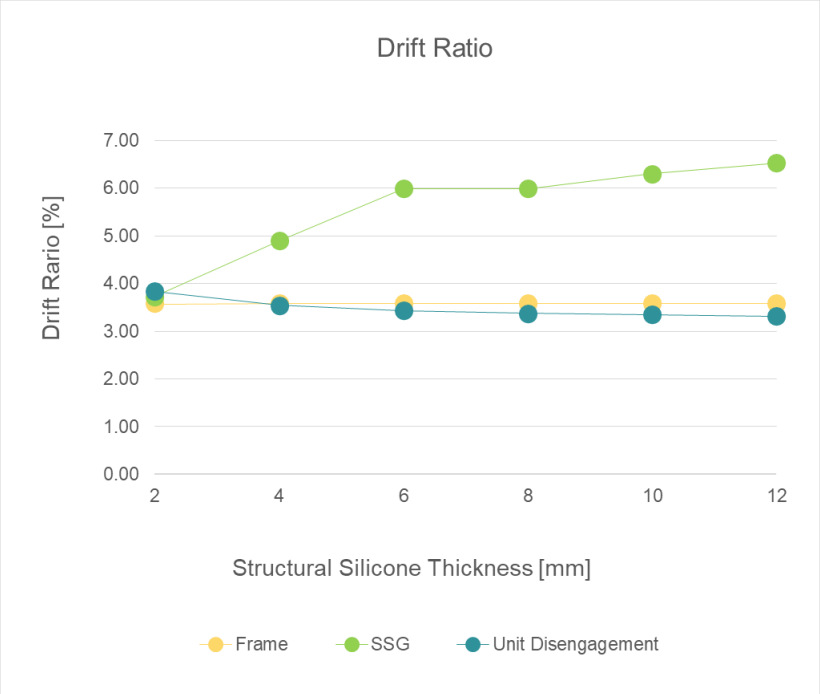

Figure 6.19: This graph displays the variation of the drift ratio with regards to the structural silicone bite.

Part III

Conclusions & Discussion

Chapter 7

Conclusions & Discussion

This final chapter initiates with a section dedicated to the discussion of this study. During the development of the numerical approach certain decisions were made, with some of them referring to various curtain wall aspects and mechanisms taken or not into consideration. Other decisions were related to the simplifications introduced in the modelling approach aiming to balance an adequate level of approximation with the minimisation of the simulation complexity and of the respective computational time. This section concentrates and presents the most important of them. Where applicable a comparison between the simulation method followed and the conditions that apply in reality is made. The previous aims to provide a better understanding of the quality of the results and to additionally substantiate certain features or responses of this specific glazed curtain wall system simulated in this numerical approach.

Initially an explanation of certain aspects implemented during this study, such as the displacement application or the in-plane curtain wall behaviour, and the omission of others, namely the action of forces or the out-of-plane façade response, is introduced. Later, the simulation approaches adopted during the modelling of the boundary conditions are described. The reason for their implementation as well as a direct collation with the almost always more complex situation realistically occurring, is presented. A list of various modelling simplifications of this modelling approach is also included, followed by the elaboration of the random effect, a parameter that can never be eliminated from the modelling attempts aiming to simulate complex configurations.

Thereafter the conclusions as originated from the current research are provided. In practice, each of the research questions formed by the research proposal is addressed. For each of those questions, the approach followed during this study accompanied by the substantiation of certain decisions is offered.

Finally, an overview of general recommendations is provided. These recommendations are initially addressed to future users and people aiming to develop simulations similar to that of the present study and later they refer to additional research. The first part of the recommendations indicated what is important to be noticed especially by people with relatively limited experience in finite element modelling while attempting a similar curtain wall simulation. This list of suggestions originates from challenges and observations made during this modelling approach, however are considered relevant for any future numerical modeller. Simultaneously these recommendations form proposals for future research. Their investigation is expected to provide valuable insight, not only related to the modelling approaches proposed but also to the better understanding of the curtain walls' behaviour and of their seismic response specifically. Finally, additional research proposals not introduced previously in this study are suggested. Their implementation in future studies is expected to contribute to the development of an integrated approach and evaluation of the glazed curtain wall post-earthquake performance as a whole.

Discussion

Modelling Aspects

Displacements vs Forces

After evaluating the considerations presented in detail in previous chapters, the decision of considering displacements, as opposed to forces, as the primary requirements for the examination of the curtain wall behaviour and the respective numerical simulation is substantiated. Displacements have been proved to constitute the main risk of curtain wall integrity when experiencing seismic events, while the equivalent

seismic action imposed on unitised curtain walls appears as less critical compared to the one imposed by the wind pressure load.

In-plane vs Out-of-plane

Additionally, based on the identification of the glazing failure or even fallout from the framing as the most common damage mechanism during an earthquake, the main principles aiming to be captured during this finite element approach were decided to be the brittle glazing behaviour as well as the easily deformable under imposed displacement framing. The simulation of the aforementioned behaviours is considered to be efficiently captured through the modelling of only the in-plane curtain wall behaviour.

While balancing the added value of the out-of-plane curtain wall incorporation into the numerical model and the additional computational complexity inevitably introduced, it was concluded that the focus should be limited to solely the in-plane behaviour. The latter can adequately recreate the key-parameters of a curtain wall system needed for the seismic design and verification, satisfying the research objectives of the present study.

Curtain Wall Units Adjacency

Contrary to other studies investigating similar topics, this research topic aimed for the simulation of a sequence of façade elements instead of only modelling an individual unit. The reason for that originated from the desire to observe the impact of adjacency of different units, the friction phenomena etc. However, the initial simulation of those connections originating between the adjacent mullions was not able to capture any different behaviour between the inward and the outward curtain wall units. The previous is verified by observing from the behaviour of the numerical model where for the application of the exact same properties and material models to the intermediate and edge curtain wall units, identical numerical values arise for the equivalent nodes.

The improvement of the connection between the adjacent curtain wall units has been decided not to be further elaborated for improvement due to lack of experimental measurements that could be used for reference. In fact, during the experimental campaign the measuring data was not obtained for both the intermediate and the outward façade units. Instead, it only referred to the intermediate façade units, making any comparison between the inward and outward units hard to realise.

Monotonic vs Cyclic Loading

The seismic loading in the present numerical approach is another important modelling aspect that needs to be introduced here since its implementation is modified compared to this applied during the experimental campaign. In reality, during the full-scale testing several displacements of different intensities as prescribed by JASS 14 (JASS 14, 2012) were applied in the curtain wall units through the seismic beam at a specified number of circles. This cyclic loading, however, has not been captured in the current modelling approach where a monotonic loading has been introduced instead. The previous is substantiated by the fact that while modelling in the DIANA environment, the introduction of a cyclic loading overrules the implementation of

the non-linear properties attributed to the various curtain wall elements in order for better recreation of the realistic façade behaviour to be achieved.

Thus, an incremental displacement is eventually applied on the curtain wall units through the use of proper factors and loading steps that result in the gradual increase of the displacement application. Although the previous approach is considered as an adequate approximation of the realistic situation, the investigation of alternative modelling solutions that would be able to simultaneously include non-linear material properties and a cyclic loading is highly suggested.

Boundary Conditions

In this particular study for the simulation of the fastening system of the curtain wall system, a common modelling approach is adopted where the complex connections are simplified and represented by a unique element. Representative examples of this study are the simulations of both the upper and the lowest boundary conditions of the façade unit through boundary springs. Below, a detailed presentation of the modelling procedure followed as opposed to the actual curtain wall mechanisms is provided. The aim of this explanation is to justify the essential modelling adaptations and to simultaneously present what are considered as important deviations of the numerical model from the actual behaviour of the actual curtain wall element examined in this study.

Bottom Transom - Starter Sill Connection

Starting from the case of the lowest fastening system of the curtain wall unit, the modelling approach adopted in this study is shortly presented below and evaluated over the more complex situation observed in the actual façade configuration. Additionally, some of the considerations regarding the absence of the gap between the two elements in the simulation as well as the attribution of different stiffness properties to the starter sill boundary springs are also mentioned.

As previously explained, in the DIANA model built during the present study, the entire connection as seen in Figure 7.1 is simulated through a boundary spring directly connecting the starter sill to the ground. In the actual façade configuration though, there are two distinguishable connections, a) the first coupling the bottom transom with the starter sill and b) another one connecting the starter sill with the bottom beam which is practically not moving, therefore could be also considered as the ground.

While observing the detailing of this connection, it becomes evident that the connection working in only one direction, allowing upward but providing resistance to the downward displacement, is the one coupling the bottom transom and the starter sill, previously mentioned as a). This type of connection is introduced in the DIANA model as a linear interface, the properties of which are restricted to linear ones. As it can be easily understood, the previous limitation of only linear properties does not allow for the scripting of the façade property facilitating movement only in one direction through this connection. So, the aforementioned property needs to be attributed to the other connection, previously referred to as connection b).

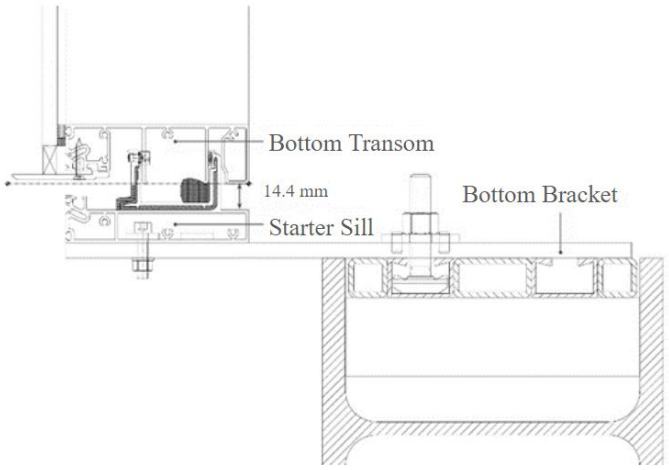

Figure 7.1: In practice this gap indicates that the interface as a whole should not provide any resistance for the cases where the transom is forced to move upwards. For the downward movement, not any resistance is presented before the gap of 14.0 mm closes.

This connection, due to its simplification for the needs of the global finite element model, is simulated through a set of boundary springs. These two boundary springs, one applied to the left and the other to the right, are provided with the façade characteristic of moving only in one direction, in other words allowing the upward but not the downward displacement. As proved from the sensitivity analyses explained, this façade feature is eventually provided through the discretization of the properties of the two starter sills.

To sum up the previous prior paragraphs, although in the actual façade configuration the component allowing the unit to displace upwards but not downwards is the one coupling the bottom transom with the starter sill, in the finite element model this function is provided through the boundary springs connecting the starter sill with the environment (ground). For a more accurate representation of the actual mechanism, the two starter sills should present symmetric behaviour. However, due to the limitations introduced by the element (linear interface) simulating the connection of interest, the properties of the actual bottom transom- starter sill connection are transferred to the starter still boundary springs through the discretization of their stiffness. There, by defining non-linear force-elongation diagrams the stiffness can be defined so that the representative connection allows the upward movement of the façade unit but provides resistance for the downward displacement.

Additionally, the relative distance, around 15.0 mm, of the bottom transom and the starter sill presented in Figure 7.1 has not been transferred into the finite element modelling. This option is based on the perceiving of the two elements combined as the bottom frame of the façade unit tested. Therefore, this internal gap provided for the accommodation and relief of various façade displacements, is assessed as an integral property of the frame, that only refers to the internal interactions of its composing elements. This is a modelling decision made for this specific façade configuration, which should be in general based on the judgement of the modeller according to the unique needs and characteristics of each modelling case.

Upper Bracket Connection

As already mentioned, during this study a second simplification approach is adopted similar to the one previously explained, namely the upper fastening system of the façade unit. The complex connection

including elements such as the bracket, the hook, the slider and the parts connecting them are collectively represented by a boundary spring. Consequently, the properties, the interconnection as well as the interrelation of those elements are attempted to be efficiently combined and attributed to a single element, which inevitably leads to simplifications and to the potential introduction of inaccuracies. A more accurate modelling of the curtain wall system tested would include the individual elements of the connection.

In the case where the previous façade and fastening components are modelled in more detail, instead of representing all the components existing between the mullion and the supporting beam solely through one element as happens in the existing study, one element could recreate the hook and a different one the bracket. There, the restraining of the vertical movement for the left bracket would be achieved in a different way from the one used for the right connection. Therefore, the decision over the set of elements introduced in a finite element model is a determinant factor significantly defining the subsequent modelling decisions and the approach in general.

In both the cases of the boundary conditions presented above, only one element, that is the boundary spring, is used for the simulation of the more complex conditions. The latter indicates that the internal components of the connection as well as their interrelations are simplified, and their properties and functions are adapted and attributed to the representative element. It is evident that another modelling approach, a more detailed one consisting of the representation of façade aspects such as the fastening systems, would be worthy of examination since interesting points of attention could arise.

Modelling Simplifications

Compressive vs Tensile Properties of Structural Silicone Material

As already mentioned, in the current study the same behaviour of the structural silicone in tensile and compressive condition was considered due to the lack of relevant references, originating both from the industry and the available literature. However, further investigation regarding the more accurate representation of the tensile vs compressive behaviour of adhesive connection is required.

Loading Application

The location of the loading applied to the curtain wall unit during its seismic loading is also one of the modelling simplifications introduced in this numerical approach. While in the experimental case the loading is applied through the seismic beam to the curtain wall unit, the numerical approach the inter-storey drift is directly applied on the façade specimen.

Additionally, another simplification introduced in the numerical approach is related to the actual location of the displacement application. Whereas in the finite element procedure the inter-storey drift is imposed on the upper left corner of the façade unit, in reality it is applied at a lower point. Due to the fastening of the mock-up unit to the load-bearing structure through the floor brackets, the displacement rate is applied at a position lower than that of the transom to mullion connection. The previous modification of the loading application in the numerical simulation compared to the experimental case introduces a small error margin, however this is not expected to considerably affect the overall curtain wall behaviour while undergoing seismic actions.

Structural Silicone Deformation Calculation

As already mentioned previously while calculating the utilisation factor of the structural silicone, only the shear stress has been determined. The reason for that originates from the fact that the current numerical model is 2D, therefore the out-of-plane movement which typically occurs in the real façade specimen, is not included in the DIANA simulation. However, for the more accurate approximation and calculation of the frame-to-glazing deformation, the axial strain should also be taken into consideration. Although in practice, it is often seen that the axial parameter is omitted from the calculations, the combined effect between the normal and the shear displacement is needed for more accurate assessment of the glazing-to frame connection strength. In a more complex modelling configuration achieved through a 3D model, the façade behaviour would be simulated incorporating also the out-of-plane movement. In this case, both the axial and the shear stresses can be determined more accurately based on the connection relative x- and y-displacements.

Glazing-to-Frame Connection Clearance

Moreover, the glazing-to-frame connection is already mentioned not to be perfectly captured in this specific modelling approach mainly for the cases of the dry-glazed configuration aimed to be captured through the structural silicone sensitivity analysis. Since the finite element model was initially developed to recreate an actual curtain wall configuration consisting only of an adhesive connection, more specifically of a structurally sealed connection, the simulation of the curtain wall clearance was not included. The latter results in a less realistic representation of the dry connections that are aimed to be approached by the structural silicone sensitivity analysis through the small bite of the structural silicone.

In order for the more accurate recreation of the glazing-to-frame connection, a modification of the modelling approach should take place focusing on the capturing of the initial gap, clearance, of the unit. Similar numerical studies that have attempted the previous, mention the use of “point contact” elements. Their application in DIANA or of equivalent elements recreating the desired behaviour are suggested for further investigation. Alternatively, the verification of the existing clearance to effectively accommodate the glazing and frame relative movements can form part of an alternative approach aiming to assess the glazing-to-frame connection.

Energy Absorption Through Silicone Materials

Moreover, the implementation of additional parameters describing the complex material properties would further increase the accuracy of the extremely complex curtain wall configuration. An instance of the previous is the contribution of the silicone materials to the energy absorption that typically affects the system’s seismic performance. For a more detailed approach, the implementation of dashpots would recreate the energy absorption by the silicone elements and eventually the damping of the forced displacements. However, as already mentioned, a decision upon the balance between the added value of each of the properties introduced in the modelling -with respect to its impact on the extracted results aiming to be later evaluated- and the prevention of the modelling complexity increase determines the aspects finally included in the simulation.

Random Effect

Finally, a possible explanation for the inconsistencies noticed in the numerical behaviour compared to the experimental values, is the occurrence of what is typically called “random effect”. The term random effect refers to the observation of the numerical results of specific façade points deviating between the subsequent loading circles. A typical example of this case is the vertical movement of point E, for the positive and largest displacement application of H/100 = 37.5 mm, which during experiment was measured as 2.55 mm, whereas in the final calibrated numerical model as -0.47 mm (Annex D, Supplement, Table 8). The latter can be substantiated through the lack of detailed information of the exact initial position of the reference point measured. Alternatively, the measurement recorded by the monitoring system might present the point relative displacement with respect to the initial position of the previous circle. Other factors, such as the existence of certain gaps between the joints or the various façade elements can also be considered responsible for variations of the numerical model compared to the experimental measurements.

Of course the random effect can apply in the finite element as a whole, however it is most likely to substantiate the upper points of the façade unit that are noticed to move downwards in the DIANA model, a behaviour which, as already mentioned, is not realistic due to the upper bracket attaching the unit to the primary structure which restrains this specific movement.

As proved above through the comparison of the numerical results with the average values of more than one circle for the third and largest displacement intensity -for more information please refer to Annex D, Reference Values Variation-, the random effect can be up to an extent considered responsible for some of the numerical model and measured values inconsistencies. In order for this effect to be eliminated in future studies of similar aims, to the extent possible of course, further attention needs to be paid to the monitoring system. In specific, a more detailed mapping of the sensors’ location is required along with more measuring points as well as a thorough understanding of what is actually measured, for example relative displacement with regards to the initial position of the measuring device or to this of the latest circle. In this way, the room for the error introduction will be considerably reduced.

In general, the information extracted during this sequence of tests is expected to provide valuable information regarding the operation of similar curtain wall systems as well as a thorough insight on their response under seismic action. However, it is essential to consider that the possible alterations of the façade elements, their geometry or properties, the different sequence of the materials, their anchorage and connections can result in a façade response that is likely to deviate from the one described previously. Thus, for the verification of each individual façade configuration further examination of its individual properties and characteristics is required.

Conclusions

Based on the findings of the present study the research questions as formed and introduced already from the introduction are addressed as presented below.

- What is the correlation of the results of the DIANA FEA numerical model, describing the behaviour of the unitised façade elements tested under seismic loading, with the experimental results observed and measured during the full-scale testing?

The development of the numerical model in this research was essentially based on the actual behaviour of the system as recorded during the experimental testing. The correlation of the previous with the reference experimental behaviour was gradually improved and basically realised through three distinct stages. Initially the properties of the main curtain wall components were attributed to the model. Additionally, the boundary conditions were applied based on a series of calculations originating from the details of the curtain wall elements and its fastening system. Through the realisation of various sensitivity analyses performed during the second modelling phase and while aiming for the better capturing of the reference experimental values, the improved version of the initial model was developed.

Eventually, after identifying the modelling aspects that determine the numerical behaviour the most, the final calibration of the numerical model took place. The properties that most determinedly define the model behaviour were found to be the boundary springs representing the upper bracket as well as the connection of the starter sill with the ground. Thus, by calibrating the non-linear stiffness properties of those boundary conditions during the third modelling phase the final version of the numerical model originated. This calibrated model managed to simulate more accurately the actual curtain wall behaviour as this was monitored during the experimental sequence.

Regarding the means of assessment used for the evaluation of the curtain wall unit with regards to the respective experimental behaviour, the principal one is the displacements examination, both vertical and horizontal, of the representative frame as well as glazing points of the examined specimen. The reference points used for the comparison of the numerical with the experimental behaviour originated from the actual façade points upon which transducers were applied monitoring their displacement. While the initial DIANA model recreated the experimental behaviour with a relatively poor approximation, with the numerical values differentiating from the experimental ones on average by 60.0 %, the numerical model improved version managed to achieve a correspondence within the range of 30.0 % which for this study is considered as accurate. However, this numerical model version managed to recreate faithfully only the curtain wall behaviour monitored for the positive displacement and not that of the negative. For the latter, the accuracy of almost all the reference points surpassed the acceptable threshold of 30.0 %.

The previous weakness of the numerical model improved version, not being able to simultaneously capture perfectly the positive and negative curtain wall behaviour, defined the third and final modelling phase and eventually led to the calibrated model version. There, the numerical model managed to capture both the positive and negative experimental behaviours accurately, with almost all the reference points recreating the experimental response within the acceptable range. The only exception is seen while examining the model behaviour to the negative displacement where the lower point of the frame presents a horizontal displacement not falling in the 30.0 % range of accuracy. However, while considering that the actual differences are no more than a few millimetres and that the comparison of the numerical and experiential behaviour is made for the third and largest displacement application, it becomes evident that small inaccuracies of the numerical model as such are both expected and acceptable.

An interesting aspect of the façade specimen examined during this specific case study, is its irregular behaviour while subjected to displacement applications of different directions. Although this irregularity of the curtain wall behaviour in reality is attributed to a specific curtain wall element, the alignment screw, its capturing in the numerical model is slightly different. In more detail, the irregularity of the facade behaviour has been achieved not through the modelling of the additional element but by slightly modifying the stiffness

properties of one of the model lower boundary conditions. In reality, this curtain wall element was attempted to be introduced in the finite element model, however, the global reaction of the system did not coincide with the expected one. The reason for this is attributed to the necessary simplifications applied during the numerical procedure, during which some curtain wall elements as well as their interrelation were combined. Their more detailed representation would significantly increase the numerical model complexity and, subsequently, the computational time, while simultaneously introducing considerable margin errors. Therefore, it was decided that the global behaviour of the curtain wall system with respect to its asymmetric behaviour to the displacements of different directions would be refined through the slight modification of the stiffness properties of one of its boundary conditions.

Additionally, further challenging aspects of the actual mock-up specimen were managed to be adequately recreated in the numerical model. These challenges were mainly driven by the limitations introduced in reality by the curtain wall fastening system and refer to the accommodation of various unit movements originating from thermal differences. In more detail, both the left upper bracket as well as the lower boundary conditions connecting the starter sill with the ground allow the curtain wall unit to move upwards, up to a certain extent, but restrain the downward movement. This behaviour, also noticed during the experimental procedure, was managed to be adequately simulated through the determination of the non-linear properties determining the stiffness of the aforementioned boundary springs. This almost faithful recreation was achieved during the processes of the improvement and calibration of the DIANA model. However, the actual experimental behaviour was not perfectly captured by the model.

In more detail, the point displacements characterised as asymmetric during both the positive and negative inter-storey applications, were not managed to be perfectly captured. While in reality the (right for the positive and the left for the negative displacement application) upper frame point appears to displace upwards by 2.50 mm on average and the lower to remain almost to its original position, in the numerical approach this is slightly different. Instead, all the points remain around their initial position, with a maximum deviation of 0.5 mm. The previous is considered an improvement compared to the original modelling where negative displacements in the range of 2.50 to 3.50 mm were recorded. This contradicts with the actual function of both the upper and lower boundary conditions that in reality restrain the downward movements. Therefore, the slight mismatch of only the asymmetric, per displacement application, points while respecting at least the actual boundary conditions restraining the downward movement is considered acceptable. The previous simplification is underlined for its accuracy when taking into account that the aim of the present numerical approach is to capture the global behaviour of the curtain wall system rather than to recreate one-to-one the displacements of all the representative points.

For this reason, alternative means of assessment, such as the unit rotation, were used for the evaluation of the global behaviour of the curtain wall system. In practice, the unit rotation was defined through the diagonal element. The creation as well as the assessment of this fictional element was realised through a Grasshopper script that was developed especially for this study. By comparing the numerical results as originating for the three levels of intensities, it becomes evident that the calibrated version of the DIANA model recreates quite closely the experimental behaviour with a maximum deviation of 0.5 degrees on average. An additional means of assessment is also utilised, the rotational behaviour as introduced by another study (Galli, 2011) focusing on the development of a similar numerical model. By comparing the accuracy of the two it is observed that the similar study reaches an approximation of 1.0 degree, therefore the numerical model developed by the present research approach better the experimental reference case.

- What are the possibilities of the results originating from this case study to be extrapolated providing insight for a wider range of similar curtain wall systems?

Aiming to answer this research question, the entire final modelling procedure phase was dedicated to the result extrapolation. In more detail, by performing a sensitivity analysis referring to the alternative types of glazing-to-frame connection, the findings originating from the present study intend to cover a broader range of curtain wall configurations. Generally, the purpose of such analyses is to provide valuable insight on various aspects related to the façade response, not only of the system examined but also of similar configurations.

In practice, by performing a structural silicone sensitivity analysis a wide variation of the curtain wall configurations, ranging from mechanically to adhesively connected systems, is examined. The evaluation of those curtain wall variations is realised on one hand by assessing their global behaviour through alternative means and on the other hand by identifying the failure mechanism that, per façade system, governs. Below, the main conclusions originating from the evaluation of the curtain wall behaviour through alternative means of assessment are presented.

Global Behaviour - Alternative Assessment Means

The impact of the structural silicone thickness on the façade unit overall behaviour is assessed through the comparison of the deformed façade units for the three representative silicone thicknesses (1.0, 6.0 and 12.0 mm) compared to the initial façade until which is presented as completely undeformed and rectangular since it does not undergo any displacement. While studying the overall behaviour of the numerical compared to the experimental behaviour it is verified that the calibrated numerical simulation follows the realistic behaviour of the façade configuration. Although the visualisation of the façade units already provides a good indication on how the variation of the structural silicone joint affects the global façade reaction to the horizontal displacement, the further elaboration on the numerical results extracted from the DIANA non-linear analysis provides an even better evaluation of the sensitivity analysis performed. For this reason, additional assessments of the structural silicone sensitivity analysis are required.

The first means of comparison refers to the rotation of the diagonal of the unit, the second to the elongation of the same diagonal expressed in mm as well as a percentage of the initial length and the third to the distortion of the curtain wall unit. The frame diagonal which is broadly used for the assessment of the unit behaviour is a fictional element connecting the diagonal frame corners and is used to correlate the overall façade movement based on individual displacement measurements of the four representative frame points.

Interesting remarks originating from the existing literature and refer to the expected curtain wall behaviour with respect to the structural silicone increase are used for the evaluation of the system response. More specifically, the transition from a dry to wet system is anticipated to result in increased rotation of the curtain wall unit and a simultaneous decrease of its distortion. By studying the curtain wall behaviour as originated from the structural silicone sensitivity analysis, the first comment can be addressed as follows.

Although the rotation of the framing separately is slightly decreased, this of the glazing pane increases. The latter results from the better collaboration achieved between the two main components of the curtain wall unit, the glazing and the frame. Consequently, a straightforward response to this question cannot be derived, since the two curtain wall elements respond differently. What can be substantiated, though, is that a better collaboration between them is for sure achieved.

Regarding the expected decrease of the unit distortion, this is also identified through the structural silicone sensitivity analysis. In practice, the distortion values of the scenarios containing larger structural silicone thickness are increased compared to those with smaller silicone bite. The better collaboration between the glazing and the frame realised through the structurally sealed connection, which in this analysis is represented by the larger structural silicone thickness, eventually results in the reduction of the frame distortion. Supplementary, the determination of a correlation between the gradual decrease of the unit distortion and the modification of the moment and shear forces of the frame cross section would be ideal, however the identification of such was not able to be found. As for the examination of the unit diagonal elongation, while studying the variation of the previous with respect to the structural silicone thickness increase, the accurate response of the system is verified for its accordance with the reference situation.

It is therefore underlined that through the result extrapolation useful insight to the seismic response of curtain wall configurations is provided. In practice, by varying over the glazing-to-frame connection, a wider range of curtain walls is covered, starting from those with mechanical connections until the structurally-sealed ones. Eventually, it is concluded that through the result extrapolation a better understanding of the different exterior envelope variations is achieved while eliminating the both costly and time consuming need for experimental testing.

- To what extent do alternative unitised curtain wall systems (dry vs wet glazed) behave differently under seismic loading in terms of the different damage mechanisms occurring on the façade element?

In order for the extrapolation of the numerical results to be reinforced, the governing per case failure mechanism was decided to be identified. Therefore, the critical parameters that typically result in each of the curtain wall components to fail needed to be also defined. For this reason, a close study of each of the curtain wall elements during the transition from a dry to wet system was performed. The latter aimed to provide a better insight to the specific façade configuration examined and more specifically to the governing failure mechanism through the determination of the respective utilisation factors.

Governing Failure Mechanisms & Utilisation Factors

While observing the impact of the structural silicone bite variation on the utilisation factors of each of the curtain wall components separately, it is concluded that in all of the cases examined during the sensitivity analysis the axial strength of the frame cross section is the factor determining the governing failure mechanism. It is also noticed that the large values of the axial forces calculated for the upper transom differ slightly with respect to the structural silicone thickness but not considerably. In practice, a small decrease of the axial stress is recorded during the transition from the dry to wet curtain wall configurations.

As for the remaining curtain wall components, the utilisation factor originating from the stress measurements of the glazing records an increase as the structural silicone bite becomes larger. This trend of the material is considered not to represent what is generally expected to occur on the glazing pane with a possible explanation being the approach followed for the recreation of the glazing-to-frame connection in this numerical model. The update of the finite element model with the simulation of the clearance occurring between the glazing and the frame can possibly return slightly different results, especially for the cases with small structural silicone bite that simulate the mechanically-captured curtain wall systems. The need for the different modelling of the clearance occurring between the glazing and the frame is indicated by the

observation of the scenario that recreates dry curtain walls where the largest stresses of the unit are noticed on the glazing areas adjacent to the mullions.

Although the sensitivity analysis interest was initially concentrated on the largest stress values observed in the pane, the respective loading path was also studied. It is found out that the examination of the stress concentration on the glazing pane provides an interesting interpretation of the expected glazing behaviour with regards to the structural silicone thickness increase. In fact, for the cases where the structural silicone bite is reduced, larger stress distribution is observed. This can increase the probability of glass cracking, when compared to the scenarios representing the structurally sealed configuration. To explain the previous, although larger stress values are measured in the latter, their distribution is limited in a small glazing area. Therefore, it is concluded that the utilisation factor as originated for the glazing serves only for describing the stress peak values occurring on the glazing but not for indicating the breakage probability. That is better expressed by the stress distribution on the glazing pane.

Regarding the response of the silicone joint utilisation factor, this appears to reduce as the silicone bite increases. This behaviour is in line with the expected one since the increase of the material accommodating the actions occurring on the unit results in the decreased stress of the glaze-to-frame connection.

Alternative Failure Mechanisms

Moreover, alternative failure mechanisms of the curtain wall unit were explored as part of the result extrapolation. Based on the outcome of a similar façade unit experimental testing, the investigation of additional failure mechanisms was decided. Therefore, instead of solely involving the mechanisms based on the components' maximum stress, the unit disengagement was also included.

Finally, while combining the two criteria determining the ultimate unit behaviour, namely the unit movement and stress, it is observed that the structural silicone bite determines the governing failure mechanism. More precisely, the axial frame strength prevails for the configurations simulating the mechanically-captured systems whereas the unit disengagement for the structurally sealed ones. The previous underlines the importance of sensitivity analyses similar to the one performed in this study since they can indicate useful conclusions regarding the susceptibility of each curtain wall configuration. By identifying the most sensitive aspects of the configuration and the most critical damage mechanisms, serious damages or even the façade unit complete failure can be prevented.

Recommendations

Future Users

Simplification Aspects, Component Mechanisms & Interaction Capturing

Be cautious of the simplifications made during the modelling. It is a general rule of course for the minimisation of the errors and inaccuracies introduced while modelling, but in this case it is mentioned to stress that while simplifying a complex mechanism/situation attention must be paid to the appropriate simulation of the overall behaviour. A representative example is this of the initial misinterpretation of the upper left vertical boundary condition of the façade unit.

At first, the focus was mostly placed on the performance of a single element of the connection, here the bracket, and how this is differentiated between the left and right area of the façade unit. In practice, although this specific element works differently inside the left and right connection, the vertical movement downwards is restricted in both cases only by different mechanisms.

So, while simplifying for the sake of the creation of a global model, it is important to carefully consider what are the actual elements and their function that are represented by each single element applied to the numerical model. Additionally, the interrelation of the individual components has to be carefully studied and translated into the properties and behaviour of the representative element. The latter indicates that although some component interactions might be omitted, the overall behaviour of the complex element aimed to be replaced by a simpler one needs careful recreation.

Early Decisions on Simulated Aspects

This specific finding mostly refers to the need of the as early as possible decision on the various mechanisms and their interrelations attempted to be recreated through the numerical process. The previous not only results in the development of the most effective modelling approach, it also prevents the need of time-consuming adaptations.

When a global finite element model of a complex configuration is attempted typically requiring the ignoring of some elements, the simplifying of others or the combined representation of adjacent ones, extra attention is needed during the initial modelling stages where the previous decisions are typically made. Therefore it is of great importance for the modeller to have the clearest view possible over the balance of the elements and their interrelation to be simulated. After the finalisation of the numerical modelling, any seemingly elementary geometry change, such as the relocation of an element, is typically labour intensive due to its numerous interrelations with adjacent elements that also need to be redefined and prone to the introduction of errors.

Therefore, attention is encouraged during the earlier modelling stages for the proper decision-making regarding the balance of the elements simulated and their interaction aimed to be captured, so that later on the process the need of adaptations will be eliminated.

The previous challenge was faced during this study when it was proven that more consideration and handling were needed regarding the simplification of the distance occurring inside the frame elements. In practice, the bottom transom-to-starter sill connection was initially simulated without any gap between the two components. However inside the frame itself, a gap of the range of 14.0 mm exists, aiming to accommodate and relieve potential displacements of the framing. The reason for not transferring this gap into the model lies on the consideration that these two elements in practice form the upper and the lowest part of the same frame and since no attention was expected to be paid to the examination of the conditions inside the frame itself, the modelling of the gap between them could be omitted. The previous originates from the fact that this interrelation between the two frame parts was not clearly stated as an objective of the study from the early design stages, instead it was specified later in the process.

Thus, the definition of the parameters needed later for the result evaluation is essential to be decided from the early phases, so that the appropriate modelling decisions can be made. Otherwise labour-intensive adaptations or even a complete remodelling is needed.

Correlation of Detailed & Global Analyses

The implementation of findings of numerical analyses focused solely on details of a complex configuration into global models is for sure an interesting topic which is expected to further increase the accuracy and effectiveness of numerical modelling. The latter is provided by examining in more detail critical aspects of complicated systems later introduced in the global approach and on the other hand by the reduction of computational time since the complexity of the global model is generally less. In this way, the increased level of accuracy is attributed to the critical areas that are analysed separately, however, the more accurate results are incorporated in the global approach, resulting in the more accurate representation of the system.

However, it is evident that combining the results of different modelling approaches with incorporating different levels of detail is a challenging topic. In order for this to function properly, the numerical approaches and simplifications followed by the detailed approach need to be in line with those of the global one. Thus, preliminary tests need to be performed prior to the actual modelling of the two approaches so that possible incompatibilities can be early identified and solved. Otherwise several time and labour-intensive adjustments of one or both the modelling procedures would be needed.

The latter has been attempted also in the present study where the results of an analysis focusing on detailed connections of the curtain wall unit were incorporated into this global model. In fact three connections, this of the mullion-to-mullion, transom-to-mullion and bottom transom-to-starter sill were tested. None of the results provided by the detailed analysis were ready to be implemented in the global modelling. After several test runs aiming to identify the property adaptations needed in order for the global model to run, it was found out that at least one modelling approach had to be adapted to the other in order for the actual impact of detailed analysis on the global behaviour to be evident.

It is expected that the parallel modelling of the two where common modelling approaches would be followed or the complete setting of one model using as a reference the other would result in collaboration of the two and eventually to a more effective representation of the curtain wall behaviour aimed to be recreated. Of course, in order for this challenging task to be completed, a lot of experience in the field of finite element modelling as well as appropriate familiarisation with the simulation software and its possibilities is needed. Thus, studies like these are expected to provide the basis for further research on similar fields to be conducted leading eventually to the better understanding and recreation of such complex systems through finite element modelling.

Parametric Post Process & Interactive Visualisation

While evaluating the impact of various property adaptations on the finite element model response it became evident that the conventional approach of exporting and evaluating the numerical result is a field in urgent need of optimisation. Although a Grasshopper script has already been developed for the quicker and more effective calculation of several means of assessment, such as the unit rotation, distortion and diagonal elongation, further improvement is expected to facilitate the evaluation of properties adaptation.

In the current procedure, the numerical results of each characteristic node used for examination were manually selected and saved in a .csv format. Later the results had to be saved into an .xls version and to be manually imported in the Grasshopper script. The post-process followed thereafter was automatically updated based on the workflow that was developed once. The latter provided a considerable reduction of the calculator process, facilitating the impact evaluation of the variation of several material properties. It also made the realisation of the various sensitivity analyses as well as the comparisons between the numerous

displacement application and directions combinations possible. The already time-consuming procedure of modifying the different properties, exporting, saving and converting the respective results and finally importing them in the Grasshopper script has potential for further improvement.

The study of the direct and automatic connection of numerical results as calculated by the DIANA environment is highly suggested. The time devoted to the development of this workflow will undeniably return considerable efficiency with regards to the data post-processing. Additionally, the interactive visualisation of the modelling changes in an environment similar to that of Rhino is regarded as considerably insightful. The direct modification of even a simplified version of the finite element model, a representative example to this originating from the current study is the comparison of the undeformed and the deformed versions of the curtain wall unit, facilitates a better and much quicker understanding of the property modification. Several flaws of the modelling procedure can be instantly identified that would otherwise require labour and time intensive processes before becoming visible to the modeller.

For this reason, the direct connection of each of the software providing the numerical results with an interactive environment allowing the parametric design with the interactive visualisation, such as the Grasshopper and Rhino combination, is considered vital for the enhancement of the numerical modelling especially when combined with sensitivity analyses that inherently require the evaluation of numerous model variations and their respective results.

Additional Research

Obviously, the entire list of the aspects previously mentioned as considerations or later listed as recommendations for future users can form additional objectives for further research. Their investigation is expected to result in an even better understanding of the glazed curtain wall function, especially when subjected to seismic loading, and eventually in more accurate simulation of the previous through finite element modelling.

Below, additional suggestions indicating research complementary to this performed during the one performed as analysed in the previous chapters are provided below. Their investigation is expected to provide an integrated assessment of the seismic performance of curtain wall systems especially when combined with finite element modelling.

Façade Multi-Performance

As already mentioned seismic actions influence the multi-performance of a curtain wall system, by affecting several aspects mainly related to its weather-proofness. In more detail seismic actions, especially the ones of large intensities, result in the degradation of elements such as gaskets for dry and structural silicone for wet systems. The aforementioned deterioration facilitates the undesired water or air intrusion through the façade detailing, therefore diminishes the weather-tightness of the exterior envelope. Therefore, the correlation of the various seismic phenomena with the subsequent failure mechanisms and their impact on the façade multi-performance which relates to its serviceability function is an interesting field providing room for additional investigation.

In order for the multi-performance of the curtain wall system to be adequately assessed a series of various tests evaluating its serviceability requirements typically needs to be performed. In the “Testing Protocol” section of the present report, Chapter 4, it has been mentioned that for the current testing sequence only air-

permeability tests were conducted, prior and after the displacement application of the first intensity H/300. However, the functionality of the curtain wall specimen can deteriorate also with respect to its wind load resistance and its water-tightness. Additionally, the influence of the displacement application on the curtain wall serviceability performance can be more integrally assessed by including tests assessing the weather-tightness prior and after all the magnitudes of the displacement applied on the specimen under examination.

A representative implementation of the above is a recent experiment evaluating the seismic and weather-tightness of a unitised curtain wall system similar to that of the present case study. This testing, which is the one previously mentioned in section "Disengagement Failure Mechanism" of Chapter 6, evaluates apart from the air-permeability of the system, also its water penetration and wind load resistance. A brief presentation of the aforementioned tests accompanied by the testing sequence are presented below aiming to serve as best practice indication for the effective assessment of multi-performance curtain wall systems while undergoing seismic verification.

Starting from the air-leakage test that has already been described in the testing protocol of the case study examined during this research topic, the testing is realised through the application of both positive and negative pressure applied on the chamber. The testing is performed with and without the implementation of tapes over the curtain wall openings in order to evaluate their impact on the response of the façade. In practice, the air flow inserting through the curtain wall unit is expressed in m^3/h. Eventually, the air leakage is identified by dividing the air flow by the specimen area as indicated by the reference regulations EN 12152 (EN 12152, 2002) and EN 12153 (EN 12153, 2000).

As for the test determining the water-tightness of the curtain wall system, this can use as a reference various standards such as EN 12154 (EN 12154, 1999), EN 12155 (EN 12155, 2000) and ASTM E 331 (ASTM E 331, 2000). In practice positive pressure increments are applied over the tested specimen while simultaneously water is sprayed over the curtain wall unit through a grid of sprinklers. These nozzles are placed in front of the tested specimen and the water is sprayed under a specific rate, which differs depending on the reference standard. The typical rate prescribed by European standards is 2.0 $l/min/m^2$ whereas ASTM E 331 suggests a larger rate of 3.4 $l/min/m^2$. Eventually, the curtain wall water-tightness is verified if no water has penetrated through the curtain wall configuration both during as well as after the test completion.

Apart from the static tests, the water-tightness of a façade system can be evaluated through dynamic tests as well. In this type of test an aero-engine is placed in front of the tested unit, generating artificial wind. Throughout the test water is also sprayed upon the mock-up unit which results in the curtain wall element being subjected to dynamic pressure. The dynamic water-tightness tests have a typical duration of fifteen minutes and after their completion a visual inspection is required in order to verify that no water penetrated through the façade system either during or after the test completion. This type of test is only prescribed by the AAMA 501.1 (AAMA 501.1, 2017) standard.

Figure 7.2: The left figure presents the implementation of water-tightness testing where water is sprayed over the curtain wall unit under testing through a grid of nozzles. The figure to the right presents the connection of the mock-up to the testing facility. During the testing it is reassured that no leakage occurs unless it penetrates through the curtain wall unit itself (Source: Permasteelisa).

Finally, the assessment of the multi-performance of a façade unit can be concluded through the implementation of wind resistance testing. There as well both positive and negative pressure is applied inside the test chamber. EN standards (EN 12179, 2000) prescribe four wind increments equal to the 25.0 % of the design wind load, reaching 100.0 % and eventually dropping to zero. The subsequent deflection of the curtain wall element is measured through displacement transducers typically placed on the mock-up specimen, on the interior of the framing. Following the finalisation of the previous tests, an additional test called safety test is performed for both the negative and positive wind design pressures with a 50.0 % increment for a security verification. After the test finalisation, the residual displacements are obtained.

To sum up, the more elaborate integration of a testing sequence including a wider range of tests evaluating the weather-tightness of a curtain wall system is proposed. A representative testing protocol is proposed below:

pre-seismic testing

- air-permeability with and without tape (600 Pa), according to EN 12152, EN 12153
- water-penetration resistance, static pressure (900 Pa), according to EN 12154, EN 12155
- wind load resistance, static pressure (1500 Pa) & static suction (1900 Pa)

seismic testing, H/300 intensity

- air-permeability with and without tape (600 Pa), according to EN 12152, EN 12153
- water-penetration resistance, static pressure (900 Pa), according to EN 12154, EN 12155

seismic testing, H/200 intensity

- air-permeability with and without tape (600 Pa), according to EN 12152, EN 12153

- water-penetration resistance, static pressure (900 Pa), according to EN 12154, EN 12155
- wind load resistance, static pressure (1500 Pa) & static suction (1900 Pa)

seismic testing, H/100 intensity

- air-permeability with and without tape (600 Pa), according to EN 12152, EN 12153
- water-penetration resistance, static pressure (900 Pa), according to EN 12154, EN 12155
- wind load resistance, static pressure (1500 Pa) & static suction (1900 Pa)

The combination of the non-seismic with the seismic testings, especially when correlated with the potentiality of the façade elements damage such as gasket or structural silicone, is expected to provide insightful information regarding the assessment of the post-seismic performance of curtain wall units.

Fragility Curves

An additional research recommendation is related to the development of tentative fragility curves that are generally known to contribute to the seismic risk assessment of unitised curtain walls. Although relevant information regarding the structural damage state of curtain walls is available, hardly any information concerning the effect of seismic loading on the weather-tightness of curtain walls is detected in the available literature. The derivation of the fragility curves, providing an indication of the performance of the unitised façade types tested under seismic loading, could form another research area with objectives similar to this thesis.

Regarding the formation methodology of tentative fragility curves, this can be attempted based on information obtained from the experimental testing. As for the background needed with respect to the typical procedure normally followed for the derivation of such curves, useful information is available on various papers and articles available in the literature. Moreover, the online database (Performance Assessment Calculation Tool) referring to the fragility functions created for FEMA guidelines (FEMA P-58-2, 2018) is proposed for investigation. Although this database is restricted to the American regulations and testing that might be slightly outdated, it is expected to be a considerably useful source of information.

Since fragility curves represent the probability of being or exceeding a specific damage state, in reality the derivation of fragility curves adequately representing the post-earthquake behaviour of the façade samples examined during a testing sequence would need to originate from a much broader range of experimental testing. However, the generation of tentative fragility curves, that can be attempted through studies similar to this, indicating the basic directions of the façade behaviour under seismic loadings, is expected to offer useful information for the design and assessment of innovative and durable façade elements that comply with serviceability and ultimate limit states. This insight provided by fragility curves can be proven even more helpful whilst considering that the current regulations prescribe scarce indications regarding the seismic performance on curtain wall systems.

Post-Earthquake Repairs & Embodied Carbon

An alternative research objective which is of great interest from a sustainability perspective relates to the investigation of the consequences of a seismic event applied on a unitised curtain wall and more specifically to the repair of the earthquake-induced damages. The carbon emissions released in the environment during a seismic repair -such as replacement of broken glazing, restoration of cracked panels or even replacement of rotated façade unit- can be investigated. It is evident that the façade damages following a seismic event require both repair costs and time. Therefore, by assessing the embodied carbon related to the restoration of the consequence damage conditions, a more comprehensive overview of the overall post-earthquake performance of the specific façade elements tested is enabled.

Regarding the evaluation of the carbon emitted during the repair of seismic-induced damages of the curtain wall systems, this can be performed through a combination of data derived from LCA (Life Cycle Analysis) and cost estimations of the seismic-induced repair actions of similar façade units previously tested. More specifically, the cost evaluation of the repair actions can be evaluated through the embodied carbon indicator of the LCAs that is a widely known and commonly used metric for the evaluation of the environmental impact of a façade. The existence of the EPDs (Environmental Product Declarations) of the materials comprising the curtain wall elements, the amount as well as the type of the environmental impact indicators used during the LCA are only a few of the topics that would need to be defined. As for the estimation of the repairing cost values, this can be assessed through the PACT (Performance Assessment Calculation Tool) generated by FEMA, a software that reproduces the probabilistic damages appearing as a consequence of seismic actions.

Thus, by accounting for the repair time and costs needed for the aforementioned repairs, subsequently the embodied carbon as well, a more comprehensive evaluation of the impact of the seismic loading on the unitised façade elements also containing the environmental impact aspect can be derived.

Chapter 8

Bibliography

AAMA 501.1. (2017). *Water Penetration of Windows, Curtain Walls and Doors Using Dynamic Pressure*. American Architectural Manufacturers Association.

AAMA 501.4. (2018). *Recommended Static Test Method for Evaluating Window Wall, Curtain Wall and Storefront Systems Subjected to Seismic and Wind-Induced Inter-Story Drift*. American Architectural Manufacturers Association.

AAMA 501.6. (2018). *Recommended Dynamic Test Method for Determining the Seismic Drift Causing Glass Fallout from Window Wall, Curtain Wall and Storefront Systems*. American Architectural Manufacturers Association.

AAMA CW-13. (1985). *Structural Sealant Glazing Systems*. American Architectural Manufacturers Association.

AC 156. (2020). Seismic Certification by Shake-table Testing of Nonstructural Components. In *AC 156*. ICC Evaluation Service.

Aiello, C., Caterino, N., Maddaloni, G., Bonati, A., Franco, A., & Occhiuzzi, A. (2018). Experimental and numerical investigation of cyclic response of a glass curtain wall for seismic performance assessment. *Construction and Building Materials*, *187*, 596–609. https://doi.org/10.1016/j.conbuildmat.2018.07.237

Alcaine, J., Lenk, P., & Forwood, E. (2020). Structural Silicone Glazing - Design & Modelling. In *Challenging Glass 7 -Conference on Architectural and Structural Applications of Glass* (Vol. 7). https://doi.org/10.7480/cgc.7.4548

Al-sheikh, A. (2019, July). ASCE 7-16 Provisions for Lateral Drift Determination. *Structural Design*. Retrieved November 16, 2022, from https://www.structuremag.org/?p=14696

ANSYS, Inc. (2017). Gasket Material. In *ANSYS, Inc.* (Release 18.2). Retrieved September 8, 2022, from https://www.mm.bme.hu/~gyebro/files/ans_help_v182/ans_thry/thy_gasket.html

ASTM C1401. (2022). *Standard Guide for Structural Sealant Glazing*.

ASTM C1401-14. (2022). *Standard Guide for Structural Sealant Glazing*. West Conshohocken, PA. Retrieved September 4, 2022, from https://www.astm.org/c1401-14r22.html

ASTM E 283. (2004). Standard Test Method for Determining Rate of Air Leakage Through Exterior Windows, Curtain Walls, and Doors Under Specified Pressure Differences Across the Specimen. In *ASTM*.

ASTM E 331. (2000). *Test Method for Water Penetration of Exterior Windows, Skylights, Doors, and Curtain Walls, by Uniform Static Air Pressure Difference*. ASTM.

AZO. (2012). Aluminium / Aluminum 6061 Alloy (UNS A96061). In *AZO Materials*. Retrieved November 15, 2022, from https://www.azom.com/article.aspx?ArticleID=6636

Baird, A., Palermo, A., & Pampanin, S. (2011). Facade Damage Assessment Of Multi-storey Buildings In The 2011 Christchurch Earthquake. *Bulletin of the New Zealand Society for Earthquake Engineering*, *44*(4), 368–376. https://doi.org/10.5459/bnzsee.44.4.368-376

Baniotopoulos, C., Nikolaidis, T., & Moutsanidis, G. (2016). Optimal Structural Design Of Glass Curtain-wall Systems. *Proceedings of the Institution of Civil Engineers*, *169*(6), 450–457. https://doi.org/10.1680/jstbu.13.00088

Bârnaure, M., & Voiculescu, M. (2013). The Seismic Behaviour Of Curtain Walls: An Analysis Based On Numerical Modelling. *Mathematical Modelling in Civil Engineering*, *9*(4), 1–8. https://doi.org/10.2478/mmce-2013-0013

Behr, R. A. (1998). Seismic Performance of Architectural Glass in Mid-Rise Curtain Wall. *Journal of Architectural Engineering*, *4*(3), 94–98.

Behr, R. A. (2001). Architectural Glass for Earthquake-resistant Buildings. In *8th Glass Processing Days Conference*. Tampere, Finland, 2001.

Behr, R. A. (2009). *Architectural Glass to Resist Seismic and Extreme Climatic Events*. ScienceDirect. Retrieved April 5, 2022, from https://www.sciencedirect.com/book/9781845693695/architectural-glass-to-resist-seismic-and-extreme-climatic-events

Behr, R. A., Belarbi, A., & Culp, J. H. (1995). Dynamic Racking Tests Of Curtain Wall Glass Elements With In-plane And Out-of-plane Motions. *Earthquake Engineering & Structural Dynamics*, *24*(1), 1–14. https://doi.org/10.1002/eqe.4290240102

Boswell, K. (2013). *Exterior Building Enclosures: Design Process and Composition for Innovative Facades*. John Wiley & Sons.

Bouwkamp, J. G. (1961). Behavior Of Window Panels Under In-plane Forces. *Bulletin of the Seismological Society of America*, *51*(1), 85–109. https://doi.org/10.1785/bssa0510010085

Bouwkamp, J. G., & Meehan, J. F. (1960). Drift Limitations Imposed By Glass. In *Proceedings of Second World Conference on Earthquake Engineering, Tokyo, Japan, 1960*.

Brenden, K. (2006, August). Dynamic Issues Drive Curtain Wall Design. *Structure Magazine*. Retrieved October 7, 2022, from https://www.structuremag.org/wp-content/uploads/2014/09/C-SD-Curtain-Wall-Aug-061.pdf

Broker, K. A., Fisher, S., & Memari, A. M. (2012). Seismic Racking Test Evaluation of Silicone Used in a Four-Sided Structural Sealant Glazed Curtain Wall System. *Journal of ASTM International*, *9*(3), 104144. https://doi.org/10.1520/jai104144

Carré, H., & Daudeville, L. (1999). Load-Bearing Capacity of Tempered Structural Glass. *Journal of Engineering Mechanics-Asce*, *125*(8), 914–921.

Caterino, N., Del Zoppo, M., Maddaloni, G., Bonati, A., Cavanna, G., & Occhiuzzi, A. (2017). Seismic Assessment And Finite Element Modelling Of Glazed Curtain Walls. *Structural Engineering and Mechanics*, *61*(1), 77–90. https://doi.org/10.12989/sem.2017.61.1.077

Cavallo, C. (n.d.). All About 6061 Aluminum (Properties, Strength and Uses). In *Thomasnet*. Thomas Publishing Company. Retrieved November 16, 2022, from https://www.thomasnet.com/articles/metals-metal-products/6061-aluminum/finite/

DOW. (2021). Dow Construction Sealants Technical Manual (Americas). In *DOW*. The Dow Chemical Company. Retrieved January 5, 2022, from https://www.dow.com/content/dam/dcc/documents/en-us/app-tech-guide/62/62-11/62-1112-01-americas-technical-manual.pdf

EN 12152. (2002). *Curtain Walling - Air Permeability - Performance Requirements and Classification*. CEN.

EN 12153. (2000). *Curtain Walling - Air Permeability - Test Method*. CEN.

EN 12154. (1999). *Curtain Walling - Watertightness - Performance Requirements and Classification*. CEN.

EN 12155. (2000). *Curtain Walling - Watertightness - Laboratory Test Under Static Pressure*. CEN.

EN 12179. (2000). *Curtain Walling – Resistance to Wind Load*. CEN.

Eurocode 8. (2004). *Design of structures for earthquake resistance - Part 1 : General rules, seismic actions and rules for buildings*. CEN.

FACETS. (2019). In *Centre for Window and Cladding Technology CWCT*. CWCT. Retrieved December 1, 2022, from https://www.cwct.co.uk/pages/facets#!articles/1222-9061-0805-frame-construction

FEMA 273. (1997). *NEHRP Guidelines For The Seismic Rehabilitation of Buildings* (FEMA 273). Building Seismic Safety Council.

FEMA 450. (2003). NEHRP Recommended Provisions For Seismic Regulations For New Buildings And Other Structures. In *FEMA*. Building Seismic Safety Council.

FEMA 461. (2007). Interim Testing Protocols for Determining the Seismic Performance Characteristics of Structural and Nonstructural Components. In *FEMA*. Applied Technology Council.

FEMA P-58-2. (2018). Seismic Performance Assessment of Buildings Volume 2 – Implementation Guide Second Edition. In *FEMA*. Federal Emergency Management Agency (FEMA). Retrieved April 5, 2022, from https://femap58.atcouncil.org/documents/fema-p-58/25-fema-p-58-volume-2-implementation-second-edition/file

FEMA P-2082-1. (2020). NEHRP Recommended Seismic Provisions for New Buildings and Other Structures. In *FEMA* (FEMA P-2082-1). Building Seismic Safety Council. Retrieved August 12, 2022, from https://www.fema.gov/sites/default/files/2020-10/fema_2020-nehrp-provisions_part-1-and-part-2.pdf

Feng, R. Q., Ye, J. H., Wu, Y., & Shen, S. Z. (2010). Seismic Response of Cable Net Facade. *Advanced Materials Research*, *163–167*, 165–168. https://doi.org/10.4028/www.scientific.net/amr.163-167.165

Filiatrault, A., Christopoulos, C., & Stearns, C. (2001). Guidelines, Specifications, and Seismic Performance Characterization of Nonstructural Building Components and Equipment. In *Pacific Earthquake Engineering Research Center*. Pacific Earthquake Engineering Research Center, College of Engineering University of California, Berkeley. Retrieved September 3, 2022, from https://peer.berkeley.edu/sites/default/files/0205_a._filiatrault_c._christopoulos_c._stearns.pdf

Frighi, V. (2022). *Smart Architecture – A Sustainable Approach for Transparent Building Components Design* (1st ed.). Springer Cham. https://doi.org/10.1007/978-3-030-77606-0

Galli, U. (2011). *Seismic Behaviour of Curtain Wall Facades, A Comparison Between Experimental Mock-up Test and Finite Element Method Analysis* [Thesis]. Politecnico di Milano.

Gil, E. M. (2019). *Computational Modeling of Glass Curtain Wall Systems to Support Fragility Curve Development* [Master of Science in Civil Engineering]. Virginia Polytechnic Institute and State University, Blacksburg, VA, USA, 15 August 2019.

Haber, M. (2021, July 15). *What is a Structural Glazing System? | W&W Glass*. W&W Glass, LLC. Retrieved September 16, 2022, from https://www.wwglass.com/blog/post/what-is-structural-glazing/

Haldimann, M., Luible, A., & Overend, M. (2008). *Structural Use of Glass*.

Hosseini, M. (2005). Behavior of Nonstructural Elements in the 2003 Bam, Iran, Earthquake. *Earthquake Spectra*, *21*(1_suppl), 439–453. https://doi.org/10.1193/1.2098829

Huang, B., Chen, S., Lu, W., & Mosalam, K. M. (2017). Seismic Demand And Experimental Evaluation Of The Nonstructural Building Curtain Wall: A Review. *Soil Dynamics and Earthquake Engineering*, *100*, 16–33. https://doi.org/10.1016/j.soildyn.2017.05.025

IBC. (2018). 2018 International Building Code (IBC). In *International Code Council, INC*. International Code Council, INC.

Iker, J., & Wolf, A. M. (1992). Secondary Stresses Induced By Shear Movement In Structural Glazing Sealants. *Matériaux Et Constructions*. https://doi.org/10.1007/bf02472426

Ilter, E., Tavil, A., & Celik, O. (2015). Full-scale Performance Testing And Evaluation Of Unitized Curtain Walls. *Journal of Facade Design and Engineering*, *3*(1), 39–47. https://doi.org/10.3233/fde-150028

JASS 14. (2012). *Curtain Wall*. Japanese Architectural Standard Specification.

Jeyamohan, K. (2022, February 27). *Construction & Design Techniques Using In The Curtain Wall System*. ResearchGate.

https://www.researchgate.net/publication/358893903_CONSTRUCTION_DESIGN_TECHNIQUES_USING_IN_THE_CURTAIN_WALL_SYSTEM

Kekan, A. (2022, September 8). *What are the types of Structural Glazing?* McCoy Mart. Retrieved November 20, 2022, from https://mccoymart.com/post/types-of-structural-glazing/

King, A. B., & Lim, K. Y. S. (1988). *The Behaviour of External Glazing Systems Under Seismic In-plane Racking*. Building Research Association of New Zealand, BRANZ.

Knaack, U., Klein, T., Bilow, M., & Auer, T. (2014). *Façades: Principles of Construction-second and revised edition* (2nd ed.). Birkhäuser. https://urbanfarmstudiowinter2015. files.wordpress.com/2015/02/principles-of-facades_structure.pdf

Le Bourhis, E. (2014). Glass. *Wiley-VCH Verlag GmbH & Co. KGaA*, 1–4. https://doi.org/10.1002/9783527679461.ch01

Lee, a. D., Shepherd, P., Evernden, M. C., & Metcalfe, D. (2017). Optimizing the Cross-sectional Shapes of Extruded Aluminium Structural Members for Unitized Curtain Wall Facades. *Structures*, *10*, 147–156. https://doi.org/10.1016/j.istruc.2017.03.002

Lee, T. H., Kato, M., Matsumiya, T., Suita, K., & Nakashima, M. (2007). Seismic Performance Evaluation Of Non-structural Components: Drywall Partitions. *Earthquake Engineering &Amp; Structural Dynamics*, *36*(3), 367–382. https://doi.org/10.1002/eqe.638

Lim, K., & King, A. (1991). *The Behaviour Of External Glazing Systems Under Seismic In-plane Racking (No. 39)*.

Lu, W., Mosalam, K. M., Chen, S., & Mosalam, K. M. (2017). Shaking Table Test Method Of Building Curtain Walls Using Floor Capacity Demand Diagrams. *Bulletin of Earthquake Engineering*, *15*(8), 3185–3205. https://doi.org/10.1007/s10518-016-9866-y

McCue, G. M., Skaff, A., & Boyce, J. W. (1978). Architectural Design of Building Components for Earthquakes. In *Nehrp*. MBT Associates.

Memari, A. M., Behr, R. A., & Kremer, P. (2000). Toward Development of a Predictive Model for Drift Limits in Architectural Glass under Seismic Loadings. In *12th World Conference on Earthquake Engineering, Auckland, New Zealand*.

Memari, A. M., Behr, R. A., & Kremer, P. A. (2003). Seismic Behavior of Curtain Walls Containing Insulating Glass Units. *Journal of Architectural Engineering*, *9*(2), 70–85.

Memari, A. M., Chen, X., Kremer, P. A., & Behr, R. A. (2006). Seismic Performance of Two-Side Structural Silicone Glazing Systems. *Journal of Astm International*, *3*(10), 100407. https://doi.org/10.1520/jai100407

Memari, A. M., Fisher, S. M., Krumenacker, C., Broker, K. A., & Modrich, R. (2012). Evaluation of the Structural Sealant for Use in a Four-Sided Structural Sealant Glazing Curtain-Wall System for a Hospital Building. *Journal of Astm International*, *9*(4), 104143. https://doi.org/10.1520/jai104143

Memari, A. M., Kremer, P. A., & Behr, R. A. (2006). Architectural Glass Panels with Rounded Corners to Mitigate Earthquake Damage. *Earthquake Spectra*, *22*(1), 129–150. https://doi.org/10.1193/1.2164875

Memari, A. M., Kremer, P. A., & Behr, R. A. (2012). Seismic Performance of Stick-Built Four-Side Structural Sealant Glazing Systems and Comparison With Two-Side Structural Sealant Glazing and Dry-Glazed Systems. *Advances in Civil Engineering Materials*, no.1 1-22. https://doi.org/10.1520/acem103159

Memari, A. M., & Shirazi, A. (2002). Development of a Seismic Rating System for Architectural Glass in Existing Curtain Walls, Storefront and Windows. In *13th World Conference on Earthquake Engineering, Vancouver, Canada*.

Memari, A. M., Shirazi, A., & Kremer, P. A. (2007). Static Finite Element Analysis of Architectural Glass Curtain Walls Under In-plane Loads and Corresponding Full-scale Test. *Structural Engineering and Mechanics*, *25*(4), 365–382. https://doi.org/10.12989/sem.2007.25.4.365

Memari, A. M., Shirazi, A., Kremer, P. A., & Behr, R. A. (2011). Development of Finite-Element Modeling Approach for Lateral Load Analysis of Dry-Glazed Curtain Walls. *Journal of Architectural Engineering*, *17*(1), 24–33. https://doi.org/10.1061/(asce)ae.1943-5568.0000027

Memari, A. M., Simmons, N. L., & Solnosky, R. L. (2021). Derivation of Kinematic Equations Based on Full-Scale Racking Tests for Seismic Performance Evaluation of Unitized Four-Sided Structural Sealant Glazing Curtain Wall Systems. *Buildings*, *11*(12), 593. https://doi.org/10.3390/buildings11120593

Mocibob, D. (2008). *Linear Connection System For Structural Application Of Glass Panels In Fully-transparent Pavilions*. Semantic Scholar. Retrieved November 22, 2022, from https://www.semanticscholar.org/paper/Linear-connection-system-for-structural-application-Mocibob-Crisinel/4843f2a174870a51f67d9409461e4397551a7f04

Mosqueda, G., Retamales, R., Filiatrault, A., & Reinhorn, A. (2008). Testing Facility For Experimental Evaluation Of Non-Structural Components Under Full-scale Floor Motions. *The Structural Design of Tall and Special Buildings*, *18*(4), 387–404. https://doi.org/10.1002/tal.441

Murty, C., Goswami, R., Ar, V., & Mehta, V. V. (2012, September 1). *Some Concepts in Earthquake Behaviour of Buildings*. ResearchGate. https://www.researchgate.net/publication/281479039_Some_Concepts_in_Earthquake_Behaviour_of_Buildings

Nhamoinesu, S., & Overend, M. (2012). The Mechanical Performance of Adhesives for a Steel-Glass Composite Façade System. *ResearchGate*. https://doi.org/10.3233/978-1-61499-061-1-293

Norton, J. A., King, A. B., Bull, D. K., Chapman, H. E., McVerry, G. H., Larkin, T. J., & Spring, K. C. (1994). Northridge Earthquake Reconnaissance Report. *Bulletin of the New Zealand Society for Earthquake Engineering*, *27*(4), 235–344. https://doi.org/10.5459/bnzsee.27.4.235-344

NZS 1170.5:2004. (2004). *New Zealand Standard, Structural design actions - Part 5: Earthquake actions - New Zealand*.

Overend, M., Jin, Q., & Watson, J. (2011). The Selection And Performance Of Adhesives For A Steel–glass Connection. *International Journal of Adhesion and Adhesives*, *31*(7), 587–597. https://doi.org/10.1016/j.ijadhadh.2011.06.001

Pantelides, C. P., & Behr, R. A. (1994). Dynamic In-plane Racking Tests Of Curtain Wall Glass Elements. *Earthquake Engineering &Amp; Structural Dynamics*, *23*(2), 211–228. https://doi.org/10.1002/eqe.4290230208

Pantelides, C. P., Truman, K. Z., Behr, R. A., & Belarbi, A. (1996). Development Of A Loading History For Seismic Testing Of Architectural Glass In A Shop-front Wall System. *Engineering Structures*, *18*(12), 917–935. https://doi.org/10.1016/0141-0296(95)00224-3

Parise, C., & Spindler, R. (1991). Structural Sealant Glazing in the 1980s. *ASTM International EBooks*, 94–24. https://doi.org/10.1520/stp20131s

Raggousis, M., & Zalok, S. S. (2016, July 9). Demystifying the Fly-By Curtain Wall Parapet. *Building Enclosure*. Retrieved January 7, 2023, from https://www.buildingenclosureonline.com/articles/ 90716-demystifying-the-fly-by-curtain-wall-parapet

Rizzo, F., Franco, A., Bonati, A., Maddaloni, G., Caterino, N., & Occhiuzzi, A. (2021). Predictive analyses for aerodynamic investigation of curtain walls. *Structures*, *29*, 1059–1077. https://doi.org/10.1016/j.istruc.2020.11.077

Sakamoto, I., Itoh, H., & Ohasjo, Y. (1984). Proposal For A Seismic Design Method On Non-Structural Elements. In *Proceedings of the Eighth World Conference on Earthquake Engineering* (Vol. 5). San Francsco, California, 1984, pp. 1093–1100.

Schmidt, C. M., Schoenherr, W. J., Carbary, L., & T. (1989). Performance Properties of Silicone Structural Adhesives. *ASTM Special Technical Publications*, 22–24. https://doi.org/10.1520/stp22987s

Schwartz, T., Z., & Kan, F. (1996). Structural Silicone Glazing: In-Service Reliability Evaluation. *ASTM International EBooks*, 3–12. https://doi.org/10.1520/stp16291s

Sie, W. W. W. (2007). *Analysis And Design Of Curtain Wall Systems For High Rise Buildings*. https://www.semanticscholar.org/paper/Analysis-and-design-of-curtain-wall-systems-for-Sie/ef09317637edfd2a12ea0f6f9622c17cf93204fb

Silvestru, V. A., Englhardt, O., & Schneider, J. (2018). Investigations on Linear Silicone Joints for Glass-Metal Elements with Composite Structural Behavior. In *Challenging Glass 6 -Conference on Architectural and Structural Applications of Glass* (Vol. 6). https://doi.org/10.7480/cgc.6.2162

Simiu, E., & Yeo, D.-H. (2019). Wind Effects on Structures:: Modern Structural Design for Wind. *John Wiley & Sons, Ltd EBooks*. https://doi.org/10.1002/9781119375890

Sivagnanasundram, S. (2011). *In-plane Seismic Performance Of Glass Facade Systems* [Doctor of Philosophy]. https://researchbank.swinburne.edu.au/file/de9a5a6d-77aa-4bf4-a329-610dba17f7bf/1/Sivanerupan%20Sivagnanasundram%20Thesis.pdf.

Sivanerupan, S., Wilson, J., Gad, F., & Lam, N. (2009). Seismic Assessment of Glazed Façade Systems. In *Annual Technical Conference of the Australian Earthquake Engineering Society, Newcastle, Australia*. https://aees.org.au/wp-content/uploads/2013/11/Sivanerupan-et-al.pdf

Stathopoulos, T., & Baniotopoulos, C. (2007). *Wind Effects on Buildings and Design of Wind-Sensitive Structures*. Springer Publishing.

Sucuoğlu, H., & Vallabhan, C. V. G. (1997). Behaviour Of Window Glass Panels During Earthquakes. *Engineering Structures*, *19*(8), 685–694. https://doi.org/10.1016/s0141-0296(96)00130-7

Thurston, S., & King, A.(1992). *Two-Directional Cyclic Racking Of Corner Curtain Wall Glazing (No.44)*.

Veer, F., Louter, C., Bos, F., & Crisinel, M. (2008, January 1). *Linear Connection System For Structural Application Of Glass Panels In Fully-transparent Pavilions*. ResearchGate. https://www.researchgate.net/publication/37462687_Linear_connection_system_for_structural_application_of_glass_panels_in_fully-transparent_pavilions

Vigener, N., & A. Brown, M. (2016). Building Envelope Design Guide - Fenestration Systems - Curtain Walls. In *Whole Building Design Guide*. Simpson Gumpertz & Heger Inc. Retrieved August 9, 2022, from https://www.wbdg.org/guides-specifications/building-envelope-design-guide/ fenestration-systems/curtain-walls

Willford, M. (2006). Recommendations for the Seismic Design of High-Rise Buildings. In *Council on Tall Buildings and Urban Habitat – CTBUH*. Retrieved July 9, 2022, from https://global.ctbuh.org/resources/papers/download/429-ctbuh-recommendations-for-the-seismic-design-of-high-rise-buildings.pdf

Zarghamee, M. S. (1996). Seismic Behavior of Structural Silicone Glazing ; Science and Technology of Building Seals, Sealants, Glazing and Waterproofing. *ASTM STP 1286*, 46–59.

Part IV

Annexes

Annex I

Insight on the Curtain Wall and its Components

Curtain Wall Basic Components

Frame

The most common material options regarding the curtain wall framing are aluminium, steel and stainless steel. Aluminium frames are often preferred in numerous applications due their light weight compared to that of steel which results in the reduction of the overall structural costs of the building. Aluminium frames also offer wide flexibility since they are highly adaptable to many designs, they are very good heat conductors and resistant to corrosion. On the downside, they are preferred only for limited frames sizes with a floor height being a representative reference. The option of steel on the other hand is approximately three times stiffer than aluminium which on one hand results in the first being comparatively stronger than the latter and additionally allows for the realisation of smaller shapes without compromising the material performance. Consequently, by applying smaller shapes of the curtain wall framing element, larger unobstructed views to the outside is provided while allowing more daylight to enter the occupied areas. Furthermore, the use of steel facilitates the span of larger heights which can reach up to 15.0 m minimising the frequent need of building connections and of additional reinforcement. One of the disadvantages of steel is its corrosion sensitivity which makes the need for treatment against corrosion an essential requirement of the steel framings.

Glass

Another integral component of a curtain wall configuration is the glazing pane. Various glazing typologies fulfilling different requirements are currently available on the market. The most common ones as listed by (A. Behr, 2009, Le Bourhis, 2014, Sivagnanasundram, 2011) are presented below:

Annealed

It is the typical float glass element undergoing a forming procedure of a float bath in a molten tin followed by a uniform and slow cooling until room temperature is reached. The latter ensures that the glazing material is stress-free which facilitates its drilling, cutting, edge working etc. Annealed glazing is listed among the weakest glazing types and is highly prone to rapture when installed inappropriately or undergoing excessive loads.

For this reason, monolithic annealed glazing is not applied on highly stressed structural glazing. It is typically not regarded as structural material due to its low strength, however it is regarded as safe when it is suitably laminated. Nevertheless, annealed glazing can be processed into different glazing products and types with advanced strength properties, safer breakage and post-failure behaviour. Such glazing types are (toughened) fully-tempered, heat-strengthened and laminated glazing.

Fully-tempered glazing (FT)

The main characteristic of fully-tempered or toughened glazing is that it is four times more resistant than the typical annealed glazing. The heating procedure implemented is continued until the glazing is soft enough to allow the uniform quenching of its both sides. The previous procedure is typically realised through air jets that rapidly solidify and cool down the external glazing layer. Later, the inner glazing skin undergoes rapid cooling, shrinkage as well as a state of compression with opposite tensile stresses acting on the nearly flawless glazing core. Regarding the breaking pattern of this glazing type, numerous glazing cubes with a size similar to the glazing thickness without sharp edges are usually seen.

Heat-strengthened (HS)

Heat-strengthened glazing is subjected to controlled heating and, later, cooling process in order for the improved resistance to thermal and mechanical stresses to be achieved. It is produced in a way similar to that of fully-tempered glass (FT). The wind-load resistance of heat-strengthened glazing is approximately twice compared to this of the annealed glazing. However, the process of quenching for the heat-strengthened glazing is less robust compared to that of the fully-tempered, resulting in the creation of reduced compression stresses on the outer glazing surfaces.

Since glass breakage is mainly due to tensile stresses, the wind actions typically leading to the bending creation need to first surpass the glazing pre-compressive stress which is built-in during the heating treatment process. For this reason, heat-strengthened glazing is considerably stronger compared to the annealed glazing where the compressive stress built-in surface is absent. Since during the manufacturing of both the FT and HT the temperature reaches the softening point of the glazing, the end product is not as flat as the annealed glazing. Additionally, the distortion of FT and HT is typically more visible. The breakage pattern typically seen on heat-strengthened glazing is similar to that of the annealed glazing, therefore large glazing pieces are observed.

Laminated

This type of glazing is typically an assembly of a minimum of two glazing plies including an adhesive interlayer, mostly of epoxy or polyvinylbutyral (PVB), which is transparent. A schematic view of a laminated unit is depicted in Figure 2.11. Generally, the sheet materials used as interlayers are flexible and thin are also known as “foils”. While the glazing plies can be either the same or different glazing layers, the interlayer is characterised by stiffness and strength similar to those of monolithic glazing when subjected to short-duration loading. An important function of this interlayer is that during the glass breaking it remains inside the frame and offers increased resistance to penetration, therefore it performs as a “safety glass”. However, the resistance to the uniform load is hard to be precisely assessed.

Laminated glazing behaves in a monolithic manner when subjected to loads of short duration due to the interlayer stiffness when located at conditions equal or lower than the room temperature under. The laminated glazing response under high temperatures or long-duration loads on the other hand is better described by a layered approach as seen in Figure I.1. While considering that all the plies are of equal thickness, each of them is assumed to transfer 50.0 % of the loading whereas no resistance to the shear stress offered by the interlayer is considered. The principal function of the laminated glazing is to provide the

building envelope with penetration protection. For this reason, the driving factor becomes the interlayer and its load resistance which is vital especially after the glass plies break.

In general, any process applied on the glazing, such as hole drilling, vee grooving, sand blasting or edge working bevelling, has to be performed before the chemical tempering or heat treatment followed for the fully-tempered or the heat-strengthened glazing. The reason for this is that it has been recorded that any type of surface treatment inserting a heat-treated glazing, more specifically to its the compressive skin, causes strength reduction therefore its avoidance is required.

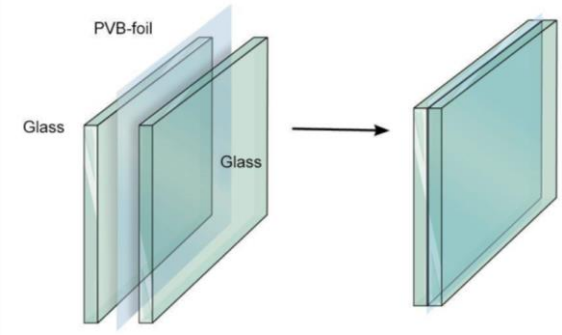

Figure I.1: Above a schematic presentation of a laminated glazing is presented. The various glazing layers are separated by one, sometimes more, synthetic films of polyvinyl butyral (PVB). For the introduction of thermal and sound insulation to the laminated glazing, the latter can also be assembled in double glazing. During the manufacturing of this glazing type both the pressure and the temperature are so high that the dissociation of the glazing from the PVB becomes impossible (Source: Glass Design Malta).

Additionally, vast progress has been observed in the development of the glazing material into a changeable building element able to simultaneously fulfil various functions (Sivagnanasundram, 2011). Some researchers (Knaack et al., 2014) concentrated the glazing developments mostly applied in the building industry which are listed below.

- Phase changing material in glazing, (PCM), which is known for its thermal storage capabilities
- Electro-chromatic coating, allowing the alteration of the radiation and daylight transmission through the application of various voltage levels
- Heated glass, balancing the increase of surface temperatures and heat loss while preserving indoor comfort levels
- Thin film cells, consisting mostly of screen-formed PV cells placed on the glazing. The energy patterns generated by those cells are laser-imprinted while the transparency of some glazing areas is preserved
- Holographic coating, offering shading irrespectively of the solar radiation angle or the focus energy.

Stack Joint

“Stack joint” is another characteristic frequently seen on façade configurations closely related to the tolerances provided on a curtain wall system. In practice, the implementation of a stack joint in the curtain wall configurations allows the system to withstand various movements without the integrity of the connection being jeopardised. These movements originate from a large variety of reasons, namely: i) Fabrication tolerances, ii) Installation tolerances, iii) Member thermal expansion, iv) Column shortening and v) Beam/slab deflection

For an efficient curtain wall design, stack joints are arranged both horizontally and vertically (Figure I.2). The movement joint provision needs to be carefully handled both during the design and the installation phase of the curtain wall system. The improper calculation or/and implementation of the stack joint is often responsible for cracking of the glaze pane and for various damages both on the glazing and the framing of the curtain wall configuration. An indication for the calculation of the minimum space of the stack joint is provided below (Jeyamohan, 2022):

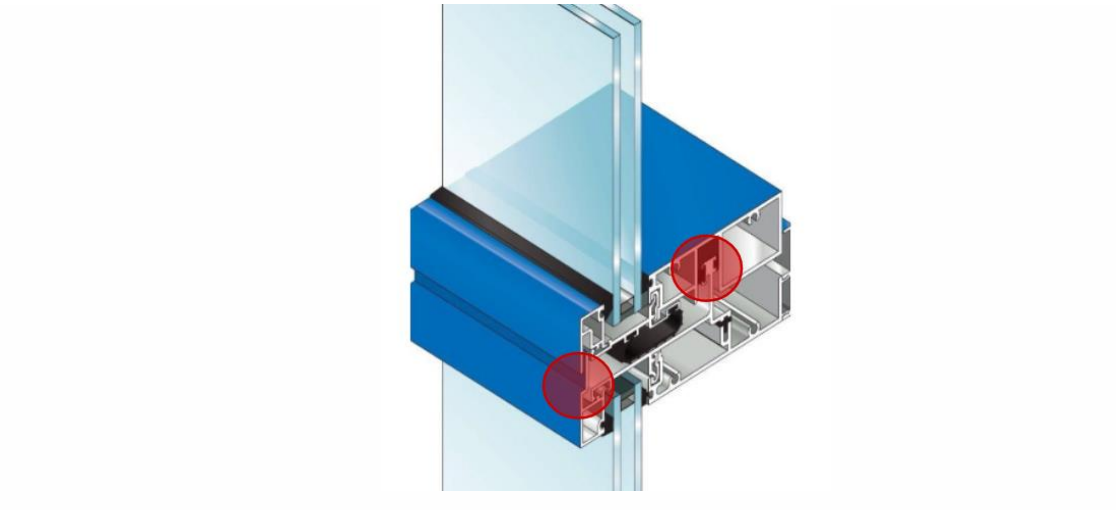

Figure I.2: In the figure above, a stack joint arrangement is presented in the coloured areas of the curtain wall section. The movement provision of the joint in the vertical direction is placed between the sill and the head transom. The horizontal provision is marked between the female and male mullions (Source: Jeyamohan, 2022).

Below the calculation of the minimum allowable joint space is presented:

Minimum allowable stack joint space	>	*[Fabrication + Installation tolerances + Thermal Expansion + Column shortening + Member deflection because of the loading]*

Structural Joint Parameters

As already mentioned, the structurally sealed design apart from providing weather protection, it also aims for the effective transfer of structural loads, with the wind load being the “primary” one, from the glazing to the supporting glazing frame. For this reason, the requirements originating from what is considered the “primary” structural load design, the wind, are in most of the cases the determining factor identifying the “bite” dimension of the sealant which in practice identifies the bead width of the sealant which is in conduct with the glazing. However, for the design of a structural sealant glazing joint to be efficient, several joint parameters need to be taken into consideration. Among others, the wind load and dead load, the structural bite as well as the thickness (DOW, 2021). A brief presentation of those parameters and their boundary values follows in the next section.

Dead Load

The dead load is typically considered to be the weight placed on the structural sealant joint by the panel in the cases where setting blocks are not implemented in the design, therefore no support to the weight of the panel is provided. The minimum allowable structural bite that meets the dead load requirements, can be derived from the following calculation:

$$bite\ [mm] = \frac{glass\ weight\ [N]}{contact\ length\ of\ sealant\ [m] * (SDS)\ design\ strength\ of\ sealant\ [kPa]}$$

Structural Bite

The term structural bite typically refers to the effective contact dimensions that the structural sealant is required to have in order to accommodate the load transfer. This required length refers to the structural sealant contact to both the structurally bonded structures, namely the frame and panel faces. Figure I.3 below identifies a typical structural bite.

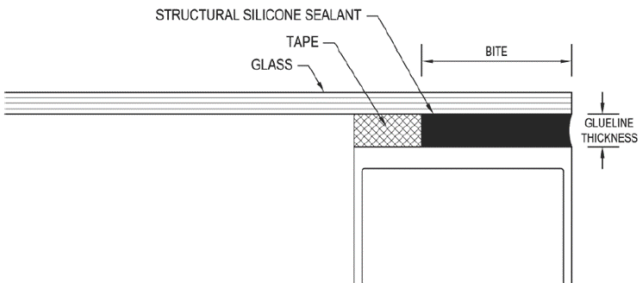

Figure I.3: A simple structural glazing design is presented on the figure above. The structural silicone sealant is depicted in the dark hatched area (Source: DOW, 2021).

Bite Thickness

The thickness of the bite defines the minimum dimension of the structural sealant needed for the facilitation of the sealant installation and for the stress reduction of the structural sealant joint itself that is introduced due to the differential thermal movement.

$$bite\ [mm] = \frac{0.5 * length\ of\ short\ span\ [mm] * wind\ load\ [kPa]}{design\ strength\ of\ sealant\ [kPa]}$$

In order for the wind loads applied to the glazing or panels of the façade elements to be efficiently transferred to the supporting structure of the curtain wall, the structural bite must be designed appropriately. The calculation of the structural bite requirement derives directly from the specified wind load applied to the building, from the panel or glass dimension and the design strength of the sealant (DOW, 2021). Therefore, the requirement for the structural bite for live load, more specifically for the wind load design, is obtained from the following relation:

$$bite\ [mm] = \frac{0.5 * length\ of\ short\ span\ [mm] * wind\ load\ [kPa]}{design\ strength\ of\ sealant\ [kPa]}$$

Setting Blocks

In the structural silicone configurations, additional elements, the “setting blocks”, are often placed underneath the glazing pane and supported on fins of the glazing frame, in order to transfer the glazing panel self-weight (Memari et al., 2012). The structural sealant is typically supplemented by the weather seals also made of silicone that are applied externally.

Since a short reference to the term “setting block” has been previously made also in the section regarding the bite design based on the dead load, a concise description of its function in the curtain wall system application is presented for matters of completeness. Setting blocks are typically applied in structurally sealed curtain wall configuration aiming to provide support to the glazing pane and to carry glazing weight. For the cases of insulating glazing, two setting blocks are recommended for the sufficient support of the two panes of the glazing. Their placement should be at a maximum distance of 30.0 mm from the glazing coroner and 100.0 mm of the glazing rebate corner. The sizing of the setting blocks is dependent on the size of the glazing that supports. Typical dimensions include 30.0 mm length for every square metre of the glazing opening and a minimum length of 25.0 mm (FACETS, 2019). For the cases where setting blocks are not included in the curtain wall design, the structural silicone joint apart from the wind load, is expected to also carry the glazing panel self-weight and thereafter transfer it to the frame. A common unitised curtain wall unit involving also setting blocks is depicted in Figure I.4.

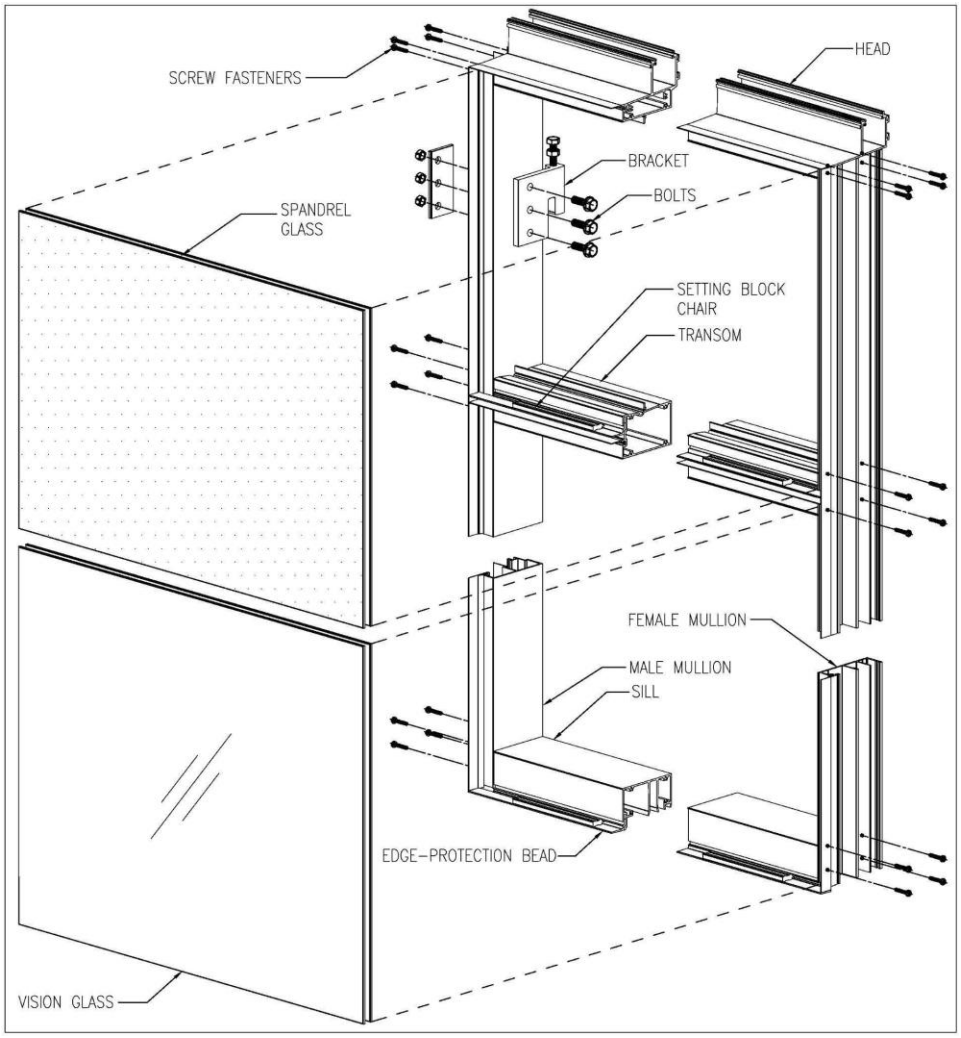

Figure I.4: In the figure above an exploded view of a typical unitised curtain wall system is presented. The interruption of the framing elements, mullions and transoms, facilitates the preview of the various cross sections. Among the various components marked, the setting block chair is also visible. Finally, the insulating material normally located behind the spandrel area is not presented in this view for purposes of clarity (Source: Lee, A. D. et al., 2017).

Annex II

Additional Seismic Regulations

FEMA 450, American Provisions

The risk of earthquake ground motions as well as their potential injuries and damages are also addressed by the American set of provisions, as provided in the form of "Recommended Provisions" by the Federal Emergency Management Agency (FEMA) and the National Earthquake Hazards Reduction Program (NEHRP).

The main purpose of these provisions is to define the minimal design aspects that ensure the primary use and function of structures while ensuring the safety, health and welfare of their users. The previous can be achieved through the minimisation of the earthquake risk that can potentially pose a threat to human life. Additionally, the provisions aspire to increase the capability of the various structures consisting of a considerable amount of hazardous elements to perform adequately both while undergoing as well as after seismic actions.

In the following section the main content of the "NEHRP Recommended Provisions for Seismic Regulations for New Buildings and Other Structures" published in 2003 (FEMA 450, 2003) regarding the seismic resistant design and construction of buildings is presented.

Main body

As already mentioned, the seismic ground motion can potentially result in damages not only of the structural elements but of the non-structural, such as the architectural ones, as well. For this reason in the Provisions document, the entire Chapter 6 is dedicated to the design criteria specification of the non-structural components, their attachments and supports that are permanently attached to the building structures.

According to the provisions, the non-structural elements are allowed to independently move from the structure. For the cases where they are rigidly tied to the structure itself, the deformation that could result in their potential cracking should be minimised. For this reason, non-structural elements such as the exterior enclosure of a building should satisfy the requirements presented in detail by the FEMA Provisions.

Component Importance Factor

An importance factor I_p is attributed to all the components and is typically equal to $I_p = 1.0$. The value of this factor shall be increased to $I_p = 1.5$ in case any of the following conditions apply for the component under examination:

- consists of hazardous materials
- it is desired to maintain its function after an earthquake
- the component belongs to or is attached to an element of Seismic Use Group III and its continued operation is required or its failure could distract the facility's continued operation

Component Force Transfer

A basic consideration introduced by the Provisions is related to the force transfer between the components. As identified by this specific standard, the different components need to be attached in a way that allows the component forces to be transferred to the load bearing structure. Every component that is aimed to withstand seismic forces needs to be either welded, bolted or positively fastened in an alternative way without the frictional resistance created due to the gravity effects being taken into consideration. As specified by the provisions, it is important that sufficient stiffness as well as strength must be continuously provided between the supporting structure and the various components. The local elements of the load bearing structure need to resist the component forces in the cases where these forces define the element design or their connections. For those cases, the component forces are defined as seismic forces as described in the following section apart from the component amplification factor (a_p) and the component response modification factor (R_p) modifications (Table II.1) based on the fact that the anchorage condition does not need to be included.

Architectural Component or Element	**ap**	**Rp**
Interior non-structural walls and partitions:		
Plain masonry walls	1.0	1.5
All other walls and partitions	1.0	2.5
Cantilever Elements, unbraced or braced (to structural frame) below their centres of mass:		
Parapets and cantilevered interior non-structural walls	2.5	2,5
Chimneys and stacks where laterally supported by structures	2.5	2.5
Cantilever elements, braced (to structural frame) above their centres of mass:		
Parapets	1.0	2.5
Chimneys and stacks	1.0	2.5
Exterior non-structural walls	1.0	2.5
Exterior non-structural wall elements and connections:		
Wall element	1.0	2.5
Body of wall-panel connections	1.0	2.5
Fasteners of the connecting system	1.3	1.0
Veneer:		
High deformability elements and attachments	1.0	2.5
Low deformability elements and attachments	1.0	1.5
Penthouses (except where framed by an extension of the building frame)	2.5	3.5
Ceilings		
All	1.0	2.5
Cabinets		
Storage cabinets and laboratory equipment	1.0	2.5
Access floors		
Special access floors	1.0	2.5
All other	1.0	1.5
Appendages and ornamentation	2.5	2.5
Signs and billboards	2.5	2.5

Other rigid components:		
High deformability elements and attachments	1.0	3.5
Limited deformability elements and attachments	1.0	2.5
Low deformability elements and attachments	1.0	1.5
Other flexible components		
High deformability elements and attachments	2.5	3.5
Limited deformability elements and attachments	2.5	2.5
Low deformability elements and attachments	2.5	1.5
a: A lower value for ap is permitted where justified by detailed dynamic analysis. The value for ap shall not be less than 1.0. The value of ap equal to 1.0 is for rigid components and rigidly attached components. The value of ap equal to 2.5 is for flexible components and flexibly attached components. b: Where flexible diaphragms provide lateral support for concrete or masonry walls or partitions, the design forces for anchorage to the diaphragm shall be as specified in Sec. 4.6.2.1.		

Table II.1: a_p and R_p coefficients for Architectural Components or Elements (Source: FEMA 450, 2003).

In the following section of the present chapter the requirements of the Provisions that are more specific to the architectural components, such as the curtain walls, will be briefly presented.

All the architectural components along with their attachments and supporting elements need to be designed to accommodate the seismic forces as described in the beginning of the present chapter. Especially for the architectural elements that can potentially cause safety hazards, an additional indication applies. Those elements are suggested to be designed to withstand also seismic relative displacements. For the design of the entire range of the architectural components, the vertical deflection caused by the joint rotation of the horizontally cantilevered structural elements should be considered.

Below the main content of the Provisions referring to the seismic forces and displacements, their transfer and application is presented.

Seismic Forces

The seismic force combined with the service loads are indicated to be applied to the component independently in the two horizontal orthogonal directions. In the case where the wind loads apply on the non-structural exterior wall elements or the building code load applied horizontally on the interior partitions surpass F_p, these loads should define the strength design.

Horizontal Seismic Forces

Seismic design force F_P is applied horizontally in the gravity centre of the non-structural component, are expected to be distributed relatively to the entire mass of the element and derives from the following equation:

$$F_p = \frac{\left(0.4 * a_p * S_{DS} * W_p\right)}{\frac{R_p}{I_p}} * \left(1 + 2\frac{z}{h}\right)$$

Where:

a_p: the amplification factor of the component as obtained from Table II.1

S_{DS}: the acceleration parameter of the short period spectra

W_p: the operating weight of the non-structural component

R_p: the response modification factor of the component originating from Table II.1

I_p: the importance factor of the component

h: the average value of the roof height above the base

z: the height of the component as measured from the base of the attachment point and upwards. It should not be less than 0 and $\frac{z}{h}$ should not exceed 1.0.

F_P is not required to exceed the following:

$$F_p = 1.6 * S_{DS} * I_p * W_P$$

And should not surpass the equation below:

$$F_p = 0.3 * S_{DS} * I_p * W_P$$

Exception: For the case where the period T_p of the component exceeds T_{flx} the upper limit of F_p is indicated to be reduced by $\frac{T_{flx}}{Tp}$. T_{flx} is calculated by the following equation:

$$T_{flx} = \left(1 + 0.25 * \frac{z}{h}\right) * \frac{S_{D1}}{S_{DS}}$$

Vertical Seismic Forces

The non-structural components should be designed to withstand vertical forces equal to:

$$\pm 0.2 * S_{DS} * W_p$$

In this case the overstrength factor Ω_O as well as the redundancy /reliability factor, ρ, are not applied.

Seismic Relative Displacements D_P

The relative displacements D_P caused due to seismic forces are widely used during the design process of the elements. Their effect should be combined with one of the displacements originating from the conventional loads. They typically derive from the following relation:

$$D_p = \delta_{xA} - \delta_{yA}$$

Where:

D_p: the relative displacement the component must be ensured to accommodate
δ_{xA}: *the deflection of structure A at level x*
δ_{yA}: *the deflection of structure A at level y* should not exceed the following value:

$$D_P = (X - Y) * \frac{\Delta_{aA}}{h_{sx}}$$

And is shall not exceed:

$$D_P = \frac{X * \Delta_{aA}}{h_{sx}} + \frac{Y * \Delta_{aB}}{h_{sx}}$$

Where:

Δ_{aA} , Δ_{aB} : the storey drift that is allowable for structure A and B respectively as obtained from Table 4.5-1 of the Provisions document

X : the height of the attachment of the upper support as measured above its base (at x level)

Y : the height of the attachment of the lower support as measured above its base (at y level)

h_{sx}: the storey height as introduced in the allowable drift Δ_a definition in the Table 4.5-1 of the Provisions document. The relation Δ_a / h_{sx} defines the allowable drift index

Exterior Elements & Connections

The non-structural elements that either form part of the exterior enclosure or are (mechanically) attached to the main building structure have to withstand both the seismic relative displacements (D_p) that were mentioned above as well as the movements generated due to temperature variations. In order to achieve so, either fasteners and mechanical connections or structural supports ensuring the direct connection with the main structural system are needed. These types of supports need to fulfil an extended list of requirements as presented below:

- Both the panel joints as well as the connections should allow relative movements between adjacent storeys. However, they should not surpass the greater value among 13.0 mm (0.5 in) or the calculated storey drift, D_p
- The connections allowing the in-plane storey drift of the panel should be either sliding ones with oversized or slotted holes, or connections allowing movements through the steel bending or alternatively, connections providing ductile capacity or equivalent sliding.
- The bodies of the connections should be able to deform sufficiently and be able to rotate in order to prevent concrete failure or failures of low deformation either on or around welds.

- The connector's body as well as every fastener comprising it, such as insert, welds, bolts and dowels, should be able to withstand the seismic force F_p as determined above applied at the mass centre of the panel. For the correct identification of F_p, the values of R_p and α_p originating from the Table 6.3-1 of the Provisions and Table II.1 of the present document need to be obtained.

- In the cases where the anchorage is done through flat straps typically embedded in masonry or concrete, the straps need to be hooked around or attached to the steel reinforcement. Alternatively, they need to be terminated in such a way to allow the effective transfer of the forces to the steel reinforcement.

Moreover, in the FEMA provisions there is an individual section (Section 6.3.7) dedicated especially to the design and installation of the glass of the glazed curtain walls. The main information of this section is summarised below.

Glass in Curtain Wall Systems & Storefronts

Especially for the case of glass in glazed storefronts, partitions and curtain walls an additional requirement needs to be met. The glass in the aforementioned situations need to be designed so that the relative seismic displacement will be sufficient to accommodate the requirement for the relative displacement $\Delta_{fallout}$.

$\Delta_{fallout}$ should be derived for the whole height of the glass element and its value is the greater one between the following:

$$\Delta_{fallout} \geq 1.25 * l * D_p$$

or (II.1)

$$\Delta_{fallout} \geq 0.5\ in\ (= 13.0\ mm)$$

Glazed curtain wall systems, glazed partition components and glazed storefronts need to be designed to withstand the relative seismic displacement $D_p = \delta_{xA} - \delta_{yA}$ as indicated previously. Their relative seismic displacement should be defined over the height of the glazing component that is analysed.

Exceptions

Below the list of the cases excluded from some of the provisions mentioned previously is presented.

- Fully tempered monolithic glass that falls into the Use Groups I & II can be excluded from the provisions of equation (I.1) when the glazing is located 3.0 m (10.0 ft) or less above the walking level

- Glass with clearance from the framing D_{clear} as defined in relation (II.2) is not required to be checked for the provisions of the relation (II.1). When the relation depicted below is met, sufficient clearance D_{clear} is achieved, ensuring the absence of physical conduct between the frame and the glass.

$$D_{clear} \geq 1.25 * D_p \quad \text{(II.2)}$$

Where:

$$D_{clear} = 2 * c_1 \ * \ (1 \ + \frac{h_p * c_2}{b_p * c_1})$$

b_p : the rectangular glass panel width
h_p: the rectangular glass panel height
c_1: the gap (clearance) between the frame and the vertical glass edges
$c_{2:}$ the gap (clearance) between the frame and the horizontal glass edges

Heat-strengthened laminated or annealed glass of a single thickness with an interlayer of at least 0.76 mm (0.030 in) which is mechanically captured in a glazing pocket of a wall system, with a secured to the frame perimeter, by means of either a gunable wet-glazed curing elastomeric sealant with a perimeter beam of at least 13.00 mm (0.5 in) with of for the contact glass or a different approved anchorage system, is also excluded from the equation 6.3.1. It can be clearly seen that the relations prescribed by the American provisions just presented above originate from the research of Bouwkamp and Meehan (Bouwkamp & Meehan, 1960) and Sucuoğlu and Vallabhan (Sucuoğlu & Vallabhan, 1997) already described earlier, in the section "Earthquake-induced Curtain Wall Damages" of the present study.

Seismic Drift Limits for the Glazing Components

Based on the FEMA provisions, the drift that is responsible for the glass fallout from the partitions, storefronts or curtain walls should be defined either by an engineering analysis or based on the AAMA 501.6 "Recommended Dynamic Test Method for Determining the Seismic Drift Causing Glass Fallout from Window Wall, Curtain Wall and Storefront Systems" standards (AAMA 501.6, 2018).

Considerations

FEMA provisions define the minimal criteria according to which a structure is considered as sufficient to resist seismic ground motions while ensuring life safety in and close to the building structure. A set of equations defining both the seismic forces F_p as well as displacements D_p is provided incorporating several coefficients. Furthermore, specifications regarding various aspects such as defining the proper clearance of the exterior cladding, the partitions and glazing the life safety of the non-structural elements is enhanced.

A specific section is devoted to the design and verification of architectural elements, attachments and supports. By providing the element's design criteria the accommodation of the inter-storey drift introduced to the structures due to the seismic events, damage to the non-structural elements is minimised. Specific attention is paid to exterior elements, to the connections of the architectural elements and also to the seismic drift limits of the glazing. In practice, the threshold for the design relative displacement $\Delta_{fallout}$ of glazed partitions, storefronts and curtain walls is provided.

It is proposed that every glass panel of a curtain wall system should have a specific in-plane drift capacity $\Delta_{fallout}$ which practically represents the inter-storey drift that could potentially result in the falling of the glass from its panel. This relative displacement $\Delta_{fallout}$ of the glazing panel should be at least 25.0 % larger than the maximum drift value that that the glass panel presents when subjected to a design earthquake.

Finally, in order for the minimum value of the inter-storey drift that results in the glass fallout to be defined, the Provisions document refers to the AAMA 501.6:2018 Standards. Based on the latter, the in-plane drift capacity $\Delta_{fallout}$ is typically identified via the realisation of mock-up tests.

New Zealand Standards (NZS 1170.5)

Seismic Requirements for Components & Parts

NZS 1170.5 Standards (NZS 1170.5, 2004), provide a set of criteria and procedures that indicate the seismic actions to be included during the limit state design of both elements and structures inside the area of New Zealand. The part of the Standard indicated to the seismic design is Section 8, "Requirements for parts and components". In this section the Standards indicate that every "part" of the building structures, from the permanent and the non-structural ones, to their connections, permanent services and also the supported by the structures equipment, is required to be designed to withstand the specified seismic actions. The complete list of the aforementioned elements is characterised by NZS 1170.5 as "parts".

The "parts" of the structure are categorised and classified according to the criteria presented on the table "Classification of Parts" that is obtained from the standard itself and is presented in Table II.2 below.

Table 8.1
Classification of Parts

Category	*Criteria*	*Part risk factor R_p*	*Structure Limit State*
P.1	*Part representing a hazard to life outside the structure*	*1.0*	*ULS*
P.2	*Part representing a hazard to a crowd of greater than 100 people within the structure*	*1.0*	*ULS*
P.3	*Past representing a hazard to individual life within the structure*	*0.9*	*ULS*
P.4	*Part necessary for the continuing function of the evacuation and life safety systems within the structure*	*1.0*	*ULS*
P.5	*Part required for operational continuity of the structure*	*1.0*	*SLS2*

P.6	*Part for which the consequential damage caused by its failure are disproportionately great*	*2.0*	*SLS1*
P.7	*All other parts*	*1.0*	*SLS1*

Table II.2 Classification criteria for the categorisation of the parts. "ULS" refers to the Ultimate Limit State and "SLS" refers to the Serviceability Limit State (Source: NZS 1170.5).

Regarding the categories P.1, P.2 and P.3, the scope is restricted to the parts weighting more than 10.0 kg and can potentially fall out of the structure more than 3.0 m in an accessible area from the public area.

Moreover, a specific category of parts is described by the standard. That category concerns the parts of the structure of which the mass exceeds the 2.00 % of the total mass of the part itself combined with the one of the primary structure and additionally their minimal translational period surpasses the 0.2 seconds. For these parts, a special study of the part aiming to define its dynamic characteristics is required by the Standard.

Seismic Design Actions on Parts

According to the New Zealand Standard, in order for the verification of a part under a seismic event to be achieved, the application of seismic actions of both horizontal and vertical direction is required. In this chapter, the determination and calculation of the horizontal and vertical design actions will be presented.

Horizontal Design Actions

The horizontal design seismic actions applied on a part can be calculated as presented in equation (II.3):

Horizontal: $$F_{ph} = C_p * (T_p) * C_{ph} * R_p * W_p \leq 3.6 * W_p \quad \text{(II.3)}$$

Where:

- $C_p * (T_p)$: the horizontal design response coefficient, practically the horizontal acceleration coefficient of the level of the structure at which the support of this part is provided as determined in the 8.2 section of the NZS Standard
- C_{ph} : the horizontal response factor of the part, as given in the 8.6 section of the Standard and Table II.3 of the present document
- R_p : the risk factor, as defined by Table 8.1 of the Standard and II.2 of this paper
- W_p: the weight of the analysed part

The horizontal response factor C_{ph} is obtained from the Table II.3 for a ductility μ_p = 1.0. For the cases where the floor level acceleration results in the part yielding, the ductility is considered otherwise.

Unless otherwise stated by a specific study, the vertical response factor C_{pv} is also provided in the Table II.3 for a ductility μ_p = 1.0.

Part Response Factor, C_{ph} and C_{pv}	
Ductility of the part μ_p	*C_{ph} and C_{pv}*
1.0	*1.0*
1.25	*0.85*
2.0	*0.55*
3.0 or greater	*0.45*

Table II.3: The table based on which the horizontal (C_{ph}) and vertical response factors (C_{pv}) in relation to the ductility μ_p of the respective parts are obtained (Source: NZS 1170.5).

Vertical Design Actions

According to the New Zealand Standard, the vertical earthquake actions should be considered for the parts that are prone to the amplification of the vertical acceleration. Unless specified otherwise, for the calculation of the vertical seismic actions on a specific part, the following equation can be utilised:

Vertical: $$F_{pv} = C_{pv} * C_{vd} * R_p * W_p \leq 2.5\, W_p$$

Where:

C_{pv}: the vertical response factor of the part as obtained from Table II.3 based on the part's ductility

C_{vd}: the design action coefficient as determined for the vertical direction from the "Design earthquake actions" Section. The period obtained is the one corresponding to the supporting system of the part

R_P the risk factor, as defined by Table 8.1 of the Standard and Table II.3 of this paper

W_P: the weight of the analysed part

Seismic Induced Deflections

According to the NZS 1170.5, every part connected to the load bearing structure on at least two levels is required to sustain any action originating from relative deflections corresponding to the respective limit state.

Horizontal Deflection Limits

The horizontal deflections of the structures should not exceed the respective boundary values for the ultimate limit state as specified in the 7.4 section of the Code document. More specifically, any part of the structure's perimeter is not allowed to transcend the distance between this point of the structure and the boundaries of the neighbouring sites. The previous is not required in the cases of the street frontages.

An additional limitation applies to the cases where the examined structure is adjacent to other structures that are located on the same site. In that case, any point of the structure placed above the ground level is allowed to have a horizontal deflection that does not cause contact with the adjacent structures even when it is paired with the design horizontal deflection of any of these adjacent structures (NZS 1170, 7.4.1.2).

Inter-storey Deflection Limits

Regarding the boundary values of the inter-storey deflections, a division between the ultimate (ULS) and the serviceability limit state (SLS) is made. Starting from the ultimate limit state (ULS), the threshold value of the inter-storey deflection equals the 2.5 % of the height of the respective storey. In case the material Standard specifies another lower value, this value forms then the limit of the inter-storey deflection of the structure.

Moving to the serviceability limit state (SLS), the Standard indicates that the inter-storey defection should be such that it will not cause deterioration of the structural components and their required performance. Moreover, the horizontal deflections should not exceed the existing separation that aims to prevent the contact between the various parts and the structure itself or between the adjacent elements of the structure. Moreover, the design horizontal deflection should not deteriorate the function of these or any other components of the structure (NZS 1170, 7.5).

Connection Parts

Various elements are seen from the New Zealand Standards as non-ductile connections. Among others, the shallow chemical anchors, the expansion anchors, and the shallow cast-in-situ anchors in tension that are not attached to the main reinforcement. The design of the non-ductile connections of the parts is prescribed to correspond to a part ductility factor $\mu_P = 1.25$.

For other connections that can be guaranteed to sustain at least the 90.0 % of the design action effects under a displacement application larger than the yield displacement originating from cycling loading multiplied by two.

Considerations

The NZS 1170.5 proposes that all the non-structural elements, also referred to as “parts” are verified under seismic actions applied to the centred of their mass. Both vertical and horizontal seismic action is required to be applied. Various deflection limits are considered separately for the two limit states, the ultimate and the serviceability one. Additionally, a minimum ductility of $\mu_P = 1.25$ is required for the connection part. Finally, the ductility of the parts (μ_P) is obtained as 1.0 for the serviceability limit state and in any other case unless otherwise stated or the floor acceleration can cause the part to yield.

Mock-up Test Guidelines, AAMA 501.4 & 501.6

As already mentioned, a common approach widely used over the years aiming for the determination of the drift capacity of a curtain wall system includes the realisation of mock-up tests performed under controlled laboratory conditions. In fact, some of the existing seismic standards and guidelines, such as FEMA 450, already prescribe the implementation of full-scale experimental testing as a prerequisite for the evaluation of the glazed curtain wall seismic behaviour.

The American Architectural Manufacturers Association (AAMA) has published a set of guidelines (AAMA 501.4) specifying the evaluation of storefronts and curtain walls serviceability limit state through a static method while undergoing inter-storey seismic drift and a set of specifications (AAMA 501.6) related to the ultimate limit state, identifying through a dynamic test the seismic drift resulting in the glass fallout from a curtain wall system.

AAMA 501.4

As previously mentioned, this first set of guidelines prescribes the windows, window walls, curtain wall or storefronts evaluation while undergoing earthquake loadings corresponding to serviceability level states. Through the application of in-plane lateral loading, the resulting damage on the systems examined is defined through the evaluation of the water- and air-leakage rates (Aiello et al., 2018).

The experimental test method by specifying the in-plane application of statical horizontal racking displacements aims to monitor the possible serviceability changes, water or air leakage rates for example, of the examined specimens. For this reason, the experimental rests are performed on 1:1 scale representative model (mock-ups) of either the storefront or the curtain wall aimed to be tested for its resistance to the specified design displacements. The testing sequence consists of a complete series of serviceability tests measuring the water- and air-infiltration, followed by the realisation of the seismic testing. After its completion, an additional complete series of the same water- and air-leakage tests is prescribed. Figure II.1 presents a typical testing configuration utilised for the seismic verification of curtain wall systems.

The standard specifies that the aforementioned testing sequence including the displacement application to the examined specimen needs to be repeated in at least three cycles. However, indications regarding the range of the movement that needs to be applied during the testing sequence are absent.

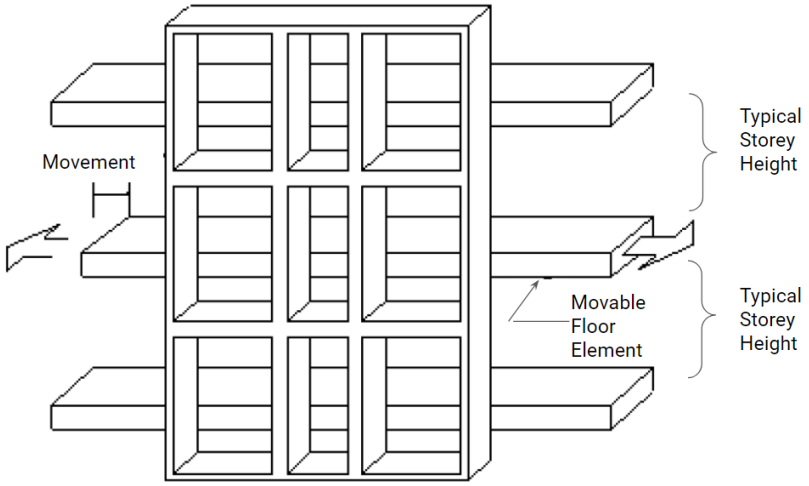

Figure II.1: A test configuration typically used for the verification of a curtain wall seismic behaviour. The racking facility in this case consists of three steel tubes. While the upper and the lowest ones are fixed, the intermediate allows horizontal movements, recreating in this way the inter-storey drift that results in the racking of the curtain all elements. As the drift amplitude gradually progresses, the potential failure modes of the examined configuration are revealed (Source: AAMA 501.4, 2018).

Additionally, although AAMA 501.4 underlines that the test must be performed slowly enough so that possible decelerations or accelerations will be prevented, the duration of the test itself remains ambiguous. More information regarding both the testing duration as well as the movement amplitude are typically determined by the "Test Agency" as mentioned by the Standards.

The serviceability limit state of the configuration tested, either storefront or curtain wall system, can be verified via the pass or fail criteria for the three discrete facility types: i) essential, ii) standard occupancy & iii) high occupancy. The detailed requirements for these three facility types are described for all the Performance Levels in both the FEMA 273 (FEMA 273, 1997) and National Earthquake Hazards Reduction Program NEHRP (FEMA P-2082-1, 2020) Provisions.

AAMA 501.6

The second set of guidelines refers to determination of the horizontal racking displacement range of an exterior wall configuration that could potentially result in the architectural glass panels to fall out of their framing while subjected to controlled laboratory conditions. Contrary to the previous guidelines (AAMA 501.4, 2018), the present aims to determine the $\Delta_{fallout}$ of a curtain wall panel through a dynamic racking crescendo test. A schematic view of a relevant testing facility is depicted in Figure II.2. As already mentioned, in practice by defining the $\Delta_{fallout}$, the in-plane dynamic inter-storey drift that leads to the glazing fallout is determined.

This specific verification method is required by the NEHRP and FEMA 450 (FEMA 450, 2003) for the glazed curtain wall cases with insufficient clearance between the glazing pane and the frame glazing pockets

is provided, allowing therefore contact of the elements when the main structural system is subjected to seismic design displacements.

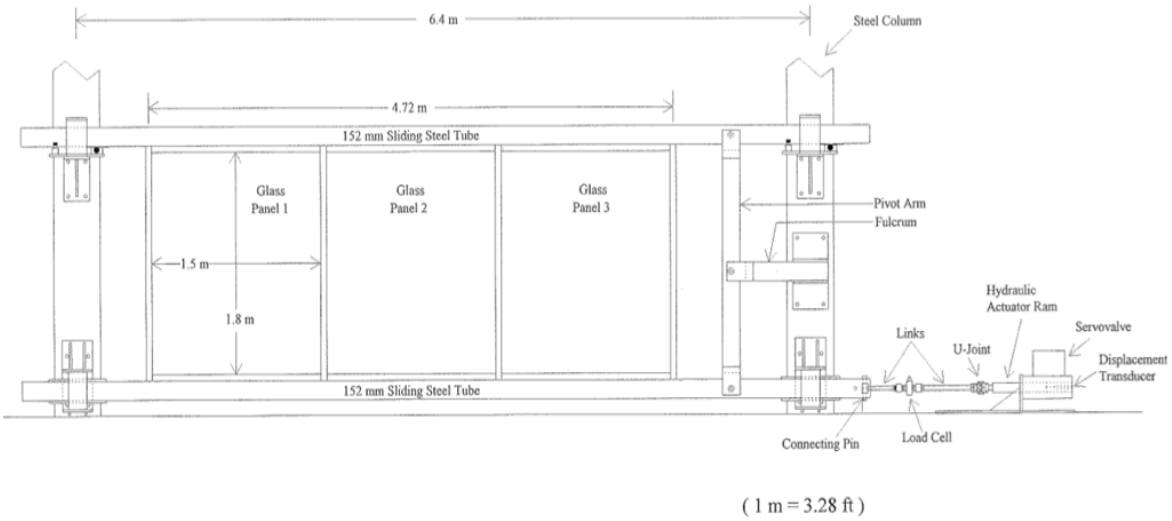

Figure II.2: A schematic view of the Dynamic Racking test facility (Source: AAMA 501.6, 2018).

According to the AAMA 501.6 Standard (AAMA 501.6, 2018), a typical crescendo test consists of a continuous series of "constant amplitude" intervals and "ramp up" intervals. It is additionally specified that four sinusoidal cycles should comprise each of the two interval types. In that way, during the testing, the glazed system examined moves sinusoidally in the horizontal direction. The experimental procedure is named after the musical term "crescendo" due to the fact that the amplitude of the racking series is progressively increasing (Figure II.3).

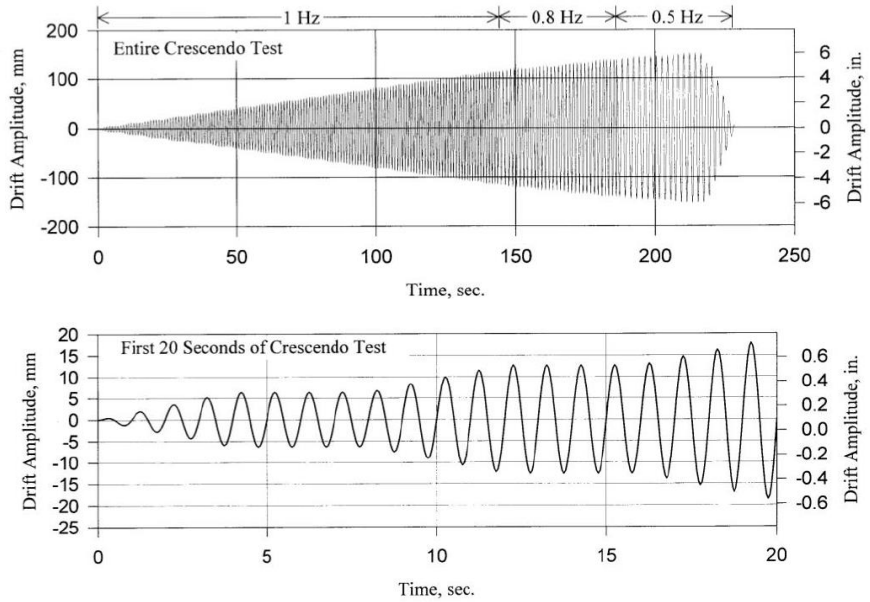

Figure II.3: The drift time history as recorded during a crescendo test of mid-rise architectural glass components (Source: AAMA 501.6, 2018).

The minimum value of the racking displacement that results in the glazing fallout of the three curtain wall specimens required by the Standard to be tested results in the $\Delta_{fallout}$ of this specific glazed curtain wall.

For actual curtain wall design applications, in the absence of numerical models or prior information adequately describing the seismic behaviour of the examined configuration, the experimental method prescribed by AAMA 501.6 Standards is followed. Complementary to AAMA 501.4 and AAMA 501.6, a report developed in 2014 by Joint Research Centre (JRC) provides "Guidance for European structural design of glass components" and functions as a supportive documentation for the harmonisation, implementation and also for the Eurocode's further development (Gil, 2019). Various key parameters relevant to the curtain walls structural performance are common in the AAMA and the JRC Guidelines (Aiello et al., 2018).

Considerations

To conclude, the main difference between AAMA 501.4 and AAMA 501.6 is that the first refers to the serviceability limit state, while the second is related to the ultimate limit state. AAMA 501.4 determines the curtain wall or a storefront performance with respect to the water- and air-tight sealing for a specific and predetermined in-plane displacement applied horizontally. AAMA 501.6-18 on the other hand, defines the ultimate in-plane displacement also applied horizontally that results in the glazing fallout from the unit framing.

Annex A

Overview of Displacements Recorded for the Characteristic Frame

& Glazing Points of the Curtain Wall System Examined

In the present Annex the displacement of the curtain wall representative points as recorded for the three different levels of displacement intensity is presented in Figures A2-A7. Figure A.1 depicts the naming convention of those representative points as well as the location of each of the displacement transducers for the frame and the glazing respectively. The transducers appear as numbers in Figure A.1 and are indicated as DT-XX in the graphs of Figures A.2-A7, where XX is the number of each transducer.

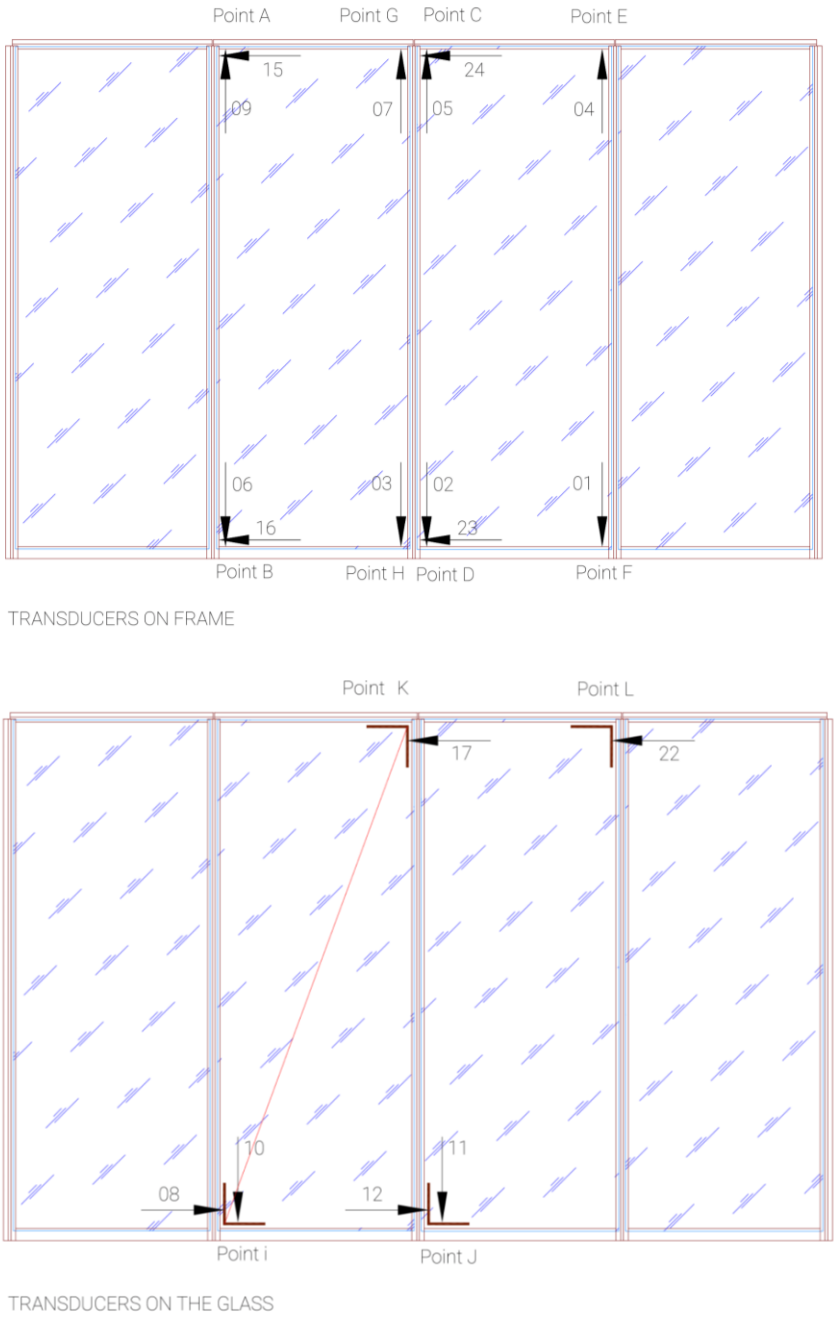

Figure A.1: The schematic representation above for the aluminium frame and below for the glazing is presented here. These figures serve as a reminder of the specific location of the transducers monitoring the curtain wall behaviour under seismic action. The naming convention (Points A-L) adopted during this study is also displayed for a matter of completeness.

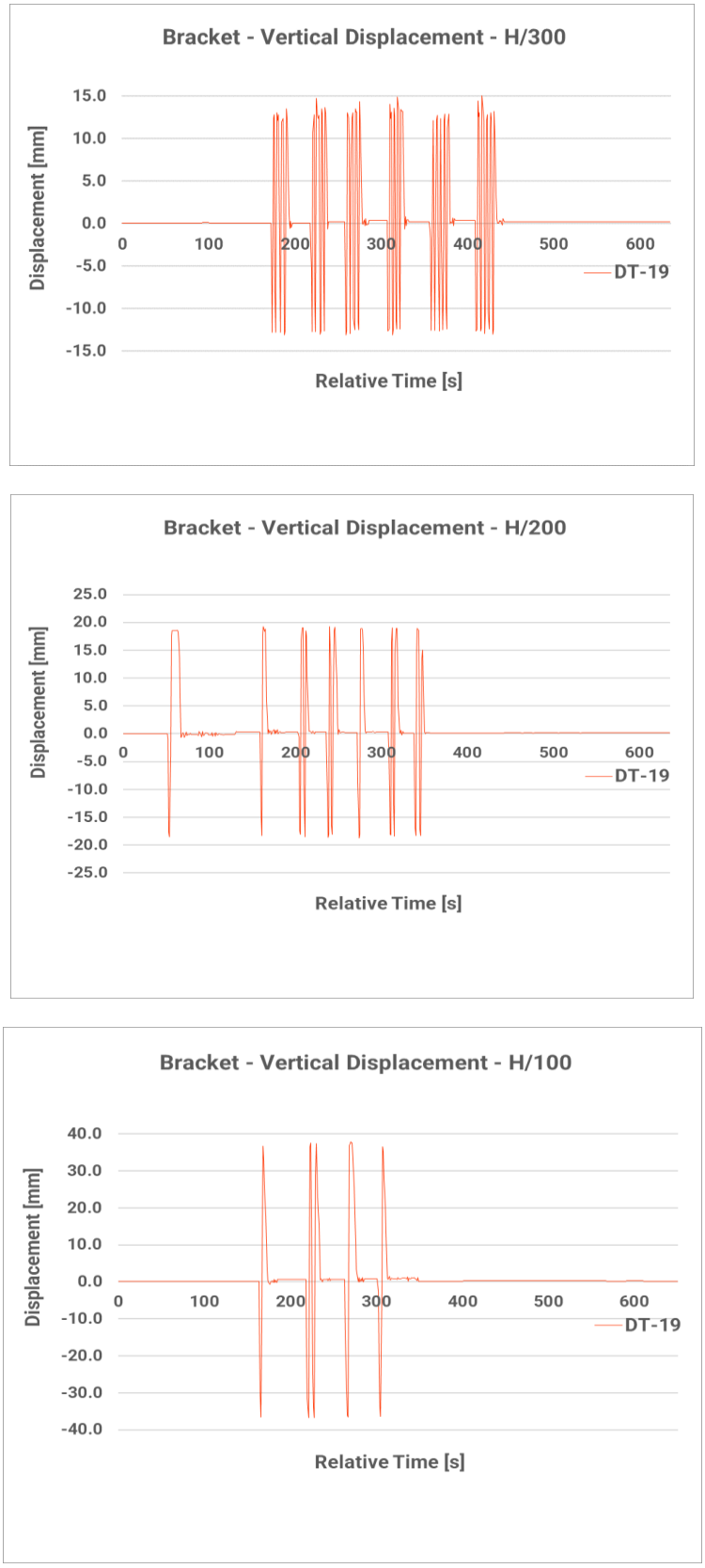

Figure A.2: The vertical displacement of one of the upper brackets of the façade specimen as monitored for H/300, H/200, H/100.

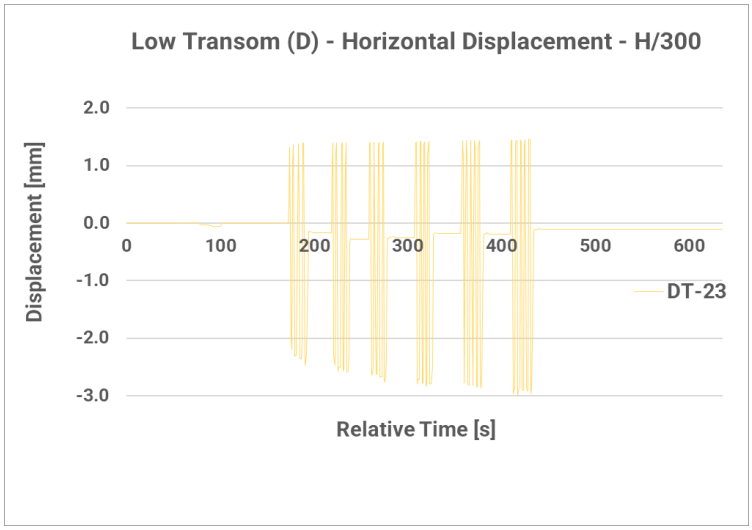

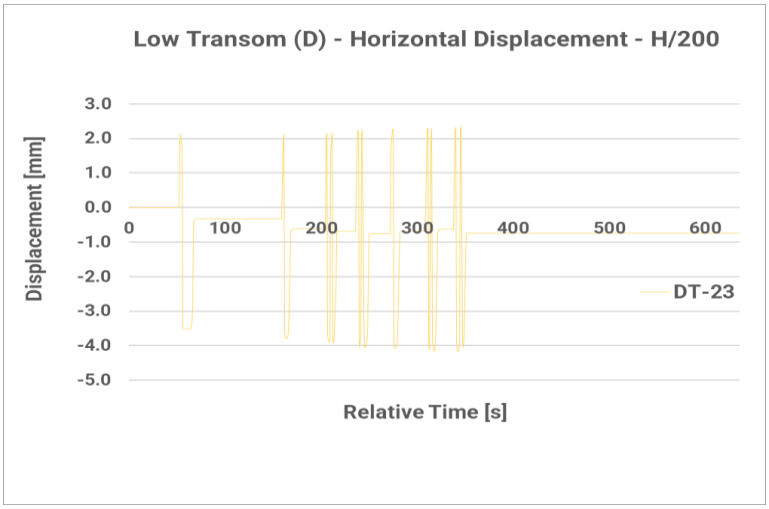

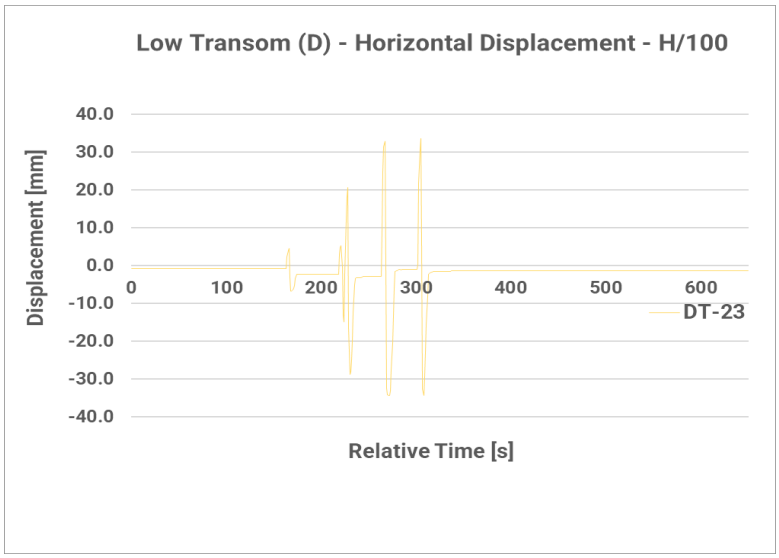

Figure A.3: The horizontal displacement of the low transom (Point D) for the different levels of the displacement application.

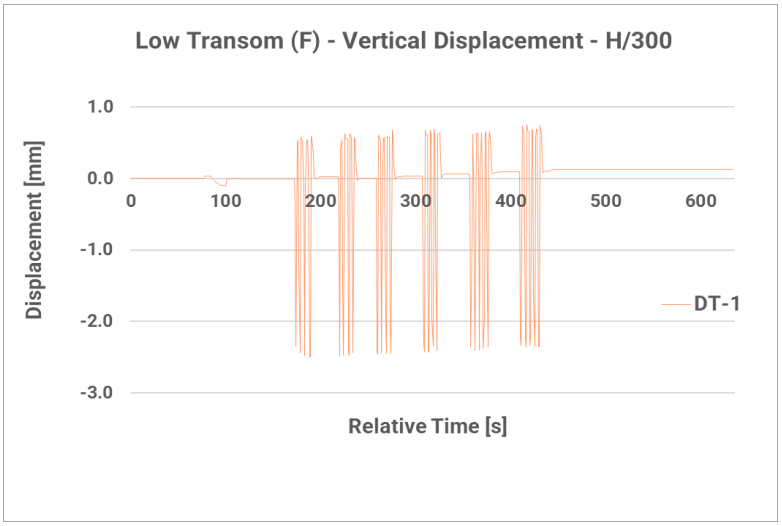

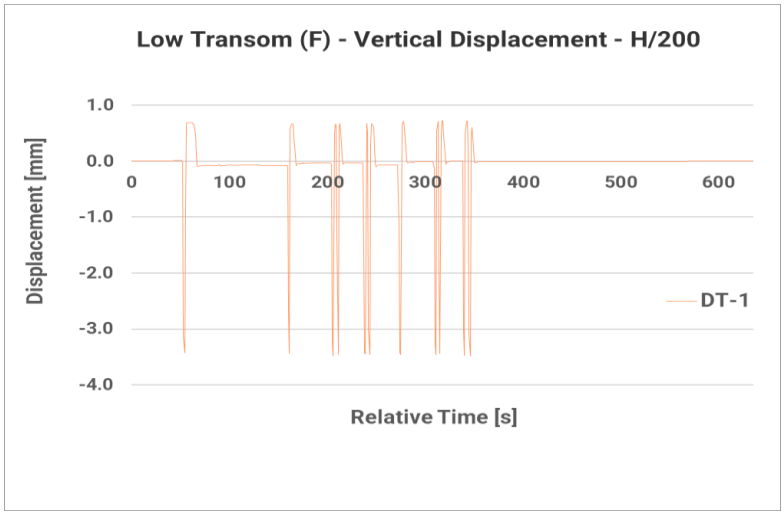

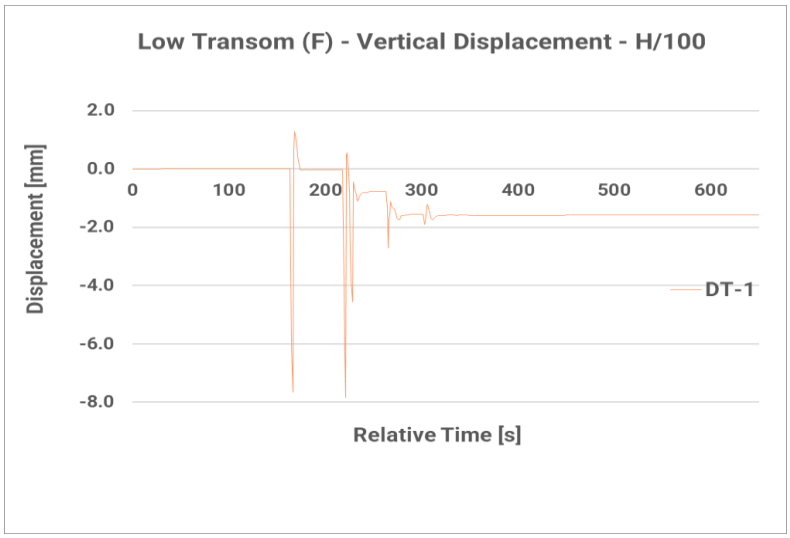

Figure A.4: The vertical displacement of the low transom (Point F) as recorded for the three intensities of the displacement application.

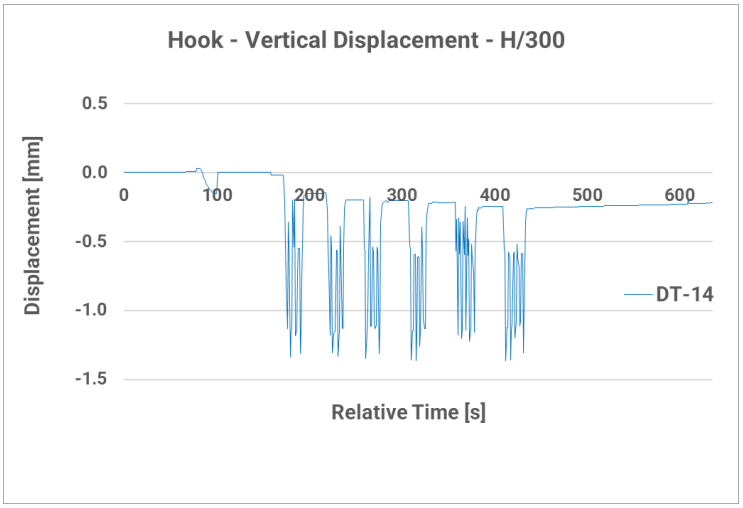

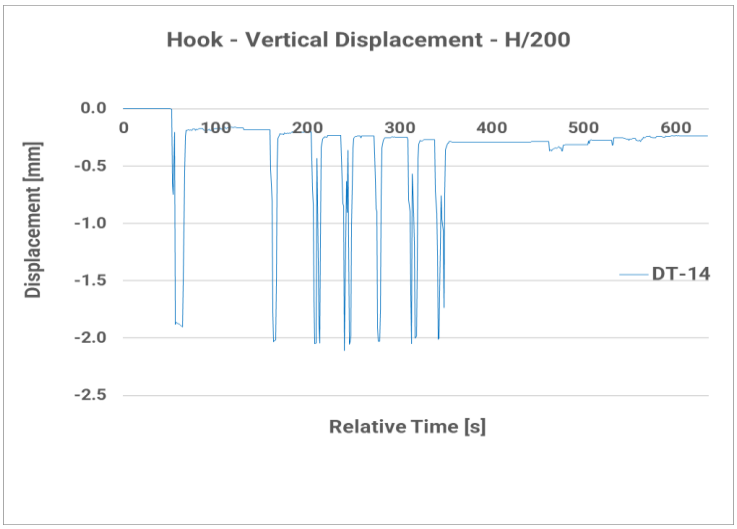

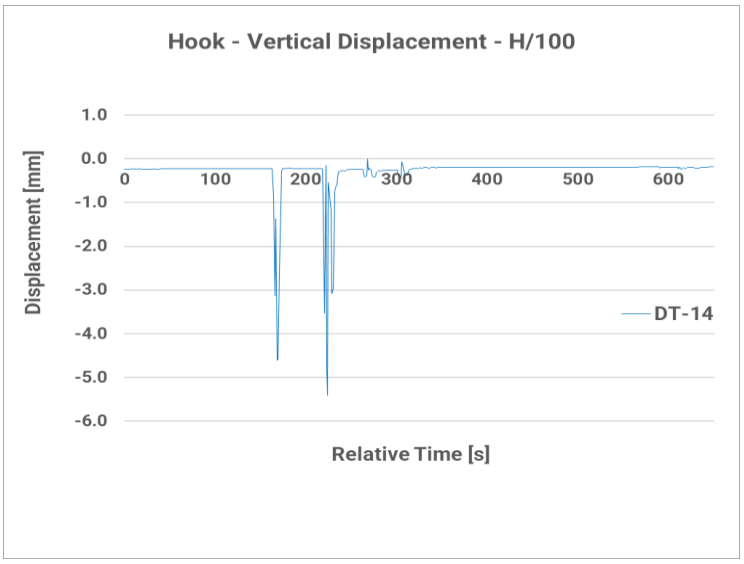

Figure A.5: The vertical displacement as monitored in the hook of the curtain wall fastening system.

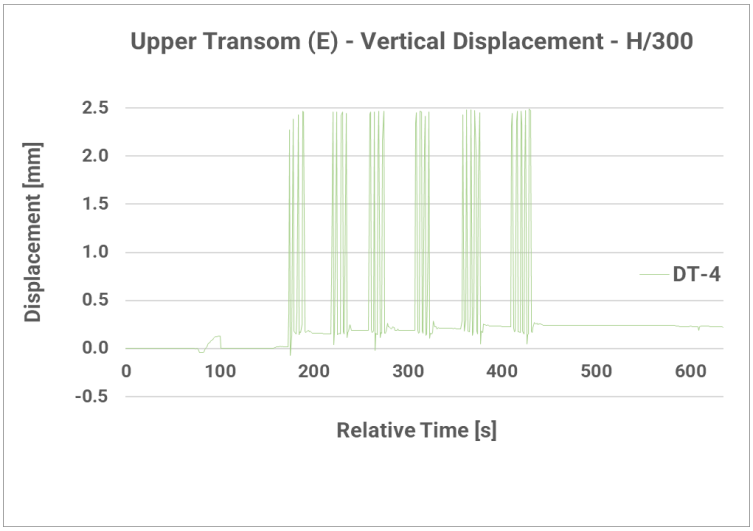

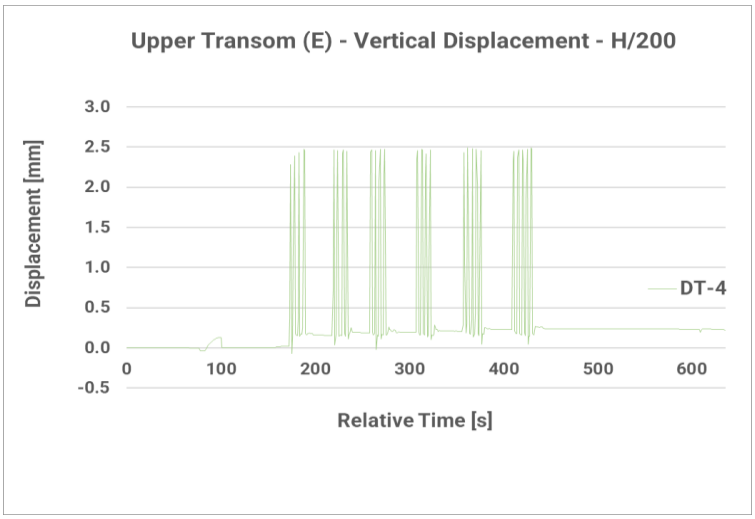

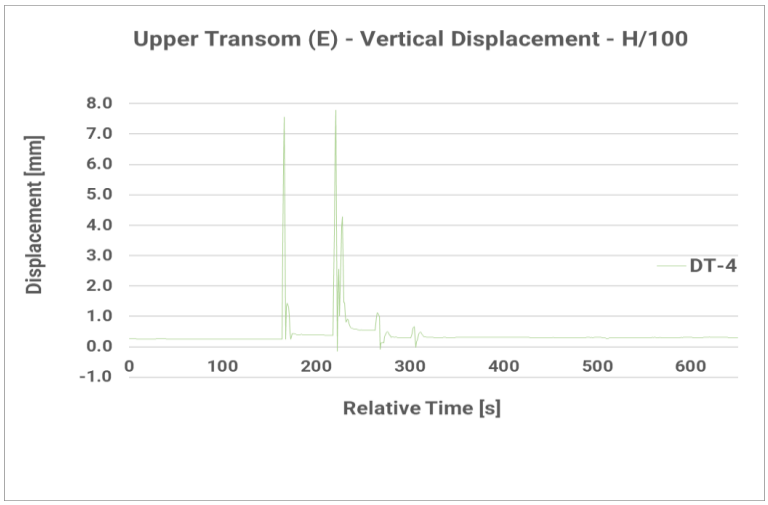

Figure A.6: The measurements of the vertical displacement of the upper transom (Point E) for the three intensities of the displacement application.

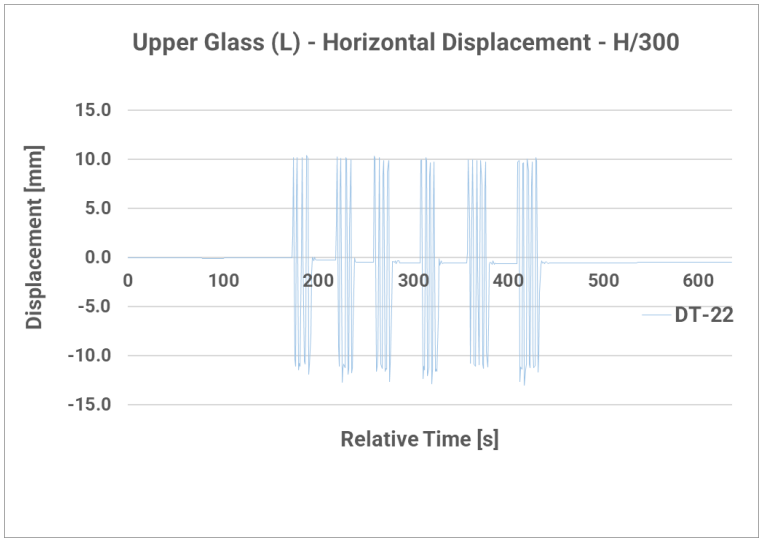

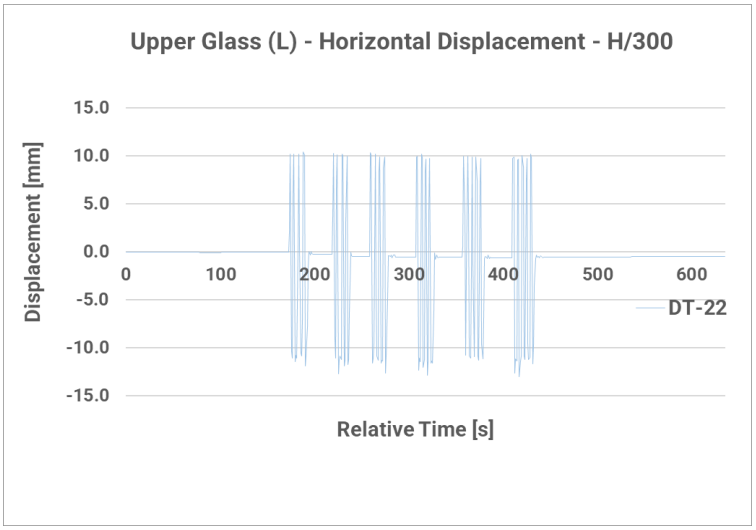

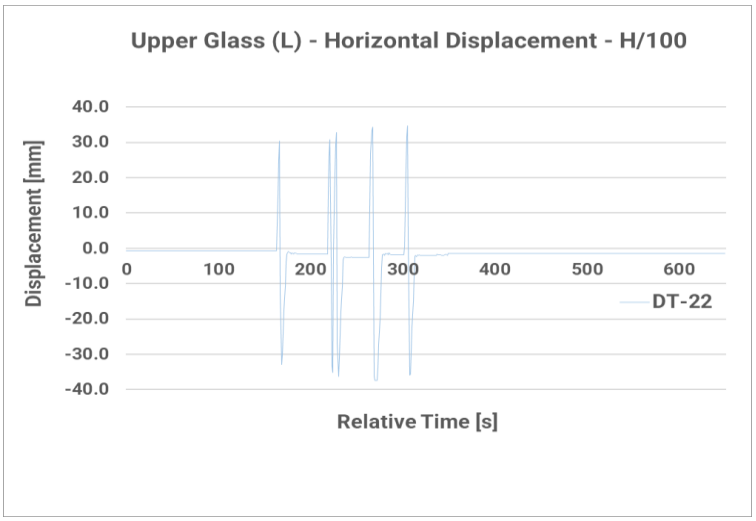

Figure A.7: The horizontal displacement of the upper glass corner (Point L) as monitored for H/300, H/200 and H/100 displacement ratios.

Annex B

Improvement of Initial Numerical Model

During the calibration of the finite element model based on the measurements of the experimental campaign, various sensitivity analyses were realised aiming to demonstrate what properties of the model affect its behaviour the most. The final goal was to acquire a better understanding of the numerical model behaviour which would facilitate the optimum calibration of the numerical model. In total thirty scenarios divided in four main categories were tested. These are presented below.

Categories of Scenarios Tested

As already mentioned, four main sensitivity analyses ran during this stage of modelling as depicted in Table B.1. Through this procedure the following goals were attempted:

- Re-introduction of the non-linear behaviour of various properties, such as of the upper bracket and starter sill
- Closer correspondence of the numerical displacements to the experimental ones
- Integration of both the negative and positive façade response in one model

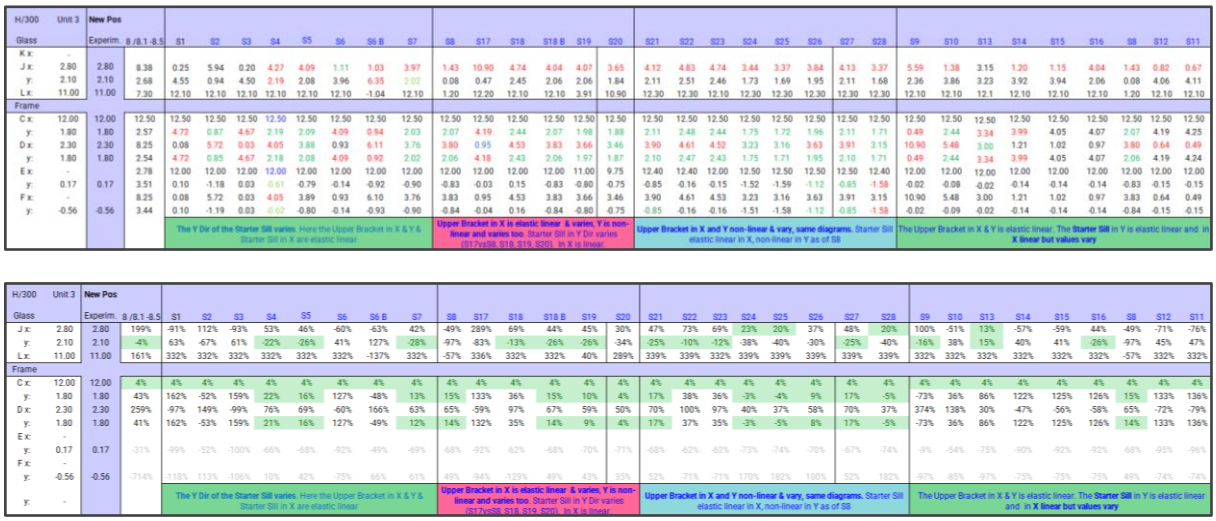

Table B.1: An overview of the scenarios tested. The different colours indicate the four main categories of the sensitivity analyses run during this stage.

Table B.1 provides a short overview of the scenarios investigated during this set of sensitivity analyses. The different scenarios are categorised in four sub-categories that are schematically presented in Figure B.2. Moreover, a brief description on each of the four main categories tested accompanied by the description of the properties varied over follows.

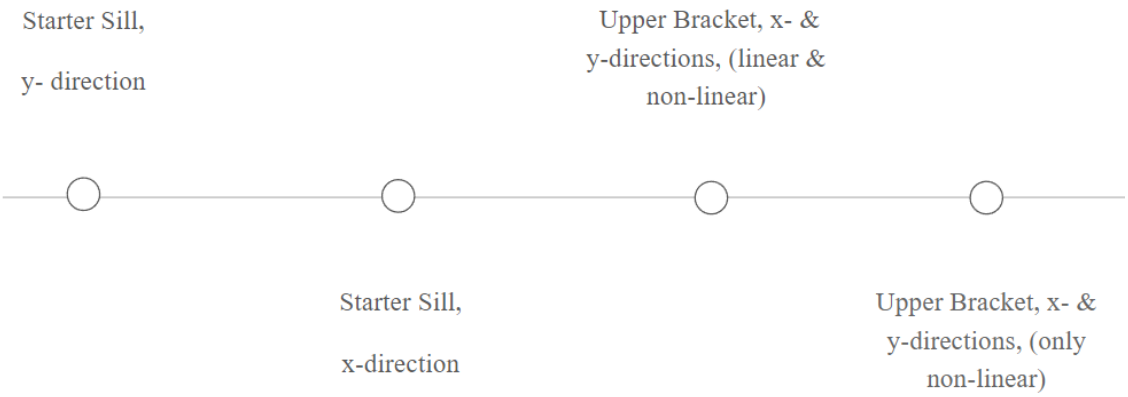

Figure B.2: The schematic view above presents four categories of material properties varied over the respective sensitivity analyses. These analysis series aimed to demonstrate what are the parameters affecting the numerical model behaviour the most.

1st Category - Starter Sill, y- direction

In this series of scenarios the parameter that was varying was the linear properties attributed to the starter sill, in particular to its movement to the Y direction. Other parameters, namely the properties of the X direction of the starter sill and of both the X and Y directions of the upper bracket remained constant. Below a closer look to the variation of the displacement values during the consequent scenarios is presented for each point.

After the completion of the seven scenarios the following conclusions were drawn.

H/300	Unit 3	**New Pos**									
Glass		Experim.	8 /8.1 -8.5	S1	S2	S3	S4	S5	S6	S6 B	S7
K x:	-										
J x:	2.80	2.80	8.38	0.25	5.94	0.20	4.27	4.09	1.11	1.03	3.97
y:	2.10	2.10	2.68	4.55	0.94	4.50	2.19	2.08	3.96	6.35	2.02
L x:	11.00	11.00	7.30	12.10	12.10	12.10	12.10	12.10	12.10	-1.04	12.10
Frame											
C x:	12.00	12.00	12.50	12.50	12.50	12.50	12.50	12.50	12.50	12.50	12.50
y:	1.80	1.80	2.57	4.72	0.87	4.67	2.19	2.09	4.09	0.94	2.03
D x:	2.30	2.30	8.25	0.08	5.72	0.03	4.05	3.88	0.93	6.11	3.76
y:	1.80	1.80	2.54	4.72	0.85	4.67	2.18	2.08	4.09	0.92	2.02
E x:	-		2.78	12.00	12.00	12.00	12.00	12.00	12.00	12.00	12.00
y:	0.17	0.17	3.51	0.10	-1.18	0.03	-0.61	-0.79	-0.14	-0.92	-0.90
F x:	-		8.25	0.08	5.72	0.03	4.05	3.89	0.93	6.10	3.76
y:	-0.56	-0.56	3.44	0.10	-1.19	0.03	-0.62	-0.80	-0.14	-0.93	-0.90
				The Y Dir of the Starter Sill varies. Here the Upper Bracket in X & Y & Starter Sill in X are elastic linear							

H/300 Glass	Unit 3	New Pos Experim.	8 /8.1 -8.5	S1	S2	S3	S4	S5	S6	S6 B	S7
J x:	2.80	2.80	199%	-91%	112%	-93%	53%	46%	-60%	-63%	42%
y:	2.10	2.10	-4%	63%	-67%	61%	-22%	-26%	41%	127%	-28%
L x:	11.00	11.00	161%	332%	332%	332%	332%	332%	332%	-137%	332%
Frame											
C x:	12.00	12.00	4%	4%	4%	4%	4%	4%	4%	4%	4%
y:	1.80	1.80	43%	162%	-52%	159%	22%	16%	127%	-48%	13%
D x:	2.30	2.30	259%	-97%	149%	-99%	76%	69%	-60%	166%	63%
y:	1.80	1.80	41%	162%	-53%	159%	21%	16%	127%	-49%	12%
E x:	-										
y:	0.17	0.17	-31%	-99%	-52%	-100%	-66%	-68%	-92%	-49%	-69%
F x:	-										
y:	-0.56	-0.56	-714%	-118%	113%	-106%	10%	42%	-75%	66%	61%
				The Y Dir of the Starter Sill varies. Here the Upper Bracket in X & Y & Starter Sill in X are elastic linear							

Table B.2: In the coloured column the displacement values as monitored during the experimental procedure are presented. To the right, the displacement values for the first 8 Scenarios (S1-S7) are presented. The values coloured in red are the ones deviating the most from the experimental results, whereas the green ones represent the cases closer to the experimental equivalents. In the green-coloured cells at the bottom the basic properties varying over the analyses are presented.

Findings

By alternating solely the negative or the positive part of the force-elongation diagram all of the test points are affected irrespectively of the sign of their movement. The above observation was anticipated since the numerical model is a dynamic one, which means that the entire range of displacements of every point examined are affected by many parameters simultaneously.

It was also concluded that when achieving closer-to-the-experimental Dy, Cy results, the values of the Dx displacement deviate considerably from the equivalent experimental. This contradiction was attempted to be solved by modifying also the properties of the upper bracket, in both X and Y directions. These variations are visible in the 3rd and 4th sensitivity analyses, the pink and blue one, that are presented later. Before them, the second sensitivity analysis is explained right below.

2nd Category - Starter Sill, x-direction

In this series of tests, the parameter varying was the linear properties in X direction of the starter sill. The rest of the parameters, the Y non-linear properties of the Upper Bracket, as well as the X and Y linear properties of the starter sill remained constant.

The aim was to calibrate the Dx movement, more specifically to decrease its value and bring it closer to the experimental one. Below the values originating from the DIANA model while undergoing positive displacement are presented.

H/300 Glass	Unit 3	New Pos Experim.	S8	S9	S10	S13	S14	S15	S16	S8	S12	S11
K x:	-											
J x:	2.80	2.80	1.43	5.59	1.38	3.15	1.20	1.15	4.04	1.43	0.82	0.67
y:	2.10	2.10	0.08	2.36	3.86	3.23	3.92	3.94	2.06	0.08	4.06	4.11
L x:	11.00	11.00	1.20	12.10	12.10	12.1	12.10	12.10	12.10	1.20	12.10	12.10
Frame												
C x:	12.00	12.00	12.50	12.50	12.50	12.50	12.50	12.50	12.50	12.50	12.50	12.50
y:	1.80	1.80	2.07	0.49	2.44	3.34	3.99	4.05	4.07	2.07	4.19	4.25
D x:	2.30	2.30	3.80	10.90	5.48	3.00	1.21	1.02	0.97	3.80	0.64	0.49
y:	1.80	1.80	2.06	0.49	2.44	3.34	3.99	4.05	4.07	2.06	4.19	4.24
E x:	-		12.00	12.00	12.00	12.00	12.00	12.00	12.00	12.00	12.00	12.00
y:	0.17	0.17	-0.83	-0.02	-0.08	-0.02	-0.14	-0.14	-0.14	-0.83	-0.15	-0.15
F x:	-		3.83	10.90	5.48	3.00	1.21	1.02	0.97	3.83	0.64	0.49
y:	-0.56	-0.56	-0.84	-0.02	-0.09	-0.02	-0.14	-0.14	-0.14	-0.84	-0.15	-0.15
				The Upper Bracket in X & Y is elastic linear. The **Starter Sill** in Y is elastic linear and in **X linear but values vary**								

H/300 Glass	Unit 3	New Pos Experim.	S8	S9	S10	S13	S14	S15	S16	S8	S12	S11
J x:	2.80	2.80	-49%	100%	-51%	13%	-57%	-59%	44%	-49%	-71%	-76%
y:	2.10	2.10	-97%	-16%	38%	15%	40%	41%	-26%	-97%	45%	47%
L x:	11.00	11.00	-57%	332%	332%	332%	332%	332%	332%	-57%	332%	332%
Frame												
C x:	12.00	12.00	4%	4%	4%	4%	4%	4%	4%	4%	4%	4%
y:	1.80	1.80	15%	-73%	36%	86%	122%	125%	126%	15%	133%	136%
D x:	2.30	2.30	65%	374%	138%	30%	-47%	-56%	-58%	65%	-72%	-79%
y:	1.80	1.80	14%	-73%	36%	86%	122%	125%	126%	14%	133%	136%
E x:	-											
y:	0.17	0.17	-68%	-9%	-54%	-75%	-90%	-92%	-92%	-68%	-95%	-96%
F x:	-											
y:	-0.56	-0.56	49%	-97%	-85%	-97%	-75%	-75%	-75%	49%	-74%	-74%
				The Upper Bracket in X & Y is elastic linear. The **Starter Sill** in Y is elastic linear and in **X linear but values vary**								

Table B.3: Similar to the previous cases, in the left part of the table the experimental values for units 2 and 3 of the experimental specimens are presented. In the coloured column the ones that are used as a reference are concentrated. In the green-coloured row an overview of the basic parameters of this specific sensitivity analyses, both constant and varying, are presented. Finally, to the right of the table the fluctuation of the values depending on the scenario tested are presented.

Findings

Based on the values presented on the table above, it can be concluded that once again, while for the vertical displacement of points C and D values closer to the experimental ones are achieved, the one representing the horizontal movement of D (Dx) is deviating from the desired reference value.

One possible solution will include an additional scenario achieving an intermediate solution of scenarios S13 and S14. An alternative approach would include the implementation of an additional support (boundary spring) in the upper right part of the frame (point C) controlling the vertical displacement of C and D. It is expected that a further run of sensitivity analysis will be needed aiming for the determination of the stiffness values of this extra boundary condition.

3rd Category - Upper Bracket, x- & y-directions, (linear & non-linear)

For the third sensitivity analysis, the properties of the upper bracket were also incorporated in the variations performed on the basic numerical model. In practice, both the X linear as well as the Y non-linear properties varied through the scenarios tested. On the contrary, the X elastic linear and Y non-linear properties attributed to the starter sill were kept unchangeable. Below the values per each of the scenarios tested are presented.

H/300 Glass	Unit 3	New Pos Experim.	S8	S17	S18	S18 B	S19	S20
K x:	-							
J x:	2.80	2.80	1.43	10.90	4.74	4.04	4.07	3.65
y:	2.10	2.10	0.08	0.47	2.45	2.06	2.06	1.84
L x:	11.00	11.00	1.20	12.20	12.10	12.10	3.91	10.90
Frame								
C x:	12.00	12.00	12.50	12.50	12.50	12.50	12.50	12.50
y:	1.80	1.80	2.07	4.19	2.44	2.07	1.98	1.88
D x:	2.30	2.30	3.80	0.95	4.53	3.83	3.66	3.46
y:	1.80	1.80	2.06	4.18	2.43	2.06	1.97	1.87
E x:	-		12.00	12.00	12.00	12.00	11.00	9.75
y:	0.17	0.17	-0.83	-0.03	0.15	-0.83	-0.80	-0.75
F x:	-		3.83	0.95	4.53	3.83	3.66	3.46
y:	-0.56	-0.56	-0.84	-0.04	0.16	-0.84	-0.80	-0.75
			Upper Bracket in X is elastic linear & varies, Y is non-linear and varies too. Starter Sill in Y Dir varies (S17vsS8, S18, S19, S20). In X is linear.					

H/300 Glass	Unit 3	New Pos Experim.	S8	S17	S18	S18 B	S19	S20
J x:	2.80	2.80	-49%	289%	69%	44%	45%	30%
y:	2.10	2.10	-97%	-83%	-13%	-26%	-26%	-34%
L x:	11.00	11.00	-57%	336%	332%	332%	40%	289%
Frame								
C x:	12.00	12.00	4%	4%	4%	4%	4%	4%
y:	1.80	1.80	15%	133%	36%	15%	10%	4%
D x:	2.30	2.30	65%	-59%	97%	67%	59%	50%
y:	1.80	1.80	14%	132%	35%	14%	9%	4%
E x:	-							
y:	0.17	0.17	-68%	-92%	-62%	-68%	-70%	-71%
F x:	-							
y:	-0.56	-0.56	49%	-94%	-129%	49%	43%	35%
			Upper Bracket in X is elastic linear & varies, Y is non-linear and varies too. Starter Sill in Y Dir varies (S17vsS8, S18, S19, S20). In X is linear.					

Table B.4: The displacement values for each of the scenarios tested are presented. The horizontal movement of point D is the main value attempted to be optimised through the analyses scenarios.

Findings

The increase of the values corresponding to the X direction of the upper bracket diagram indeed results in more accurate results, compared to the experimental values, but simultaneously negatively affects Cy and Dy. In order for more certain conclusions regarding the sensitivity of the model to the properties attributed to the upper bracket and for a better understanding of the impact of the linear vs non-linear upper bracket property for the X direction, the following sensitivity analysis scenario was realised.

4th Category - Upper Bracket, x- & y-directions, (only non-linear)

In this final set of scenarios which comprises the fourth sensitivity analysis of this stage, the parameters tested for their impact on the model were the non-linear properties in both X and Y direction of the upper bracket. Actually, the exact same properties were used for the behaviour of the upper bracket in both directions. The purpose of this analysis category, combined with the 3rd one, is to evaluate the impact of the non-linearity of the upper bracket on the behaviour of the numerical model.

Moreover, the non-linear properties of the Y direction as well as the X elastic linear ones of the starter sill were kept the same.

H/300 Glass	Unit 3	New Pos Experim.	S8	S21	S22	S23	S24	S25	S26	S27	S28
K x:	-										
J x:	2.80	2.80	1.43	4.12	4.83	4.74	3.44	3.37	3.84	4.13	3.37
y:	2.10	2.10	0.08	2.11	2.51	2.46	1.73	1.69	1.95	2.11	1.68
L x:	11.00	11.00	1.20	12.30	12.30	12.10	12.30	12.30	12.30	12.30	12.30
Frame											
C x:	12.00	12.00	12.50	12.50	12.50	12.50	12.50	12.50	12.50	12.50	12.50
y:	1.80	1.80	2.07	2.11	2.48	2.44	1.75	1.72	1.96	2.11	1.71
D x:	2.30	2.30	3.80	3.90	4.61	4.52	3.23	3.16	3.63	3.91	3.15
y:	1.80	1.80	2.06	2.10	2.47	2.43	1.75	1.71	1.95	2.10	1.71
E x:	-		12.00	12.40	12.40	12.00	12.50	12.50	12.50	12.50	12.40
y:	0.17	0.17	-0.83	-0.85	-0.16	-0.15	-1.52	-1.59	-1.12	-0.85	-1.58
F x:	-		3.83	3.90	4.61	4.53	3.23	3.16	3.63	3.91	3.15
y:	-0.56	-0.56	-0.84	-0.85	-0.16	-0.16	-1.51	-1.58	-1.12	-0.85	-1.58
				Upper Bracket in X and Y non-linear & vary, same diagrams. Starter Sill elastic linear in X, non-linear in Y as of S8							

H/300 Glass	Unit 3	New Pos Experim.	S8	S21	S22	S23	S24	S25	S26	S27	S28
J x:	2.80	2.80	-49%	47%	73%	69%	23%	20%	37%	48%	20%
y:	2.10	2.10	-97%	-25%	-10%	-12%	-38%	-40%	-30%	-25%	-40%
L x:	11.00	11.00	-57%	339%	339%	332%	339%	339%	339%	339%	339%
Frame											
C x:	12.00	12.00	4%	4%	4%	4%	4%	4%	4%	4%	4%
y:	1.80	1.80	15%	17%	38%	36%	-3%	-4%	9%	17%	-5%
D x:	2.30	2.30	65%	70%	100%	97%	40%	37%	58%	70%	37%
y:	1.80	1.80	14%	17%	37%	35%	-3%	-5%	8%	17%	-5%
E x:	-										
y:	0.17	0.17	-68%	-68%	-62%	-62%	-73%	-74%	-70%	-67%	-74%
F x:	-										
y:	-0.56	-0.56	49%	52%	-71%	-71%	170%	182%	100%	52%	182%
				Upper Bracket in X and Y non-linear & vary, same diagrams. Starter Sill elastic linear in X, non-linear in Y as of S8							

Table B.5: The displacement values for both the glazing and the frames are presented for each of the scenarios tested (S21-S28) during this final sensitivity analysis.

Findings

An interesting finding originating from this set of scenarios consists of the observation originating from the two final scenarios, S27 and S28. In practice, these two scenarios occurred from the combination of the scenarios resulting in the displacements closer to the experimental ones (S22 and S25) for this analysis

category. While S22, accompanied by S23 as well, results in the Ey and Fy movements closer to the experimental, S25 leads to more accurate numerical values for Cx, Cy and Dy.

So in the first case, S27, the negative part of the upper bracket diagram of S22 was combined with the positive part of the respective diagram implemented in S25. In a similar fashion, S28 consisted of upper bracket diagrams composed of the negative part of the diagram under examination of S22 and of the positive of the S25 scenario.

As observed from the displacement results, the results of S27 scenario are the same as of S22 and those of S28 to the ones of S25. This observation leads to the conclusion that the positive part of the diagram is practically not affecting the model behaviour. An interesting point of further investigation would be the testing of these two scenarios for the negative displacement. This comparison would allow for a more concrete conclusion regarding the part of the diagram of the upper bracket affecting the model behaviour in relation to the direction of the displacement applied to the façade specimen.

Conclusion

As already mentioned in all of the categories analyses described above, the behaviour of the model is characterised as dynamic. By altering over the properties of either starter sill or upper bracket, even when one direction is affected and irrespectively of the elastic linear or non-elastic character, it is impossible to improve the displacement values of a certain point without compromising the results of other points.

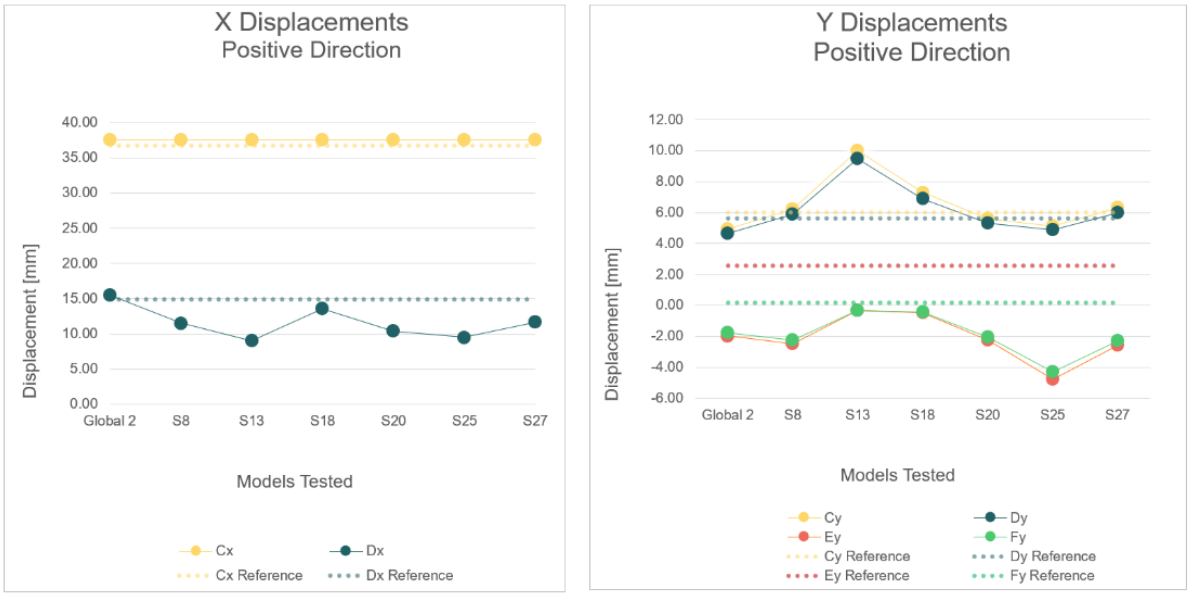

Figure B.3: The charts above represent the fluctuation of the displacement values of each of the representative frame points analysed. Initially the experimental values are plotted and, thereafter, the respective values as obtained per scenario. The scenarios presented above are the ones considered as more accurate since their numerical results are closer to the experimental ones.

In order for the more conservative evaluation of the model to be assessed, the most representative scenarios as resulted from the sensitivity analyses above and depicted in Figure B.3 and Table B.6 were analysed for

the displacement with the largest intensity (H/100). In this case, the deviations of the numerical model values and those monitored during the experiment were expected to be increased compared to the case of the H/300 displacement.

A possible improvement of the model that would bring the Ey and Fy movements if not closer to the experimental ones, at least around 0.0 could be related to the implementation of an additional support in the vertical direction in the upper right point of the frame, point C. Additionally, although the testing of the scenarios above for the other direction of displacement, the negative one, is not presented above in detail, this was investigated for some of the representative scenarios. It was observed that the displacement values originating from these additional runs were not different from those of the positive displacement. Actually, their absolute values were identical whereas the signs were opposite.

H/100			Displacement Sign: Positive					
	Unit 3	Experim.	S8	S13	S18	S20	S25	S27
J x:	15.74	15.74	12.10	9.45	14.20	10.90	10.10	12.40
y:	6.42	6.42	6.18	9.69	7.35	5.51	5.05	6.32
L x:	35.10	35.10	36.20	36.30	36.20	32.70	37.00	36.90
Frame								
C x:	36.80	36.80	37.50	37.50	37.50	37.50	37.50	37.50
y:	6.03	6.03	6.21	10.00	7.30	5.61	5.14	6.33
D x:	14.90	14.90	11.50	9.02	13.60	10.40	9.48	11.70
y:	5.76	5.76	6.18	10.00	7.27	5.58	5.12	6.30
E x:	-		36.00	36.00	36.00	29.30	37.50	37.50
y:	2.55	2.55	-2.50	-0.35	-0.47	-2.25	-4.77	-2.56
F x:	-		11.50	9.02	13.60	10.40	9.48	11.70
y:	0.20	0.20	-2.51	-0.35	-0.49	-2.26	-4.75	-2.56

H/100			Displacement Sign: Positive					
	Unit 3	Experim.	S8	S13	S18	S20	S25	S27
Glass								
J x:	15.74	15.74	-23%	-40%	-10%	-31%	-36%	-21%
y:	6.42	6.42	-4%	51%	14%	-14%	-21%	-2%
L x:	35.10	35.10	3%	3%	3%	-7%	5%	5%
C x:	36.80	36.80	2%	2%	2%	2%	2%	2%
y:	6.03	6.03	3%	66%	21%	-7%	-15%	5%
D x:	14.90	14.90	-23%	-39%	-9%	-30%	-36%	-21%
y:	5.76	5.76	7%	74%	26%	-3%	-11%	9%
E x:	-							
y:	2.55	2.55	-198%	-114%	-118%	-188%	-287%	-200%
F x:	-							
y:	0.20	0.20	-1387%	-278%	-352%	-1259%	-2536%	-1413%

Table B.6: The collection of the numerical values of the most representative scenarios selected out of the complete set of scenarios run during the sensitivity analyses of this chapter is presented in this table. The respective values measured during the experimental campaign are displayed in yellow.

It is important to mention that the sensitivity analyses presented above as well as their subsequent results were evaluated only for the case of the positive displacement application on the façade specimens. Although the behaviour of the specimens is not exactly the same for the two displacement directions, it was considered that not both the cases were needed for the evaluation of the numerical behaviour.

The previous argument was reinforced by the observation that, up to this point of modelling at least, the displacements of the finite element model occurring due to the negative displacement application are a mirrored version of the ones of the positive. To rephrase the latter, the displacements of the points examined in negative and positive directions are identical in absolute values and their only difference is the sign. The values with a positive sign in one case, appear a negative sign in the other case.

Annex C

Alignment Screw Implementation

In the present section a brief explanation of the steps followed during the modelling of the alignment screw accompanied by the respective behaviour of the model is presented. As also mentioned in the main body of the study, the implementation of this additional façade element which was not included in the initial version of the finite element modelling, the alignment screw attempts to recreate the different behaviour of the DIANA model in the two directions (positive and negative) as noticed during the experimental phase.

In more detail, the alignment implementation is expected on one hand to introduce to the numerical model the asymmetrical behaviour in the two displacement directions and, on the other hand, to introduce the different behaviour of the vertical displacement of Ey and Fy, different with respect to each other, as noticed in the experimental values of the tables above. The previous is practically translated in larger movement of points E and F in Y direction for the case of the negative displacement and smaller for the positive. Especially for the positive displacement, as seen from Table B.6 of Annex B, the upper right point (E) of the frame moves upwards, 2.5 mm for the case of the largest intensity applied (H/100), whereas the lowest right point barely moves upwards at a value of 0.20 mm.

In practice, the model behaviour is expected to be affected, mainly due to the position of the alignment screw, which is closer to the right mullion of the frame, roughly at a distance of L/3 where L is the length of the transom (Figure C.1). Its implementation is expected to allow the frame to behave differently while subjected to a positive displacement compared to its response to the application of a negative displacement.

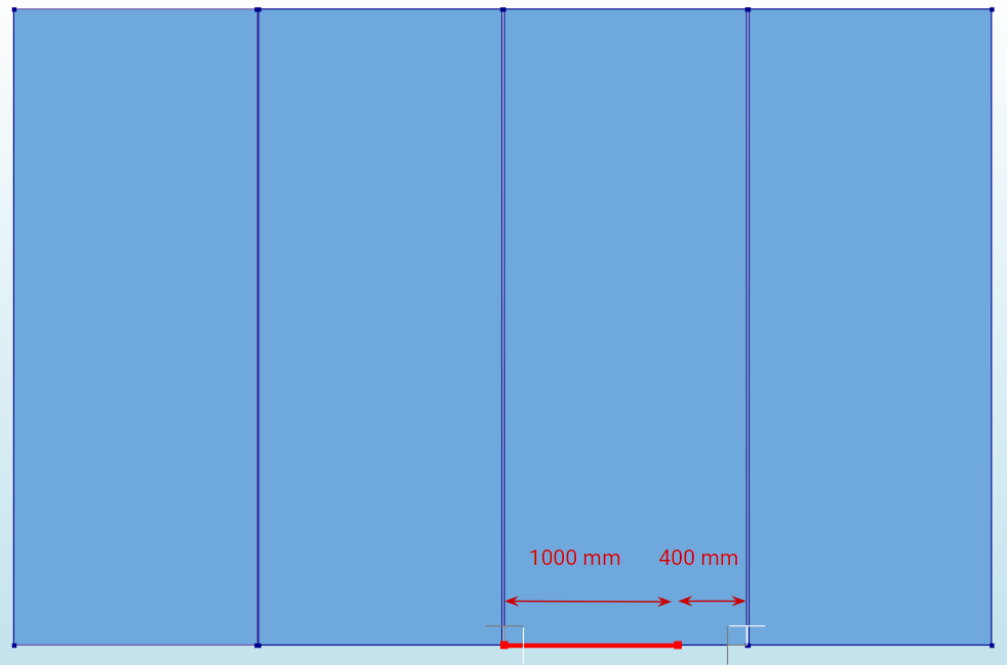

Figure C.1: In the above picture the four façade elements of the DIANA numerical model are presented. The marked element represents the "bottom transom left" element which is supplementary to the corresponding right one. The two of them comprise the bottom transom of each of the façade elements. In like manner, the starter sill of each unit consists of a left and right part. It is clearly seen that the point representing the alignment screw is placed closer to the right mullion of the façade in a 400.0 mm distance. Some of the "unite" connections, in particular the ones connecting the bottom transom with the adjacent mullions, are also visible in the figure above. The connections are represented as black and white lines forming a corner configuration.

Initial Modelling

Consequently, the four façade elements examined, along with their connections, interfaces and properties had to be redesigned. At first, the alignment screw had to be placed in the model at the appropriate location through the introduction of a point element. After that, the bottom transom of each of the façade elements had to be divided into two sub elements, the “bottom transom left” and the “bottom transom right”.

Similarly to the bottom transoms, all the starter sills had to be redrawn; this time each of the elements was defined by two elements, the left and the right one. In order for the two sub-elements of both the bottom transom and the starter sill to operate uniformly, their movements in their adjacent location had to be coupled. This was achieved through the connection of the (right) end-point of the left element with the (left) start-point of the right element through a “Unite” element. This “unite” connection rigidly connects the connected parts in the DIANA environment, ensuring their uniform behaviour. It is also presented in Figure C.2. This type of connection was also used already from the previous stages of modelling for the connection of the transoms with the adjacent mullions aiming to provide a joined movement of the corner area. In the absence of the “unite” connection all the elements comprising the façade perimeter would move independently, therefore the collaboration of the adjacent elements which occurs in the corners of the façade unit would have been missing.

After the redrawing of the bottom transoms and starter sill, the interfaces were introduced to the model. Similarly to the previous DIANA models, an interface connecting the bottom transom with the glazing was introduced. In this case, where the bottom transom consisted of a left and right part, two identical interfaces were introduced connecting the adjacent edges. Two identical interfaces were then modelled connecting the bottom transom elements with the ones of the starter sill. The interfaces used had the similar properties as the ones applied for the connection of the adjacent mullions.

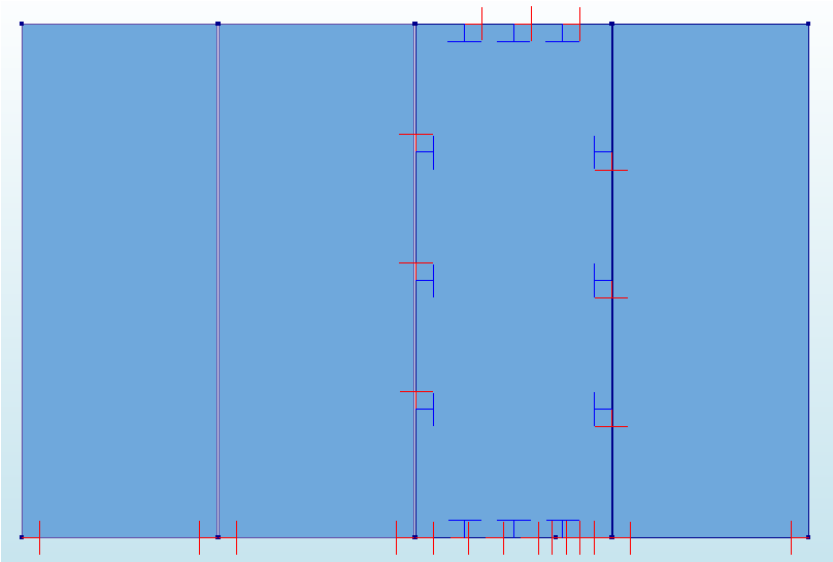

Figure C.2: In the figure above some of the connections introduced in the numerical model are presented. In the bottom transoms of the four façade elements the boundary springs connecting the starter sill with the ground are seen. The interfaces connecting the glazing with the frame are previewed only for the third façade segment.

Then, the connection of the bottom transom with the starter sill followed via the introduction of a rigid link in the location of the alignment screw. Initially, the T1 and T2 movements were restrained, whereas the R3 rotation was set free. Finally, the boundary springs were applied to the new starter sill elements, providing the connection of the frame to the ground.

After the setting of the numerical model, the scenarios selected from the preceded sensitivity analyses as the most representative ones recreating as close as possible the experimental behaviour, were analysed again. The aim was to observe the possible differences of the model displacements and to understand whether the above approach aiming to recreate the alignment screw behaviour was successful. The cases of the largest displacement were selected, aiming to determine the largest deviation of the numerical results from the experimental measurements. As previously explained, in the case of H/100 displacement application due to the introduction of the maximum prescribed deformation, displacements of larger values are noticed in the façade units. In that way, the difference of the numerical model from the experimental ones reaches the largest value. From that respect, checking the model through the H/100 displacements is the most conservative approach compared to the lower intensities of H/200 and H/100.

Façade Response

After the introduction of the alignment screw, the most representative scenarios concluded from the sensitivity analyses of the previous step were updated with the alignment screw implementation and were rerun. The measurements of the reference points examined (A - L) through the current study were collected and are presented in the following table.

H/100 Towards the Right Frame			
Displacement Sign		Positive	
Glass	Exper.	S25	S27
I x:	15.74	10.20	12.30
y:	6.42	5.12	6.35
K x:	35.10	36.90	36.90
Frame			
C x:	36.80	37.50	37.50
y:	6.03	5.22	6.36
D x:	14.90	9.49	11.60
y:	5.76	5.19	6.33
E x:	-	37.50	37.50
y:	2.55	-4.67	-2.56
F x:	-	0.15	11.60
y:	0.20	-4.67	-2.59

H/100 Towards the Right Frame			
Displacement Sign		Positive	
Glass	Exper.	S25	S27
I x:	15.74	-35%	-22%
y:	6.42	-20%	-1%
K x:	35.10	5%	5%
Frame			
C x:	36.80	2%	2%
y:	6.03	-13%	5%
D x:	14.90	-36%	-22%
y:	5.76	-10%	10%
E x:	-		
y:	2.55	-283%	-200%
F x:	-		
y:	0.20	-2495%	-1428%

Table C.1: Above the displacement values for two of the representative scenarios (S25 and S27) are presented. Since not a considerable difference is noticed between these cases and the ones where the alignment screw was not implemented, not all of the representative scenarios were re-calculated.

As it can be clearly seen from the results above, the displacement of the points tested was slightly affected but not up to the extent initially expected. Although some variations are visible, the introduction of the

alignment screw does not affect the results considerably compared to the cases where the alignment screw was missing from the façade configuration.

H/100				
Displacement Sign	Positive		Negative	
Glass	Exper.	Num.	Exper.	Num.
I x:	15.74	10.10	-6.63	-10.10
y:	6.42	5.05	0.62	-5.07
K x:	35.10	37.00	-30.70	-36.90
Frame				
C x:	36.80	37.50	-34.16	-37.50
y:	6.03	5.14	2.82	-5.16
D x:	14.90	9.48	-5.26	-9.41
y:	5.76	5.12	0.92	-5.14
E x:	-	37.50	-	-37.50
y:	2.55	-4.77	7.78	4.77
F x:	-	9.48	-	-9.41
y:	0.20	-4.75	7.85	4.75

H/100				
Displacement Sign	Positive		Negative	
Glass	Exper.	Num.	Exper.	Num.
I x:	15.74	-36%	-6.63	52%
y:	6.42	-21%	0.62	-918%
K x:	35.10	5%	-30.70	20%
Frame				
C x:	36.80	2%	-34.16	10%
y:	6.03	-15%	2.82	-283%
D x:	14.90	-36%	-5.26	79%
y:	5.76	-11%	0.92	-657%
E x:	-		-	
y:	2.55	-287%	7.78	-39%
F x:	-		-	
y:	0.20	-2536%	7.85	-39%

Table C.2: In the above tables the experimental and the numerical results of one representative scenario (S25) are presented for the positive and negative displacement application respectively. By comparing the values, it can be concluded that during the negative displacement façade's response is identical to that of the positive displacement with the only exception being the sign.

For the sake of completeness, the façade behaviour while undergoing negative displacement was also tested. The negative displacement was tested only on scenario S25, since from this very first one it was noticed that the façade behaviour matched completely that of the positive displacement. Therefore, the desired asymmetry of the façade reaction with respect to the vertical movement of points E and F which was attempted through the implementation of the alignment screw is not observed.

Variations Tested

In an attempt to understand the extent to which the numerical model is sensitive to the alignment screw, some alternative cases were tested. In these additional scenarios, initially the alignment screw was relocated and later on the restraint conditions alternated. In more details, the first alternative case tested included the transfer of the alignment screw from its initial location to the middle of the bottom transom. This relocation, compared to the first scenario where the screw was placed, should result in the increase of the movements of points E and F in the Y direction under the negative displacement and their reduction for the case of the positive displacement. The rest of the options tested included variations over the restraints applied to the alignment screw, affecting the collaboration of the bottom transom with the starter sill located right below it.

After the evaluation of the displacement values extracted from the numerical model it became obvious that none of the cases above affected the façade behaviour, not even the case where all the degrees of freedom were restrained. This leads to the conclusion that the façade behaviour is not at all sensitive to the alignment screw, at least for the case implemented as explained above.

H/100 Middle Location		
Displacement Sign		Positive
Glass	Exper.	S27
I x:	15.74	8.87
y:	6.42	7.83
K x:	35.10	36.90
Frame		
C x:	36.80	37.50
y:	6.03	8.23
D x:	14.90	8.48
y:	5.76	8.23
E x:	-	37.50
y:	2.55	-2.51
F x:	-	8.48
y:	0.20	-2.51

H/100 Middle Location		
Displacement Sign		Positive
Glass	Exper.	S27
I x:	15.74	-44%
y:	6.42	22%
K x:	35.10	5%
Frame		
C x:	36.80	2%
y:	6.03	36%
D x:	14.90	-43%
y:	5.76	43%
E x:	-	
y:	2.55	-198%
F x:	-	
y:	0.20	-1387%

Table C.3: Above the displacement results of the examined points for the case of the alignment screw relocation. For the sake of simplicity, only one of the representative scenarios is included since it was observed that, for this specific numerical model, the relocation of the alignment screw from the initial point to the middle of the mullion does not affect the façade behaviour.

Variations of the Alignment Screw Tested	
Alignment Screw Location	Restraints
400.0 mm from the right mullion	T1 & T2 restrained, R3 free
L/2, where L: the mullion length	T1 restrained, T2 & R3 free
	T2 restrained, T1 & R3 free
	T2 & T2 & R3 restrained
	T1 & T2 & R3 free

Table C.4: An overview of the alternative cases tested while attempting to define the impact of the alignment screw implementation in the numerical model.

A possible explanation for the non-sensitivity of the model to the alignment screw application can lie on the fact that during the initial setting of the model, both the starter sill and the bottom transom were placed without any distance between them, therefore, they were placed in the exact same location. However, the actual thickness of the structural silicone connecting the bottom transom with the starter sill was attributed as thickness to the geometry properties of the respective interface.

Moreover, it is important to mention that the interfaces as well as the connections and boundary conditions were assigned in each case to the appropriate element, either the starter sill or the bottom transom. The implementation of the “unites” for example connecting the bottom transom with the adjacent mullions recreating the corner collaboration of the neighbouring elements, as well as the rest of boundary conditions, ensure that the bottom transom and the starter sill behave differently. Therefore, the argument that the two elements respond identically is not substantiated.

Alternative Modelling

The implementation of the alignment screw in the finite element model had to be repeated since after the evaluation of the first results, inconsistencies on the numerical values were noticed. An approach similar to the one previously explained was followed. However, after consulting researchers with more experience in the sector of finite element modelling regarding this topic, it was concluded that the replacement of the rigid connection recreating the alignment screw behaviour with tyings could lead to different results of the façade, recreating closer the experimental behaviour.

For this reason, the following calibration of the DIANA model initially focused on the re-modelling of the alignment screw through an alternative connection type, tyings, instead of the rigid connections originally used. After noticing the limited sensitivity of the DIANA model to the alignment screw application, the stiffness of the related bottom transom-to-starter sill connection was reduced. Through a new series of modifications of the numerical model, the correlation between the stiffness of the aforementioned connection with the alignment screw application and its restraints was investigated. As a supplement to this sensitivity analysis, additional tests aiming to identify the impact of stiffness properties of the shear vs normal direction were performed.

Modifications Applied

As already mentioned, the alignment screw implementation was originally realised through the introduction of rigid connections to the DIANA model. Since the sensitivity of the numerical model to the alignment screw was found to be extremely limited, an alternative modelling approach through tyings was investigated. Before diving into the details of that, though, a general overview of the first results originating from the implementation of the alignment screw in the DIANA model as a rigid connection will be presented.

Following the remodelling of the alignment screw, again some variations regarding the restrains of the connection representing the actual alignment screw element were tested. For an overview of the degrees of freedom of the alignment screw that can either be set free or restrained, see Figure C.3.

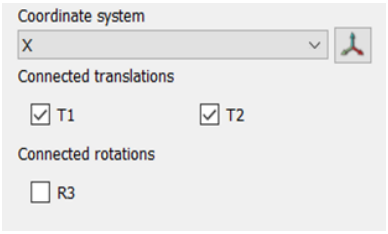

Figure C.3: The translations and rotations of the alignment screw that can be either restrained or set free are presented as seen in the DIANA environment. Above, T1 as well as T2 were selected, but for the sake of completeness, the complete series of restrain combinations was tested.

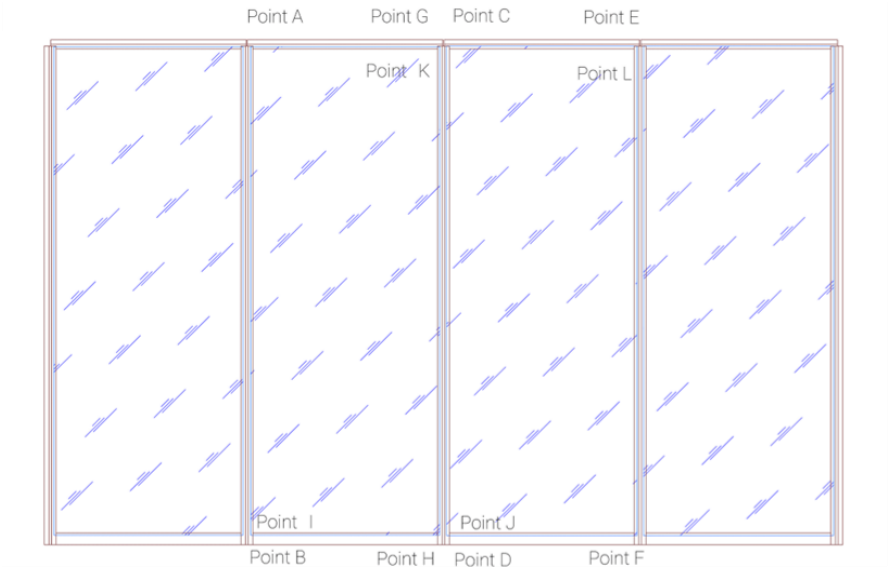

Figure C.4: The naming convention followed in the study is presented. Above, the points of the frames for which the displacements were measured during the experiment are located outside the façade units. The reference points for which the glazing movement is measured are the ones placed on the inside of the frame and are also included on the following table.

The results of the cases tested are presented in Table C.5. The way or representation is similar to the one followed previously. In the coloured column the experimental results as measured for the respective displacement amplitude and direction during the experimental campaign are presented. In the following columns, the numerical values of the different versions on the DIANA model are presented. The reference scenario used for this circle of analyses was scenario 8 (S8), therefore the results of this scenario are also presented on this table, aiming to clarify the sensitivity of the model to the alignment screw implementation and to the specific property changed in each scenario tested.

			i	ii	iii	iv
Glass	Unit 3	Experiment Values	S8	rigid T1 restrained	rigid T2 restrained	Tying T1/T2/T1T2 restrained
J x:	15.74	15.74	12.10	12.00	12.10	11.90
y:	6.42	6.42	6.18	6.21	6.19	6.30
L x:	35.10	35.10	36.20	36.20	36.20	36.20
Frame						
C x:	36.80	36.80	37.50	37.50	37.50	37.50
y:	6.03	6.03	6.21	6.23	6.22	6.33
D x:	14.90	14.90	11.50	11.40	11.50	11.30
y:	5.76	5.76	6.18	6.20	6.19	6.29
E x:	-		36.00	36.00	36.00	36.00
y:	2.55	2.55	-2.50	-2.52	-2.50	-2.49
F x:	-		11.50	11.30	11.50	11.30
y:	0.20	0.20	-2.51	-2.52	-2.51	-2.51

			i	ii	iii	iv
Glass	Unit 3	Experiment Values	S8	rigid T1 restrained	rigid T2 restrained	Tying T1/T2/T1T2 restrained
J x:	15.74	15.74	-23%	-24%	-23%	-24%
y:	6.42	6.42	-4%	-3%	-4%	-2%
L x:	35.10	35.10	3%	3%	3%	3%
Frame						
C x:	36.80	36.80	2%	2%	2%	2%
y:	6.03	6.03	3%	3%	3%	5%
D x:	14.90	14.90	-23%	-23%	-23%	-24%
y:	5.76	5.76	7%	8%	7%	9%
E x:	-					
y:	2.55	2.55	-198%	-199%	-198%	-198%
F x:	-					
y:	0.20	0.20	-1387%	-1392%	-1387%	-1387%

Table C.5: The numerical results of the different versions of the DIANA model attempted for the implementation of the alignment screw are seen above. In the coloured row the property modification applied on each scenario is explained. Apart from the reference scenario, S8, two scenarios with translation T1 and T2 restrained

respectively are presented in columns ii and iii. In column iv the numerical results of the DIANA model incorporating tyings instead of rigid connections for the representation of the alignment screw are presented.

It can be noticed that for the first two scenarios tested no impact of the different restraints implemented on the alignment screw is noticed on the numerical results of the façade model. In the case of the two first scenarios, the function of the actual alignment screw was represented in the DIANA model through a rigid connection. Although T1, T2, T1 & T2 were successively restrained and the numerical values of all the values were extracted respectively, no difference between the element's behaviour was noticed as seen while comparing columns ii and iii of Table C.5. This behaviour initiated the idea of modelling the alignment screw through tyings instead of rigid connections. This alternative modelling approach was attempted aiming for the increase of the model sensitivity to the alignment screw application.

Prior to the results related to the alignment screw representation as a tying connection instead of a rigid one, an introductory explanation to the tying connection is presented.

Tying Connections in DIANA

Tyings are a typical option provided in some finite element software, including DIANA, to provide nodal variables with linear dependency. The most common example of tying applications is sliding connections, hinges, symmetry, eccentric connection, maintaining planes or edges straight, connection for incompatibility cases, connection with eccentricity and mesh refinement (DIANA FEA, 2017). Through those linear dependencies that are defined by the software user the degrees of freedom for the equation system, namely rotations, displacements, temperatures etc., are specified. Similarly to the case of the rigid support, the degrees of freedom are defined as either rotation or translation and a number that specifies the direction (DIANA FEA, n.d.)

In general for the determination of a tying, a master node as well as a slave node, or a set of slave nodes, need to be defined. DIANA defines a few types of tyings which are equalities, interconnections and eccentricities. For the recreation of the alignment screw in the finite element modelling, the last case has been selected. Eccentricities are typically recommended for connections that although in the actual model comprise eccentricities, the respective nodes coincide in the numerical model. Since this is the exact same case for the connection between the bottom transom and the starter sill, this type of connection was selected for the recreation of the alignment screw.

Consequently, the implementation of the tying was realised using the left node of the right bottom transom as a master node and the group of the right node of the left bottom transom and the two adjacent nodes of left and right starter sill as slave points. Additionally the unites previously used for the connection of the left and right parts of both the starter sill and the bottom transom were deleted since the adjacent elements were already coupled through the implementation of the tying with the. Following the alignment screw implementation, scenarios similar to the ones used for the case of rigid connections, where T1, T2, T1 & T2 were restrained followed. The numerical results of all those models are presented in one column of Table C.5, column iv since no differentiation between the respective displacement values is noticed.

Shear vs Normal Direction of Transom-to-Starter Sill Connection

After reducing the stiffness of the frame to starter sill connection, not only the displacement values of the test points were altered, an outcome that was obviously expected, but the impact of the alignment screw on the façade behaviour was increased as well. At this stage of the analysis, an additional property parameter was evaluated, namely the impact of normal vs the shear direction of the interface connecting the bottom transom element with the starter sill. For that reason, and while the alignment screw was represented as tying, initially the shear elastic stiffness of the aforementioned connection was reduced at a range of 10.0 whereas the normal elastic stiffness remained the same.

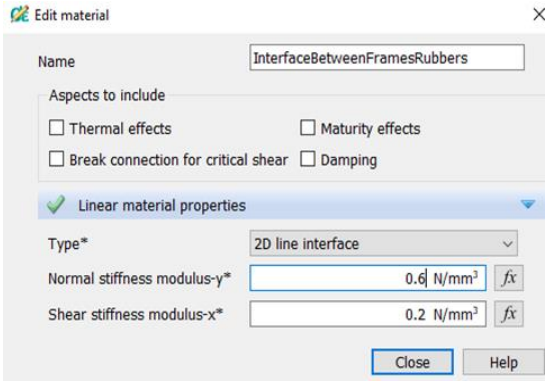

Figure C.5: The environment where the linear material properties of the interface connecting bottom transom with the starter sill are defined. In the image presented above, the original scenario is presented, where the Normal stiffness modulus – y is defined as 0.6 N/mm³ whereas the Shear stiffness modulus-x equals 0.2 N/mm³.

			i	ii	iii	iv	v	vi	vii	viii
Glass	Unit 3	Experiment Values	S8	rigid T1 restrained	rigid T2 restrained	**Tying** T1/T2/T1T2 restrained	Tying T1T2 interface StarterSill Transom less stiff only shear (elastic)	Tying T1 T2 interface StarterSill Transom less stiff both shear & normal (elastic)	Tying T1 only normal less stiff	Tying T2 only normal less stiff
J x:	15.74	15.74	12.10	12.00	12.10	11.90	12.00	7.66	6.87	7.73
y:	6.42	6.42	6.18	6.21	6.19	6.30	6.25	8.54	9.00	8.51
L x:	35.10	35.10	36.20	36.20	36.20	36.20	36.20	36.20	36.20	36.20
Frame										
C x:	36.80	36.80	37.50	37.50	37.50	37.50	37.50	37.50	37.50	37.50
y:	6.03	6.03	6.21	6.23	6.22	6.33	6.27	8.74	9.23	8.72
D x:	14.90	14.90	11.50	11.40	11.50	11.30	11.40	7.06	6.31	7.12
y:	5.76	5.76	6.18	6.20	6.19	6.29	6.23	8.72	9.21	8.70
E x:	-		36.00	36.00	36.00	36.00	36.00	36.00	36.00	36.00
y:	2.55	2.55	-2.50	-2.52	-2.50	-2.49	-2.49	-1.98	-1.84	-1.98
F x:	-		11.50	11.30	11.50	11.30	11.40	7.06	6.31	7.17
y:	0.20	0.20	-2.51	-2.52	-2.51	-2.51	-2.50	-1.99	-1.85	-1.99

			i	ii	iii	iv	v	vi	vii	viii
Glass	Unit 3	Experiment Values	S8	rigid T1 restrained	rigid T2 restrained	**Tying** T1/T2/T1T2 restrained	Tying T1T2 interface StarterSill Transom less stiff only shear (elastic)	Tying T1 T2 interface StarterSill Transom less stiff both shear & normal (elastic)	Tying T1 only normal less stiff	Tying T2 only normal less stiff
J x:	15.74	15.74	-23%	-24%	-23%	-24%	-24%	-51%	-56%	-51%
y:	6.42	6.42	-4%	-3%	-4%	-2%	-3%	33%	40%	33%
L x:	35.10	35.10	3%	3%	3%	3%	3%	3%	3%	3%
Frame										
C x:	36.80	36.80	2%	2%	2%	2%	2%	2%	2%	2%
y:	6.03	6.03	3%	3%	3%	5%	4%	45%	53%	45%
D x:	14.90	14.90	-23%	-23%	-23%	-24%	-23%	-53%	-58%	-52%
y:	5.76	5.76	7%	8%	7%	9%	8%	51%	60%	51%
E x:	-									
y:	2.55	2.55	-198%	-199%	-198%	-198%	-198%	-178%	-172%	-178%
F x:	-									
y:	0.20	0.20	-1387%	-1392%	-1387%	-1387%	-1382%	-1121%	-1049%	-1121%

Table C.6: In these similar to the previous tables, the numerical results obtained from the sensitivity analysis aiming to evaluate the impact of the normal and the shear direction of the transom to starter sill connection are presented in columns v-viii. The test cases belonging to the same category are obtained inside the framed columns.

The extracted results, as seen in column v of Table C.6 did not present considerable deviation from those of column iv. On the contrary, when also modifying the values regarding the normal direction (column vi), it was observed that the displacements of the numerical values were considerably affected.

Additionally, for this level of reduced stiffness the impact of restraining the different degrees of freedom was evaluated. For this reason, two additional scenarios where initially T1 and then T2 translation were restrained. While studying the columns vii and viii of Table C.6 it can be noticed that the restraining of different degrees of freedom of the tying affects the model behaviour. Contrary to the sensitivity checks for which the results were almost identical as presented in columns ii, iii and iv, the different degrees of freedom in the cases where the transom to starter sill connection is less stiff affect the test points displacements (columns v and vi).

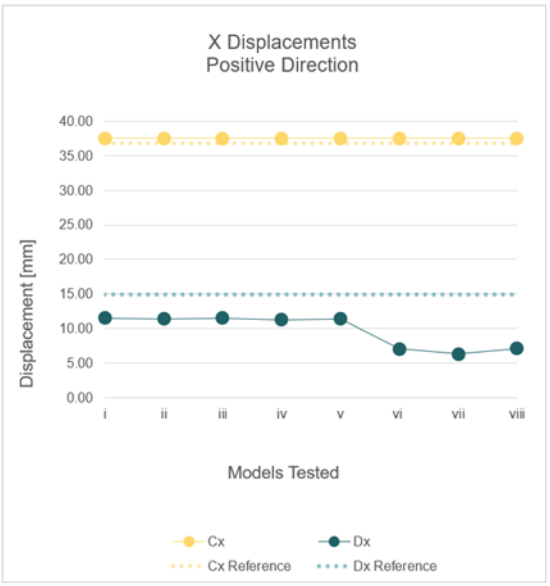

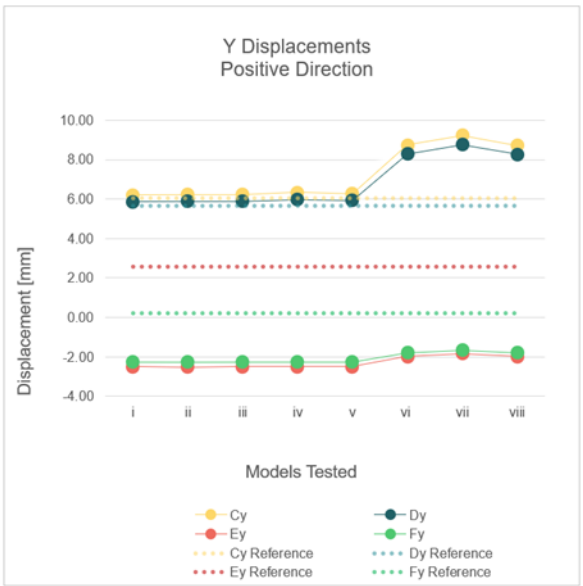

Figure C.6: The graphs above represent the variation of the numerical results for the scenarios previously discussed. As explained also in the legend, the dashed lines represent the reference values which resulted from the experimental campaign.

Conclusions

Based on the results presented on the previous table, it can be concluded that the implementation of the alignment screw in both modelling approaches, as a rigid connection as well as a tying, does not instantly provide the numerical model with the desired behaviour. In fact, the stiffness of the interface connecting the bottom transom with the starter sill appears to be increased up to the degree that does not allow for the different restraints of degrees of freedom to affect the façade model behaviour. The previous argumentation is underlined by the fact that all the five scenarios of Table C.6 presented right after the S8 scenario (columns ii-iv) and previewing the numerical displacement of the DIANA model where initially alignment screw is applied as rigid and afterwards as tying connection, provide almost the same displacement values.

By comparing the results of columns v and vi of Table C.6 with the ones of column iv, the following conclusion based on the impact of the shear vs the normal properties of the bottom transom-starter sill connection can be derived. The linear properties of this particular connection regarding the normal stiffness modulus are critical for the façade behaviour whereas the equivalent of the shear stiffness modulus do not extensively affect the façade behaviour.

Finally, between the two cases of restraining only the tying degree of freedom T1 and T2 for the reduced stiffness of transom-to-starter sill connection (columns vii and viii), slightly different values for the test point displacements were noticed. In practice, for the last case where T2 translation was restrained it was observed that the subsequent numerical results recreate better the actual façade behaviour.

According to the previous findings, it can be concluded that implementation of the alignment screw into the numerical model affects the façade global response more when the connection between the bottom transom and the starter sill is less stiff. However, these reduced stiffness properties of the transom-to-starter sill connection applied in order for the sensitivity of the model to the alignment crew implementation to be increased, do not correspond to the actual values for linear properties of this connection that originated from realistic properties of similar products typically used by the industry.

Alignment Screw Affect, Final Verification

In order for the conclusions drawn above to be verified, after the final calibration of the numerical model that is presented in detail in the following section, Annex D, an additional check of the final version of the DIANA model was made. In more detail, the exact same numerical model was tested for its behaviour both in the negative and positive displacement application initially with and later without the implementation of the alignment screw. The respective results are presented below.

Figure C.7: The displacements both in X and Y direction of the reference points. As it can be clearly seen from the graphs, the façade response in the positive displacement recreated better the experimental behaviour compared to the negative one. A possible area of improvement is the horizontal movement of Point D.

As it can be seen both through Figure C.7 and Table C.7, the numerical values of the finite element model for both the positive and negative displacement application were not affected considerably by the removal of the alignment screw.

Therefore, the initial hypothesis regarding the insensitivity of this type of DIANA modelling to the alignment screw application is verified.

Impact of the Alignment Screw Application							
Experiment Values		Alignment Screw		Alignment Screw		Experiment Values	
		Yes	No	Yes	No		
Positive Displacement				Negative Displacement			
Glass							Glass
J x:	15.74	14.20	14.30	-14.20	-14.40	-6.63	J x:
y:	6.42	7.36	7.29	-0.56	-0.61	0.62	y:
L x:	35.10	36.20	36.20	-36.20	-36.20	-30.70	L x:
Frame							Frame
C x:	36.80	37.50	37.50	-37.50	-37.50	-34.16	C x:
y:	6.03	7.28	7.23	-0.46	-0.47	2.82	y:
D x:	14.90	13.50	13.70	-13.60	-13.70	-5.26	D x:
y:	5.76	7.24	7.20	-0.49	-0.50	0.92	y:
E x:							E x:
y:	2.55	-0.49	-0.49	7.28	7.20	7.78	y:
F x:							F x:
y:	0.20	-0.05	-0.52	7.25	7.13	7.85	y:

Impact of the Alignment Screw Application							
Experiment Values		Alignment Screw		Alignment Screw		Experiment Values	
		Yes	No	Yes	No		
Positive Displacement				Negative Displacement			
Glass							Glass
J x:	15.74	-10%	-9%	114%	117%	-6.63	J x:
y:	6.42	15%	14%	-191%	-199%	0.62	y:
L x:	35.10	3%	3%	18%	18%	-30.70	L x:
Frame							Frame
C x:	36.80	2%	2%	10%	10%	-34.16	C x:
y:	6.03	21%	20%	-116%	-117%	2.82	y:
D x:	14.90	-9%	-8%	158%	160%	-5.26	D x:
y:	5.76	26%	25%	-153%	-154%	0.92	y:
E x:							E x:
y:	2.55	-119%	-119%	-6%	-7%	7.78	y:
F x:							F x:
y:	0.20	-127%	-368%	-8%	-9%	7.85	y:

Table C.7: For the final calibrated scenario the alignment screw was removed and the results are presented in the columns where "No" is indicated referring to the implementation of the Alignment Screw. As it can be seen, the removal of this specific façade element does not affect the façade behaviour neither on the positive nor on the negative direction of the applied displacement.

Annex Bibliography

DIANA FEA. (n.d.). 9.3 Linear Dependencies or Tyings. In *DIANA FEA b.v.* Retrieved May 4, 2022, from https://manuals.dianafea.com/d103/Theory/Theoryse57.html#x73-1440009.3

DIANA FEA. (2017). 8.3 Linear Dependencies or Tyings. In *DIANA FEA*. DIANA FEA BV. Retrieved April 3, 2022, from https://manuals.dianafea.com/d101/Theory/node89.html

Annex D

Numerical Model Calibration

Throughout the calibration of the finite element model based on the measurements of the experimental campaign, various sensitivity analyses were realised aiming to demonstrate what properties of the model affect its behaviour the most. The final goal was to acquire a better understanding of the numerical model behaviour which would facilitate the optimum calibration of the numerical model. In total thirty scenarios were tested divided in four main categories that are going to be presented right below.

During this specific modelling phase, a wide range of the modelling properties were investigated for their impact on the overall behaviour of the finite element model. The ultimate goal of the various sensitivity analyses run during this stage includes not only the thorough understanding of the numerical model and its response, but also its further calibration with respect to the reference experimental value. In more detail, displacement values as presented for the reference points are attempted to recreate more accurately those measured during the experimental campaign during which representative glazed curtain wall units were tested.

Additionally, the implementation of both the negative and positive façade behaviours as observed during the aforementioned experimental procedure and described in the earlier sections of the present study into one numerical model was another primary goal of this modelling phase. Below, a detailed description of the modelling approach followed is presented.

Further Calibration – Boundary Springs Sensitivity Analysis

Initially, an additional calibration of the model was attempted, varying over the two main properties, the stiffness of the boundary springs connecting the upper bracket and the starter sill with the environment. The aim of this calibration was the further approximation of the current finite element model to the realistic façade behaviour through the introduction of the non-linear behaviours of the aforementioned boundary conditions, which in practice recreates the restraining of the downward and the allowing of the upward displacements of the façade unit. It is important to mention that although the properties of the boundary springs were modified in this study for simplification reasons the changing parameters are often referred to as upper bracket and starter sill.

The behaviour of the façade unit intended to be attributed to both the upper and the lower boundary conditions, namely the upper bracket and the starter sill boundary springs, through the implementation of the non-linear properties was clearly identified. Both boundary conditions should allow the upward and restrain the downward movement of the unit. However, the exact interpretation of upward and downward through the introduction of force-elongation properties on the respective material model was not perfectly understood therefore all the possible non-linear combinations of both the starter sill and the upper bracket boundary spring were examined as explained in the following paragraphs.

In short, four additional scenarios were tested where the stiffness of the starter sill initially and of the upper bracket later varied. In Figure D.1 the qualitative modifications of the respective force-elongation diagrams are presented. In more detail, the symmetric diagrams of starter sill and upper bracket presented on the left section of the figure above represent the properties attributed to the scenarios tested previously. For scenario a, the numerical results of which are presented in Table D.1, the force-elongation diagram of the upper bracket remained the symmetric one but the properties of the boundary spring connecting the starter sill to the environment originate from the diagram presented in the upper middle section of Figure D.1 marked as “a”. In a similar manner, for scenario b, the properties of the aforementioned boundary spring were defined

by the graph marked as “b” located on the upper right section of the figure whereas the upper bracket stiffness properties were still defined by the symmetric diagram.

Respectively, for scenarios c and d the properties identifying the stiffness of the upper bracket boundary spring are described by the diagrams marked with the respective letter, located on the lower middle and right part of the figure respectively. Similarly to the previous case, the stiffness properties of the starter sill in both scenarios c and d are described by the symmetric diagram presented on the upper left section of Figure D.1. The numerical model behaviour for each of the scenarios tested is seen below in Table D.1 and Figure D.2.

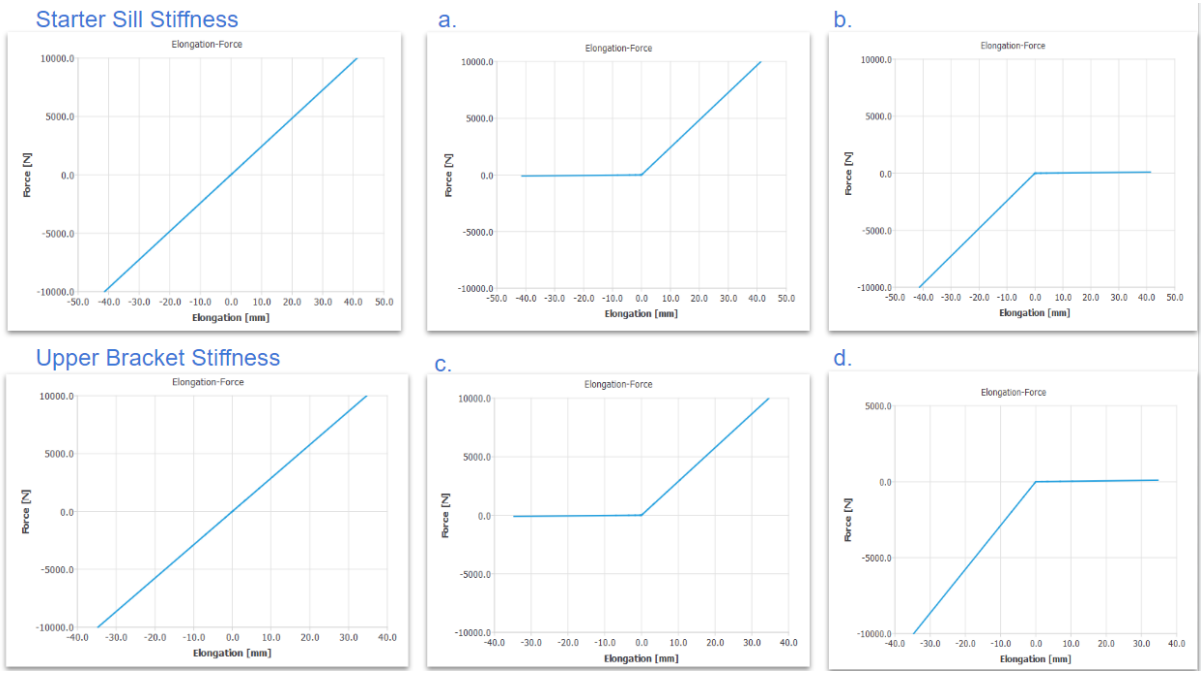

Figure D.1: Qualified presentation of the properties varied over the additional sensitivity analysis performed focused on the stiffness of the Starter Sill and the Upper Bracket boundary springs.

			S8	ii,iii	viii	a	b	c	d
Glass	Unit 3	Experiment Values	S8	Rigid T1, T2 restrained	Tying T2 only normal less stiff	Tying T2 only normal less stiff - a.	Tying T2 only normal less stiff - b.	Tying T2 only normal less stiff - c.	Tying T2 only normal less stiff - d.
J x:	15.74	15.74	12.10	12.00	7.73	7.44	0.82	5.48	7.73
y:	6.42	6.42	6.18	6.21	8.51	8.16	13.20	5.66	8.51
L x:	35.10	35.10	36.20	36.20	36.20	36.20	36.20	36.20	36.20
Frame									
C x:	36.80	36.80	37.50	37.50	37.50	37.50	37.50	37.50	37.50
y:	6.03	6.03	6.21	6.23	8.72	8.38	13.70	5.96	8.72
D x:	14.90	14.90	11.50	11.40	7.12	6.83	0.31	4.89	7.12
y:	5.76	5.76	6.18	6.20	8.70	8.36	13.70	5.95	8.70
E y:	2.55	2.55	-2.50	-2.52	-1.98	-2.45	-0.09	-5.76	-1.98
F y:	0.20	0.20	-2.51	-2.52	-1.99	-2.45	-0.09	-5.75	-1.99

			S8	ii,iii	viii	a	b	c	d
Glass	Unit 3	Experiment Values	S8	Rigid T1, T2 restrained	Tying T2 only normal less stiff	Tying T2 only normal less stiff - a.	Tying T2 only normal less stiff - b.	Tying T2 only normal less stiff - c.	Tying T2 only normal less stiff d.
J x:	15.74	15.74	-23%	-24%	-51%	-53%	-95%	-65%	-51%
y:	6.42	6.42	-4%	-3%	33%	27%	106%	-12%	33%
L x:	35.10	35.10	3%	3%	3%	3%	3%	3%	3%
Frame									
C x:	36.80	36.80	2%	2%	2%	2%	2%	2%	2%
y:	6.03	6.03	3%	3%	45%	39%	127%	-1%	45%
D x:	14.90	14.90	-23%	-23%	-52%	-54%	-98%	-67%	-52%
y:	5.76	5.76	7%	8%	51%	45%	138%	3%	51%
E y:	2.55	2.55	-198%	-199%	-178%	-196%	-103%	-326%	-178%
F y:	0.20	0.20	-1387%	-1392%	-1121%	-1356%	-145%	-3049%	-1121%

Table D.1. The results of the additional sensitivity analysis are presented in the last four columns of the table above. On the coloured row the description of the parameters checked is described. The red or green colouring of certain values indicates the worse or better correspondence of the numerical to the experimental results respectively.

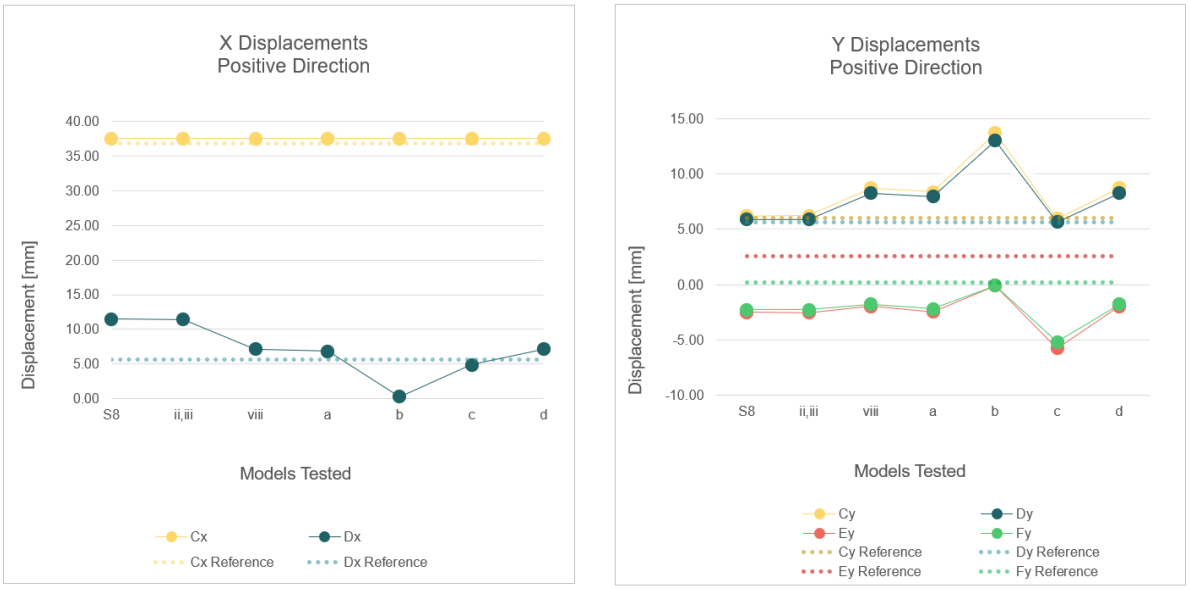

Figure D.2: The graphs above visualise the gradual change of displacements in X and Y direction for the positive displacement application. By studying this figure as well as on Table D.1 an insightful indication regarding the impact of the stiffness non-linearity of the model's boundary conditions is provided More specifically, an indication of the more appropriate scenario recreating better the stiffness property of the upper bracket spring being scenario d can already be made. For a matter of completion though, all the possible scenarios, including the ones containing the force - elongation curve of scenario c, is included in this and the following tables and figures.

As already stated in the previous paragraphs, at this stage of analysis the asymmetric properties of the boundary springs were not combined but were tested separately. Half of the scenarios examined the impact of the modification of symmetric to asymmetric stiffness properties of the starter sill boundary condition whereas the rest of the test cases focused on the equivalent alteration of the stiffness properties of the upper bracket boundary conditions.

This analysis stage operates as an introduction to the better understanding of the proper scripting of the allowable movements of the façade unit through the restraining of the boundary springs. Based on the indications provided during this analysis stage, the need for further model calibration through the simultaneous combination of the asymmetric behaviour of the starter sill and the upper bracket boundary springs became obvious. This specific sensitivity analysis is explained in detail later in this document.

Additionally a final test run in one of the DIANA variations above where the displacement applied on the model was negative was performed. The aim of this test was to verify whether one of the goals of this calibration stage, the incorporation of the positive and negative behaviour of the façade units into one numerical model through the application of the alignment screw, was achieved. The different behaviour of the model based on the sign of the displacement applied on the façade unit is presented in Figure D.3.

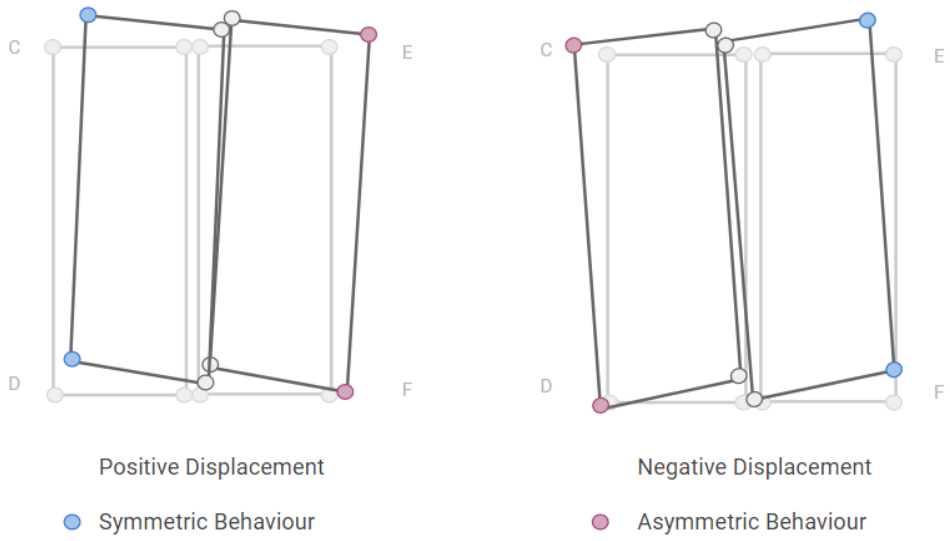

Figure D.3: The reaction of the façade under positive to the left and negative to the right displacement application is presented. The points marked in blue represent the test point displacing symmetrically with respect to each other. On the contrary, the points marked in red are those that display asymmetric behaviour. The term "asymmetric" aims to express the numerical inequality of the points belonging to the same mullion, points C and D for the positive and E and F for the negative displacement.

Reflection

By studying Table D.1, it becomes evident that the introduction of the alignment screw in this specific DIANA model through a "rigid" connection does not affect the model behaviour as initially expected. In practice, it is evidenced that any type of connection between the starter sill and the bottom transom results in further deviation from the experimental values of both the vertical and horizontal displacements of points C and D when compared to the initial scenario S8. Additionally, the vertical displacement of points E and F is not improved as desired by preventing the downward movement. These characteristics of the façade behaviour are present in all the cases tested, irrespectively of alignment screw modelling approach and of the different restraints applied to this façade component.

Additional attempts to modify the vertical displacement of point E, which based on the experiment moves upwards by 2.55 mm whereas in almost all of the cases presented above experiences negative displacement

of equal or even larger values, were made. In practice the stiffness of the upper bracket located on the upper right corner, point E, of each façade element tested was adjusted. As seen from the two last columns of Table D.1, the modification of this property did not affect the model behaviour as desired, leading to the conclusion that other façade parameters are either responsible for this behaviour or overcome this specific property variation, namely the stiffness of the upper bracket in the Y direction.

Proposals

Some of the parameters that are expected to affect the overall behaviour of the façade model and to eliminate the desired displacement on points E and F are presented shortly in the following section of the paper. They are also schematically presented in Figure D.4. Figure D.5 aims to serve as a reminder of the boundary conditions applied until this specific modelling phase.

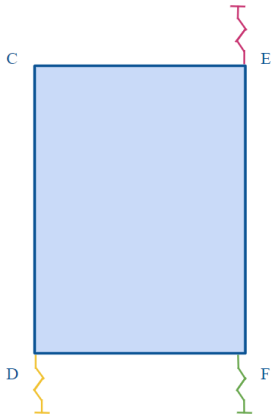

Figure D.4: Schematic representation of the boundary conditions applied up until this modelling phase. As seen for the figure, only one upper bracket is introduced in the numerical modelling procedure and two below, dedicated to the starter sills. Additionally, the same properties are attributed to both the starter sills.

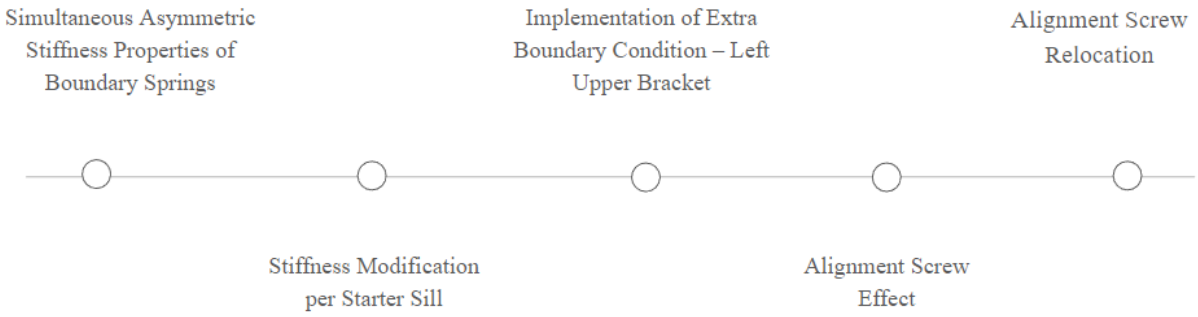

Figure D.5: The present schematic representation depicts the various aspects of the finite element modelling that intend to improve the numerical behaviour.

Simultaneous Asymmetric Stiffness Properties of Boundary Springs

A previously explained during the previous scenarios tested the asymmetric force-elongation stiffness properties were introduced separately. The effect of the asymmetric stiffness diagram was initially for the starter sill was examined while the stiffness of the upper bracket boundary spring remained symmetric. Later on, the asymmetry in the upward vs downward movement of the upper bracket boundary condition was evaluated while the stiffness properties of the starter sill were preserved symmetric.

For the better approximation of the experimental measurements as well as the effective incorporation of the positive and negative façade behaviour in solely one numerical model, the combination of the asymmetric behaviour of starter sill and upper bracket boundary conditions simultaneously is proposed to be examined. Therefore, another series of tests investigating the impact of merging scenario a with c and d and thereafter scenario b with c and d covering in this way all the possible combinations of the asymmetric properties of the existing boundary conditions is expected to provide valuable insight for the further calibration of the DIANA finite element model.

Stiffness Modification per Starter Sill

Moreover, the differentiation of the stiffnesses of the two lower boundary springs serving as boundary conditions connecting the starter sill with the surrounding environment was decided to be investigated. The above proposal originates from a conclusion drawn not only from the latest campaign of sensitivity analyses, but also from the earlier ones. Practically, it was observed that the modification of solely one parameter, e.g. the stiffness of the upper bracket in the Y direction, apart from altering the desired displacement, for example the vertical direction of points E and F, also affects other movements, such as the horizontal displacement of point D. Additionally, the vertical displacement variation of points C and D for the positive displacement which relates to this of points E and F of the negative displacement application (6.03 and 5.76 mm & 7.78 and 7.85 mm respectively resulting from the largest H/100 displacement) underlines the need for different stiffnesses of the boundary springs representing the left and the right starter sills.

Implementation of Extra Boundary Condition – Left Upper Bracket

The fact that the façade model did not react as expected in the application of the displacement with a negative displacement underlines the need for a more accurate defining of the boundary conditions, mainly through the modification of the force-elongation diagrams determining the properties of the boundary springs of both the upper bracket and the starter sill. As already explained previously, in this study the positive displacement refers to a displacement applied to the façade units under examination as seen in Figure D.6. On the contrary, when the displacement is applied in the opposite direction, then this is considered as a negative displacement.

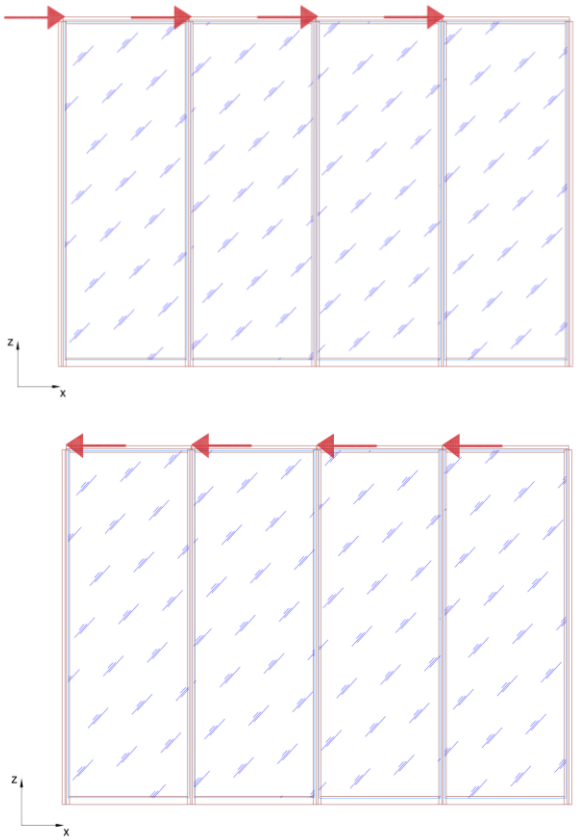

Figure D.6: Representation of the positive (above) and negative (below) displacement application. The displacements are applied on the upper left part of each of the façade units tested.

What is more, the implementation of an additional boundary condition on the upper left part of the façade is proposed to be investigated. The implementation of this new boundary condition aims to recreate the upper left bracket which is also present in the realistic situation and restrains the vertical direction of the upper left frame part when needed. It is expected that this additional boundary condition is going to restrain the movement of the façade unit in one direction but allow it in the other. The detailed reasoning justifying the implementation of the extra boundary spring simulating the left upper bracket of the façade unit will be later explained in detail.

Alignment Screw Effect

Based on the testing of several cases, some of which included the lowering of the connection stiffness of the bottom transom and the starter sill, it was concluded that for the initial stiffness (both normal and shear) values of the aforementioned connection, the alignment screw implementation did not affect the façade behaviour. To rephrase the previous, the connection between the bottom transom and the starter sill due to

the properties attributed to it is already stiff up the extent where the extra restrain introduced by the alignment screw does not introduce a coupling of the bottom transom with the starter sill that could result in different displacements of the points tested. So a verification of the previous statement could be realised through the comparison of two versions of the final calibrated model, one with and the other without the alignment screw implementation.

Alignment Screw Relocation

The location of the alignment screw in the finite element model that might deviate from the actual location can be one of those reasons. In case the previous hypothesis is realistic, due to the coupling of the starter sill and the bottom transom in an exact location the movement of the façade element is practically determined at its largest extent, eliminating the option of further calibrating the model behaviour through the modification of further properties.

To sum up, the detailed examination of all the property modification in both the positive and negative displacement application is considered as essential for the better understanding of the numerical model recreating the curtain wall global response to the seismic actions. The application of the alignment screw is suggested to be maintained for the following scenarios tested. A final comparison of the optimised DIANA model which will result from this final series of calibration with an equivalent one without the alignment screw implementation is expected to provide a confirmation on the hypothesis previously made.

Final Model Calibration

A final sensitivity analysis of the DIANA numerical model was attempted while taking into consideration all the valuable output originating from the previous sensitivity analysis runs. In practice all the ideas proposed during the previous section were tested, therefore the implementation of each of them will be successively explained in the following section.

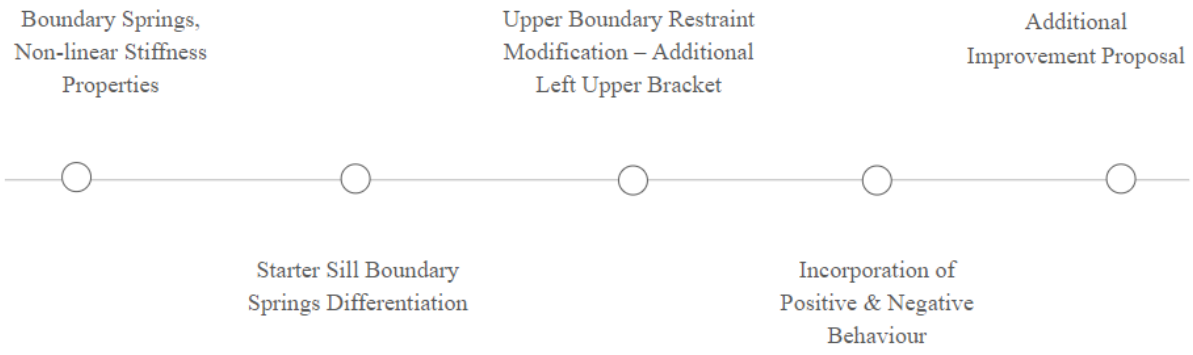

Figure D.7: Similarly to the previous schematic representation this as well concentrates the different parameters tested during this modelling stage that aspire to improve the curtain wall behaviour with regards to the experimental reference.

Boundary Springs, Non-linear Stiffness Properties

As already explained, the latest run of sensitivity analysis was related to the stiffness of the boundary springs. Up until then symmetric behaviours for negative and positive displacement were attributed to both the upper bracket and the starter sill boundary springs. During the latest scenarios tested, which are also presented in the last four columns of Table D.1, those symmetric stiffness properties were replaced by asymmetric ones. The reasoning behind those replacements lied on the better representation of the actual façade behaviour.

In reality, due to the restrains introduced from the upper boundary conditions, the spring simulating the bracket connecting the top transom with the surrounding environment, and the lower boundary conditions, the springs connecting the starter sill to the environment, the façade unit is allowed to move upwards while the downward movement is restrained. In an attempt to understand what is the proper modelling approach that would recreate the situation described previously, scenarios a-d as presented in Figure D.1 were tested.

An indication of the façade positive response to the implementation of non-linear instead of linear properties defining the stiffness of the boundary conditions can be recognised already from the previous scenarios, for which the results are presented on Table D.1. In order for the even more accurate representation of the actual façade behaviour the optimum combination of the non-linear properties of both the starter sill and the upper bracket was attempted.

Consequently the calibration of the DIANA model continued with the run of scenarios ad, ac, bc and bd. In practice all the possible scenarios between the non-symmetric properties of the upper bracket and the starter sill were tested. The combination of the non-symmetric diagrams per scenario tested is presented in Figure D.8. The subsequent results of the numerical model are presented for both the positive and the negative displacement direction on Figure D.9 and Tables D.2 and D.3 of the Supplement respectively.

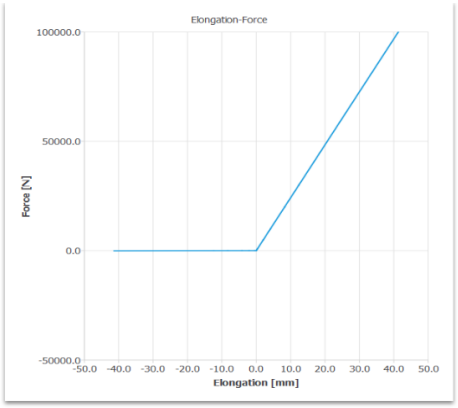

Starter Sill Stiffness (a)

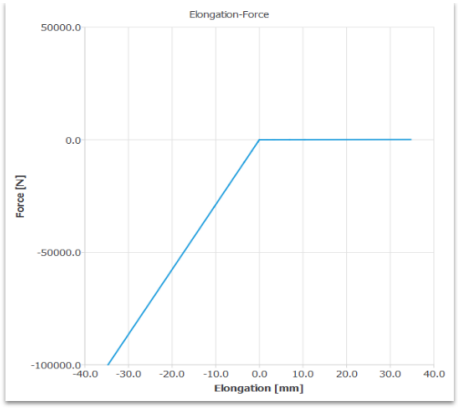

Upper Bracket Stiffness (d)

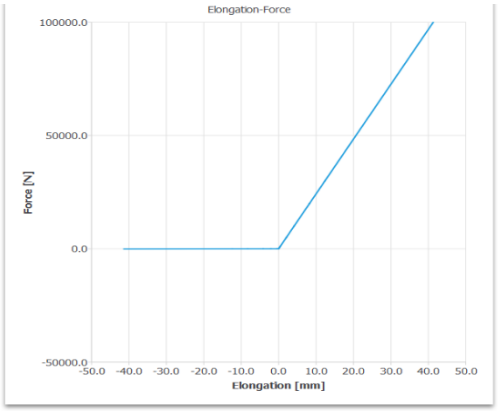

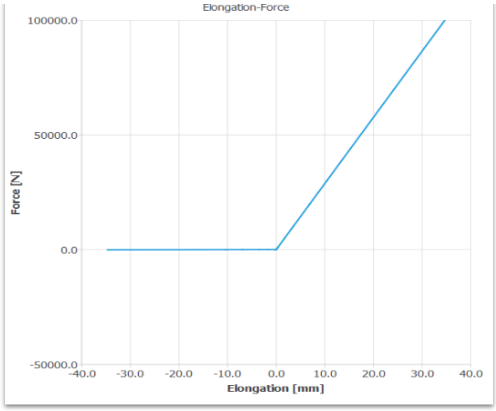

Starter Sill Stiffness (a)

Upper Bracket Stiffness (c)

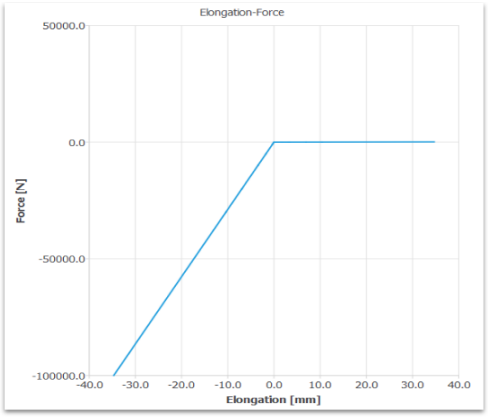

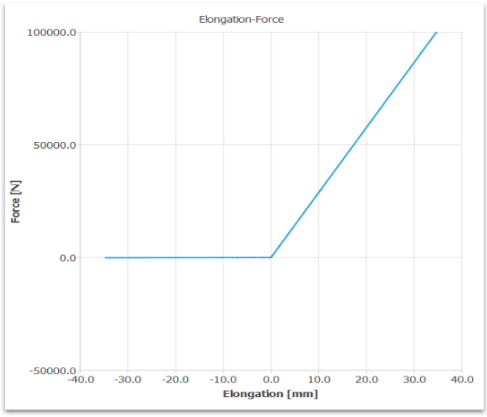

Starter Sill Stiffness (b)

Upper Bracket Stiffness (c)

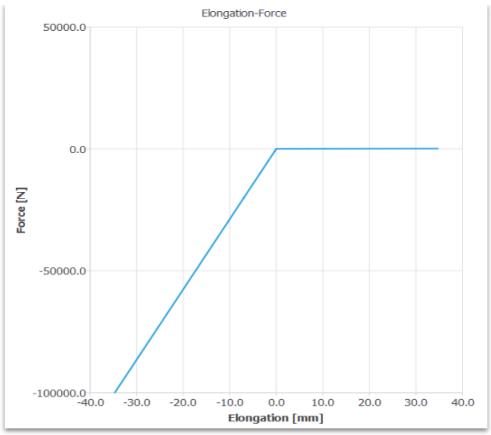

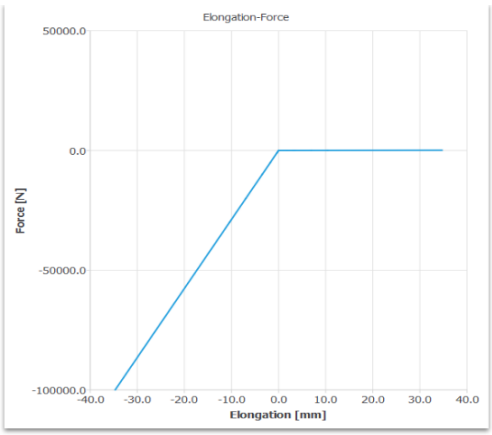

Starter Sill Stiffness (b)

Upper Bracket Stiffness (d)

Figure D.8: The stiffness properties of the starter sill and the upper bracket boundary springs for the scenarios ad, ac, bc and bd respectively.

Based on the numerical values presented on Tables D.2 and D.3 of the Supplement which is located at the end of the present document as well as on Figure D.9, it can already be concluded that scenarios ac and bc result in displacements that are quite far from the equivalent experimental results. In more detail the horizontal and displacement of point D as well as the vertical movement of C and D provide numerical results that deviate the most in both positive and negative displacements with the only exception being the vertical displacement of points E and F that for scenario bc provide values close to the target ones. Scenarios ad and bd on the other hand seem to simulate slightly better the experimental behaviour as it can also be seen from the values marked as green in the respective tables. Especially scenario bd appears to resemble closer compared to the other scenarios the vertical movement of E and F for the positive displacement and of C and D for the negative displacement.

Figure D.9: The response of the façade unit to the simultaneous combination of the non-linear properties of the boundary conditions are presented above for both the positive and negative displacement application.

Starter Sill Boundary Springs Differentiation

According to the insight provided form the previous set of scenarios, a further hypothesis that could result in numerical values even closer to the experimental ones arose. Aiming to incorporate effectively the negative and positive displacements of the façade unit into solely one model, the differentiation of the properties attributed to the left and right starter sill was introduced. The combination of the stiffness properties incorporated is presented in Figure D.10. The numerical results of the scenarios de, df, ce and cf are presented for the positive and negative displacement in Tables D.4 and D.5 of the Supplement.

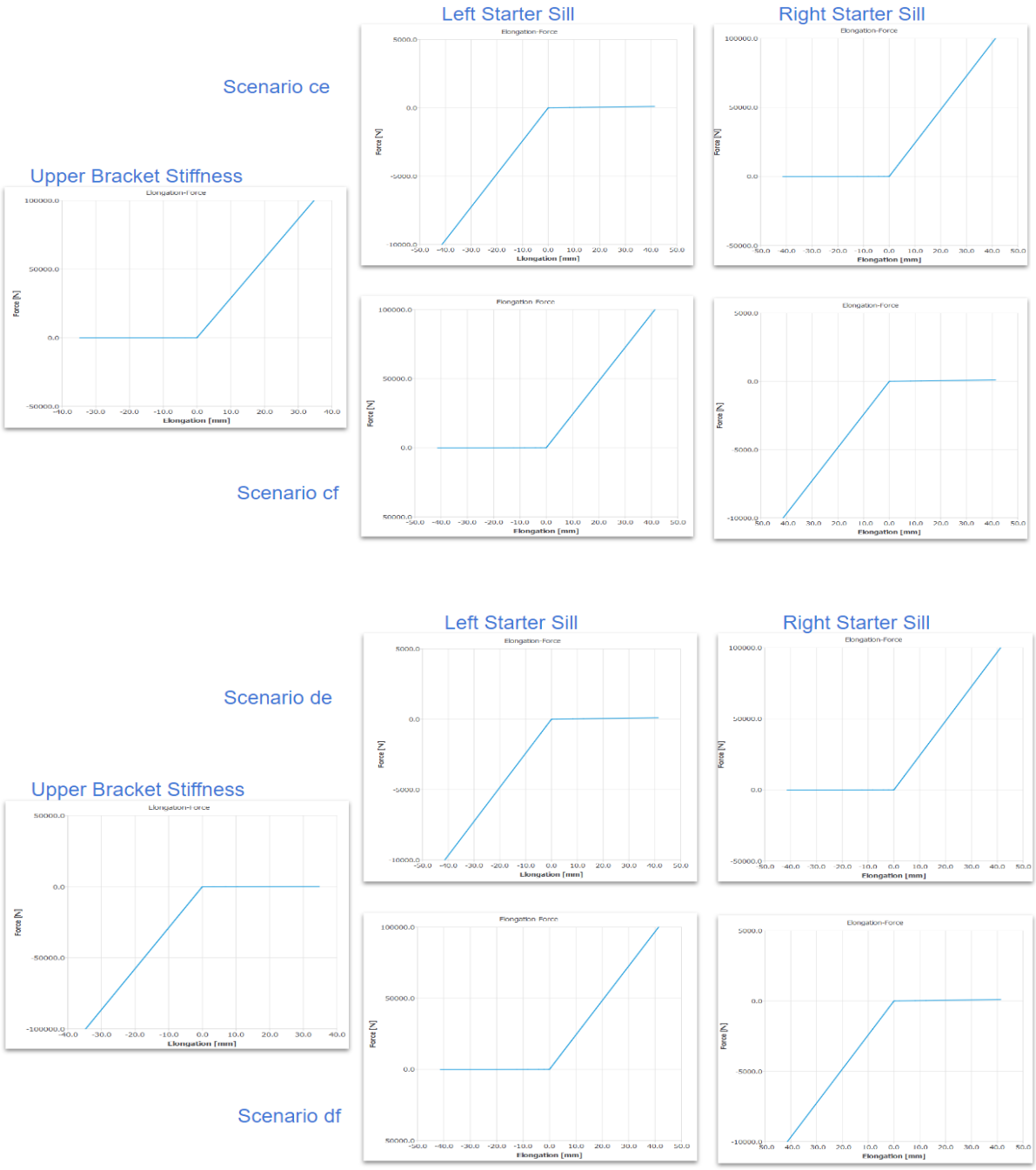

Figure D.10: The properties of the stiffness attributed to the boundary conditions per scenario tested. To the left the force – elongation diagram defining the upper bracket stiffness is provided. The diagrams for stiffnesses of the left and the right starter sills are displayed separately.

It is important to mention, that already from the previous numerical results it was observed that between scenarios c and d, d is the one better recreating the stiffness properties of the upper bracket, allowing the unit to move upwards but not downwards. However, for reasons of completeness, since additional parameters were also varying during this final stage of calibration, all the possible scenarios, including c, were performed and evaluated as seen in the following sensitivity analyses.

The discretisation of the stiffness properties of the left and right boundary springs led to the creation of Tables D.4 and D.5 of the Supplement. The study of those tables and of Figure D.11 provide the ground for some interesting findings. One of the scenarios tested, df, resulted for the positive displacement application in numerical values close to the experimental ones and the reference scenario S18 as well. In more detail, the horizontal displacement of point D and J as well as the vertical movement of all the façade and glazing points tested approximated the reference values quite faithfully. The previous is an important topic, especially for points E and F where an almost 0 displacement was achieved as opposed to the extremely large negative displacements (-4.84 and -4.24 mm) originating from scenarios cf and ce.

For the case of the negative displacement application, again the scenarios that include the upper bracket stiffness properties as defined by scenario d seem to result in better correspondence of the numerical results with the experimental measurements. The largest improvement is noticed in the vertical displacement of points E and F, which although are eligible for further improvement, they provide the closest until now relation to the target values.

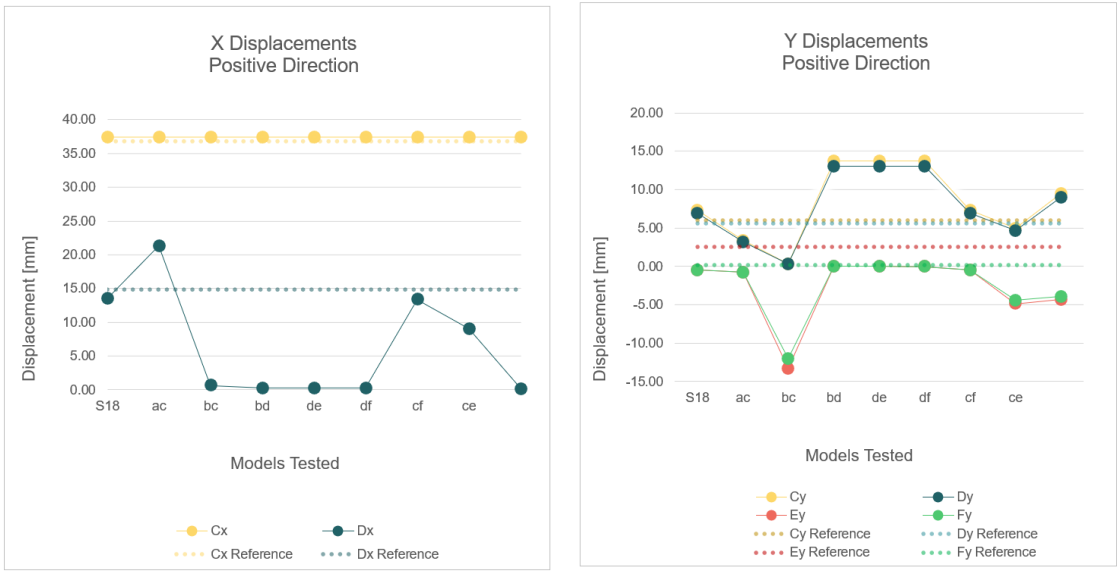

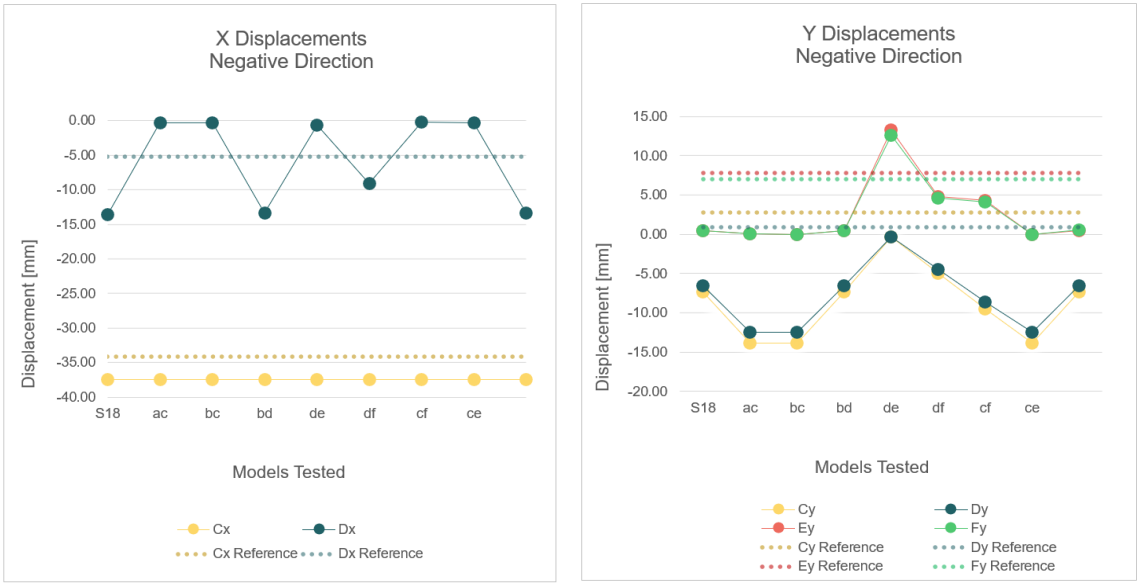

Figure D.11: The numerical values of the DIANA model for the previous scenarios tested are now accompanied by the new series of scenarios (de, df, cf and ce). The diagrams of the upper row describe the curtain wall reaction to the positive displacement application, whereas the ones of the lower row of the opposite direction.

Based on the observations described in the previous paragraphs, it can be confirmed that the preliminary conclusion extracted from the preceding set of analysis as well, indicating that the stiffness properties of scenario d, as opposed to scenario c, approximate the actual stiffness mechanism of the bracket applied to the glazed curtain wall system. Additionally it can be noticed that through the implementation of those additional scenarios (de, df, cf and ce) some of the target displacement values are approximated quite close for the first time, with the greatest example being the vertical displacement of points E and F for the negative displacement application.

Aiming for the additional correction of the behaviour of the numerical model, the implementation of an extra boundary condition representing the upper left bracket of the façade unit was investigated and explained in the following section.

Upper Boundary Restraint Modification – Additional Upper Bracket

Up until the previous scenarios tested, the upper boundary conditions were restrained to one boundary spring connecting the upper right frame corner to the surrounding environment. The remaining left corner of the framing was set free to move vertically. The concept behind that originated from the different function of the right compared to the left bracket.

While taking a closer look through to the curtain wall detailing, especially the details presenting the bracket area and reconsidering the modelling approach adopted during this study it became obvious that the implementation of an additional boundary spring restraining the vertical movement of the left part of the frame (points C and D) as well was essential. Figure D.12 depicts the complete set of boundary conditions, including the upper left one depicted in magenta colour.

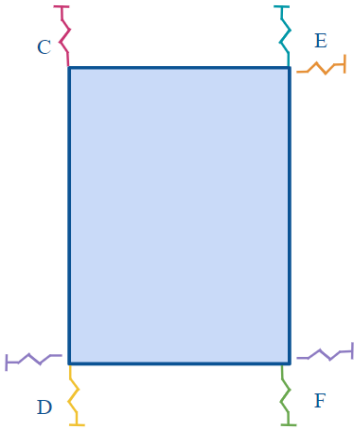

Figure D.12: This schematic representation of the boundary conditions is an updated version of the one presented previously. Here the additional upper bracket implemented to the upper left corner of the façade unit is additionally implemented.

For this reason the complete series of the scenarios previously tested reran with the implementation of this extra boundary condition, of the upper left bracket of the façade unit. Once again, based on the precious sensitivity analyses some of the scenarios tested were expected not to adequately capture the actual curtain wall behaviour. However, they were also tested for the implementation of the extra boundary spring for matters of completeness. The properties attributed to this new boundary spring were identical to the ones applied to the existing upper bracket. Of course, when a change was indicated on these specific stiffness properties, this was applied to both the upper bracket boundary springs. The numerical results are presented in Tables D.6 and D.7 of the Supplement and are visualised in Figure D.13.

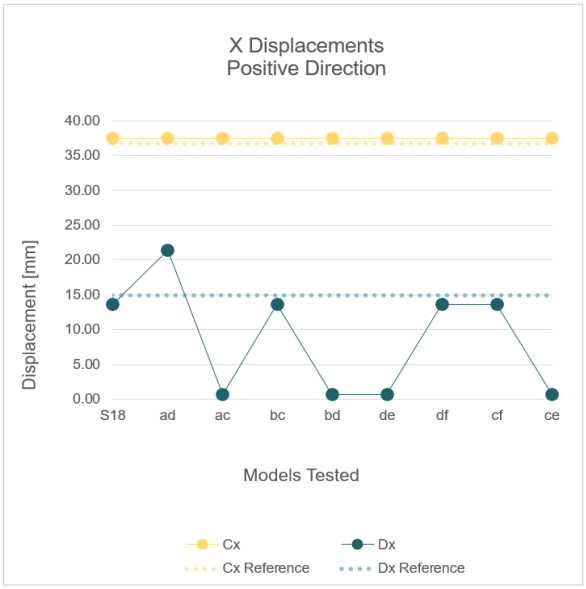

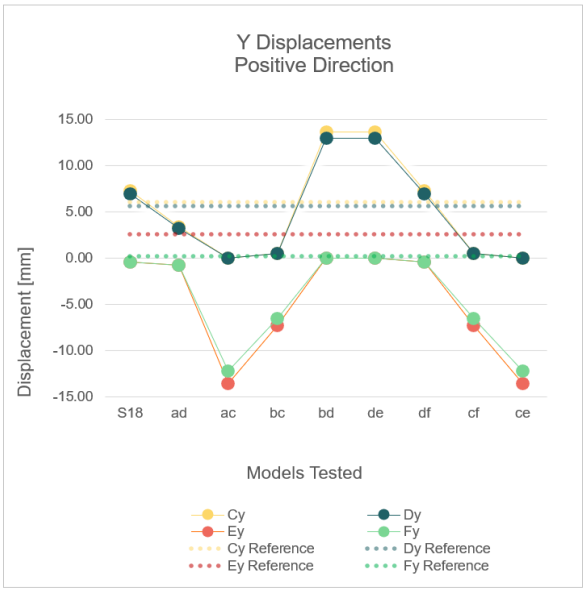

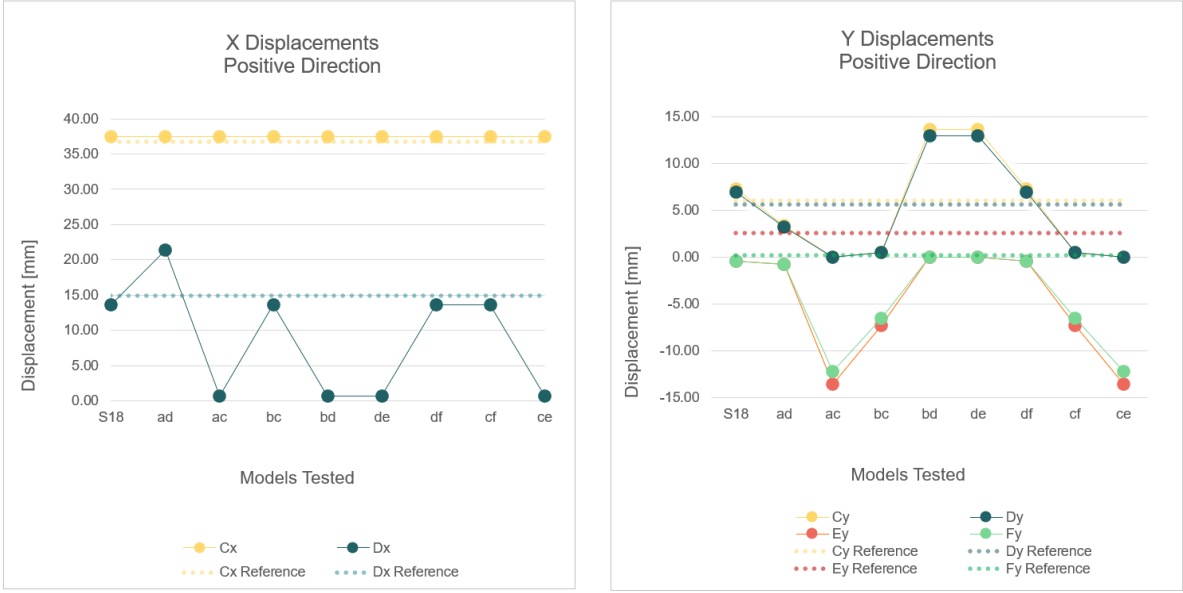

Figure D.13: The numerical values of the DIANA models of all the previous scenarios with the implementation of the extra boundary condition on the upper left frame of the unit presented above for the positive and negative displacement application respectively.

As it can be concluded by examining the numerical values of the Tables D.8 and D.9 of the Supplement, the implementation of an extra boundary spring in the upper left part of the façade configuration resulted in some scenarios generating improved numerical results, especially for the case of the negative displacement application. More precisely, both scenarios ad and de provided considerable improvement to the vertical displacement of especially points E and F compared to the experimental ones.

On the contrary, not an equivalent improvement in the approximation of the numerical results to the experimental values was noticed for the case of the positive displacement application. The latter can be explained by the fact that the previous calibrations of the DIANA model were performed based on the positive displacement application since the respective experimental measurements were taken as a reference. Therefore, the combined exploration of additional stiffness combinations of the boundary springs, as realised through the testing of scenarios de, df, cf and ce, and the implementation of the left upper boundary spring were proven to result in numerical results more accurate to the reference values.

Incorporation of Positive & Negative Behaviour

Following the study of the latest numerical result for the positive and the negative displacement application, it was noticed that not solely one variation of the DIANA model provided the optimum displacement results simultaneously for both the directions tested. In fact, while scenario df provides better representation of the actual façade behaviour as experienced during the experimental sequence for the positive displacement application, scenario de results in a more realistic simulation of the negative displacement application, especially while approximating the vertical movement of points E and F.

Based on the observation made above, an additional run of sensitivity analysis was decided aiming for the merging of the two scenarios into a unique case where both the negative and positive façade behaviours

aimed to be optimally reached. The numerical results of this final recalibration of the DIANA model are presented in Table D.8 of the Supplement and in Figure D.14.

In practice the additional change that led to the efficient merging of the previously two optimal scenarios (de and df) each of which performed better in the one of the two displacement directions examined was the further modification of the stiffness properties of the left starter sill. Those non-linear properties of the base case were modified to the initial linear ones and that resulted in the correction of the problematic response (points C and D) of the numerical model while undergoing positive displacement.

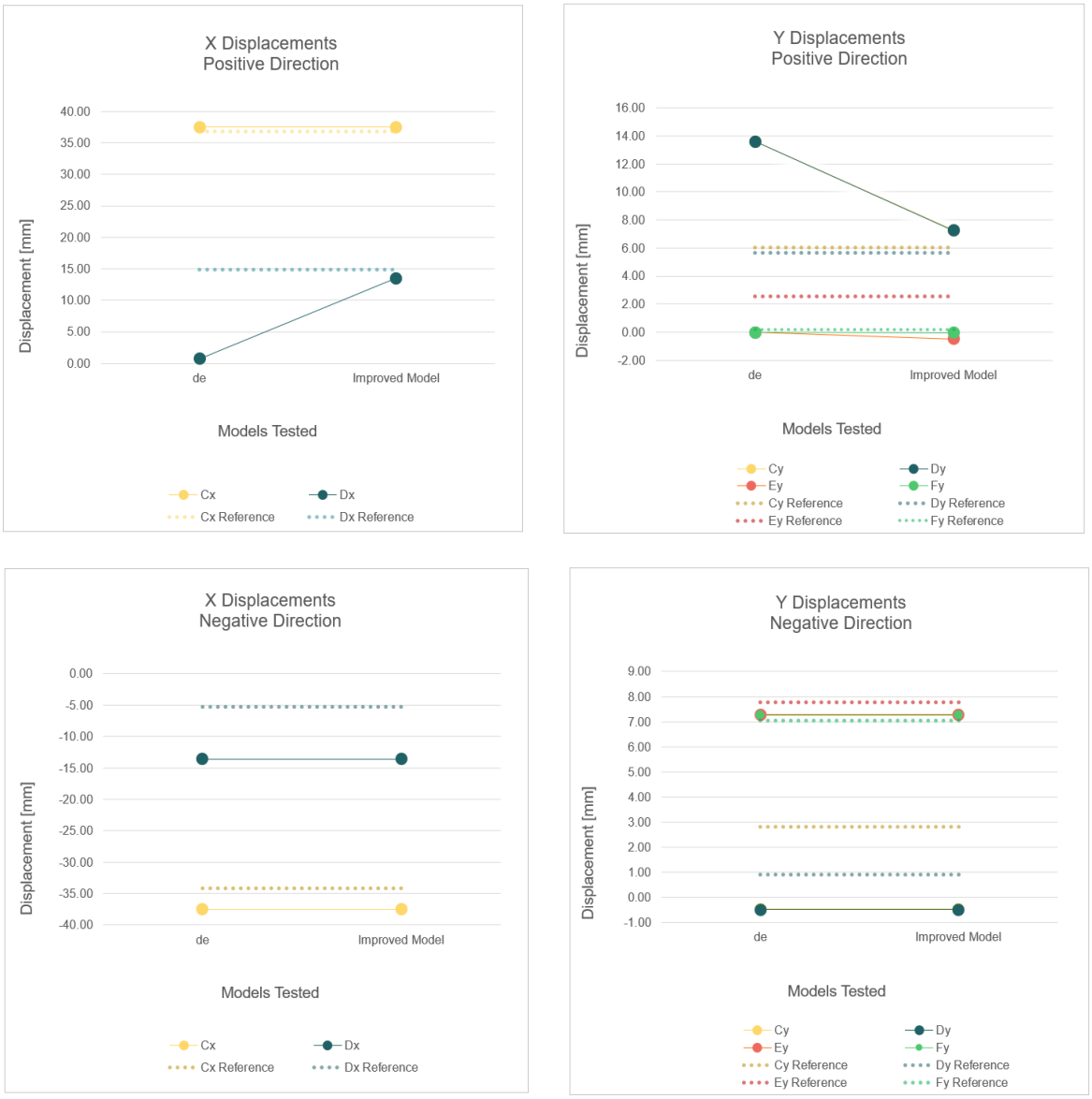

Figure D.14: The modification of the displacements of the frame points tested are presented above. During this improvement of the previous scenario de, the positive behaviour of the numerical model appears to be optimised, whereas the negative remains unaffected.

Unfortunately, since the implementation of the extra upper boundary condition via the modelling of an extra boundary spring on the upper left part of the façade unit, the horizontal movement of point D was observed

to deviate from the equivalent experimental value more compared to the scenarios tested before. Consequently, the adjacent test point J of the glazing, presents larger displacement compared to the experimental one. The above largest variations from the actual values measured during the experimental behaviour were noticed only for the negative displacement application. On the contrary, the façade units tested behave closer to the experimental results for the case of the positive displacement.

Additional Improvement Proposal

In an attempt to fix the above inconsistency with the realistic façade behaviour, additional scenarios run where the boundary condition restraining the horizontal movement of the starter sills was modified in terms of its stiffness properties. Although a difference from the previous value for this linear property resulted in more accurate results for the positive façade behaviour, simultaneously negatively affected the equivalent positive values. The reason behind that is that up until this stage of analysis the stiffness properties of this boundary spring were linear. Consequently, the conversion to the non-linear ones, without negatively affecting the previous calibration, is a topic requiring additional attention and a series of test runs in order for the better understanding of the optimum modelling to be achieved.

Reference Values Variation

Finally, while taking a closer look at the values recorded by the monitoring system during the experimental procedure, an inconsistency of the measurements is often noticed. The previous is even more obvious in the measurements of the third and largest displacement application, where the unit behaviour varies considerably between the subsequent loading circles. The above is in detail mentioned in the section dedicated to the presentation of the façade response as observed during the testing sequence. For this reason, the values originating from the final calibrated model have been compared to the average values of more loading circles to verify whether the numerical values match better with the numerical results. The results are presented in Figure D.15 and Table D.9 of the Supplement provided at the end of this section.

As seen from Figure D.15, the utilisation of the measurements of more loading cycles in some cases provide better correspondence of the numerical to the experimental results. The latter applies for the case where the first two loading circles are considered as reference values. Although more circles were also considered as reference, more specifically four subsequent ones, it was proven that during this loading consequence the façade unit already presents an irregular behaviour while heading to its failure. For this reason, the use of values representing the façade unit already entered into its failure phase cannot be considered as a safe means of comparison for the numerical results.

It is important to underline that the finding above, proving that better approximation of the finite element model to the experimental behaviour is achieved through the comparison of the first with averaged values of more loading circles, only refers to the negative displacement application. On the contrary, for the positive displacement application it was noticed that the initial reference values provide results closer to the values of the DIANA model.

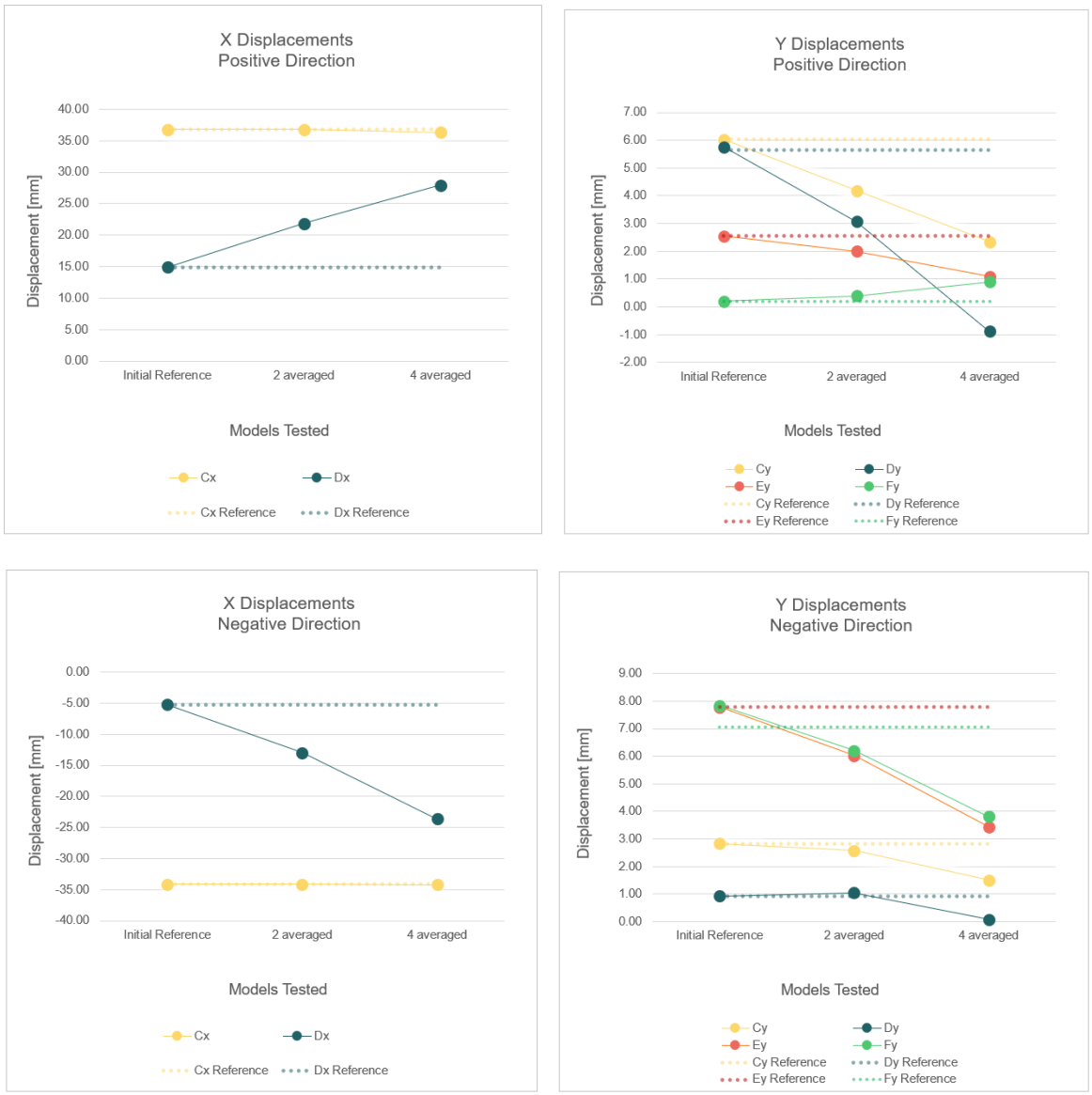

Figure D.15: In the figure above, the approximation of the final numerical models to different reference values is presented for the x and y displacements of both the positive and negative displacement application. In the first case, the initial reference values are used, originating from the first loading cycle of H/100 = 37.5 mm. Later, the reference values occur from the averaged measurements of the first two loading circles and finally, from the averaged four loading circles.

Conclusions

Undeniably, one of the most important modelling improvements of this stage is the introduction of the additional boundary condition at the upper left point of the façade unit which was excluded during the previous modelling approaches.

Following its implementation, the study of the respective unit behaviour led to an interesting observation. The beneficiary impact of the extra boundary condition to the numerical values indicated that the initial

interpretation of the façade behaviour and its modelling simulation were lacking an important parameter. By not modelling the upper left vertical boundary condition of the façade unit, which in reality allows the façade to move upwards but not downwards through a slightly different mechanism compared to this of the right vertical boundary condition, the concept of the load distribution of the actual unit was overruled. In practice, by not providing a boundary condition restricting the downward façade movement to the left as well as the right of the unit, the façade self-weight is sustained only by the right bracket whereas to the left no reaction from the fastening system occurs. So, for the modelling approach followed during this study, where connection elements such as the hook and slider were combined into a single boundary spring covering practically whatever occurs between the framing and the bracket, no difference in the modelling of the left and right boundary springs was needed.

So, here the contribution of the numerical modelling to the better interpretation of the function and response of the actual unit to be simulated is underlined. By setting up a representative numerical model, studying its reaction under various conditions and comparing it with the actual one originating from observations and measurements, either the accurate recreation of the realistic situation can be verified or fundamental misinterpretations can be identified. The latter finding is also considered as valuable, since not only leads to more accurate numerical simulations but also to the better understanding of the system-under-study as a whole.

Another important conclusion originating from the previous analysis which is related to the accuracy of this specific modelling approach is that the current numerical model cannot capture completely faithfully what has been previously called as asymmetric behaviour. This observation is mostly related to the vertical movement of point C for the negative and point E for the positive displacement applications that in the experimental values are presented to reach a positive displacement of 2.82 mm and 2.55 mm respectively.

On the contrary, in most of the numerical scenarios tested these displacement values were reaching negative values, an option that can for sure be regarded as unrealistic since in reality the implementation of the upper bracket prevents the downward movement of the façade unit. As already explained, the negative vertical displacement in the existing façade configuration is restricted in both the areas of the left and right upper brackets. Therefore, since the positive displacement movement is practically not achieved through the numerical models checked previously, at least the 0, or almost 0, movement in the vertical direction of points C and D for the negative and the positive displacement applications are considered as acceptable. This misalignment of the numerical with the experimental results can be possibly substantiated by what is commonly known as “random effect”. The relevant explanation is presented in one of the following sections of the present study.

Therefore, even after the final calibration of the numerical model, the asymmetric behaviour of the actual façade behaviour as presented during the experimental sequence referring to the uneven displacement of points E and F for the positive and C and D for the negative displacement application as presented in Figure D.14 is not properly captured in the DIANA model. Instead, the aforementioned points are presented to move symmetrically with respect to each other following the actual movement of the lowest point of the framing while for the upper point the unrealistic negative movement is eventually eliminated.

Regarding the alignment screw effect, it can be concluded that its simulation is not presented to affect the numerical values of the finite element model, in neither the positive nor the negative displacement applications tested. However, since the implementation of this additional façade element was proven to affect the curtain wall behaviour for the cases where the stiffness of the bottom transom-to-starter sill connection was reduced, it can be assumed that impact of the alignment screw is greater for the structurally sealed façade configurations than this of the dry glazed systems.

Finally, the variation of the experimental values used as a reference, based on the results of the present study the following can be concluded. The incorporation of experimental values of more than one loading circles might result in better approximation of the numerical model with the actual façade behaviour as measured during an experimental sequence. The previous can be possibly explained by the elimination of the random effect, which is typically responsible for the deviation of the simulated and actual behaviour of complex configurations, such as glazed curtain wall systems. However, a limitation regarding the number of loading circles used as reference for the model calibration is recommended to be introduced. This constraint should incorporate the correspondence of the model behaviour to the loading circle above which the curtain wall system is considered to have failed.

Supplement

Further Calibration, Non-linear Stiffness Properties of Boundary Springs

Positive Displacement, H/100, Different Stiffness Properties on Left vs Right Starter Sill							
Glass	Unit 3	Experiment Values	S18	ad	ac	bc	bd
J x:	15.74	15.74	14.20	22.10	1.18	0.82	0.82
y:	6.42	6.42	7.35	3.83	-0.11	13.30	13.30
L x:	35.10	35.10	36.20	36.20	36.20	36.20	36.20
Frame							
C x:	36.80	36.80	37.50	37.50	37.50	37.50	37.50
y:	6.03	6.03	7.30	3.41	0.38	13.80	13.80
D x:	14.90	14.90	13.60	21.30	0.68	0.32	0.32
y:	5.76	5.76	7.27	3.35	0.37	13.80	13.80
E x:	-		36.00	36.00	36.00	36.00	36.00
y:	2.55	2.55	-0.47	-0.77	-13.30	-0.01	-0.01
F x:	-		13.60	21.50	0.68	0.32	0.32
y:	0.20	0.20	-0.49	-0.82	-13.30	-0.01	-0.01

Positive Displacement, H/100, Different Stiffness Properties on Left vs Right Starter Sill							
Glass	Unit 3	Experiment Values	S18	ad	ac	bc	bd
J x:	15.74	15.74	-10%	40%	-93%	-95%	-95%
y:	6.42	6.42	14%	-40%	-102%	107%	107%
L x:	35.10	35.10	3%	3%	3%	3%	3%
Frame							
C x:	36.80	36.80	2%	2%	2%	2%	2%
y:	6.03	6.03	21%	-43%	-94%	129%	129%
D x:	14.90	14.90	-9%	43%	-95%	-98%	-98%
y:	5.76	5.76	26%	-42%	-94%	139%	139%
E x:	-						
y:	2.55	2.55	-118%	-130%	-621%	-100%	-100%
F x:	-						
y:	0.20	0.20	-352%	-519%	-6921%	-106%	-106%

Table D.2: The numerical values of scenarios ad, ac, bc and bd for the positive displacement application. Scenario 18 that was selected as the most representative one from the previous sensitivity analysis was used this time as the basic model upon which the appropriate per case property modifications were applied. The numerical values of Scenario 18 are also presented since they serve as a reference for the impact assessment of each of the variations introduced.

Negative Displacement, H/100, Different Stiffness Properties on Left vs Right Starter Sill							
Glass	Unit 3	Experiment Values	S18	ad	ac	bc	bd
J x:	-6.63	-6.63	-14.20	-0.82	-0.82	-14.10	-1.18
y:	0.62	0.62	-7.35	-13.30	-13.30	-7.41	0.12
L x:	-30.70	-30.70	-36.20	-36.20	-36.20	-36.20	-36.20
Frame							
C x:	-34.16	-34.16	-37.50	-37.50	-37.50	-37.50	-37.50
y:	2.82	2.82	-7.30	-13.80	-13.80	-7.33	-0.37
D x:	-5.26	-5.26	-13.60	-0.32	-0.32	-13.40	-0.68
y:	0.92	0.92	-7.27	-13.80	-13.80	-7.29	-0.37
E x:	-		-36.00	-36.00	-36.00	-36.00	-36.00
y:	7.78	7.78	0.47	0.05	0.01	0.49	13.30
F x:	-		-13.60	-0.32	-0.32	-13.50	-0.68
y:	7.85	7.85	0.49	0.05	0.01	0.52	13.30

Negative Displacement, H/100, Different Stiffness Properties on Left vs Right Starter Sill							
Glass	Unit 3	Experiment Values	S18	ad	ac	bc	bd
J x:	-6.63	-6.63	114%	-88%	-88%	113%	-82%
y:	0.62	0.62	-1285%	-2245%	-2245%	-1295%	-81%
L x:	-30.70	-30.70	18%	18%	18%	18%	18%
Frame							
C x:	-34.16	-34.16	10%	10%	10%	10%	10%
y:	2.82	2.82	-358%	-589%	-589%	-360%	-113%
D x:	-5.26	-5.26	158%	-94%	-94%	155%	-87%
y:	0.92	0.92	-889%	-1597%	-1597%	-891%	-140%
E x:	-						
y:	7.78	7.78	-94%	-99%	-100%	-94%	71%
F x:	-						
y:	7.85	7.85	-94%	-99%	-100%	-93%	71%

Table D.3: The respective displacements of the DIANA model are presented above for the negative displacement application. Similarly to previous situations, the marking of some values with red determines the further deviation of the numerical results compared to the reference scenario whereas with green the better approximation is introduced due to the property modification applied through the scenario case tested.

Positive Displacement, H/100, Different Stiffness Properties on Left vs Right Starter Sill											
Glass	Unit 3	Experiment Values	S18	ad	ac	bc	bd	de	df	cf	ce
J x:	15.74	15.74	14.20	22.10	1.18	0.82	0.82	0.82	14.10	9.74	0.72
y:	6.42	6.42	7.35	3.83	-0.11	13.30	13.30	13.30	7.42	4.82	9.00
L x:	35.10	35.10	36.20	36.20	36.20	36.20	36.20	36.20	36.20	36.20	36.20
Frame											
C x:	36.80	36.80	37.50	37.50	37.50	37.50	37.50	37.50	37.50	37.50	37.50
y:	6.03	6.03	7.30	3.41	0.38	13.80	13.80	13.80	7.34	4.94	9.52
D x:	14.90	14.90	13.60	21.30	0.68	0.32	0.32	0.32	13.40	9.10	0.22
y:	5.76	5.76	7.27	3.35	0.37	13.80	13.80	13.80	7.34	4.92	9.52
E x:	-		36.00	36.00	36.00	36.00	36.00	36.00	36.00	36.00	25.00
y:	2.55	2.55	-0.47	-0.77	-13.30	-0.01	-0.01	-0.01	-0.46	-4.84	-4.34
F x:	-		13.60	21.50	0.68	0.32	0.32	0.32	13.50	9.11	0.11
y:	0.20	0.20	-0.49	-0.82	-13.30	-0.01	-0.01	-0.01	-0.48	-4.84	-4.34

Positive Displacement, H/100, Different Stiffness Properties on Left vs Right Starter Sill											
Glass	Unit 3	Experiment Values	S18	ad	ac	bc	bd	de	df	cf	ce
J x:	15.74	15.74	-10%	40%	-93%	-95%	-95%	-95%	-10%	-38%	-95%
y:	6.42	6.42	14%	-40%	-102%	107%	107%	107%	16%	-25%	40%
L x:	35.10	35.10	3%	3%	3%	3%	3%	3%	3%	3%	3%
Frame											
C x:	36.80	36.80	2%	2%	2%	2%	2%	2%	2%	2%	2%
y:	6.03	6.03	21%	-43%	-94%	129%	129%	129%	22%	-18%	58%
D x:	14.90	14.90	-9%	43%	-95%	-98%	-98%	-98%	-10%	-39%	-99%
y:	5.76	5.76	26%	-42%	-94%	139%	139%	139%	27%	-15%	65%
E x:	-										
y:	2.55	2.55	-118%	-130%	-621%	-100%	-100%	-100%	-118%	-290%	-270%
F x:	-										
y:	0.20	0.20	-352%	-519%	-6921%	-106%	-106%	-107%	-348%	-2582%	-2326%

Table D.4: The numerical values of the additional scenarios de, df, cf and ce are presented above for the positive displacement application. Below, the same values expressed as percentages presenting either the positive or the negative deviation from the reference values are shown. A deviation range of ±30.0 % has been accepted as allowable. The values between this range are highlighted in green.

Negative Displacement, H/100, Different Stiffness Properties on Left vs Right Starter Sill											
Glass	Unit 3	Experiment Values	S18	ad	ac	bc	bd	de	df	cf	ce
J x:	-6.63	-6.63	-14.20	-0.82	-0.82	-14.10	-1.18	-9.74	-0.72	-0.82	-14.10
y:	0.62	0.62	-7.35	-13.30	-13.30	-7.41	0.12	-4.82	-9.02	-13.30	-7.42
L x:	-30.70	-30.70	-36.20	-36.20	-36.20	-36.20	-36.20	-36.20	-36.20	-36.20	-36.20
Frame											
C x:	-34.16	-34.16	-37.50	-37.50	-37.50	-37.50	-37.50	-37.50	-37.50	-37.50	-37.50
y:	2.82	2.82	-7.30	-13.80	-13.80	-7.33	-0.37	-4.94	-9.52	-13.80	-7.34
D x:	-5.26	-5.26	-13.60	-0.32	-0.32	-13.40	-0.68	-9.10	-0.22	-0.32	-13.40
y:	0.92	0.92	-7.27	-13.80	-13.80	-7.29	-0.37	-4.92	-9.52	-13.80	-7.31
E x:	-		-36.00	-36.00	-36.00	-36.00	-36.00	-36.00	-36.00	-36.00	-36.00
y:	7.78	7.78	0.47	0.05	0.01	0.49	13.30	4.85	4.34	0.01	0.46
F x:	-		-13.60	-0.32	-0.32	-13.50	-0.68	-9.11	-0.22	-0.32	-13.50
y:	7.85	7.85	0.49	0.05	0.01	0.52	13.30	4.84	4.34	0.01	0.58

Negative Displacement, H/100, Different Stiffness Properties on Left vs Right Starter Sill											
Glass	Unit 3	Experiment Values	S18	ad	ac	bc	bd	de	df	cf	ce
J x:	-6.63	-6.63	114%	-88%	-88%	113%	-82%	47%	-89%	-88%	113%
y:	0.62	0.62	-1285%	-2245%	-2245%	-1295%	-81%	-877%	-1555%	-2245%	-1297%
L x:	-30.70	-30.70	18%	18%	18%	18%	18%	18%	18%	18%	18%
Frame											
C x:	-34.16	-34.16	10%	10%	10%	10%	10%	10%	10%	10%	10%
y:	2.82	2.82	-358%	-589%	-589%	-360%	-113%	-275%	-437%	-589%	-360%
D x:	-5.26	-5.26	158%	-94%	-94%	155%	-87%	73%	-96%	-94%	155%
y:	0.92	0.92	-889%	-1597%	-1597%	-891%	-140%	-634%	-1133%	-1597%	-893%
E x:	-										
y:	7.78	7.78	-94%	-99%	-100%	-94%	71%	-38%	-44%	-100%	-94%
F x:	-										
y:	7.85	7.85	-94%	-99%	-100%	-93%	71%	-38%	-44%	-100%	-93%

Table D.5: The equivalent values of the additional scenarios tested for different properties of the starter sill are presented this time for the negative displacement application. Below, the same results are shown in the form of percentages representing the deviation range from the values measured. The values marked in light grey instead of the typical black colour are the ones accepted as allowable since their movement remains in the area of 0.0 displacement.

Positive Displacement, H/100, Extra Boundary Condition - Upper Left Bracket											
Glass	Unit 3	Experiment Values	S18	ad	ac	bc	bd	de	df	cf	ce
J x:	15.74	15.74	14.20	22.10	1.20	14.20	1.20	1.20	14.20	14.20	1.20
y:	6.42	6.42	7.35	3.83	-0.46	0.60	13.10	13.10	7.37	0.56	-0.46
L x:	35.10	35.10	36.20	36.20	36.20	36.20	36.20	36.20	36.20	36.20	36.20
Frame	0.00										
C x:	36.80	36.80	37.50	37.50	37.50	37.50	37.50	37.50	37.50	37.50	37.50
y:	6.03	6.03	7.30	3.41	0.02	0.49	13.60	13.60	7.29	0.46	0.02
D x:	14.90	14.90	13.60	21.40	0.70	13.60	0.69	0.69	13.60	13.60	0.70
y:	5.76	5.76	7.27	3.35	0.02	0.52	13.60	13.60	7.26	0.49	0.03
E x:	-		36.00	36.00	36.00	36.00	36.00	36.00	36.00	36.00	36.00
y:	2.55	2.55	-0.47	-0.77	-13.60	-7.26	-0.02	-0.02	-0.46	-7.28	-13.60
F x:	-		13.60	21.50	0.70	13.50	0.70	0.70	13.60	13.60	0.70
y:	0.20	0.20	-0.49	-0.82	-13.60	-7.23	-0.03	-0.03	-0.48	-7.25	-13.60

Positive Displacement, H/100, Extra Boundary Condition - Upper Left Bracket											
Glass	Unit 3	Experiment Values	S18	ad	ac	bc	bd	de	df	cf	ce
J x:	15.74	15.74	-10%	40%	-92%	-10%	-92%	-92%	-10%	-10%	-92%
y:	6.42	6.42	14%	-40%	-107%	-91%	104%	104%	15%	-91%	-107%
L x:	35.10	35.10	3%	3%	3%	3%	3%	3%	3%	3%	3%
Frame	0.00										
C x:	36.80	36.80	2%	2%	2%	2%	2%	2%	2%	2%	2%
y:	6.03	6.03	21%	-43%	-100%	-92%	125%	125%	21%	-92%	-100%
D x:	14.90	14.90	-9%	44%	-95%	-9%	-95%	-95%	-9%	-9%	-95%
y:	5.76	5.76	26%	-42%	-100%	-91%	136%	136%	26%	-92%	-100%
E x:	-										
y:	2.55	2.55	-118%	-130%	-633%	-384%	-101%	-101%	-118%	-385%	-633%
F x:	-										
y:	0.20	0.20	-352%	-519%	-7074%	-3808%	-113%	-114%	-348%	-3818%	-7074%

Table D.6: The numerical values representing the façade behaviour under the implementation of a positive displacement equal to H/100 is presented above. In this set of scenarios an additional boundary spring has been introduced in the upper left part of the façade unit recreating the left upper bracket fastening the curtain wall system to supporting structure. It is obvious that scenarios de and df are the ones approaching better the experimental measurements with df recreating better the positive and de the negative displacement application.

Negative Displacement, H/100, Extra Boundary Condition - Upper Left Bracket											
Glass	Unit 3	Experiment Values	S18	ad	ac	bc	bd	de	df	cf	ce
J x:	-6.63	-6.63	-14.20	-22.20	-1.20	-14.20	-1.20	-14.20	-1.20	-1.20	-14.20
y:	0.62	0.62	-7.35	-1.24	-13.30	-7.36	0.46	-0.56	0.46	-13.10	-7.37
L x:	-30.70	-30.70	-36.20	-36.20	-36.20	-36.20	-36.20	-36.20	-36.20	-36.20	-36.20
Frame	0.00										
C x:	-34.16	-34.16	-37.50	-37.50	-37.50	-37.50	-37.50	-37.50	-37.50	-37.50	-37.50
y:	2.82	2.82	-7.30	-0.77	-13.60	-7.28	-0.02	-0.46	-0.03	-13.60	-7.29
D x:	-5.26	-5.26	-13.60	-21.50	-0.69	-13.40	-0.69	-13.60	-0.69	-0.69	-13.60
y:	0.92	0.92	-7.27	-0.83	-13.60	-7.24	-0.02	-0.49	-0.03	-13.60	-7.26
E x:	-		-36.00	-36.00	-36.00	-36.00	-36.00	-36.00	-36.00	-36.00	-36.00
y:	7.78	7.78	0.47	3.37	0.02	0.49	13.60	7.28	13.60	0.02	0.46
F x:	-		-13.60	-21.40	-0.70	-13.50	-0.70	-13.60	-0.70	-0.69	-13.60
y:	7.85	7.85	0.49	3.32	0.03	0.52	13.60	7.25	13.60	0.03	0.49

Negative Displacement, H/100, Extra Boundary Condition - Upper Left Bracket											
Glass	Unit 3	Experiment Values	S18	ad	ac	bc	bd	de	df	cf	ce
J x:	-6.63	-6.63	114%	235%	-82%	114%	-82%	114%	-82%	-82%	114%
y:	0.62	0.62	-1285%	-300%	-2245%	-1287%	-26%	-191%	-26%	-2213%	-1289%
L x:	-30.70	-30.70	18%	18%	18%	18%	18%	18%	18%	18%	18%
Frame	0.00										
C x:	-34.16	-34.16	10%	10%	10%	10%	10%	10%	10%	10%	10%
y:	2.82	2.82	-358%	-127%	-582%	-358%	-101%	-116%	-101%	-582%	-358%
D x:	-5.26	-5.26	158%	309%	-87%	155%	-87%	158%	-87%	-87%	158%
y:	0.92	0.92	-889%	-190%	-1575%	-885%	-103%	-153%	-103%	-1575%	-887%
E x:	-										
y:	7.78	7.78	-94%	-57%	-100%	-94%	75%	-6%	75%	-100%	-94%
F x:	-										
y:	7.85	7.85	-94%	-58%	-100%	-93%	73%	-8%	73%	-100%	-94%

Table D.7: The equivalent numerical values are presented for the negative displacement application. The most interesting improvements introduced by the modification of the stiffness properties of the two starter sills separately are marked in coloured background. The green background marks an important improvement compared to the previous results whereas the red colour indicates the points approximating less the experimental results.

Further Improvement, Incorporation of Positive & Negative Behaviour							
Experiment Values		de	Improved Version	Improved Version	de	Experiment Values	
Positive Displacement				Negative Displacement			
Glass							Glass
J x:	15.74	1.20	14.20	-14.20	-14.20	-6.63	J x:
y:	6.42	13.10	7.36	-0.56	-0.56	0.62	y:
L x:	35.10	36.20	36.20	-36.20	-36.20	-30.70	L x:
Frame							Frame
C x:	36.80	37.50	37.50	-37.50	-37.50	-34.16	C x:
y:	6.03	13.60	7.28	-0.46	-0.46	2.82	y:
D x:	14.90	0.69	13.50	-13.60	-13.60	-5.26	D x:
y:	5.76	13.60	7.24	-0.49	-0.49	0.92	y:
E x:							E x:
y:	2.55	-0.02	-0.49	7.28	7.28	7.78	y:
F x:							F x:
y:	0.20	-0.03	-0.05	7.25	7.25	7.85	y:

Further Improvement, Incorporation of Positive & Negative Behaviour							
Experiment Values		de	Improved Version	Improved Version	de	Experiment Values	
Positive Displacement				Negative Displacement			
Glass							Glass
J x:	15.74	-92%	-10%	114%	114%	-6.63	J x:
y:	6.42	104%	15%	-191%	-191%	0.62	y:
L x:	35.10	3%	3%	18%	18%	-30.70	L x:
Frame							Frame
C x:	36.80	2%	2%	10%	10%	-34.16	C x:
y:	6.03	125%	21%	-116%	-116%	2.82	y:
D x:	14.90	-95%	-9%	158%	158%	-5.26	D x:
y:	5.76	136%	26%	-153%	-153%	0.92	y:
E x:							E x:
y:	2.55	-101%	-119%	-8%	-8%	7.78	y:
F x:							F x:
y:	0.20	-114%	-127%	-8%	-8%	7.85	y:

Table D.8: The table of the final calibration is presented. The blue and orange columns present the reference values of the positive and negative displacement respectively. Additionally, the results of scenario de are seen for both the displacement options. In red the final calibrated scenario is presented, that is an optimised version of scenario de. In practice the properties of the left starter sill were modified to the initial linear ones. In this way a façade behaviour recreating both the positive and negative displacement application was achieved.

Positive Displacement Application						
Experiment	Initial Reference		Averaged 2 Cycles		Averaged 4 Cycles	
Glass						
J x:	15.74	14.20	17.28	14.20	18.04	14.20
y:	6.42	7.36	2.01	7.36	0.74	7.36
L x:	35.10	36.20	35.70	36.20	36.18	36.20
Frame						
C x:	36.80	37.50	36.80	37.50	36.32	37.50
y:	6.03	7.28	4.18	7.28	2.34	7.28
D x:	14.90	13.50	21.85	13.50	27.89	13.50
y:	5.76	7.24	3.08	7.24	-0.88	7.24
E x:	-		-		-	
y:	2.55	-0.49	2.01	-0.49	1.09	-0.49
F x:	-		-		-	
y:	0.20	-0.05	0.39	-0.05	0.89	-0.05

Negative Displacement Application						
Experiment	Initial Reference		Averaged 2 Cycles		Averaged 4 Cycles	
Glass						
J x:	-6.63	-14.20	-13.97	-14.20	-22.59	-14.20
y:	0.62	-0.56	0.81	-0.56	0.58	-0.56
L x:	-30.70	-36.20	-31.75	-36.20	-33.13	-36.20
Frame						
C x:	-34.16	-37.50	-34.16	-37.50	-34.17	-37.50
y:	2.82	-0.46	2.57	-0.46	1.50	-0.46
D x:	-5.26	-13.60	-12.98	-13.60	-23.63	-13.60
y:	0.92	-0.49	1.05	-0.49	0.07	-0.49
E x:	-		-		-	
y:	7.78	7.28	6.03	7.28	3.43	7.28
F x:	-		-		-	
y:	7.85	7.25	6.20	7.25	3.81	7.25

Positive Displacement Application						
Experiment	Initial Reference		Averaged 2 Cycles		Averaged 4 Cycles	
Glass						
J x:	15.74	-10%	17.28	-18%	18.04	-21%
y:	6.42	15%	2.01	266%	0.74	891%
L x:	35.10	3%	35.70	1%	36.18	0%
Frame						
C x:	36.80	2%	36.80	2%	36.32	3%
y:	6.03	21%	4.18	74%	2.34	211%
D x:	14.90	-9%	21.85	-38%	27.89	-52%
y:	5.76	26%	3.08	135%	-0.88	-920%
E x:	-		-		-	
y:	2.55	-119%	2.01	-124%	1.09	-145%
F x:	-		-		-	
y:	0.20	-127%	0.39	-113%	0.89	-106%

Negative Displacement Application						
Experiment	Initial Reference		Averaged 2 Cycles		Averaged 4 Cycles	
Glass						
J x:	-6.63	114%	-13.97	2%	-22.59	-37%
y:	0.62	-191%	0.81	-169%	0.58	-196%
L x:	-30.70	18%	-31.75	14%	-33.13	9%
Frame						
C x:	-34.16	10%	-34.16	10%	-34.17	10%
y:	2.82	-116%	2.57	-118%	1.50	-131%
D x:	-5.26	158%	-12.98	5%	-23.63	-42%
y:	0.92	-153%	1.05	-147%	0.07	-99%
E x:	-		-		-	
y:	7.78	-6%	6.03	21%	3.43	112%
F x:	-		-		-	
y:	7.85	-8%	6.20	17%	3.81	90%

Table D.9: The correspondence of the numerical behaviour to the variation of the experimental values used as a reference is presented above. It can be easily seen that while taking into account four loading circles as reference, worse approximation of the experimental results occurs. On the contrary, while considering only two circles, the problematic areas for the negative displacement application are corrected. So it can be concluded that by using the experimental values of the first two loading cycles as a reference, the DIANA model approximates closely the respective experimental behaviour for the negative displacement application. In fact, all the numerical values, with the exception of those marked in light grey, approach the experimental results at a range of 30.0 %. The above does not apply for the positive displacement application. In this case, better correspondence of the numerical to the actual behaviour is achieved when comparing the first with the initial reference values.

List of Figures

2.12 Two-sided structural glazing application. In this particular case, the horizontal edges of the glass panes are attached to the mullions mechanically whereas the vertical ones through structural silicone. To the right the structural glazing horizontal (top) and the vertical (bottom) details are seen (Source: DOW, 2021).

2.13 Four-sided structural glazing application. To the right the horizontal (top) and the vertical (bottom) details /section are presented (Source: DOW, 2021).

2.14 Comparison of the load-displacement correlation of typical four-, two-sided SSG and dry-glazed curtain wall systems. The mock-up configurations tested during this study were stick-built systems and consisted of nine glass panes, with the central panel being the largest one. The dimensions of the central element, which was utilised as a test panel, were 1.83 m high * 1.52 m wide. The drift values measured in the central panel are presented in the displacement scale at the bottom horizontal axis. The actual drift experienced by the complete mock-ups is presented at the top of the graph, in its appropriate scale (Source: Memari et al., 2012).

2.15 The correlation of the dynamic drift ratio and the air-leakage rates measured on the gasket seal and the silicone sealant for the dry and the wet mock-up configurations are presented respectively (Source Memari et al., 2012).

2.16 Typical stack joints and anchoring system for a unitised four-sided SSG configuration. The stack joints are placed at the top of each floor slab accommodating both vertical deflection and lateral movement. In the renderings above the curtain wall system is presented to be attached to the floor slab above the pair of the primary mullions through a set of hook plates, a pair at each panel, that are vertically attached to the stack mullions placed below the stack joint of the horizontal direction (Source: Memari, Fisher, et al., 2012).

2.17 The drawing above presents different types of anchorage of a curtain wall system to the load bearing structure of a building. The type of connection defines the load transfer. To the left, the option of a suspended curtain wall is presented, followed by a single-storey configuration in the middle of the figure. Finally, a two-storey curtain wall system is depicted to the right (Source: Knaack et al., 2014).

3.1 Determination of the storey-drift of a typical structure (Source: ASCE 7-16).

3.2 The difference between the seismic-proof and seismic-resistant design is depicted above. To the left, a representation of a seismic-proof building, remaining undamaged even after being subjected to earthquake actions, and to the left, the depiction of a damaged structure (Source: Murty et al., 2012).

3.3 The requirements identified by the seismic-resistant building concept applied for typical building structures are depicted above for the three of the seismic intensities individually. (a) Minor seismic intensity: hardly any damage is accepted, (b) Intermediate shaking: minor damage of the structural elements and limited of the non-structural ones (c) Severe seismic intensity: minor damages of structural elements, prevention of the building collapse (Source: Murty et al., 2012).

3.4 In the figure above, the design effect of a building for the seismic is presented to the left. The seismically-imposed displacement is applied at the base of the structure. To the right, the wind pressure acting on the building's exposed area is depicted (Source: Murty et al., 2012).

3.5 In the figure above the in-plane deformation observed in glazed panels when undergoing horizontal shear is presented. To the left the undeflected panel, where the initial frame deformation and the glazing translation within the framing is presented for a displacement applied from the right towards the left. In the middle the in-plane deflection due to the glazing movement is depicted and finally, to the right, the combined in-plane deflection due to both the rotational and the horizontal movement of the glazing (Source: Bârnaure & Voiculescu, 2013).

3.6 The different breaking patterns for typical glazing types. To the left a representation of the large, pointed and sharp splinters created after the annealed or heat-strengthened glazing rapture are depicted. In the middle, the image of a tempered glazing panel being completely shattered is observed, with most of the shivers falling out of the framing. To the right, a view of a laminated glazing is presented. As seen in the picture, the panel integrity is preserved, with most of the splinters remaining on the frame, adhered to the interlayer (Source: Pioneer Glass).

4.1 Chamber 1. The seismic and weather performance testing facility of Permasteelisa is presented. The seismic beam of the test set up can be noticed in blue (Source: Permasteelisa).

4.2 The seismic beam used for the seismic performance tests as seen from the interior of the Chamber. To the right of the picture the interesting feature of the seismic beam is visible, allowing the seismic beam to make a turn of 90.0 degrees. This feature which makes the testing of the corner of two storefronts of a building possible, was not utilised in the case study examined during this study (Source: Permasteelisa).

4.3 The fastening system through two halfen channels at the top of the seismic beam is depicted. In the lower part of the image, the hydraulic system responsible for the displacement or acceleration induction is presented (Source: Permasteelisa).

4.4 The façade units used for the testing campaign are presented. The type of silicone joint applied on each of the units is described (Source: Permasteelisa).

4.5 Detail drawings of the fastening system of the curtain wall system which is fixed to the seismic beam. The left drawing describes the vertical whereas the right one the horizontal detail of the upper constraint points of the curtain wall system (Source: Permasteelisa).

4.6 Vertical detail presenting the bottom constrain point of the curtain wall system. In particular the connection of the bottom transom to the starter sill is presented (Source: Permasteelisa).

4.7 View of the fastening system of the curtain wall units as seen from the inside (Source: Permasteelisa).

4.5 Detail drawings of the fastening system of the curtain wall system which is fixed to the seismic beam. The left drawing describes the vertical whereas the right one the horizontal detail of the upper constraint points of the curtain wall system (Source: Permasteelisa).

4.6 Vertical detail presenting the bottom constrain point of the curtain wall system. In particular the connection of the bottom transom to the starter sill is presented (Source: Permasteelisa).

4.7 View of the fastening system of the curtain wall units as seen from the inside (Source: Permasteelisa).

4.8 In the figure above the different stages at which the glazed curtain wall unit undergoes deformation and, consequently, the glazing gets in conduct with the framing, are depicted. The above representation refers to the cases where relatively weak adhesion is provided between the glazing pane and the frame. The previous allows for the relative movement of the glazing with respect to the curtain wall framing (Source: Sucuoğlu & Vallabhan, 1997).

4.9 Above the location of the displacement transducers is mapped. On top the transducers placed on the framing and below the ones located for the glazing monitoring are presented.

4.10 The displacement transducers located upon the fastening system to which the façade unit containing SG-500 (to the left) and SG-550 (to the right) is attached to (Source: Permasteelisa).

4.11 In this graph the cyclic displacement applied on the curtain wall units during the testing procedure is presented. The displacement values originate from the measurements as recorded by the transducer DT-19 applied on the fastening system of the unit under examination (see also Figure 4.10). In the

present graph, the loading introduced during the first intensity H/300 is depicted. However, the remaining two drift ratios were applied in the same cyclical manner.

4.12 The figure above represents the deformed space of two adjacent out of the four adjacent curtain wall units examined during the experimental sequence. The deformed shapes originate from the plotting of the measurements taken during the experimental procedure, therefore recreate the actual curtain wall behaviour as observed during the mock-up test. To the left the façade reaction to the positive and to the right to the negative displacement application are presented.

4.13 The detail to the left presents the connection of the bottom transom and the starter sill. In red the alignment screw is marked, the component that is responsible for the different curtain wall unit behaviour with regards to the horizontal displacement direction. To the right, the 3D drawing provides a better view of the alignment screw location in the curtain wall configuration (Source Permasteelisa).

4.14 In the schematic views presented above the curtain wall response while undergoing the three levels of inter-storey drift is presented. The darker and lighter colours represent the positive and negative behaviour respectively.

4.15 The procedure followed for both the positive and negative pressure application during the air-leakage testing is presented above (Source: EN 12153, 2000).

4.16 The air-leakage as measured before the implementation of the H/300 displacement application both for the cases of Suction and Pression.

4.17 To the left, the slot on the transom of the curtain wall unit where the alignment screw is placed is depicted. To the right, the alignment screw after bearing the hole in the transom, is completely extracted from the transom (Source Permasteelisa).

4.18 The extraction of the alignment screw from its original location in the transom of the façade element. The bearing phenomena after the performance tests recreating the seismic intensities are depicted above (Source: Permasteelisa).

4.19 In this schematic view the curtain wall unit diagonal is presented to connect the diagonal corners of the curtain wall unit. The coloured deformed shape represents the unit response to the horizontal displacement application. As seen in the visualisation, the diagonal is also affected. Therefore, the rotation, elongation or contraction of the diagonal can be defined based on the initial state of the diagonal.

4.20 In the figure above the variation of the frame rotation is presented as recorded during the experimental campaign for each of the three displacement rates.

4.21 Similar to the previous figure, the response of the glazing rotation with regards to the different displacement values, in practice drift rations, is presented.

4.22 In the figure above the rotational behaviour of both the glazing and the framing combined are presented for the case of the structural silicone joint SG-500 to the left and of SG-550 to the right respectively.

4.23 In the figure above the rotational behaviour of both the glazing and the framing combined are presented for the case of the structural silicone joint SG-500 to the left and of SG-550 to the right respectively.

5.1 In the details above, the division between the adjacent framing profiles, to the left of the left and right mullion and to the right the lower transom on top from the bottom transom/ starter sill, are presented. The red line indicates the boundary between the framing areas used for the calculation of the

respective equivalent area and moment of inertia eventually introduced as properties to the arbitrary shapes of the aluminium framing elements in the DIANA environment.

5.2 Above, the connection between the glazing and the adjacent aluminium framing is presented by the red arrows of the schematic representation. Through the implementation of this element in the numerical procedure, all the non-linearities of the material, its time-dependent behaviour as well as the mechanisms occurring on its interface with the frame and the glazing are attempted to be included.

5.3 The stress-strain curves for the adhesive connections for the uniaxial tensile tests found in the literature are depicted. These curves were used as a reference for the plotting of force-elongation diagrams of the interface connecting the glazing with the frame (Image Source: Silvestru et al., 2018).

5.4 The non-linear elasticity of the structural silicone connecting the glazing with the frame is introduced in the DIANA environment through the traction-relative displacement curve as seen above. In order for the analysis to run for the two displacement directions, apart from the tensile, the compressive behaviour also had to be provided. For this reason, the information found for the tensile behaviour was mirrored with respect to axes x and y that are also marked in red dotted lines in the figure above.

5.5 In the schematic presentation above the implementation of the interfaces to the glazing-to-frame and frame-to-frame connections is depicted. The blue arrows identify the connection realised between adjacent frames, bonding right and left mullion profiles on one hand and the bottom transom with the starter sill below on the other hand.

5.6 In the figure above, the connection detail of the adjacent framing elements is presented. To the left, it can be seen that although the units can move almost freely away from each other, while an external action forces them to move towards each other, a certain distance of almost 10.0 mm has to be overcome before the actual connection of the left and right mullion. To the right, a similar case is observed for the bottom transom and starter sill connection. Here the distance that needs to be surpassed before the elements are in conduct is slightly larger, around 15.0 mm.

5.7 The figure above is obtained from the DIANA environment and visualises the modelling of the different curtain wall elements comprising the mock-up unit of the four subsequent units. The larger blue area represents the glazing, whereas the perimetrical thin lines that are coloured in darker blue depict the framing. Although not visible in the picture, the starter sills are placed right where the bottom transoms of each curtain wall unit are located. The blue and red lines forming represent the various interfaces, connecting either the glazing with the frame, the adjacent mullions or the bottom transom with the starter sill.

5.8 A preview of the result section of the four curtain wall units is presented above. In this specific case the units have undergone a negative displacement equal to the largest displacement applied on the unit H/100 = 37.5 mm. It is observed that the meshing is uniform throughout the area analysed.

5.9 The convention of the positive and negative sign used in the current study. To the left the positive and to the right the negative displacement applications are depicted. The displacements are always applied on the upper left framing corner of each of the curtain wall units tested.

5.10 In the schematic representation above, the different boundary conditions applied on the numerical model are represented. The different colours indicate different properties, whereas the asterisk (*) the cases were linear properties were attributed. Obviously, the non-linear properties were provided to the boundary springs not characterised by an asterisk.

5.11 In this figure the curtain wall response to the positive inter-storey ratio of H /300 is depicted. Similar behaviour is noticed for the negative direction as well. Regarding the horizontal movement of the curtain wall unit, the upper part of the frame is noticed to displace at a value almost equal to the

imposed displacement. On the contrary, the lower part of the façade unit presents a smaller horizontal displacement.

5.12 The naming convention used for the points under examination is presented. The figure above depicts the points of the framing whereas the scheme below the ones of the glazing. The direction of the arrows was used for the appropriate interpretation of the experimental values monitored during the experiment.

5.13 The reaction of the façade under positive to the left and negative to the right displacement application is presented.

5.14 In this figure the detail of the connection of the bottom transom with the starter sill is presented. The alignment screw connecting the two elements is highlighted in red.

5.15 In the figure above the scenarios referring to the variation of the upper bracket and starter sill boundary springs are presented. To the left, the completely linear properties of the starter sill and the upper bracket brackets initially calculated from Hooke's Law, based on the spring stiffness initially defined, are presented respectively. Scenarios a, b, refer to the two possible ways of implementing to DIANA the desired behaviour of the starter sill allowing upward but no downward movement of the unit. Scenarios c and d are the equivalent for the upper bracket. Initially the scenarios referring to the starter sill and later for the upper bracket boundary conditions were tested separately while preserving the properties of the other boundary spring linear. This sensitivity analysis attempted to determine the most appropriate combination of upper bracket and starter sill boundary spring properties that more accurately recreate the experimental, therefore actual, curtain wall behaviour. Later, all the possible combinations of joined non-linearity of the upper and lowest boundary springs were tested (ac, ad, bc, bd).

5.16 The figures above represent the different displacement values of the characteristic points C, D, E & F that are used as a reference for the evaluation of the proximity of the numerical behaviour to that of the actual experimental response to the positive and negative displacement application respectively. In dotted lines, the experimental values that are used as a reference are presented, following the same colour coding as defined for each of the characteristic points. It is seen that less values are presented for the x displacements and this is due to the lack of the experimental reference. It has been decided that only the values for which a reference exist, will be presented since only by means of comparison as such the proximity of each scenario tested can be indicated. Based on the response of the numerical model to the implementation of non-linear properties to the boundary springs, it can be concluded that the combinations including the upper bracket properties defined by scenario d are the ones approximating better the reference behaviour plotted in dotted lines.

5.17 The above figure concentrates all the cases tested in order for the impact of the implementation of opposite non-linear properties on each of the starter sills to be assessed. The diagrams viewed correspond to the force-elongation properties attributed to the respective boundary condition. For better visualisation, the same colour coding of the properties defined to each of the boundary springs tested is identical to that of the simplified scheme presented to the left.

5.18 The schematic representation of the final boundary conditions applied to the numerical model is depicted above. The implementation of the additional boundary spring located on the top left corner of the curtain wall frame is visible in pink colour.

5.19 Detail of the upper fastening of the façade unit to the supporting structure. The difference between the left and right upper boundary conditions of the façade unit is the reaction of the floor bracket and the hook and lies on the need for the displacement accommodation. In practice in the right connection the screw, which is more accurately referred to as grain, connects the hook with the floor bracket rigidly. Therefore, the hook is fixed to the floor bracket which results in these rigidly connected elements having the same vertical displacement. On the other hand, the upward vertical movement of the unit is possible since the hook is allowed to slide inside the slider. This upward movement, though, is only allowed until a certain point above which the unit disengages from the hook. Although

the aforementioned screw is not present in the left connection, the vertical movement downwards is still restrained due to the conduct of the hook and the slider. The upward movement is also allowed since there as well the hook can slide inside the slider.

5.20 In the schematic representation presented above the different boundary springs applied to the curtain wall unit are depicted. Each colour indicates different material properties. The slightly different trend of the properties attributed to the two boundary springs of the starter sills are depicted to the right. It is clearly seen that for the left case, the non-linear properties were reversed to the linear ones.

5.21 In the figure above the variation of the vertical and horizontal displacements for the positive and negative displacement application is presented above for the three distinctive versions of the numerical model, namely the initial, the improved and finally the calibrated version.

5.22 A schematic representation used as a reminder for the naming convention followed during this numerical approach.

5.23 In the schematic representation above the undeformed shape of the unit prior to its loading is depicted in pink. The curtain wall response to the horizontal displacement implementation is presented in light blue colour. The angle marked in the scheme indicates the rotation angle based on which the following evaluation is realised.

5.24 An overview of the script developed in grasshopper aiming for facilitation and the standardisation of the result post-process is presented above.

5.25 Above the concept followed during the grasshopper script starting from the initial undeformed condition and gradually moving to the deformed one and the creation of the diagonal element is presented.

5.26 In the graph presented above an overview of the frame rotation as captured by the transducers during the experimental procedure or simulated through the different modelling approaches is presented. The experimental values monitored during the full-scale testing campaign are presented in the turquoise dotted line. The light green dashed line depicts the numerical values originating from the similar study performed for the same case study while following a slightly different modelling approach (Galli, 2011). Finally, the continuous pink, yellow and purple lines display the different versions of the DIANA model. This graph provides an insightful indication of the level of proximity achieved by each of the numerical simulations.

5.27 The alternative means used for the evaluation of the curtain wall behaviour are seen in this schematic representation. The diagonal elongation is assessed both in terms of mm and as percentage with respect to the initial diagonal length. The unit distortion is calculated as the relative difference of the initial and final angle of the mullion and transom connection.

6.1 The façade behaviour under the largest positive displacement applied during this testing sequence of H/100 = 37.5 mm is seen in the figures above. In grey, the initial undeformed shape of the façade unit is presented. In light blue the façade behaviour as monitored during the experimental procedure is shown, and finally the representative DIANA models with the different silicone joints (1.0, 6.0 and 12.0 mm) are depicted in purple, blue and pink respectively. In order for the façade behaviour to be clearly seen, a magnification factor of 10.0 has been applied to both the x- and y-displacements of the façade unit. The same behaviour is presented to the left in continuous and to the right in dashed lines for the better assessment of the unit behaviour.

6.2 In the figure above the response of one of the curtain wall units imposed to a positive in-plane horizontal displacement is depicted. In grey the initial position of the curtain wall unit is presented. In light blue the experimental behaviour as monitored by the displacement sensors is depicted. Finally, in purple, blue and pink the representative scenarios of the structural silicone sensitivity analysis are presented. A magnification factor of 10.0 has been applied to both the vertical and horizontal displacements for illustrative purposes. Additionally, for the better evaluation of the model response a closer look is provided to the framing corners.

6.3 The variation of the diagonal and framing rotation with respect to the structural silicone thickness is presented in the figure above for the three representative scenarios of structural silicone bite of 1.0, 6.0 and 12.0 mm. The previous are referred to as SSG 1, SSG 6 and SSG 12.0 respectively. Although an increase of the glazing rotation is observed with the increase of the structural silicone bite, a decrease is noticed in the case of the aluminium framing.

6.4 In this figure the variation of diagonal elongation expressed in the form of percentage is presented.

6.5 The same variation of the frame diagonal is visualised here in the form of millimetres. Again, the variation is depicted with respect to the three representative structural silicone scenarios.

6.6 In the figure above the response of the curtain wall unit to the alteration of the structural silicone bite is presented through the frame distortion. Similarly to the previous cases, the values presented correspond to three representative scenarios of the structural silicone sensitivity analysis.

6.7 In the figure above the relation between the maximum stress observed on the glazing pane for the positive displacement application with the largest intensity H/100 is depicted with respect to the increase of the structural silicone bite.

6.8 Above the loading path of the glazing unit as changing based on the different thickness of the structural silicone connection is presented for the positive (left) and negative (right) displacement application and the largest inter-storey ratio (H/100).

6.9 The variation of the axial and shear forces (top) and the moment (below) with regards to the structural silicone thickness increase is presented above.

6.10 The figure above provides a qualitative indication of the results obtained from the Result tab of the DIANA environment. To the left, the contouring expressing the orientation as well as the magnitude of stresses on the curtain wall unit as resulted from the run of the non-linear analysis is seen. In the middle, the shear as well as the axial forces as calculated from the cross section of the frame and to the right the relative displacement of the glazing-to-frame connection as measured for the x-axis are presented.

6.11 The aluminium frame utilisation factor as calculated for the axial and shear strength. As seen above, the factor deriving from the axial strength is much larger compared to that of the shear strength.

6.12 The variation of the shear stress measured on the glazing-to-frame connection in relation to the silicone thickness is presented. Several silicone materials were considered as depicted in the coloured legend.

6.13 The utilisation factor of the main façade components, frame, silicone joint and the glazing are presented in the figure above.

6.14 The graphs presented above express variation of the utilisation factor (to the left) and of the drift ratio (to the right) with respect to the structural silicone thickness. The influence of the glazing-to-frame connection on the ultimate failure mechanism can be easily assessed.

6.15 In the details above the left and right brackets connecting the curtain wall unit of the recent experiment to the structural system are presented. The vertical distance that the curtain wall unit needs to overcome in order for the disengagement to occur is different for the two brackets. As seen above, this distance is limited in the case of the left bracket, around 25.0 mm whereas for the right case is considerably larger (Source: Permasteelisa).

6.16 To the left, the vertical distance the unit needs to surpass in order for the disengagement to occur. To the right, the much larger vertical displacement that the façade unit needs to undergo is depicted. The difference between the two is substantiated through the screw located on the right connection, here depicted also in red, fixing the hook to the floor bracket. For the left connection, in the absence of this screw, the hook is free to disengage from the floor bracket if exceeding the 25.0 mm vertical displacement, leading to the disengagement of the curtain wall unit (Source: Permasteelisa).

6.17 The maximum vertical displacement of the façade unit under examination observed on the upper frame corners of the façade unit.

6.18 In the figure above the two maximum stress-based failure mechanisms of the frame and the structural silicone joint are presented accompanied by the additional failure mechanism indicating the possibility of the unit disengagement.

6.19 This graph displays the variation of the drift ratio with regards to the structural silicone bite.

7.1 In practice this gap indicates that the interface as a whole should not provide any resistance for the cases where the transom is forced to move upwards. For the downward movement, not any resistance is presented before the gap of 14.0 mm closes.

7.2 The left figure presents the implementation of water-tightness testing where water is sprayed over the curtain wall unit under testing through a grid of nozzles. The figure to the right presents the connection of the mock-up to the testing facility. During the testing it is reassured that no leakage occurs unless it penetrates through the curtain wall unit itself (Source: Permasteelisa).

I.1 Above a schematic presentation of a laminated glazing is presented. The various glazing layers are separated by one, sometimes more, synthetic films of polyvinyl butyral (PVB). For the introduction of thermal and sound insulation to the laminated glazing, the latter can also be assembled in double glazing. During the manufacturing of this glazing type both the pressure and the temperature are so high that the dissociation of the glazing from the PVB becomes impossible (Source: Glass Design Malta).

I.2 In the figure above, a stack joint arrangement is presented in the coloured areas of the curtain wall section. The movement provision of the joint in the vertical direction is placed between the sill and the head transom. The horizontal provision is marked between the female and male mullions (Source: Jeyamohan, 2022).

I.3 A simple structural glazing design is presented on the figure above. The structural silicone sealant is depicted in the dark hatched area (Source: DOW, 2021).

I.4 In the figure above an exploded view of a typical unitised curtain wall system is presented. The interruption of the framing elements, mullions and transoms, facilitates the preview of the various cross sections. Among the various components marked, the setting block chair is also visible. Finally, the insulating material normally located behind the spandrel area is not presented in this view for purposes of clarity (Source: Lee, A. D. et al., 2017).

II.1 A test configuration typically used for the verification of a curtain wall seismic behaviour. The racking facility in this case consists of three steel tubes. While the upper and the lowest ones are fixed, the intermediate allows horizontal movements, recreating in this way the inter-storey drift that results in the racking of the curtain all elements. As the drift amplitude gradually progresses, the potential failure modes of the examined configuration are revealed (Source: AAMA 501.4, 2018).

II.2 A schematic view of the Dynamic Racking test facility (Source: AAMA 501.6, 2018).

II.3 The drift time history as recorded during a crescendo test of mid-rise architectural glass components (Source: AAMA 501.6, 2018).

A.1 The schematic representation above for the aluminium frame and below for the glazing is presented here. These figures serve as a reminder of the specific location of the transducers monitoring the curtain wall behaviour under seismic action. The naming convention (Points A-L) adopted during this study is also displayed for a matter of completeness.

A.2 The vertical displacement of one of the upper brackets of the façade specimen as monitored for H/300, H/200, H/100.

A.3 The horizontal displacement of the low transom (Point D) for the different levels of the displacement application.

A.4 The vertical displacement of the low transom (Point F) as recorded for the three intensities of the displacement application.

A.6 The vertical displacement as monitored in the hook of the curtain wall fastening system.

A.7 The measurements of the vertical displacement of the upper transom (Point E) for the three intensities of the displacement application.

B.1 An overview of the scenarios tested. The different colours indicate the four main categories of the sensitivity analyses run during this stage.

B.2 The schematic view above presents four categories of material properties varied over the respective sensitivity analyses. These analysis series aimed to demonstrate what are the parameters affecting the numerical model behaviour the most.

B.3 The charts above represent the fluctuation of the displacement values of each of the representative frame points analysed. Initially the experimental values are plotted and, thereafter, the respective values as obtained per scenario. The scenarios presented above are the ones considered as more accurate since their numerical results are closer to the experimental ones.

C.1 In the above picture the four façade elements of the DIANA numerical model are presented. The marked element represents the “bottom transom left” element which is supplementary to the corresponding right one. The two of them comprise the bottom transom of each of the façade elements. In like manner, the starter sill of each unit consists of a left and right part. It is clearly seen that the point representing the alignment screw is placed closer to the right mullion of the façade in a 400.0 mm distance. Some of the “unite” connections, in particular the ones connecting the bottom transom with the adjacent mullions, are also visible in the figure above. The connections are represented as black and white lines forming a corner configuration.

C.2 In the figure above some of the connections introduced in the numerical model are presented. In the bottom transoms of the four façade elements the boundary springs connecting the starter sill with the ground are seen. The interfaces connecting the glazing with the frame are previewed only for the third façade segment.

C.3 The translations and rotations of the alignment screw that can be either restrained or set free are presented as seen in the DIANA environment. Above, T1 as well as T2 were selected, but for the sake of completeness, the complete series of restrain combinations was tested.

C.4 The naming convention followed in the study is presented. Above, the points of the frames for which the displacements were measured during the experiment are located outside the façade units. The reference points for which the glazing movement is measured are the ones placed on the inside of the frame and are also included on the following table.

C.5 The environment where the linear material properties of the interface connecting bottom transom with the starter sill are defined. In the image presented above, the original scenario is presented, where the Normal stiffness modulus – y is defined as 0.6 N/mm^3 whereas the Shear stiffness modulus-x equals 0.2 N/mm^3.

C.6 The graphs above represent the variation of the numerical results for the scenarios previously discussed. As explained also in the legend, the dashed lines represent the reference values which resulted from the experimental campaign.

C.7 The displacements both in X and Y direction of the reference points. As it can be clearly seen from the graphs, the façade response in the positive displacement recreated better the experimental behaviour compared to the negative one. A possible area of improvement is the horizontal movement of Point D.

D.1 Qualified presentation of the properties varied over the additional sensitivity analysis performed focused on the stiffness of the Starter Sill and the Upper Bracket boundary springs.

D.2 The graphs above visualise the gradual change of displacements in X and Y direction for the positive displacement application. By studying this figure as well as on Table D.1 an insightful indication regarding the impact of the stiffness non-linearity of the model's boundary conditions is provided More specifically, an indication of the more appropriate scenario recreating better the stiffness property of the upper bracket spring being scenario d can already be made. For a matter of completion though, all the possible scenarios, including the ones containing the force - elongation curve of scenario c, is included in this and the following tables and figures.

D.3 The reaction of the façade under positive to the left and negative to the right displacement application is presented. The points marked in blue represent the test point displacing symmetrically with respect to each other. On the contrary, the points marked in red are those that display asymmetric behaviour. The term "asymmetric" aims to express the numerical inequality of the points belonging to the same mullion, points C and D for the positive and E and F for the negative displacement.

D.4 Schematic representation of the boundary conditions applied up until this modelling phase. As seen for the figure, only one upper bracket is introduced in the numerical modelling procedure and two below, dedicated to the starter sills. Additionally, the same properties are attributed to both the starter sills.

D.5 The present schematic representation depicts the various aspects of the finite element modelling that intend to improve the numerical behaviour.

D.6 Representation of the positive (above) and negative (below) displacement application. The displacements are applied on the upper left part of each of the façade units tested.

D.7 Similarly to the previous schematic representation this as well concentrates the different parameters tested during this modelling stage that aspire to improve the curtain wall behaviour with regards to the experimental reference.

D.8 The stiffness properties of the starter sill and the upper bracket boundary springs for the scenarios ad, ac, bc and bd respectively.

D.9 The response of the façade unit to the simultaneous combination of the non-linear properties of the boundary conditions are presented above for both the positive and negative displacement application.

D.10 The properties of the stiffness attributed to the boundary conditions per scenario tested. To the left the force – elongation diagram defining the upper bracket stiffness is provided. The diagrams for stiffnesses of the left and the right starter sills are displayed separately.

D.11 The numerical values of the DIANA model for the previous scenarios tested are now accompanied by the new series of scenarios (de, df, cf and ce). The diagrams of the upper row describe the curtain wall reaction to the positive displacement application, whereas the ones of the lower row of the opposite direction.

D.12 This schematic representation of the boundary conditions is an updated version of the one presented previously. Here the additional upper bracket implemented to the upper left corner of the façade unit is additionally implemented.

D.13 The numerical values of the DIANA models of all the previous scenarios with the implementation of the extra boundary condition on the upper left frame of the unit presented above for the positive and negative displacement application respectively.

D.14 The modification of the displacements of the frame points tested are presented above. During this improvement of the previous scenario de, the positive behaviour of the numerical model appears to be optimised, whereas the negative remains unaffected.

D.15 In the figure above, the approximation of the final numerical models to different reference values is presented for the x and y displacements of both the positive and negative displacement application. In the first case, the initial reference values are used, originating from the first loading cycle of H/100 = 37.5 mm. Later, the reference values occur from the averaged measurements of the first two loading circles and finally, from the averaged four loading circles.

List of Tables

6.4 The table presents the actual numbers as originated from the calculation of the diagonal elongation through the grasshopper script.

6.5 The numerical values describing the frame distortion are presented above. As seen both from both the figure and the table, the distortion is expressed as the difference between the initial right angle of 90.0 degrees and the deformed angle as calculated for the unit which responds to the horizontal displacement application.

6.6 Four different assessment methods of the structural silicone sensitivity analysis are presented above. On the table below, the values for which their approximation to the equivalent experimental result fluctuates between -20.0 % and 20.0 % are presented in green background.

6.7 The different means of evaluation are collected facilitating the assessment of the glazing (up) and the frame (below). Both the experimental values including a less stiff silicone connection (SG-500) and a stiffer one (SG-550) are presented aiming to provide a direct comparison to the similar stiffness increase introduced by the silicone sensitivity analysis. The numerical values observed here refer to the last and largest intensity of displacement application, with a range of 37.50 mm, which responds to a drift ratio of H/100.

6.8 The variation of the axial stress S_{xx} as measured in the top transom is presented in the table above in relation to the gradual increase of the structural silicone thickness. It is quickly observed that the axial stress is slightly decreasing as the structural silicone thickness increases. Additionally, the yield stress of the aluminium alloy 6061 used for the frame of the façade configuration is also presented. Based on the two previous the utilisation factor of the aluminium frame is calculated and presented on the latest column.

6.9 Geometrical and mechanical properties of the various structural silicone joints examined.

II.1 a_p and R_p coefficients for Architectural Components or Elements (Source: FEMA 450, 2003).

II.2 Classification criteria for the categorisation of the parts. “ULS” refers to the Ultimate Limit State and “SLS” refers to the Serviceability Limit State (Source: NZS 1170.5).

II.3 The table based on which the horizontal (C_{ph}) and vertical response factors (C_{pv}) in relation to the ductility μ_p of the respective parts are obtained (Source: NZS 1170.5).

B.1 An overview of the scenarios tested. The different colours indicate the four main categories of the sensitivity analyses run during this stage.

B.2 In the coloured column the displacement values as monitored during the experimental procedure are presented. To the right, the displacement values for the first 8 Scenarios (S1-S7) are presented. The values coloured in red are the ones deviating the most from the experimental results, whereas the green ones represent the cases closer to the experimental equivalents. In the green-coloured cells at the bottom the basic properties varying over the analyses are presented.

B.3 Similar to the previous cases, in the left part of the table the experimental values for units 2 and 3 of the experimental specimens are presented. In the coloured column the ones that are used as a reference are concentrated. In the green-coloured row an overview of the basic parameters of this specific sensitivity analyses, both constant and varying, are presented. Finally, to the right of the table the fluctuation of the values depending on the scenario tested are presented.

B.4 The displacement values for each of the scenarios tested are presented. The horizontal movement of point D is the main value attempted to be optimised through the analyses scenarios.

B.5 The displacement values for both the glazing and the frames are presented for each of the scenarios tested (S21-S28) during this final sensitivity analysis.

B.6 The collection of the numerical values of the most representative scenarios selected out of the complete set of scenarios run during the sensitivity analyses of this chapter is presented in this table. The respective values measured during the experimental campaign are displayed in yellow.

C.1 Above the displacement values for two of the representative scenarios (S25 and S27) are presented. Since not a considerable difference is noticed between these cases and the ones where the alignment screw was not implemented, not all of the representative scenarios were re-calculated.

C.2 In the above tables the experimental and the numerical results of one representative scenario (S25) are presented for the positive and negative displacement application respectively. By comparing the values, it can be concluded that during the negative displacement façade's response is identical to that of the positive displacement with the only exception being the sign.

C.3 Above the displacement results of the examined points for the case of the alignment screw relocation. For the sake of simplicity, only one of the representative scenarios is included since it was observed that, for this specific numerical model, the relocation of the alignment screw from the initial point to the middle of the mullion does not affect the façade behaviour.

C.4 An overview of the alternative cases tested while attempting to define the impact of the alignment screw implementation in the numerical model.

C.5 The numerical results of the different versions of the DIANA model attempted for the implementation of the alignment screw are seen above. In the coloured row the property modification applied on each scenario is explained. Apart from the reference scenario, S8, two scenarios with translation T1 and T2 restrained respectively are presented in columns ii and iii. In column iv the numerical results of the DIANA model incorporating tyings instead of rigid connections for the representation of the alignment screw are presented.

C.6 In these similar to the previous tables, the numerical results obtained from the sensitivity analysis aiming to evaluate the impact of the normal and the shear direction of the transom to starter sill connection are presented in columns v-viii. The test cases belonging to the same category are obtained inside the framed columns.

C.7 For the final calibrated scenario the alignment screw was removed and the results are presented in the columns where “No” is indicated referring to the implementation of the Alignment Screw. As it can be seen, the removal of this specific façade element does not affect the façade behaviour neither on the positive nor on the negative direction of the applied displacement.

D.1 The results of the additional sensitivity analysis are presented in the last four columns of the table above. On the coloured row the description of the parameters checked is described. The red or green colouring of certain values indicates the worse or better correspondence of the numerical to the experimental results respectively.

D.2 The numerical values of scenarios ad, ac, bc and bd for the positive displacement application. Scenario 18 that was selected as the most representative one from the previous sensitivity analysis was used this time as the basic model upon which the appropriate per case property modifications were applied. The numerical values of Scenario 18 are also presented since they serve as a reference for the impact assessment of each of the variations introduced.

D.3 The respective displacements of the DIANA model are presented above for the negative displacement application. Similarly to previous situations, the marking of some values with red determines the further deviation of the numerical results compared to the reference scenario whereas with green the better approximation is introduced due to the property modification applied through the scenario case tested.

D.4 The numerical values of the additional scenarios de, df, cf and ce are presented above for the positive displacement application. Below, the same values expressed as percentages presenting either the positive or the negative deviation from the reference values are shown. A deviation range of ±30.0 % has been accepted as allowable. The values between this range are highlighted in green.

D.5 The equivalent values of the additional scenarios tested for different properties of the starter sill are presented this time for the negative displacement application. Below, the same results are shown in the form of percentages representing the deviation range from the values measured. The values marked in light grey instead of the typical black colour are the ones accepted as allowable since their movement remains in the area of 0.0 displacement.

D.6 The numerical values representing the façade behaviour under the implementation of a positive displacement equal to H/100 is presented above. In this set of scenarios an additional boundary spring has been introduced in the upper left part of the façade unit recreating the left upper bracket fastening the curtain wall system to supporting structure. It is obvious that scenarios de and df are the ones approaching better the experimental measurements with df recreating better the positive and de the negative displacement application.

D.7 The equivalent numerical values are presented for the negative displacement application. The most interesting improvements introduced by the modification of the stiffness properties of the two starter sills separately are marked in coloured background. The green background marks an important improvement compared to the previous results whereas the red colour indicates the points approximating less the experimental results.

D.8 The table of the final calibration is presented. The blue and orange columns present the reference values of the positive and negative displacement respectively. Additionally, the results of scenario de are seen for both the displacement options. In red the final calibrated scenario is presented, that is an optimised version of scenario de. In practice the properties of the left starter sill were modified to the initial linear ones. In this way a façade behaviour recreating both the positive and negative displacement application was achieved.

D.9 The correspondence of the numerical behaviour to the variation of the experimental values used as a reference is presented above. It can be easily seen that while taking into account four loading circles as reference, worse approximation of the experimental results occurs. On the contrary, while considering only two circles, the problematic areas for the negative displacement application are corrected. So it can be concluded that by using the experimental values of the first two loading cycles as a reference, the DIANA model approximates closely the respective experimental behaviour for the negative displacement application. In fact, all the numerical values, with the exception of those marked in light grey, approach the experimental results at a range of 30.0 %. The above does not apply for the positive displacement application. In this case, better correspondence of the numerical to the actual behaviour is achieved when comparing the first with the initial reference values.